NTNU – Trondheim
Norwegian University of
Science and Technology

L1 Adaptive Control of the Inner Control Loops of an F-16 Aircraft

Øystein Hov Holhjem

Master of Science in Engineering Cybernetics
Submission date: June 2012
Supervisor: Tor Arne Johansen, ITK

Norwegian University of Science and Technology
Department of Engineering Cybernetics

"There is an art, it says, or rather, a knack to flying. The knack lies in learning how to throw yourself at the ground and miss. (...) Clearly, it is this second part, the missing, which presents the difficulties."

From "Life, the Universe and Everything"
Douglas Adams, Pan Books, 1982

Problem description

Candidate: Øystein Hov Holhjem

Title: $\mathcal{L}_1$ Adaptive Control of the Inner Control Loops of an F-16 Aircraft.

Problem formulation: $\mathcal{L}_1$ adaptive control is a new and promising field of study. This master's thesis aims at getting a good understanding of of the theory of $\mathcal{L}_1$ adaptive control, and document this. The goal of the master's thesis is a simulator based testing of the $\mathcal{L}_1$ adaptive control strategy on aircraft with strong nonlinearities.

The task consists of the following subtasks:

- Develop a linear mathematical model for the longitudinal and the lateral modes of a suitable aircraft as a basis for the control design.
- Choose a control architecture and a problem formulation for the adaptive control. Evaluate which architectures of $\mathcal{L}_1$ adaptive control are suitable for control of the inner loops of an autopilot with regards to uncertainties and modelling errors (parametric, unmatched, actuator dynamics, etc.).
- Test controllers for longitudinal and lateral inner loop with simulations with realistic unmatched modelling errors, actuator dynamics and disturbances etc. Emphasis on simulations where the controller is implemented in discreet time with realistic values for the sampling frequencies.
- Compare the results of the $\mathcal{L}_1$ adaptive controller with results from MRAC and PID for chosen scenarios.

Supervisor: Tor Arne Johansen, NTNU

Co-advisor: Åge Skullestad, KDS

Abstract

This report is written as a master's thesis given at NTNU, and in collaboration with Kongsberg Defence System. This text investigates the use of $\mathcal{L}_1$ adaptive control for multi-variable systems with unknown nonlinear unmatched uncertainties and unmodeled actuator dynamics, particularly for the inner longitudinal and lateral loops of a nonlinear F-16 aircraft model.

Chapter 1 gives an introduction to the report by introducing the basic principles of aircraft control and specifying the goals of the text. Chapter 2 introduces the theory of linear aircraft modelling, which specifies the starting point for the $\mathcal{L}_1$ adaptive control design. Chapter 3 presents the $\mathcal{L}_1$ adaptive control theory considered in this text, together with the main theoretical results. Chapter 4 presents the simulations results and the discussion, together with the specific $\mathcal{L}_1$ adaptive control design used in the simulations. Chapter 5 concludes this report and points toward possible future work.

The $\mathcal{L}_1$ adaptive control theory has proven to give good results. This was also found in this report. The controller handles unmatched nonlinearities and disturbances very well and manages to track the reference signal. For the longitudinal controller, this has also been shown through simulations on a realistic nonlinear F-16 model. Compared to the MRAC-formulation we see that the introduction of the filter in the $\mathcal{L}_1$ adaptive control formulation gives great improvements with regards to performance. The results of this text shows how the $\mathcal{L}_1$ adaptive controller manages to separate adaptation from control and thus be able to introduce fast adaptation without introducing high gain feedback. This text also discusses how implementation issues like limited sampling rate affects the performance of the $\mathcal{L}_1$ adaptive controller, and shows how this can be handled by a proper redesign of the architecture.

The results of the $\mathcal{L}_1$ adaptive controller for the longitudinal mode are compared to a simple PID-controller. We actually see that the PID-controller performs almost as good as the $\mathcal{L}_1$ adaptive controller for the simple longitudinal system.

Sammendrag

Denne rapporten er skrevet som en masteroppgave gitt ved NTNU og i samarbeid med Kongsberg Defence System. Denne teksten undersøker bruken av $\mathcal{L}_1$ adaptiv regulering for multivariable systemer med ukjente ulineære umatchede usikkerheter, og umodellert aktuatordynamikk. Dette er spesefikt undersøkt med tanke på bruk for de indre langsgående og laterale sløyfene av en ulineær F-16 flymodell.

Kapittel 1 gir en introduksjon til rapporten ved å forklare de grunnleggende prinsippene for flykontroll og ved å spesifisere målene med teksten. Kapittel 2 introduserer teorien om lineær flymodellering, som angir utgangspunktet for designet av en $\mathcal{L}_1$ adaptiv regulator. Kapittel 3 presenterer teorien bak $\mathcal{L}_1$ adaptiv regulering som behandles i denne teksten, sammen med de viktigste teoretiske resultatene. Kapittel 4 presenterer simulerings resultatene og diskusjonen, sammen med det konkrete $\mathcal{L}_1$ adaptiv reguleringsdesignet som benyttes i simuleringene. Kapittel 5 konkluderer denne rapporten og peker mot mulig fremtidig arbeid.

$\mathcal{L}_1$ adaptiv reguleringsteorien har vist seg å gi gode resultater. Dette ble også funnet i denne rapporten. Regulatoren håndterer umatchede ulinearitеter og forstyrrelser meget godt og klarer å følge referansesignalet. For den langsgående kontrolleren har dette også blitt vist gjennom simuleringer på en realistisk ulineær F-16 modell. Sammenlignet med MRAC-formuleringen ser vi at innføringen av filteret i $\mathcal{L}_1$ adaptiv reguleringsformuleringen gir store forbedringer med hensyn til ytelse. Resultatene av denne teksten viser hvordan $\mathcal{L}_1$ adaptiv regulatoren klarer å skille adapsjonen fra reguleringen og dermed kan introdusere rask adapsjon uten å resultere i tilbakekobling med stor forsterkning (high gain feedback). Denne teksten drøfter også hvordan implementasjonsvansker som begrenset samplingsfrekvens påvirker ytelsen til $\mathcal{L}_1$ adaptiv regulatoren, og viser hvordan dette kan håndteres av et redesign av arkitekturen.

Resultatene av $\mathcal{L}_1$ adaptive regulering for langsgående sløyfen er sammenlignet med en enkel PID-regulator. Vi ser faktisk at PID-regulatoren resulterer i nesten like god regulering som $\mathcal{L}_1$ adaptiv regulatoren for det enkle langsgående systemet.

Contents

List of figures **XI**

Nomenclature **XIII**

Preface **XVII**

1 Introduction **1**
1.1 Background . . . 1
1.2 Historical perspective . . . 1
1.3 Principles of aircraft control . . . 3
1.3.1 Sensors . . . 3
1.3.2 Actuators . . . 3
1.3.3 Automatic control . . . 5
1.3.4 Autopilots . . . 6
1.3.5 Current state of the art in aircraft control . . . 7
1.4 Principles of $\mathcal{L}_1$ adaptive control . . . 9
1.5 Goals of the report . . . 9

2 Aircraft modelling **11**
2.1 Kinematics . . . 11
2.1.1 Reference systems . . . 11
2.1.2 State vector . . . 13
2.1.3 Transformation between BODY and NED . . . 14
2.1.4 Transformation between BODY and WIND axes . . . 15
2.2 Rigid body kinetics . . . 16
2.3 Aerodynamics . . . 18
2.3.1 Forces and moments . . . 18
2.4 Linear models . . . 19
2.4.1 Trimmed flight condition . . . 19
2.4.2 Linearisation of the kinetics . . . 20
2.4.3 Linearisation of the aerodynamic forces and moments . . . 22
2.4.4 Aerodynamic control . . . 26
2.4.5 Thrust . . . 27

2.4.6 Total models . . . 29
2.4.7 Dimensionless aerodynamic coefficients . . . 30
2.4.8 Simplifications and change of states . . . 30
2.5 F-16 model . . . 31

3 Theory of $\mathcal{L}_1$ adaptive control **33**
3.1 Main theoretical results for systems with unknown constant parameters. . . . 34
3.2 SISO systems with matched unknown parameters and disturbance, and uncertain system input gain . . . 35
3.2.1 Problem formulation . . . 35
3.2.2 Limitations in the problem formulation . . . 36
3.2.3 Model Reference Adaptive Control with state predictor . . . 38
3.2.4 Why $\mathcal{L}_1$ adaptive control? . . . 41
3.2.5 $\mathcal{L}_1$ adaptive control architecture . . . 41
3.2.6 Theoretical results . . . 43
3.3 Design challenges: Trade-off between robustness and performance . . . 46
3.4 SISO systems with matched nonlinear uncertainties . . . 48
3.4.1 Problem formulation . . . 48
3.4.2 Limitations in the problem formulation . . . 49
3.4.3 $\mathcal{L}_1$ adaptive control architecture . . . 50
3.4.4 Theoretical results . . . 52
3.5 MIMO systems with unmatched nonlinear uncertainties . . . 56
3.5.1 Problem formulation . . . 56
3.5.2 $\mathcal{L}_1$ adaptive control architecture . . . 58
3.5.3 Theoretical results . . . 62
3.6 Systems with unmodeled actuator dynamics . . . 65
3.6.1 Problem formulation . . . 65
3.6.2 Control architecture . . . 66

4 Simulation results and discussion **69**
4.1 Simulation values . . . 69
4.2 $\mathcal{L}_1$ adaptive control design for the longitudinal system . . . 71
4.2.1 Design of the feedback gain K_m . . . 72
4.2.2 Specifying the projection bounds . . . 73
4.2.3 Designing the filter $C(s)$ . . . 76
4.2.4 Choosing the adaptation gain Γ . . . 78
4.3 Simulation results and discussion for the longitudinal system . . . 79
4.3.1 Design system . . . 80
4.3.2 Simulation case 1 . . . 83
4.3.3 Simulation case 2 . . . 88
4.3.4 MRAC control of simulation case 2 . . . 93
4.3.5 Discussion . . . 98
4.4 $\mathcal{L}_1$ adaptive control design for the lateral system . . . 101
4.4.1 Design of the feedback gain K_m . . . 101
4.4.2 Specifying the projection bounds . . . 104

4.4.3 Designing the filter $C(s)$ . . . 106
4.4.4 Choosing the adaptation gain Γ . . . 109
4.5 Simulation results and discussion for the lateral system . . . 110
4.5.1 Design system . . . 110
4.5.2 Simulation case 1 . . . 113
4.5.3 Simulation case 2 . . . 118
4.5.4 Discussion . . . 123
4.6 Alternative control . . . 125
4.6.1 PID control design . . . 125
4.6.2 Simulations . . . 126
4.6.3 Discussion . . . 130
4.7 Simulation of the nonlinear F-16 model . . . 131
4.7.1 Simulations . . . 131
4.7.2 Discussion . . . 133
4.8 Implementation issues and assumptions made . . . 135
4.8.1 Control redesign for limited sampling rate . . . 135
4.8.2 Simulation with limited sample rate . . . 137
4.8.3 Discussion . . . 141

5 Conclusion **143**
5.1 Future work . . . 144

Bibliography **147**

A Simulink diagrams **149**

List of Figures

1.1 Aircraft with control surfaces, from [9]. 4
1.2 Aircraft response to control surfaces, from [9]. 4
1.3 Feedback control system. 5
1.4 Adaptive control system. 6
1.5 Aircraft control system. 7
1.6 Controller with gain scheduling. 8

2.1 Illustration showing the states of an aircraft. 13
2.2 Body fixed coordinate systems. 14

3.1 Closed loop MRAC architecture with state predictor, from [22]. 40
3.2 L1 adaptive control architecture, from [22]. 44

4.1 Bode plot of $\frac{y}{r}(s) = \mathbf{C}\left(s\mathbb{I}_n - \left(\mathbf{A}_{id} - \mathbf{B}_{id}F(s)K_m\right)\right)^{-1} k_g \mathbf{B}_{id}F(s)$ 74
4.2 $\mathcal{L}_1$-norm condition as a function of k. 77
4.3 Control input, case 2, with k = 150, and reference r_1. 78
4.4 Bode plot of $C(s)$ 79
4.5 System output in the case of no modelling error. 81
4.6 Control input in the case of no modelling error. 81
4.7 System states in the case of no modelling error. 82
4.8 System output of the $\mathcal{L}_1$ adaptive controlled longitudinal system, for simulation case 1. 84
4.9 L1 adaptive control input to the longitudinal system, for simulation case 1. . . 84
4.10 Adaptive estimates for the $\mathcal{L}_1$ adaptive controlled longitudinal system, for simulation case 1. 85
4.11 Real and predicted states of the $\mathcal{L}_1$ adaptive controlled longitudinal system, for simulation case 1. 86
4.12 System output of the $\mathcal{L}_1$ adaptive controlled longitudinal system, for simulation case 1, without adaptation. 87
4.13 System output of the $\mathcal{L}_1$ adaptive controlled longitudinal system, for simulation case 2. 89
4.14 $\mathcal{L}_1$ adaptive control input to the longitudinal system, for simulation case 2. . . 89

4.15 Adaptive estimates for the $\mathcal{L}_1$ adaptive controlled longitudinal system, for simulation case 2. 90
4.16 Predicted and real system states of the $\mathcal{L}_1$ adaptive controlled longitudinal system, for simulation case 2. 91
4.17 System output of the $\mathcal{L}_1$ adaptive controlled longitudinal system, for simulation case 2, without adaptation. 92
4.18 MRAC controlled system output of simulation case 2. 95
4.19 MRAC control input of simulation case 2. 95
4.20 Adaptive estimates for MRAC controlled system, simulation case 2. 96
4.21 MRAC controlled system states of simulation case 2. 97
4.22 Bode plot of $\frac{y}{r}(s) = \mathbf{C}\left(s\mathbb{I}_n - (\mathbf{A}_{id} - \mathbf{B}_{id}F(s)K_m)\right)^{-1} k_g \mathbf{B}_{id}F(s)$ 103
4.23 $\mathcal{L}_1$-norm condition as a function of k. 107
4.24 Simulation of case 1 with $K = \mathbb{I}_m 12.5$, and reference r_1. 108
4.25 System output of simulation case 2, with $K = \mathbb{I}_m 12.5$, and reference r_1. 108
4.26 Bode plot of $C(s)$. 109
4.27 System output in the case of no modelling error. 111
4.28 Control input in the case of no modelling error. 111
4.29 System states in the case of no modelling error. 112
4.30 System output of the $\mathcal{L}_1$ adaptive controlled lateral system, for simulation case 1. 114
4.31 Control input to the $\mathcal{L}_1$ adaptive controlled lateral system, for simulation case 1. 114
4.32 Adaptive estimates for the $\mathcal{L}_1$ adaptive controlled lateral system, for simulation case 1. 115
4.33 Predicted and real system states of the $\mathcal{L}_1$ adaptive controlled lateral system, for simulation case 1. 116
4.34 System output of the $\mathcal{L}_1$ adaptive controlled lateral system, for simulation case 1, without adaptation. 117
4.35 System output of the $\mathcal{L}_1$ adaptive controlled lateral system, for simulation case 2. 119
4.36 Control input to the $\mathcal{L}_1$ adaptive controlled lateral system, for simulation case 2. 119
4.37 Adaptive estimates for the $\mathcal{L}_1$ adaptive controlled lateral system, for simulation case 2. 120
4.38 Predicted and real system states of the $\mathcal{L}_1$ adaptive controlled lateral system, for simulation case 2. 121
4.39 System output of the $\mathcal{L}_1$ adaptive controlled lateral system, for simulation case 2, without adaptation. 122
4.40 PID-controlled longitudinal system output, with no modelling error. 127
4.41 PID control input to the longitudinal system, with no modelling error. 127
4.42 System output of the PID-controlled longitudinal system, for simulation case 1. 128
4.43 Control input to the PID-controlled longitudinal system, for simulation case 1. 128
4.44 System output of the PID-controlled longitudinal system, for simulation case 2. 129
4.45 Control input to the PID-controlled longitudinal system, for simulation case 2. 129
4.46 Simulation of the nonlinear F-16 model, with $\mathcal{L}_1$ adaptive controlled pitch. . . 132

4.47 Simulation of the nonlinear F-16 model, with $\mathcal{L}_1$ adaptive controlled pitch, without adaptation. 133
4.48 Simulation of the nonlinear F-16 model, with PID controlled pitch. 134
4.49 Simulation of the original $\mathcal{L}_1$ adaptive control design for simulation case 2 of the longitudinal system, with a limited sample rate of 20 Hz. 138
4.50 System output of the $\mathcal{L}_1$ adaptive controlled longitudinal system, for simulation case 2, with limited sampling rate and reference r_1. 138
4.51 Control input to the $\mathcal{L}_1$ adaptive controlled longitudinal system, for simulation case 2, with limited sampling rate and reference r_1. 139
4.52 Adaptive estimates of the $\mathcal{L}_1$ adaptive controlled longitudinal system, for simulation case 2, with limited sampling rate and reference r_1. 139
4.53 Predicted and real system states of the $\mathcal{L}_1$ adaptive controlled longitudinal system, for simulation case 2, with limited sampling rate and reference r_1. . . 140

A.1 Simulink implementation of the $\mathcal{L}_1$ adaptive control structure. 149
A.2 Simulink implementation of controller. 150
A.3 Simulink implementation of the state predictor. 150
A.4 Simulink implementation of the adaptive law. 151
A.5 Simulink implementation of the state predictor with limited sampling rate. . 151
A.6 Simulink implementation of the adaptive law with limited sampling rate. . . 151

Nomenclature

A	Aspect ratio
$\mathbf{A}$	State matrix
$\mathbf{A}_m$	Hurwitz state matrix
b	Wing span
$\mathbf{B}$	Input matrix
$\bar{c}$	Chord
C	Low-pass filter
$\mathbf{C}$	Output matrix
C_D	Drag coefficient
C_{D_0}	Zero lift drag coefficient
C_l	Rolling moment coefficient
C_L	Lift coefficient
C_m	Pitching moment coefficient
C_{m_α}	Slope of $C_m - \alpha$ plot
C_n	Yawing moment coefficient
C_x	Axial force coefficient
C_y	Lateral force coefficient
C_z	Normal force coefficient
$\mathbf{C}_{RB}$	Rigid body Coriolis matrix
D	Drag, filter
e	Oswald efficiency factor
g	Acceleration due to gravity
I_{xx}	Moment of inertia in roll
I_{yy}	Moment of inertia in pitch
I_{zz}	Moment of inertia in yaw
$\mathbf{I}$	Identity matrix
$\mathbf{I_{CG}}$	Inertia matrix about center of gravity
I_{xy}	Product of inertia about x^b and y^b axes
I_{xz}	Product of inertia about x^b and z^b axes
I_{yz}	Product of inertia about y^b and y^b axes
$\mathbf{K}$	Feedback gain matrix
$\mathbf{K}_g$	Feed forward gain matrix
$\mathbf{K}_m$	Feedback gain matrix

l_{ref}	Reference length, equal wing mean aerodynamic chord
L	Lift: Rolling moment
L_α	Lift due to incidence
m	Mass
M	Pitching moment
$\mathbf{M}_{RB}$	Rigid body inertia matrix
N	Yawing moment
ΔP	Roll rate perturbation
P	Roll rate, matrix solving the Lyapunov equation
ΔQ	Pitch rate perturbation
Q	Pitch rate
ΔR	Yaw rate perturbation
R	Yaw rate
$\mathbf{R}$	Rotation matrix
S	Wing area
S_{ref}	Wing reference area
$\mathbf{S}$	Skew-symmetric matrix
$\mathcal{T}$	Time delay margin
T_s	Sampling time
$\mathbf{u}$	Input vector
u	Axial velocity perturbation, control input
U	Total axial velocity
U_0	Axial component of steady equilibrium velocity
v	Lateral velocity perturbation
V	Total lateral velocity, Lyapunov function candidate
V_0	Lateral component of steady equilibrium velocity
V_T	Total speed
V_{T0}	Total steady equilibrium speed
w	Normal velocity perturbation
W	Total normal velocity
W_0	Normal component of steady equilibrium velocity
x	Longitudinal coordinate in axis system
$\mathbf{x}$	State vector
X	Axial force component
y	Lateral coordinate in axis system
$\mathbf{y}$	Output vector
Y	Lateral force component
z	Normal coordinate in axis system
Z	Normal force component

Greek letter

α	Angle of attack
β	Side-slip angle
$Gamma$	Adaptation gain

δ	Control input
Δ	Convex compact set
$\boldsymbol{\eta}$	Position and attitude vector
θ	Pitch angle perturbation
$\boldsymbol{\theta}$	Unknown parameter
$\hat{\boldsymbol{\theta}}$	Adaptive estimate
Θ	Euler pitch angle
$\boldsymbol{\Theta}$	Vector of euler angles
$\boldsymbol{\nu}$	Vector of speeds and rates
ρ	Density
σ	Unmodelled disturbance
$\hat{\sigma}$	Adaptive estimate
$\boldsymbol{\tau}$	Vector of forces and moments
$\boldsymbol{\tau}_0$	Equilibrium forces and moments
$\boldsymbol{\tau}_{RB}$	Vector of rigid body forces and moments
ϕ	Roll angle perturbation
Φ	Euler roll angle
ψ	Yaw angle perturbation
ψ_m	Phase margin
Ψ	Euler yaw angle
ω	Input gain
Ω	Convex set
$\hat{\omega}$	Adaptive estimate
$\omega_g c$	Gain crossover frequency

Subscripts

0	Equilibrium value, initial value
a	Aerodynamic
A	Aileron
c	Control
D	Drag
E	Elevator
g	Gravitational
id	Ideal, identified
l	Roll moment, lower
lat	Lateral
$long$	Longitudinal
L	Lift
m	Pitch moment, desired, matched
n	Yaw moment
p	Roll rate
q	Pitch rate
r	Yaw rate
R	Rudder

T	Thrust
u	Axial velocity perturbation, upper
um	Unmatched
v	Lateral velocity perturbation
w	Normal velocity perturbation
x	Axial
y	Lateral

α	Angle of attack
$\dot{\alpha}$	Angle of attack rate
δ	Control input

Superscripts

b	BODY reference frame
n	NED reference frame
T	Transpose
w	WIND reference frame

Preface

This text presents the work done in my master's thesis in the spring 2012 at NTNU. The general goal was to get a good understanding of the newly developed theory of $\mathcal{L}_1$ adaptive control. Similar to the way the theory is presented in the text, this understanding was achieved through a step by step expanding of the problem formulation. For each of the problem formulations considered I implemented the architecture in Simulink and simulated it on the computer. In this way I got a good insight to the control architectures. In this text however, only the final control architecture is presented. This is obviously the most interesting architecture to consider since it handles all the earlier problem formulations. After finishing this report I feel I have a good understanding of the $\mathcal{L}_1$ adaptive control theory and can definitely see the advantages of this formulation. Further I feel have a much better understanding of the theory of aircraft control in general and the challenges of this control field.

I would like to thank my supervisor Tor Arne Johansen for the help and the constructive feedback throughout this work. I would also like to thank Åge Skullestad for the help and motivation throughout this work. Finally, I would like to thank my lovely wife Ida Pernille Holhjem for her patient and support when I spent most of the time at school.

Chapter 1

Introduction

1.1 Background

This master's thesis is written in collaboration with Kongsberg Defence System (KDS). The work done in this text is a continuation of the work done in my project report [1]. The project report concerned modelling of an RC-plane and developing an $\mathcal{L}_1$ adaptive controller for the pitch of this aircraft. The system considered included constant matched parameter uncertainty, and the control goal was to design an $\mathcal{L}_1$ adaptive controller who compensated for the modelling error and produced a desired response. This master thesis takes the principles of $\mathcal{L}_1$ adaptive control further to include unmatched uncertainties for multi-variable nonlinear systems, and unmodeled actuator dynamics. The models considered in this master thesis is obtained from a nonlinear F-16 model implemented in Simulink and Matlab. This model is developed at the University of Minnesota and introduced in section 2.5.

1.2 Historical perspective

Ever since man invented the float regulator to keep track of time in the antiquity, automatic control systems have been used to make life easier. Together with the industrial revolution around 1750, new self-driven machines was invented, and the need for automatic control of for instance temperature, pressure and liquid level was introduced. Now, we use automatic controllers in our everyday life without even thinking about it. Examples of this are the thermostat of our coffee machine, the ABS-brakes in our car or the water system in our WC. The developments within control theory have made us able to achieve things not before possible, and made lot of processes more cost efficient.

In aviation, automatic control also plays an important role. Ever since the Wright brothers had the world's first controlled, powered flight in December 1903, the goals for flying faster, higher, longer, and making more and more challenging manoeuvres has demanded new and better control systems. In addition, safety plays an important role, which demands

robust and polite control systems. In 1912 the Sperry Gyroscope Company developed the first aircraft autopilot, and by 1914 the "Sperry Aeroplane Stabilizer" was so good that a public flying demonstration was given where the mechanic was walking along the wing while the pilot raised his hands from the controls [2]. The principles of these first autopilots where simple. A gyroscope was used as the reference for the plane's orientation, and any offset detected from the desired heading was fed back to the control surfaces to counter the error. More on the principles of gyroscopes in section 1.3.1. World War I (1914-1918) led to great improvements in aircraft design. The planes designed at this time however, was designed so that the pilots was capable of controlling the planes without the help of automatic control systems. Thus, the developments within automatic control at this time was not that great.

In the 1930s, automatic control was mostly practically-oriented without many theoretical tools, and the design methods consisted mostly of "trial and error" [3]. Further, the developments within automatic control was divided between different disciplines that had little or no communication between them. This prevented a unified theoretical foundation for automatic control. Similar to World War I, World War II also led to developments within automatic control and aviation. For instance, the developments within servomechanisms for positioning of canons was adapted to control the control surfaces of the aircraft. The war also helped the different disciplines within automatic control meet and create a universal vocabulary and a unified fundamental theory. One slowly moved away from the "trial and error" methods, and towards theoretical research based on mathematics. The developments of computers made it possible to make calculations much faster than before, and made the theoretical analysis easier. In October 1947, the American rocket-powered X-1 became the first manned aircraft to brake the sound barrier. At this time automatic control was well established as a discipline, while interest in adaptive control grew significantly in the mid-1950s [4].

The design of autopilots for high-performance aircraft was one of the primary motivations for active research on adaptive control in the early 1950s [5]. However, a crash of the X-15 test vehicle on November 15, 1967 [6], which was partially because of the adaptive system, gave adaptive flight control a bad reputation [7]. The work on adaptive control continued mostly in other disciplines and it would take about two decades before problems associated with adaptive control were reasonably well understood and adaptive techniques were finding use in industry [4]. The interest for adaptive flight control reappeared in the new century. The first result on $\mathcal{L}_1$ adaptive control, which is inspired by flight control, was presented in [8] in 2006. Since then, a large number of flight tests have been performed, showing great promise for the $\mathcal{L}_1$ adaptive control theory [7]. However, since the 1960s, lot of research has been performed on other areas of automatic control, and led to the flight control systems most commonly used today. Only time will tell if $\mathcal{L}_1$ adaptive control becomes an alternative to the current state of the art.

1.3 Principles of aircraft control

As a background to the theory presented in this text, this section presents the basic principles of aircraft control.

1.3.1 Sensors

To be able to control anything, we need information about the state of the controlled object. This is in itself a separate field of study and is not a focus of this master thesis. In this master thesis, it is assumed that more or less correct measurements of the states is provided, but how this is achieved is ignored. However, to give an understanding of how these measurements can be achieved, a short general introduction to the different sensors is given in this section.

The choices of sensors depend highly on the considered system, and which states we need information about. In aircraft control, common states we need information about are the attitude, rate of rotation, velocity and position. Common sensors used on aircraft are accelerometers and gyroscopes. An accelerometer is a sensor which senses proper acceleration. These measurements are fed to a computer which based on the previous known speed, can calculate the new speed. This principle is called dead reckoning. This can again be used to calculate position and orientation. The gyroscope measures the orientation. It consists of a fast spinning rotor, which due to the principles of angular momentum wants to keep its initial attitude. Thus, as this rotor continues to spin in its initial plane, we can measure the orientation of the aircraft relative to this. These measurements are combined with the measurements from the accelerometers to calculate the orientation and rotation rates. The combination of the accelerometers, the gyroscopes, and the computer calculating the desired states are called an inertial measurement unit, or IMU.

To get the position of the aircraft, it is also common to use a GPS. This gives the absolute position of the aircraft based on measuring the distance to 3 or more satellites. To find the altitude of aircraft it is common to use measurements of the air pressure. The lower the air pressure, the higher the altitude.

1.3.2 Actuators

To be able to control the orientation of the aircraft, one need actuators or control surfaces to apply the desired forces on the aircraft. This section gives a short introduction to the control surfaces used on the aircraft considered in the text, and an intuitive explanation on how they affect the aircraft.

Figure 1.1 shows an aircraft with its main control surfaces. These are the ailerons, which are mainly used to get a roll motion, the elevator which are mainly used to get a pitching motion, and the rudder, which are mainly used to get a yaw motion.

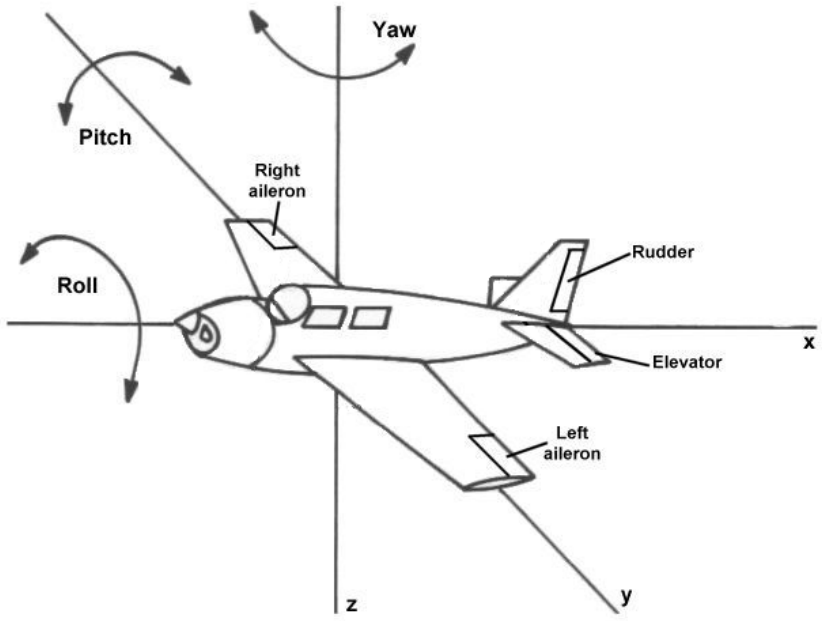

Figure 1.1: Aircraft with control surfaces, from [9].

The right and left aileron moves in opposite directions to create a rolling motion. If for instance the left aileron moves up and the right moves down (see the upper left picture in figure 1.2), the left wing get less lift while the right wing gets more lift. Thus, a moment is induced, forcing the aircraft to roll to the left.

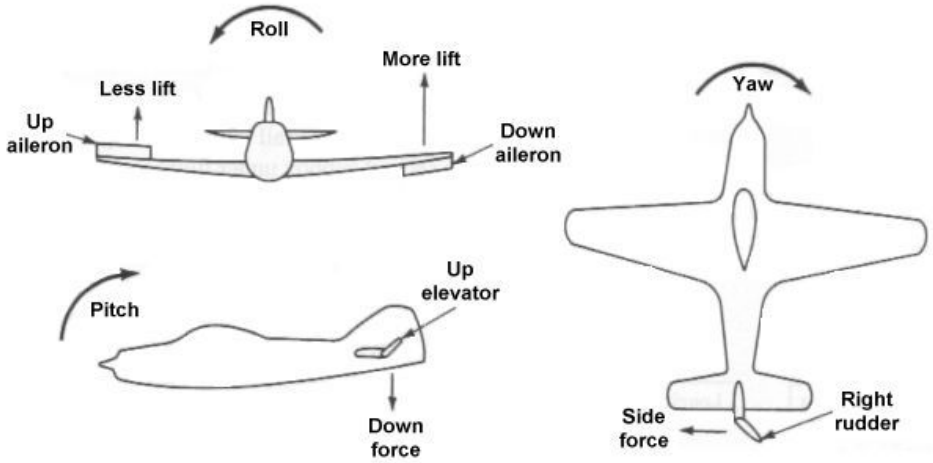

Figure 1.2: Aircraft response to control surfaces, from [9].

The elevator is mainly used to create a pitching motion. If the elevator is moved upwards, a down force is created, and equivalently if the elevator is moved downwards, a force is created upwards (see the bottom left picture in figure 1.2). Since the elevator is located behind the center of gravity, we have a moment arm, and a pitching motion is induced.

The rudder is mainly used to create a yaw motion. Just like the elevator, the force created by the deflection in the rudder together with the moment arm creates a moment which makes the aircraft turn in a yawing motion (see the picture to the right in figure 1.2).

1.3.3 Automatic control

As mentioned, this text concerns the newly developed $\mathcal{L}_1$ adaptive control of aircraft. To understand this control strategy, it is important to have a good understanding of automatic feedback control in general, and the principles of adaptive control. This section thus introduces the basic principles of automatic feedback control and adaptive control.

Principles of feedback control

Figure 1.3 shows the principal components of a feedback control system. In all control systems, we have a controller. This is typically implemented in a computer. This controller gives an output to the actuators which affects the system in the desired way. On an aircraft, these actuators are typically the control surfaces described in section 1.3.2. The controller also needs to know something about the state of the system. Typical states of an aircraft includes velocity, attitude and position. Without this, it would be very difficult to know what the right control would be. This information is given by the measurement sensors available. On an aircraft, these are typically the ones described in section 1.3.1. These measurements are feed back to the controller through the feedback connection. The controller also takes a reference as an input which includes information about the desired output of the system. The reference is compared to the measurements and based on the error between reference and measurements, new actions from the controller are produced.

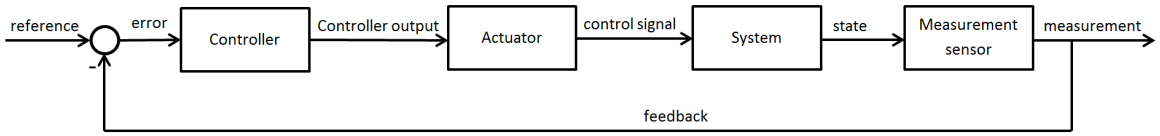

Figure 1.3: Feedback control system.

To be able to get the best possible control result, good information about the system response is important. That is, the response of the states, to the output from the controller. This can be expressed mathematically by a differential equation. Let $\mathbf{x}$ be the states of the system, $\mathbf{u}$ be the controller output and t be the time. Then the relationship between the states and the input can be expressed as

$$\dot{\mathbf{x}} = f(\mathbf{x}, \mathbf{u}, t), \tag{1.1}$$

where $f(\cdot)$ is an arbitrary function mapping $\mathbf{x}$, $\mathbf{u}$ and t to $\dot{\mathbf{x}}$. The difficulty lies in identifying the function $f(\cdot)$. Chapter 2 concerns the modelling of aircraft. When a good model is obtained, this can be used to simulate the feedback control system on a computer. Thus, we are able to test the controller without the need to implement it on the real system. If

the model is a good approximation of the real system, one would expect to get a similar responce on the real system as in the simulation. The mathematical model can also be used directly in the design of the controller to give the desired response.

Principles of adaptive control

As described, an important part of the control design is to identify the controlled system. However, it is impossible to develop models who incorporate all the dynamics of the real system. Systems may also include highly nonlinear dynamics. This may imply that a mathematical model describes the system well for some combination of states, while it gives a completely wrong dynamic response in a different combination of states. This effect is true for aircraft. As described, the way we control an aircraft is by moving the control surfaces. The desired forces is obtained by changing the flow of the air around the aircraft. Thus, it is easy to understand that the forces acting on the aircraft is highly dependent on the speed relative to the air. The difficulty appear since this dependency in nonlinear. Thus, one single controller based on linear theory, soon to be introduced, can not be used for the entire flight envelope. The flight also experience nonlinear dependencies to air pressure and different flight conditions. This is where the adaptive controller has its strengths. The controller can be designed for a single flight condition, and adapt to the changes in the system on-line.

Figure 1.4 shows the basic components of an adaptive control system. It uses the control signal together with the system output to change the control-parameters based on an adaptive law. Thus, as the system dynamics change, the controller adapt to this change, to give the best possible control.

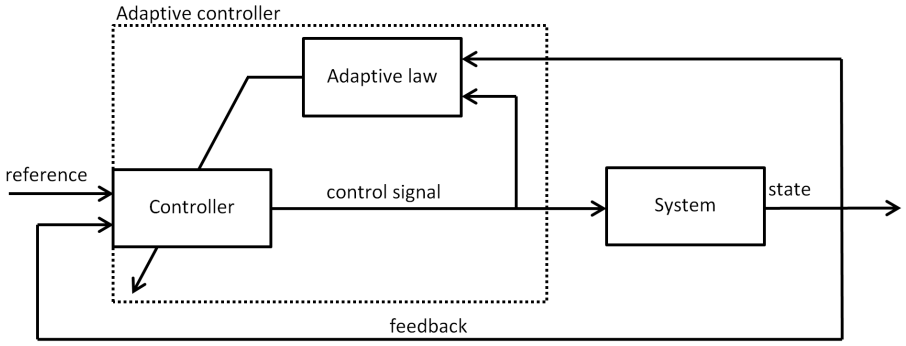

Figure 1.4: Adaptive control system.

1.3.4 Autopilots

Figure 1.3 shows a general feedback control loop. When considering aircraft control, it is common to separate the controller in an inner and an outer control loop. The inner control loop typically controls the actuators to achieve a given attitude reference, while the outer control loop specifies the desired attitude references based on desired waypoints or desired manoeuvres. A simple example of an outer loop controller is an altitude controller. If the

measured altitude is lower than the desired altitude, the outer reference controller would demand a larger pitch angle from the inner loop controller, and visa versa. The outer loop can also be replaced by the pilot who directly through the steering, demands a given response of the aircraft.

The principles of this separation in shown in figure 1.5. Further it is common to decouple the control of the inner loop between the so called longitudinal and lateral modes. This decoupling is explained in more detail in chapter 2, but in simple words we design one controller to control the pitch angle, the longitudinal controller, and one controller to control the roll and yaw angles, the lateral controller. This is also shown in figure 1.5. It is in these inner loops we experience the nonlinear aerodynamic effects, and thus it is here it is relevant to implement the $\mathcal{L}_1$ adaptive control law. Therefore, these inner loop controllers are the focus of this text. In this text we will test how well the inner loops react to given references, but the logic behind these reference signals is not a concern in this text.

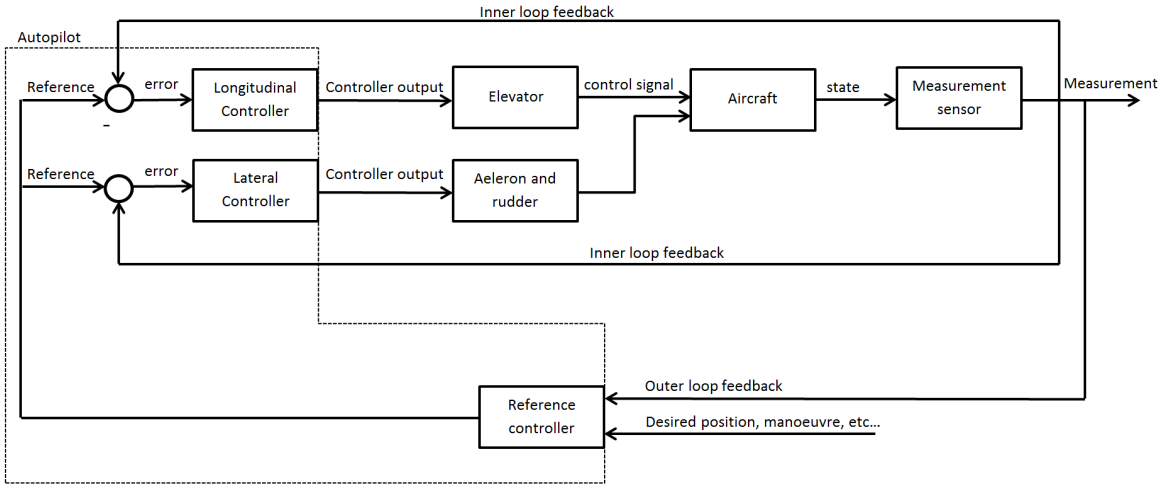

Figure 1.5: Aircraft control system.

1.3.5 Current state of the art in aircraft control

As discussed, we know that since the dynamics of the aircraft is changing nonlinearly dependent of the altitude speed and flight condition, it is advantageous with a controller that can adapt to this changes. However, as mentioned in section 1.2 research on automatic flight control since the crash of X-15 has mostly been on other areas than adaptive control. And apparently, as we can see, these control systems seem to work pretty well. This section introduces the concepts of the current state of the art within aircraft control, and discusses the pros and cons of these techniques.

Linear design with gain scheduling

The state of the art within aircraft control can mostly be divided between two main categories: linear control design with gain scheduling [10], and nonlinear control design. Most

aircraft control systems used today are based on linear system design in combination with gain scheduling [2]. With this strategy, the aircraft dynamics are linearised at given operating points and flight conditions, that is, different combination of states and manoeuvres. Then, different linear controllers are designed for each of these modes. A gain scheduler changes between the different controllers based on auxiliary measurements. Figure 1.6 shows the structure of a gain scheduled controller.

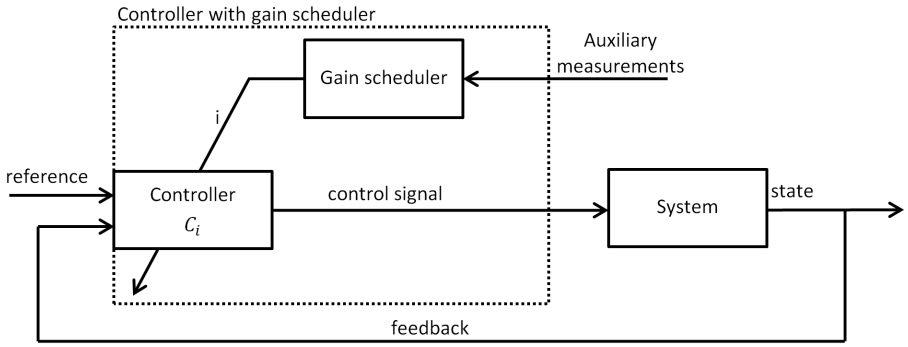

Figure 1.6: Controller with gain scheduling.

The advantage to gain scheduling is that one can use linear control theory for nonlinear systems. Linear control are a well established field and consists a lot of design techniques including PID-control [11], pole-placement [12] and LQG/LQR [2] [13] [14]. Further, the stability analysis is easily performed for linear systems. A different advantage is that scheduler can change between the different controllers quickly, and thus respond to the changing environment fast. However, frequent and rapid changes of the controllers may lead to instability, and thus there is a limit to how often and how fast the changes can be performed [5].

One disadvantage of gain scheduling is that it takes a lot of time to develop the controller. One have to identify and linearise the system for all the different combinations of states and manoeuvres the aircraft can encounter, and design and analyse the controller for all these cases. Thus, the implementation of a gain scheduled controller is costly. Also, compared to an adaptive system, the control strategy and controller gains are computed off-line. Thus, there are no feedback in the control loop to compensate for incorrect schedules. Unpredictable changes in the system dynamics may lead to deterioration or even to complete failure [5].

Nonlinear design

Nonlinear control strategies are based on the complete nonlinear model of the system, and the goal is to make one universal controller which is valid for all the flight conditions. Examples of such control strategies are sliding mode control [10] [14], backstepping [10] [14], passivity-based control[10] and nonlinear MPC [13]. Feedback-linearisation [10] [14] is also an important nonlinear control strategy. The strategy involves inverting the nonlinearities of the real system through feedback, such that the resulting systems becomes linear. Thus, one may design the controller using classical linear design strategies.

Developing good nonlinear mathematical models is a difficult and time consuming process. Also, as mentioned, it is almost impossible to find models who incorporate all the dynamics of a system. Thus, nonlinear control strategies who are based on mathematical models will not perform as good in practice as in theory. If the mathematical model is used directly in the control design, as with feedback-linearisation or nonlinear MPC, the modelling errors may cause performance degradation or even instability. A different problem with nonlinear controllers are that the implementation involves intensive on-line computations due to the complex models. If the computations can not be performed fast enough the control will lag behind and be useless in a real implementation.

1.4 Principles of $\mathcal{L}_1$ adaptive control

Since we already have plenty of well working control strategies for aircraft, one may ask oneself why we need a new control strategy for this purpose. However, as discussed in the previous section, the current state of the art have different limitations and challenges. This chapter has also argued for the need of an adaptive controller due to the changing system dynamics. However, the different adaptive controllers designed up until now, have not been able to prove robustness a priori. Further, the tuning of adaptive systems represents a great challenge and has mostly relied on heavy Monte Carlo simulations or trial-and-error methods. Up until now this has largely remained an open question in the literature [7]. This is where the $\mathcal{L}_1$ adaptive control theory finds its strength, by decoupling adaptation from robustness, and proving robustness in the presence of fast adaptation. The authors of [7] promise:

> "The architectures of $\mathcal{L}_1$ adaptive control theory have guaranteed transient performance and guaranteed robustness in the presence of fast adaptation, without introducing or enforcing persistence of excitation, without any gain scheduling in the controller parameters, and without resorting to high-gain feedback. (...) These features of $\mathcal{L}_1$ adaptive control theory were verified-consistently with theory-in a large number of flight tests and mid- to high-fidelity simulation environments."

1.5 Goals of the report

The journey from the the sketch board to a finished fully automatic aircraft includes plenty of steps. Before we even start thinking about any control system, choices about the material, the shape of the aircraft, control surfaces and much more has to be made. All of these choices affects the system we are to control. Further, as have been discussed, proper measurement tools need to be designed and implemented to get the desired feedback information. All these issues are important for the resulting aircraft, and are in them selves separate fields of study.

In this text, the focus is on the design of the inner loop control systems for the longitudinal and the lateral modes. The controllers are to be designed based on a given system, while the design of the system, the aircraft, is of no concern. Further, we assume full state measurements without considering the design of the IMU. The goal of this text is to investigate and get a good understanding of the newly developed $\mathcal{L}_1$ adaptive control theory. The goal is to achieve a control strategy with an associated problem formulation which puts as few limitations to the considered systems as possible. This is achieved by the final problem formulation considered in this text, considering MIMO systems with unmatched nonlinear uncertainties and unmodeled actuator dynamics.

Further, the goal of this text is to design and simulate an $\mathcal{L}_1$ adaptive controller for the longitudinal and the lateral modes of an F-16 model. As opposed to the current state of the art presented in section 1.3.5, we want to design a single $\mathcal{L}_1$ adaptive controller based on one linearised model for the longitudinal and the lateral modes of the F-16 model, which is able to handle all the changing dynamics during a flight, on-line. The results are to be compared with the simulation results of a basic PID-controller. Further, the goal is to investigate and test the $\mathcal{L}_1$ adaptive control theory with regards to realistic implementation issues, with special focus on the issue of limited sampling rate.

Since the goal is to base the $\mathcal{L}_1$ adaptive controller on a linear aircraft model, the linear aircraft modelling theory is of interest. This is covered in chapter 2. This chapter is mainly based on the project report [1], with some corrections.

Chapter 2

Aircraft modelling

As discussed, system modelling is an important part of the control design process. This chapter presents the theory of aircraft modelling, and results in the final linear models considered in the remainder of the text. To be able to identify the different parameters, wind tunnel tests are needed. Since this identification is not the focus of this thesis, the numerical values for the aircraft model considered obtained from a nonlinear F-16 model, implemented in Matlab. This model is developed at the University of Minnesota, and further introduced in section 2.5. The theory presented in this chapter is mainly based on [15], [2] ,[16], [17], [18] and [19].

This chapter is mostly taken from my project report [1] with some minor corrections. An important change is however done in this text due to the formulation in the nonlinear model, namely the choice of states. I refer to section 2.4.8 for a discussion on this topic.

2.1 Kinematics

Classical mechanics are usually divided in two branches: kinematics and kinetics. Kinematics is the branch which studies the motion of bodies without considering the forces acting on them. This section concerns the kinematics for aircraft.

2.1.1 Reference systems

When deriving the equations of motion of the aircraft, well defined reference systems are required. This section explains the different reference systems used in the remainder of the text.

NED

The North-East-Down (NED) reference system (x^n, y^n, z^n) is located at the surface of the earth. x^n points toward the north pole, y^n points toward east and z^n downward. The aircraft considered in this text only travels within a radius of a couple of hundred meters. Thus the surface of the earth can be assumed flat, and therefore the NED reference frame is assumed inertial such that Newton's laws apply.

BODY

The BODY reference system (x^b, y^b, z^b) is fixed to the aircraft. The position of the aircraft is expressed relative to the NED frame, while the attitude of the aircraft is expressed as the orientation of the aircraft BODY axis system relative to the NED frame.

The origin of the BODY reference system is located in the lift center of the aircraft. Since the lift center is not a static point in the aircraft, we have assumed its location to middle of the aircraft at one fourth of the mean aerodynamic chord(MAC) of the aircraft wings, measured from the leading edge of the wing. For more information about this assumption see [15] and [2]. This point on the wing is called the aerodynamic center or the quarter chord of the wing. The MAC is defined as $\bar{c} = \frac{S}{b}$, where S is the wing area and b is the wing span.

x^b is pointing forward in the aircraft, y^b pointing out of the right wing and z^b downward out of the belly of the aircraft. See figure 2.1 for an illustration of the BODY axis.

Wind axes

It is the movement of the air around the aircraft that creates the aerodynamic forces and moments. The WIND axes system is a body-fixed reference system that aligns with the movement of the aircraft relative to the air, see figure 2.2. In aerodynamics it is normal to calculate everything in the WIND axes system. In figure 2.2 from [16], we can find α and β, corresponding to the angle of attack and the side-slip angle respectively.

Angle of attack and side-slip angle are defined as:

$$\tan(\alpha) = \frac{W}{U} \tag{2.1}$$

$$\sin(\beta) = \frac{V}{V_T} \tag{2.2}$$

and V_T is the length of the velocity vector i.e:

$$V_T = \sqrt{U^2 + V^2 + W^2} \tag{2.3}$$

The WIND axes is later used to calculate the linear models of the aircraft motion.

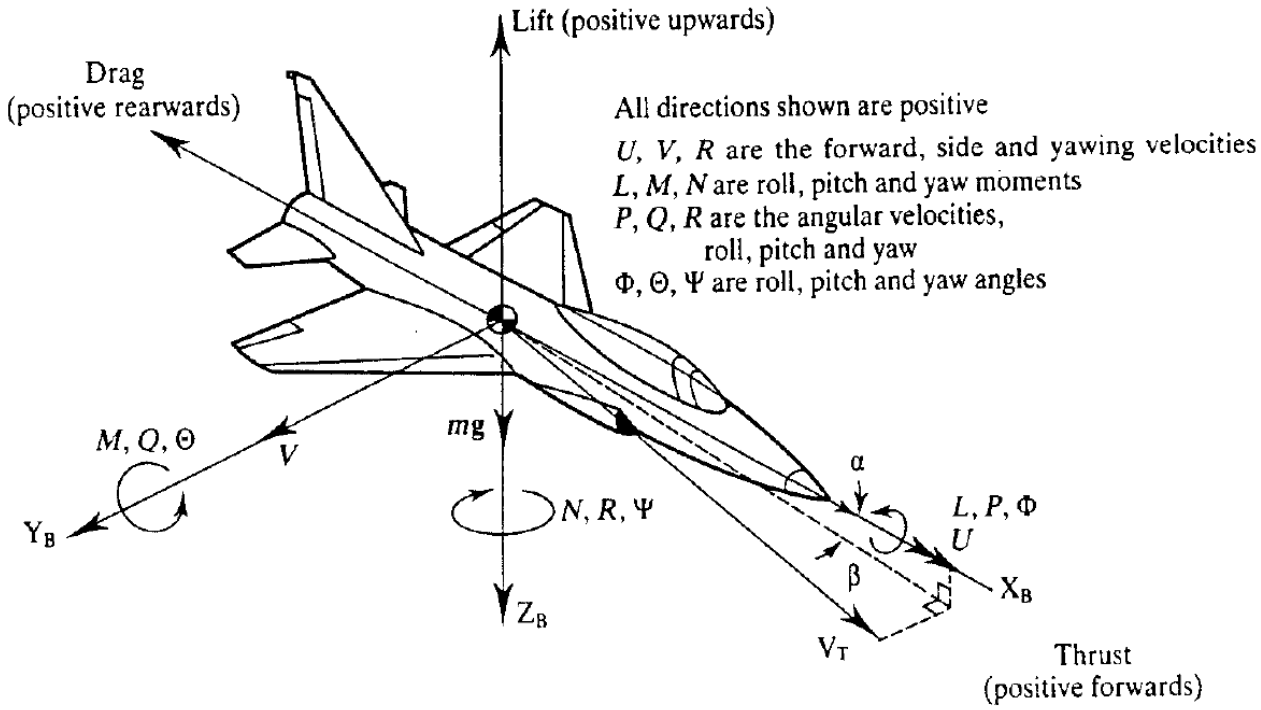

Figure 2.1: Illustration showing the states of an aircraft.

2.1.2 State vector

Before stating the equations of motions it is useful to define the state vectors.

The position and orientation vector, $\boldsymbol{\eta}$, for a body, {b}, relative to the NED frame is defined as

$$\boldsymbol{\eta} := \begin{bmatrix} x^n \\ y^n \\ z^n, -h \\ \Phi_{nb} \\ \Theta_{nb} \\ \Psi_{nb} \end{bmatrix} = \begin{bmatrix} \text{north} \\ \text{east} \\ \text{down} \\ \text{roll} \\ \text{pitch} \\ \text{yaw} \end{bmatrix}$$

The velocity vector, $\boldsymbol{\nu}$, in a general body reference frame is defined as (see figure 2.1):

$$\boldsymbol{\nu} := \begin{bmatrix} U \\ V \\ W \\ P \\ Q \\ R \end{bmatrix} = \begin{bmatrix} \text{axial velocity} \\ \text{lateral velocity} \\ \text{normal velocity} \\ \text{roll rate} \\ \text{pitch rate} \\ \text{yaw rate} \end{bmatrix}$$

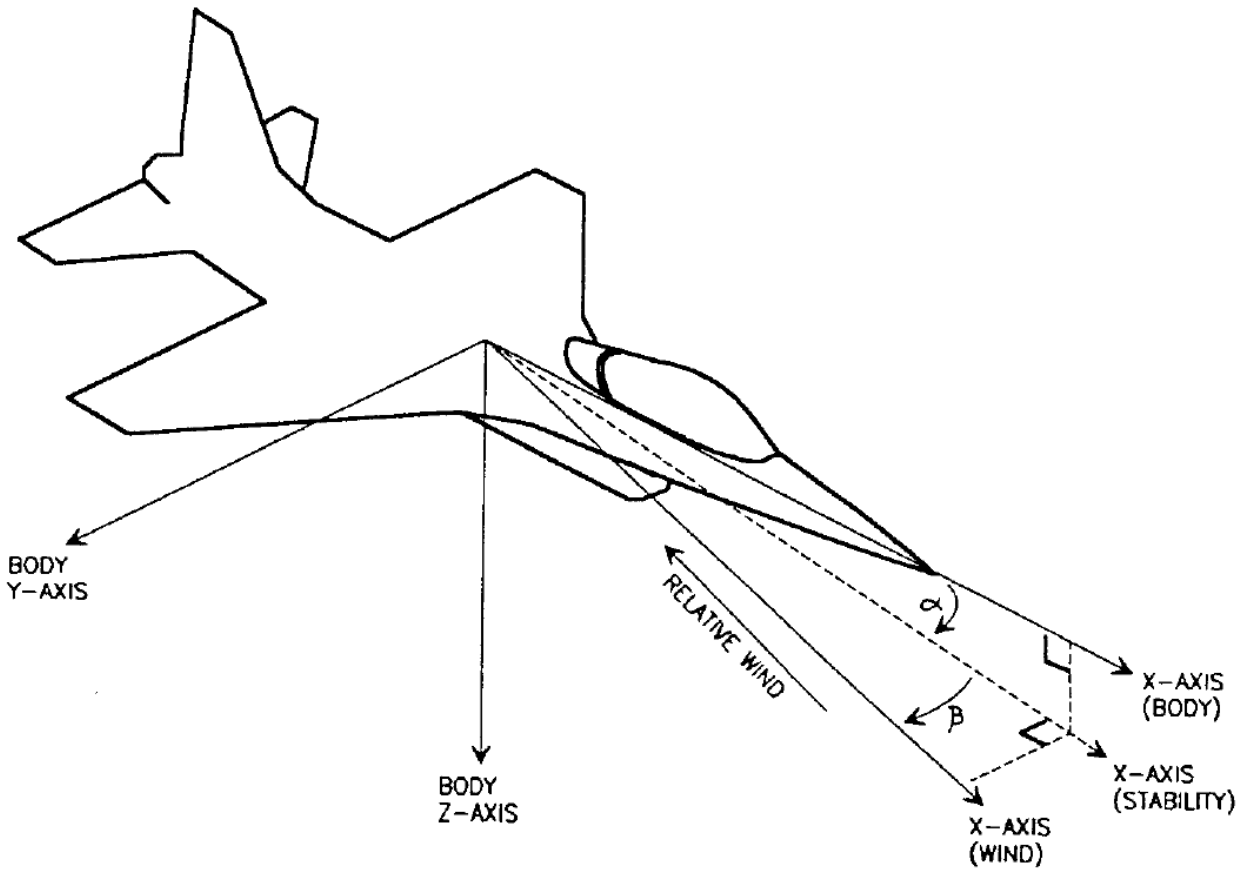

Figure 2.2: Body fixed coordinate systems.

The force and moment vector, $\boldsymbol{\tau}$, in a general body reference frame is defined as (see figure 2.1):

$$\boldsymbol{\tau} := \begin{bmatrix} X \\ Y \\ Z \\ L \\ M \\ N \end{bmatrix} = \begin{bmatrix} \text{axial force} \\ \text{lateral force} \\ \text{normal force} \\ \text{roll moment} \\ \text{pitching moment} \\ \text{yawing moment} \end{bmatrix}$$

We now relate the different reference frames to each other, which are used to calculate attitude.

2.1.3 Transformation between BODY and NED

The relationship between a vector, $\mathbf{p}^n$, in NED and a vector, $\mathbf{p}^b$, in BODY is given by:

$$\mathbf{p}^n = \mathbf{R}_b^n \mathbf{p}^b$$

where $\mathbf{R}_b^n$ is the Euler angle rotation matrix from BODY to NED, and given by:

$$\mathbf{R}_b^n = \begin{bmatrix} c\Psi_{nb}c\Theta_{nb} & -s\Psi_{nb}c\Phi_{nb} + c\Psi_{nb}s\Theta_{nb}s\Phi_{nb} & s\Psi_{nb}s\Phi_{nb} + c\Psi_{nb}c\Phi_{nb}s\Theta_{nb} \\ s\Psi_{nb}c\Theta_{nb} & c\Psi_{nb}c\Phi_{nb} + s\Psi_{nb}s\Theta_{nb}s\Phi_{nb} & -c\Psi_{nb}s\Phi_{nb} + s\Psi_{nb}c\Phi_{nb}s\Theta_{nb} \\ -s\Theta_{nb} & c\Theta_{nb}s\Phi_{nb} & c\Theta_{nb}c\Phi_{nb} \end{bmatrix}$$

where $s\cdot = \sin(\cdot)$ and $c\cdot = \cos(\cdot)$.

This gives the relationship between the translation motion in BODY and NED:

$$\begin{bmatrix} \dot{x}^n \\ \dot{y}^n \\ \dot{z}^n \end{bmatrix} = \mathbf{R}_b^n \begin{bmatrix} U^b \\ V^b \\ W^b \end{bmatrix}$$

For rotation motion, the relationship between BODY and NED is given by

$$\begin{bmatrix} \dot{\Phi}_{nb} \\ \dot{\Theta}_{nb} \\ \dot{\Psi}_{nb} \end{bmatrix} = \begin{bmatrix} 1 & s\Phi_{nb}t\Theta_{nb} & c\Phi_{nb}t\Theta_{nb} \\ 0 & c\Phi_{nb} & -s\Phi_{nb} \\ 0 & s\Phi_{nb}/c\Theta_{nb} & c\Phi_{nb}/c\Theta_{nb} \end{bmatrix} \begin{bmatrix} P^b \\ Q^b \\ R^b \end{bmatrix}$$

where $t\cdot = \tan(\cdot)$.

2.1.4 Transformation between BODY and WIND axes

The relationship between a vector, $\mathbf{p}^w$, in the WIND axes and a vector, $\mathbf{p}^b$, in BODY is given by:

$$\mathbf{p}^w = \mathbf{R}_b^w \mathbf{p}^b$$

where $\mathbf{R}_b^w$ is the rotation matrix from BODY to WIND axes, and given by:

$$\mathbf{R}_b^w = \begin{bmatrix} c\alpha c\beta & s\beta & s\alpha c\beta \\ -c\alpha s\beta & c\beta & -s\alpha s\beta \\ -s\alpha & 0 & c\alpha \end{bmatrix}$$

This gives the relationship between the velocity, $[U^b, V^b, W^b]^T$ in BODY and the velocity, $\mathbf{v}^w$ in the WIND axes:

$$\begin{bmatrix} U \\ V \\ W \end{bmatrix} = (\mathbf{R}_b^w)^T \mathbf{v}^w = (\mathbf{R}_b^w)^T \begin{bmatrix} V_T \\ 0 \\ 0 \end{bmatrix} = \begin{bmatrix} V_T \cos\alpha\cos\beta \\ V_T \sin\beta \\ V_T \sin\alpha\cos\beta \end{bmatrix}$$

Thus,

$$\begin{aligned} U^b &= V_T \cos\alpha\cos\beta \\ V^b &= V_T \sin\beta \\ W^b &= V_T \sin\alpha\cos\beta \end{aligned} \tag{2.4}$$

2.2 Rigid body kinetics

The derivation of the equations of motions for a general body starts with Euler's first and second axioms:

$$\frac{^n\mathrm{d}}{\mathrm{d}t}\overrightarrow{p}_b = \overrightarrow{f}_b \qquad \overrightarrow{p}_b = m\overrightarrow{v}_{nb} \tag{2.5}$$

$$\frac{^n\mathrm{d}}{\mathrm{d}t}\overrightarrow{h}_b = \overrightarrow{m}_b \qquad \overrightarrow{h}_b = I_{cg}\overrightarrow{\omega}_{nb} \tag{2.6}$$

where $\overrightarrow{f}_b$ and $\overrightarrow{m}_b$ are the forces and moments acting on the body's center of gravity, $\overrightarrow{\omega}_{nb}$ is the angular velocity of the body with respect to NED. $^n\mathrm{d}/\mathrm{d}t$ means the time differentiation in the NED frame.
Following the derivation in [14], the aircraft rigid body kinetics can be expressed as

$$m(\dot{\boldsymbol{\nu}}_{\mathbf{1}} + \mathbf{S}(\boldsymbol{\nu}_{\mathbf{2}})\boldsymbol{\nu}_{\mathbf{1}}) = \boldsymbol{\tau}_1 \tag{2.7}$$

$$\mathbf{I_{CG}}\dot{\boldsymbol{\nu}}_{\mathbf{2}} - \mathbf{S}(\mathbf{I_{CG}}\boldsymbol{\nu}_{\mathbf{2}})\boldsymbol{\nu}_{\mathbf{2}} = \boldsymbol{\tau}_{\mathbf{2}} \tag{2.8}$$

where $\boldsymbol{\nu}_{\mathbf{1}} = [U, V, W]^T$, $\boldsymbol{\nu}_{\mathbf{2}} = [P, Q, R]^T$, $\boldsymbol{\tau}_{\mathbf{1}} = [X, Y, Z]^T$, $\boldsymbol{\tau}_{\mathbf{2}} = [L, M, N]^T$ and $\mathbf{S}$ is a skew symmetric matrix. The resulting 6 degree of freedom(DOF) model is written

$$\mathbf{M}_{RB}\dot{\boldsymbol{\nu}} + \mathbf{C}_{RB}\boldsymbol{\nu} = \boldsymbol{\tau}_{RB} \tag{2.9}$$

where

$$\mathbf{M}_{RB} = \begin{bmatrix} m\mathbf{I}_{3x3} & \mathbf{0}_{3x3} \\ \mathbf{0}_{3x3} & \mathbf{I_{CG}} \end{bmatrix} \tag{2.10}$$

is the rigid body inertia matrix, and

$$\mathbf{C}_{RB} = \begin{bmatrix} m\mathbf{S}(\boldsymbol{\nu}_{\mathbf{2}}) & \mathbf{0}_{3x3} \\ \mathbf{0}_{3x3} & -\mathbf{S}(\mathbf{I_{CG}}\boldsymbol{\nu}_{\mathbf{2}}) \end{bmatrix} \tag{2.11}$$

In these equations it is assumed that the body reference system is located at the center of gravity. In our model, this is not the case (see section 2.1.1). The arm between center of gravity and the coordinate origin is small, thus the resulting error is small. The equations could be corrected by introducing the transformation matrix, but for simplicity and since the error will be small, we assume the origin of the body reference system to be at center of gravity when deriving the rigid body kinetics.

Assuming xz-plane symmetry ($I_{xy} = I_{yz} = 0$) the inertia matrix is defined

$$\mathbf{I_{CG}} := \begin{bmatrix} I_{xx} & 0 & -I_{xz} \\ 0 & I_{yy} & 0 \\ I_{xz} & 0 & I_{zz} \end{bmatrix} \tag{2.12}$$

where I_{xx}, I_{yy} and I_{zz} are the moments of inertia about the body x, y and z axes, and I_{xz} is the product of inertia defined as

$$\begin{aligned} I_{xx} &:= \int_V (y^2 + z^2)\rho_m \mathrm{d}V \\ I_{yy} &:= \int_V (x^2 + z^2)\rho_m \mathrm{d}V \\ I_{zz} &:= \int_V (x^2 + y^2)\rho_m \mathrm{d}V \\ I_{xz} &:= \int_V (xz)\rho_m \mathrm{d}V \end{aligned}$$

The forces and moments acting on the body can be expressed as

$$\boldsymbol{\tau}_{RB} = -\mathbf{g}(\boldsymbol{\eta}) + \boldsymbol{\tau} \tag{2.13}$$

where $\boldsymbol{\tau}$ includes the aerodynamic, control and propulsion forces and moments defined as

$$\boldsymbol{\tau} := \boldsymbol{\tau}_a + \boldsymbol{\tau}_c + \boldsymbol{\tau}_p, \tag{2.14}$$

and $\mathbf{g}(\boldsymbol{\eta})$ is the force of gravity. The gravity force is given in the body reference frame by

$$\mathbf{g}(\boldsymbol{\eta}) = (\mathbf{R}_b^n)^T \begin{bmatrix} 0 \\ 0 \\ mg \\ 0 \\ 0 \\ 0 \end{bmatrix} = \begin{bmatrix} mg\sin(\Theta) \\ -mg\cos(\Theta)\sin(\Phi) \\ -mg\cos(\Theta)\cos(\Phi) \\ 0 \\ 0 \\ 0 \end{bmatrix} \tag{2.15}$$

The 6-DOF model can now be written in matrix form:

$$\mathbf{M}_{RB}\dot{\boldsymbol{\nu}} + \mathbf{C}_{RB}\boldsymbol{\nu} + \mathbf{g}(\boldsymbol{\eta}) = \boldsymbol{\tau} \tag{2.16}$$

or in component form as in [17]:

$$\begin{aligned} m(\dot{U} + QW - RV + g\sin(\Theta)) &= X \\ m(\dot{V} + UR - WP - g\cos(\Theta)\sin(\Phi)) &= Y \\ m(\dot{W} + VP - QU - g\cos(\Theta)\cos(\Phi)) &= Z \\ I_{xx}\dot{P} - I_{xz}(\dot{R} + PQ) + (I_{zz} - I_{yy})QR &= L \\ I_{yy}\dot{Q} - I_{xz}(P^2 - R^2) + (I_{xx} - I_{zz})PR &= M \\ I_{zz}\dot{R} - I_{xz}\dot{P} + (I_{yy} - I_{xx})PQ + I_{zz}QR &= N \end{aligned} \tag{2.17}$$

In the next chapter we will derive the aerodynamic forces and moments. These forces and moments are derived in the WIND axes. To be able to combine the equations of motion with the aerodynamics, the equations of motion need to be derived for the WIND axes, or the aerodynamic forces need to be rotated to the BODY axes through $\mathbf{R}_b^w$.

In this text the models will be expressed in the WIND axes. Since the equations in (2.17) are derived for a general body, they still hold for the WIND axes. In the remainder of the text all the forces, moments and velocities will be in the WIND axes. Thus we make the following definition for the rest of the text:

$$\boldsymbol{\nu} = \begin{bmatrix} U \\ V \\ W \\ P \\ Q \\ R \end{bmatrix} := \begin{bmatrix} U^w \\ V^w \\ W^w \\ P^w \\ Q^w \\ R^w \end{bmatrix} \tag{2.18}$$

$$\boldsymbol{\tau} = \begin{bmatrix} X \\ Y \\ Z \\ L \\ M \\ N \end{bmatrix} := \begin{bmatrix} X^w \\ Y^w \\ Z^w \\ L^w \\ M^w \\ N^w \end{bmatrix} \tag{2.19}$$

2.3 Aerodynamics

In this section we will make a short introduction to aerodynamics. We will define the aerodynamic forces and moments.

2.3.1 Forces and moments

The aerodynamic forces and moments are usually written as a product of dynamic pressure $\frac{1}{2}\rho V_T^2$, reference area S_{ref} and/or reference length l_{ref} and dimensionless coefficients C. The reference area is usually the wing area and the reference length is almost always the wing mean aerodynamic chord (MAC) [15]. The only unknowns are the dimensionless coefficients which are nonlinear functions of the velocity, the rates and the attitude. These can not be found analytically, but are normally estimated by wind tunnel testing, physical experiments, approximated calculation etc. Due to nonlinearities, these coefficients are difficult to compute correctly. The aerodynamic forces and moments can be written as [20]

$$\begin{bmatrix} -X \\ Y \\ -Z \\ L \\ M \\ N \end{bmatrix} = \begin{bmatrix} Drag \\ Sideforce \\ Lift \\ Roll\ moment \\ Pitch\ moment \\ Yaw\ moment \end{bmatrix} = \frac{1}{2}\rho V_T^2 S_{ref} \begin{bmatrix} C_D \\ C_y \\ C_L \\ C_l l_{ref} \\ C_m l_{ref} \\ C_n l_{ref} \end{bmatrix}$$

where the coefficients are for drag, side force, lift, roll-, pitch- and yaw moment respectively. Further, the coefficients can be split into contribution from control surfaces, rates, speeds

and so forth. The most dominating contributions are [18]

$$
\begin{aligned}
C_D &= C_{D_0} + \frac{C_L^2}{\pi e A} + C_{D_u} u + C_{D_{\delta_E}} \delta_E \\
C_L &= C_{L_0} + C_{L_\alpha} \alpha \ + C_{L_u} u + C_{L_{\delta_E}} \delta_E \\
C_y &= C_{y_0} + C_{y_\beta} \beta \ + C_{y_{\delta_R}} \delta_R \\
C_l &= C_{l_0} + C_{l_\beta} \beta + C_{l_p} p + C_{l_r} r + C_{l_{\delta_R}} \delta_R + C_{l_{\delta_A}} \delta_A \\
C_m &= C_{m_0} + C_{m_u} u + C_{m_\alpha} \alpha + C_{m_{\dot{\alpha}}} \dot{\alpha} + C_{m_q} q + C_{m_{\delta_E}} \delta_E \\
C_n &= C_{n_0} + C_{n_\beta} \beta + C_{n_p} p + C_{n_r} r + C_{n_{\delta_R}} \delta_R + C_{n_{\delta_A}} \delta_A
\end{aligned}
$$

Where A is the aspect ratio of the wings, and e is Oswald's efficiency factor. The coefficients will be affected by several other factors, but the effects above are the ones we have taken into account.

We have used the following notation for the coefficients, given a force/moment a and a state b: C_{a_b} is change in coefficient C_a due to change in b, that is $C_{a_b} = \frac{\delta C_a}{\delta b}$, where b could be velocities, rates, angle of attack, side-slip angle etc.

2.4 Linear models

This section concerns the derivations of the linear models used in the remainder of the text. The starting point for this linearisation is the results from section 2.2 and 2.3. The linearisation of the kinetics follows the derivations in [17], while the linearisation of the aerodynamic forces and moments, aerodynamic control and thrust follows the derivations in [15]. Further, the constant dimensionless coefficients for our given case are found together with the final system matrices.

2.4.1 Trimmed flight condition

An aircraft is said to be in trim if it is in a steady state, that is the moments are balanced and the forces are constant. There are several steady states, but in this text only one is considered, namely the steady straight flight condition. Steady straight flight is when a aircraft keeps its attitude and altitude constant. Thus, the lift must equal the weight, and the thrust must equal the drag. Further, the control surfaces must be trimmed for the specific altitude and speed such that the moments are zero. The forces and moments acting on the aircraft are thus

$$
\begin{aligned}
X_0 &= -mg \sin(\Theta) \\
Y_0 &= mg \cos(\Theta) \sin(\Phi) \\
Z_0 &= mg \cos(\Theta) \cos(\Phi) \\
L_0 &= M_0 = N_0 = 0
\end{aligned}
$$

We are later going to linearise for these equilibrium forces and moments. For symmetric flight we have a roll angle equal to zero, and we get

$$\begin{aligned} X_0 &= -mg\sin(\Theta) \\ Y_0 &= 0 \\ Z_0 &= mg\cos(\Theta) \\ L_0 &= M_0 = N_0 = 0 \end{aligned}$$

See [16] and [2] for more information.

2.4.2 Linearisation of the kinetics

The states are linearised about the trimmed flight conditions. The trimmed flight condition of interest is described in section 2.4.1. The states are written as a sum of a nominal value and a perturbation:

Total state = nominal value + perturbed state

This gives the following definitions:

$$\boldsymbol{\tau} := \boldsymbol{\tau_0} + \delta\boldsymbol{\tau} = \begin{bmatrix} X_0 \\ Y_0 \\ Z_0 \\ L_0 \\ M_0 \\ N_0 \end{bmatrix} + \begin{bmatrix} \delta X \\ \delta Y \\ \delta Z \\ \delta L \\ \delta M \\ \delta N \end{bmatrix} \tag{2.20}$$

$$\boldsymbol{\nu} := \boldsymbol{\nu_0} + \delta\boldsymbol{\nu} = \begin{bmatrix} U_0 \\ V_0 \\ W_0 \\ P_0 \\ Q_0 \\ R_0 \end{bmatrix} + \begin{bmatrix} u \\ v \\ w \\ p \\ q \\ r \end{bmatrix} \tag{2.21}$$

$$\begin{bmatrix} \Phi \\ \Theta \\ \Psi \end{bmatrix} := \begin{bmatrix} \Phi_0 \\ \Theta_0 \\ \Psi_0 \end{bmatrix} + \begin{bmatrix} \phi \\ \theta \\ \psi \end{bmatrix} \tag{2.22}$$

Expressing the forces and moments, velocities and angles as defined above in (2.16), the aircraft's equilibrium point ($\dot{\boldsymbol{\nu}} = 0$) will satisfy:

$$\mathbf{C}_{RB}(\boldsymbol{\nu_0})\boldsymbol{\nu_0} + \mathbf{g}(\boldsymbol{\eta_0}) = \boldsymbol{\tau_0} \tag{2.23}$$

or on component form:

$$\begin{aligned} m(Q_0W_0 - R_0V_0 + g\sin(\Theta_0)) &= X_0 \\ m(U_0R_0 - P_0W_0 - g\cos(\Theta_0)\sin(\Phi_0)) &= Y_0 \\ m(P_0V_0 - Q_0U_0 - g\cos(\Theta_0)\cos(\Phi_0)) &= Z_0 \\ (I_{zz} - I_{yy})Q_0R_0 - P_0Q_0I_{xz} &= L_0 \\ (P_0^2 - R_0^2)I_{xz} + (I_{xx} - I_{zz})P_0R_0 &= M_0 \\ (I_{yy} - I_{xx})P_0Q_0 + Q_0R_0I_{xz} &= N_0 \end{aligned} \tag{2.24}$$

The linearised equations are found by substituting (2.20), (2.21) and (2.24) into (2.17). By neglecting higher order terms of the perturbed states, setting $\sin(\cdot) = \cdot$ and $\cos(\cdot) = 1$, where $\cdot$ is a perturbed state, and assuming steady straight flight (see section 2.4.1) we get the following linearised 6 DOF equations:

$$\begin{aligned} m(\dot{u} + Q_0w + W_0q - R_0v - V_0r + g\cos(\Theta_0)\theta) &= \delta X \\ m(\dot{v} + U_0r + R_0u - W_0p - P_0w - g\cos(\Theta_0)\cos(\Phi_0)\phi + g\sin(\Theta_0)\sin(\Phi_0)\theta) &= \delta Y \\ m(\dot{w} + V_0p + P_0v - U_0q - Q_0u + g\cos(\Theta_0)\sin(\Phi_0)\phi + g\sin(\Theta_0)\cos(\Phi_0)\theta) &= \delta Z \\ I_{xx}\dot{p} - I_{xz}\dot{r} + (I_{zz} - I_{yy})(Q_0r + R_0q) - I_{xz}(P_0q + Q_0p) &= \delta L \\ I_{yy}\dot{q} + (I_{xx} - I_{zz})(P_0r + R_0p) - 2I_{xz}(R_0r + P_0p) &= \delta M \\ I_{zz}\dot{r} - I_{xz}\dot{p} + (I_{yy} - I_{xx})(P_0q + Q_0p) + I_{xz}(Q_0r + R_0q) &= \delta N \end{aligned} \tag{2.25}$$

Where the forces/moments consist of aerodynamic forces/moments, control forces/moments and propulsion forces/moments:

$$\begin{aligned} \delta X &= X_a + X_c + X_p \\ \delta Y &= Y_a + Y_c + Y_p \\ \delta Z &= Z_a + Z_c + Z_p \\ \delta L &= L_a + L_c + L_p \\ \delta M &= M_a + M_c + M_p \\ \delta N &= N_a + N_c + N_p \end{aligned} \tag{2.26}$$

For aircrafts it is common to decouple the 6 DOF model in two 3 DOF models, longitudinal and lateral. The main assumptions are that the aircraft's body is much longer than its height and width, and that the forward velocity is much larger than the vertical and transverse velocity. For our aircraft, these assumptions hold quite good. In the longitudinal model, only the the states u, w, q and θ are considered, while the states v, p, r and ϕ is assumed negligible. For the lateral model the opposite assumptions are made. This gives the following equations:

Longitudinal model

$$\begin{aligned} m(\dot{u} + Q_0w + W_0q + g\cos(\Theta_0)\theta) &= \delta X \\ m(\dot{w} - U_0q - Q_0u + g\sin(\Theta_0)\cos(\Phi_0)\theta) &= \delta Z \\ I_{yy}\dot{q} &= \delta M \\ \dot{\theta} &= q \end{aligned}$$

In trim the rates are zero, and the downward equilibrium velocity is zero in WIND, $Q_0 = W_0 = 0$. The equilibrium pitch angle is also zero in WIND $\Theta_0 = 0$, because we are in trim and we are flying parallel to the earth. For steady straight flight the equilibrium roll angle $\Phi_0 = 0$. Inserting these values in the equations above, and solving for $\dot{u}$, $\dot{w}$, $\dot{q}$ and $\dot{\theta}$ gives:

$$\dot{u} = \frac{\delta X}{m} - g\theta \tag{2.27}$$

$$\dot{w} = \frac{\delta Z}{m} + U_0 q \tag{2.28}$$

$$\dot{q} = \frac{\delta M}{I_{yy}} \tag{2.29}$$

$$\dot{\theta} = q \tag{2.30}$$

Lateral model

$$\begin{aligned} m(\dot{v} + U_0 r - W_0 p - g\cos(\Theta_0)\cos(\Phi_0)\phi) &= \delta Y \\ I_{xx}\dot{p} - I_{xz}\dot{r} + (I_{zz} - I_{yy})Q_0 r - I_{xz}Q_0 p &= \delta L \\ I_{zz}\dot{r} - I_{xz}\dot{p} + (I_{yy} - I_{xx})Q_0 p + I_{xz}Q_0 r &= \delta N \\ \dot{\phi} &= p \end{aligned}$$

In trim we have zero equilibrium pitch rate and zero downward equilibrium velocity in WIND, $Q_0 = W_0 = 0$. As above $\Theta_0 = \Phi_0 = 0$ for trim. Inserting these value in the equations above, and solving for $\dot{p}$ and $\dot{r}$, we get:

$$\dot{v} = \frac{\delta Y}{m} - U_0 r + g\phi \tag{2.31}$$

$$\dot{p} = \left(\frac{\delta L}{I_{xx}} + \frac{\delta N}{I_{zz}}\frac{I_{xz}}{I_{xx}}\right)\left(\frac{1}{1 - \frac{I_{xz}^2}{I_{xx}I_{zz}}}\right) \tag{2.32}$$

$$\dot{r} = \left(\frac{\delta N}{I_{zz}} + \frac{\delta L}{I_{xx}}\frac{I_{xz}}{I_{xx}}\right)\left(\frac{1}{1 - \frac{I_{xz}^2}{I_{xx}I_{zz}}}\right) \tag{2.33}$$

$$\dot{\phi} = p \tag{2.34}$$

In the following we will assume that $\left(\frac{1}{1-\frac{I_{xz}^2}{I_{xx}I_{zz}}}\right) = 1$, because I_{xz} is small.

2.4.3 Linearisation of the aerodynamic forces and moments

In linear aerodynamic theory it is assumed that the aerodynamic forces and moments are only dependent on perturbation of rates and velocity, and their derivatives. The alignment of the WIND axis system with respect to the body axis system changes as a function of the trim condition. When an aircraft is disturbed from its trim condition, the WIND axis rotate with the airframe and consequently, the perturbed X axis may or may not be parallel to the relative wind while the aircraft motion is being disturbed. For perturbations around

an equilibrium velocity, the aerodynamic derivatives can be expressed as a Taylor series expansion. For example, the aerodynamic term X_a in the axial force may be expressed [15]:

$$\begin{aligned}
X_a = X_{a_0} &+ \left(\frac{\partial X}{\partial u}u + \frac{\partial^2 X}{\partial u^2}\frac{u^2}{2!} + \frac{\partial^3 X}{\partial u^3}\frac{u^3}{3!} + \frac{\partial^4 X}{\partial u^4}\frac{u^4}{4!} + ...\right) \\
&+ \left(\frac{\partial X}{\partial v}v + \frac{\partial^2 X}{\partial v^2}\frac{v^2}{2!} + \frac{\partial^3 X}{\partial v^3}\frac{v^3}{3!} + \frac{\partial^4 X}{\partial v^4}\frac{v^4}{4!} + ...\right) \\
&+ \left(\frac{\partial X}{\partial w}w + \frac{\partial^2 X}{\partial w^2}\frac{w^2}{2!} + \frac{\partial^3 X}{\partial w^3}\frac{w^3}{3!} + \frac{\partial^4 X}{\partial w^4}\frac{w^4}{4!} + ...\right) \\
&+ \left(\frac{\partial X}{\partial p}p + \frac{\partial^2 X}{\partial p^2}\frac{p^2}{2!} + \frac{\partial^3 X}{\partial p^3}\frac{p^3}{3!} + \frac{\partial^4 X}{\partial p^4}\frac{p^4}{4!} + ...\right) \\
&+ \left(\frac{\partial X}{\partial q}q + \frac{\partial^2 X}{\partial q^2}\frac{q^2}{2!} + \frac{\partial^3 X}{\partial q^3}\frac{q^3}{3!} + \frac{\partial^4 X}{\partial q^4}\frac{q^4}{4!} + ...\right) \\
&+ \left(\frac{\partial X}{\partial r}r + \frac{\partial^2 X}{\partial r^2}\frac{r^2}{2!} + \frac{\partial^3 X}{\partial r^3}\frac{r^3}{3!} + \frac{\partial^4 X}{\partial r^4}\frac{r^4}{4!} + ...\right) \\
&+ \left(\frac{\partial X}{\partial \dot{u}}\dot{u} + \frac{\partial^2 X}{\partial \dot{u}^2}\frac{\dot{u}^2}{2!} + \frac{\partial^3 X}{\partial \dot{u}^3}\frac{\dot{u}^3}{3!} + \frac{\partial^4 X}{\partial \dot{u}^4}\frac{\dot{u}^4}{4!} + ...\right) \\
&+ \left(\frac{\partial X}{\partial \dot{v}}\dot{v} + \frac{\partial^2 X}{\partial \dot{v}^2}\frac{\dot{v}^2}{2!} + \frac{\partial^3 X}{\partial \dot{v}^3}\frac{\dot{v}^3}{3!} + \frac{\partial^4 X}{\partial \dot{v}^4}\frac{\dot{v}^4}{4!} + ...\right) \\
&+ \left(\frac{\partial X}{\partial \dot{w}}\dot{w} + \frac{\partial^2 X}{\partial \dot{w}^2}\frac{\dot{w}^2}{2!} + \frac{\partial^3 X}{\partial \dot{w}^3}\frac{\dot{w}^3}{3!} + \frac{\partial^4 X}{\partial \dot{w}^4}\frac{\dot{w}^4}{4!} + ...\right) \\
&+ \left(\frac{\partial X}{\partial \dot{p}}\dot{p} + \frac{\partial^2 X}{\partial \dot{p}^2}\frac{\dot{p}^2}{2!} + \frac{\partial^3 X}{\partial \dot{p}^3}\frac{\dot{p}^3}{3!} + \frac{\partial^4 X}{\partial \dot{p}^4}\frac{\dot{p}^4}{4!} + ...\right) \\
&+ \left(\frac{\partial X}{\partial \dot{q}}\dot{q} + \frac{\partial^2 X}{\partial \dot{q}^2}\frac{\dot{q}^2}{2!} + \frac{\partial^3 X}{\partial \dot{q}^3}\frac{\dot{q}^3}{3!} + \frac{\partial^4 X}{\partial \dot{q}^4}\frac{\dot{q}^4}{4!} + ...\right) \\
&+ \left(\frac{\partial X}{\partial \dot{r}}\dot{r} + \frac{\partial^2 X}{\partial \dot{r}^2}\frac{\dot{r}^2}{2!} + \frac{\partial^3 X}{\partial \dot{r}^3}\frac{\dot{r}^3}{3!} + \frac{\partial^4 X}{\partial \dot{r}^4}\frac{\dot{r}^4}{4!} + ...\right) \\
&+ \text{series terms in higher order derivatives}
\end{aligned} \tag{2.35}$$

where X_{a_0} is a constant aerodynamic force acting on the aircraft.

Since we assume that the aircraft is in trim, the constant aerodynamic force is equal to the constant contribution from the gravity force specified in 2.4.1. Trim also imply that the constant aerodynamic moments are zero. Therefore, the constant aerodynamic forces and moments will be omitted from the derivation, together with the constant contribution from gravity.

We assume that the velocity and rate perturbations are small, such that only the first term in each of the series is significant, and higher order derivatives can be neglected. This simplifies (2.35) to

$$\begin{aligned}
X_a = &\frac{\partial X}{\partial u}u + \frac{\partial X}{\partial v}v + \frac{\partial X}{\partial w}w + \frac{\partial X}{\partial p}p + \frac{\partial X}{\partial q}q + \frac{\partial X}{\partial r}r \\
&+ \frac{\partial X}{\partial \dot{u}}\dot{u} + \frac{\partial X}{\partial \dot{v}}\dot{v} + \frac{\partial X}{\partial \dot{w}}\dot{w} + \frac{\partial X}{\partial \dot{p}}\dot{p} + \frac{\partial X}{\partial \dot{q}}\dot{q} + \frac{\partial X}{\partial \dot{r}}\dot{r}
\end{aligned}$$

In our work we use the American normalized form, which means both sides of the equation is divided by mass/inertia:

$$\begin{aligned}\frac{X_a}{m} = &\frac{\partial X}{\partial u}\frac{u}{m} + \frac{\partial X}{\partial v}\frac{v}{m} + \frac{\partial X}{\partial w}\frac{w}{m} + \frac{\partial X}{\partial p}\frac{p}{m} + \frac{\partial X}{\partial q}\frac{q}{m} + \frac{\partial X}{\partial r}\frac{r}{m} \\ &+ \frac{\partial X}{\partial \dot{u}}\frac{\dot{u}}{m} + \frac{\partial X}{\partial \dot{v}}\frac{\dot{v}}{m} + \frac{\partial X}{\partial \dot{w}}\frac{\dot{w}}{m} + \frac{\partial X}{\partial \dot{p}}\frac{\dot{p}}{m} + \frac{\partial X}{\partial \dot{q}}\frac{\dot{q}}{m} + \frac{\partial X}{\partial \dot{r}}\frac{\dot{r}}{m}\end{aligned}$$

From now on we use the notation

$$X_u = \frac{\partial X}{\partial u}\frac{1}{m}, \tag{2.36}$$

where X_u is called "aerodynamic derivative". This gives the aerodynamic forces and moments a more compact form.

Similar to the axial force, this assumptions can be made for all forces and moments. Expressed by the aerodynamic derivatives, the forces and moments become:

$$\begin{aligned}\frac{X_a}{m} &= X_u u + X_v v + X_w w + X_p p + X_q q + X_r r + X_{\dot{u}}\dot{u} + X_{\dot{v}}\dot{v} + X_{\dot{w}}\dot{w} + X_{\dot{p}}\dot{p} + X_{\dot{q}}\dot{q} + X_{\dot{r}}\dot{r} \\ \frac{Y_a}{m} &= Y_u u + Y_v v + Y_w w + Y_p p + Y_q q + Y_r r + Y_{\dot{u}}\dot{u} + Y_{\dot{v}}\dot{v} + Y_{\dot{w}}\dot{w} + Y_{\dot{p}}\dot{p} + Y_{\dot{q}}\dot{q} + Y_{\dot{r}}\dot{r} \\ \frac{Z_a}{m} &= Z_u u + Z_v v + Z_w w + Z_p p + Z_q q + Z_r r + Z_{\dot{u}}\dot{u} + Z_{\dot{v}}\dot{v} + Z_{\dot{w}}\dot{w} + Z_{\dot{p}}\dot{p} + Z_{\dot{q}}\dot{q} + Z_{\dot{r}}\dot{r} \\ \frac{L_a}{I_{xx}} &= L_u u + L_v v + L_w w + L_p p + L_q q + L_r r + L_{\dot{u}}\dot{u} + L_{\dot{v}}\dot{v} + L_{\dot{w}}\dot{w} + L_{\dot{p}}\dot{p} + L_{\dot{q}}\dot{q} + L_{\dot{r}}\dot{r} \\ \frac{M_a}{I_{yy}} &= M_u u + M_v v + M_w w + M_p p + M_q q + M_r r + M_{\dot{u}}\dot{u} + M_{\dot{v}}\dot{v} + M_{\dot{w}}\dot{w} + M_{\dot{p}}\dot{p} + M_{\dot{q}}\dot{q} + M_{\dot{r}}\dot{r} \\ \frac{N_a}{I_{zz}} &= N_u u + N_v v + N_w w + N_p p + N_q q + N_r r + N_{\dot{u}}\dot{u} + N_{\dot{v}}\dot{v} + N_{\dot{w}}\dot{w} + N_{\dot{p}}\dot{p} + N_{\dot{q}}\dot{q} + N_{\dot{r}}\dot{r}\end{aligned}$$

According to [15] and [16], the following derivatives are negligible $X_{\dot{u}}$, X_q, $X_{\dot{w}}$, $X_{\dot{q}}$, $Z_{\dot{u}}$, $Z_{\dot{w}}$, $Z_{\dot{q}}$, $M_{\dot{u}}$, $M_{\dot{q}}$, $Y_{\dot{u}}$, $Y_{\dot{w}}$, $Y_{\dot{v}}$, Y_p, $Y_{\dot{p}}$, Y_r, $Y_{\dot{r}}$, $L_{\dot{u}}$, $L_{\dot{v}}$, $L_{\dot{p}}$, $L_{\dot{p}}$, $L_{\dot{r}}$, $N_{\dot{u}}$, $N_{\dot{v}}$, $N_{\dot{p}}$, $N_{\dot{q}}$ and $N_{\dot{r}}$.

[15] states that $X_{\dot{w}}$ could give a contribution, but we were unable to find a values for this derivative due to insufficient knowledge about the drag acting on the aircraft. Z_q is negligible according to [16].

As for the kinetics, we decouple the system in a lateral and a longitudinal model, assuming negligibly small aerodynamic coupling derivatives.

Longitudinal

In the longitudinal model, movement is described by the forces in WIND x-axis and z-axis, as well as the moment about the y-axis. The lateral motion is assumed not to affect this

movement. Thus, the aerodynamic forces and moments involving v, p, r and their derivatives are neglected. We get

$$X_v = X_p = X_r = Z_v = Z_p = Z_r = M_v = M_p = M_r = 0$$
$$X_{\dot{v}} = X_{\dot{p}} = X_{\dot{r}} = Z_{\dot{v}} = Z_{\dot{p}} = Z_{\dot{r}} = M_{\dot{v}} = M_{\dot{p}} = M_{\dot{r}} = 0$$

The longitudinal aerodynamic forces and moments are

$$\frac{X_a}{m} = X_u u + X_w w \tag{2.37}$$
$$\frac{Z_a}{m} = Z_u u + Z_w w \tag{2.38}$$
$$\frac{M_a}{I_{yy}} = M_u u + M_w w + M_{\dot{w}} \dot{w} + M_q q \tag{2.39}$$

where

$$X_u = \frac{\rho V_{T0} S_{ref}}{2m}(-C_D - C_{D_u}) \qquad M_u = \frac{\rho V_{T0} S_{ref} l_{ref}}{2I_{yy}}(C_{m_u} + C_m)$$
$$X_w = \frac{\rho V_{T0} S_{ref}}{2m}(C_L - C_{D_\alpha}) \qquad M_w = \frac{\rho V_{T0} S_{ref} l_{ref}}{2I_{yy}} C_{m_\alpha}$$
$$Z_u = \frac{\rho V_{T0} S_{ref}}{2m}(-C_L - C_{L_u}) \qquad M_{\dot{w}} = -\frac{\rho V_{T0} S_{ref} l_{ref}^2}{4I_{yy}} C_{m_{\dot{\alpha}}}$$
$$Z_w = \frac{\rho V_{T0} S_{ref}}{2m}(-C_{L_\alpha} - C_D) \qquad M_q = \frac{\rho V_{T0} S_{ref} l_{ref}^2}{4I_{yy}} C_{m_q}$$

Here, the dimensionless coefficients, C, are constants, identified by for instance wind tunnel tests. More on this topic in section 2.4.7.

Lateral

In the lateral model, movement is described by the force in WIND y-axis as well as the moments about the x-axis and z-axis. The lateral motion is assumed independent of the longitudinal motion. Thus, the aerodynamic forces and moments from u, w, q and their derivatives are neglected in the lateral model. This leads to

$$Y_u = Y_w = Y_q = L_u = L_w = L_q = N_u = N_w = N_q = 0$$
$$Y_{\dot{u}} = L_{\dot{w}} = N_{\dot{w}} = 0$$

We get

$$\frac{Y_a}{m} = Y_v v \tag{2.40}$$
$$\frac{L_a}{I_{xx}} = L_v v + L_p p + L_r r \tag{2.41}$$
$$\frac{N_a}{I_{zz}} = N_v v + N_p p + N_r r \tag{2.42}$$

where

$$Y_v = \frac{\rho V_{T0} S_{ref}}{2m} C_{y_{\delta\beta}} \qquad N_v = \frac{\rho V_{T0} S_{ref} l_{ref}}{2I_{zz}} C_{n_v}$$
$$L_v = \frac{\rho V_{T0} S_{ref} l_{ref}}{2I_{xx}} C_{l_v} \qquad N_p = \frac{\rho V_{T0} S_{ref} l_{ref}^2}{4I_{zz}} C_{n_p}$$
$$L_p = \frac{\rho V_{T0} S_{ref} l_{ref}^2}{4I_{xx}} C_{l_p} \qquad N_r = \frac{\rho V_{T0} S_{ref} l_{ref}^2}{4I_{zz}} C_{n_r}$$
$$L_r = \frac{\rho V_{T0} S_{ref} l_{ref}^2}{4I_{xx}} C_{l_r}$$

Here, the dimensionless coefficients, C, are constants, identified by for instance wind tunnel tests. More on this topic in section 2.4.7.

2.4.4 Aerodynamic control

The aircraft's aerodynamic controls are the elevator, aileron and rudder. The forces and moments created by the control deflections are due to changes in aerodynamic condition of the aircraft. Similar to the aerodynamic derivatives in 2.4.3, we introduce the "aerodynamic control derivatives". The assumptions stated above about the aerodynamic forces and moments apply to the control terms, [15]. Further, according to [15] and [16], aerodynamic derivatives where first or higher order derivatives of the aerodynamic controls are present, are negligible. We continue using American normalized form for the control derivatives and get:

$$\frac{X_c}{m} = X_{\delta_A}\delta_A + X_{\delta_E}\delta_E + X_{\delta_R}\delta_R$$
$$\frac{Y_c}{m} = Y_{\delta_A}\delta_A + Y_{\delta_E}\delta_E + Y_{\delta_R}\delta_R$$
$$\frac{Z_c}{m} = Z_{\delta_A}\delta_A + Z_{\delta_E}\delta_E + Z_{\delta_R}\delta_R$$
$$\frac{L_c}{I_{xx}} = L_{\delta_A}\delta_A + L_{\delta_E}\delta_E + L_{\delta_R}\delta_R$$
$$\frac{M_c}{I_{yy}} = M_{\delta_A}\delta_A + M_{\delta_E}\delta_E + M_{\delta_R}\delta_R$$
$$\frac{N_c}{I_{zz}} = N_{\delta_A}\delta_A + N_{\delta_E}\delta_E + N_{\delta_R}\delta_R$$

Since aileron and rudder do not usually cause longitudinal motion and in addition, due to airframe symmetry, elevator do not cause lateral motion, X_{δ_A}, X_{δ_R}, Y_{δ_A}, X_{δ_E}, Z_{δ_A}, Z_{δ_R}, L_{δ_E}, M_{δ_A}, M_{δ_R}, N_{δ_E} and Z_{δ_E} are zero or negligible. This gives the longitudinal control derivative

model

$$\frac{X_c}{m} = X_{\delta_E}\delta_E \tag{2.43}$$
$$\frac{Z_c}{m} = Z_{\delta_E}\delta_E \tag{2.44}$$
$$\frac{M_c}{m} = M_{\delta_E}\delta_E, \tag{2.45}$$

where

$$X_{\delta_E} = -\frac{\rho V_{T0}^2 S_{ref}}{2m} C_{D_{\delta_E}} \qquad M_{\delta_E} = -\frac{\rho V_{T0}^2 S_{ref} l_{ref}}{2I_{yy}} C_{m_{\delta_E}} \tag{2.46}$$
$$Z_{\delta_E} = -\frac{\rho V_{T0}^2 S_{ref}}{2m} C_{L_{\delta_E}}$$

The lateral control derivative model becomes

$$\frac{Y_c}{m} = Y_{\delta_R}\delta_R \tag{2.47}$$
$$\frac{L_c}{I_{xx}} = L_{\delta_A}\delta_A + L_{\delta_R}\delta_R \tag{2.48}$$
$$\frac{N_c}{I_{xx}} = N_{\delta_A}\delta_A + N_{\delta_R}\delta_R, \tag{2.49}$$

where

$$Y_{\delta_R} = \frac{\rho V_{T0}^2 S_{ref}}{2m} C_{y_{\delta_R}} \qquad N_{\delta_A} = \frac{\rho V_{T0}^2 S_{ref} l_{ref}}{2I_{zz}} C_{n_{\delta_A}}$$
$$L_{\delta_A} = \frac{\rho V_{T0}^2 S_{ref} l_{ref}}{2I_{xx}} C_{l_{\delta_A}} \qquad N_{\delta_R} = \frac{\rho V_{T0}^2 S_{ref} l_{ref}}{2I_{zz}} C_{n_{\delta_R}} \tag{2.50}$$
$$L_{\delta_R} = \frac{\rho V_{T0}^2 S_{ref} l_{ref}}{2I_{xx}} C_{l_{\delta_R}}$$

The dimensionless coefficients, C, in (2.46) and (2.50) are constants, identified by for instance wind tunnel tests. More on this topic in section 2.4.7.

2.4.5 Thrust

In our model we have for simplicity neglected actuator dynamics. The thrust on our aircraft, δ_T, has a value between 0 and 1. We have assumed that the thrust only acts in BODY x-axis, and we need to rotate this to WIND.

The the thrust is not necessarily perfectly aligned level with the center of gravity, and will therefore give a small pitch moment. We have chosen to neglect this effect. We have also for simplicity assumed that the thruster has zero mass. For more information see [16].

The thrust forces in BODY becomes

$$\begin{aligned}
\frac{X_p^b}{m} &= X_{\delta_T}^b \delta_T = \frac{T}{m}\delta_T \\
\frac{Y_p^b}{m} &= \frac{Z_p^b}{m} = \frac{L_p^b}{m} = \frac{M_p^b}{m} = \frac{N_p^b}{m} = 0
\end{aligned}$$

where T is the maximum thrust force from the propeller. The thrust derivatives in WIND becomes

$$\begin{aligned}
\begin{bmatrix} X_{\delta_T} \\ Y_{\delta_T} \\ Z_{\delta_T} \end{bmatrix} &= \mathbf{R}_b^w \begin{bmatrix} X_p^b \\ Y_p^b \\ Z_p^b \end{bmatrix} \\
&= \begin{bmatrix} c\alpha c\beta & s\beta & s\alpha c\beta \\ -c\alpha s\beta & c\beta & -s\alpha s\beta \\ -s\alpha & 0 & c\alpha \end{bmatrix} \begin{bmatrix} \frac{T}{m} \\ 0 \\ 0 \end{bmatrix} \\
&= \begin{bmatrix} \frac{T}{m} c\alpha c\beta \\ -\frac{T}{m} c\alpha s\beta \\ -\frac{T}{m} s\alpha \end{bmatrix} \qquad (2.51) \\
\begin{bmatrix} L_{\delta_T} \\ M_{\delta_T} \\ N_{\delta_T} \end{bmatrix} &= \begin{bmatrix} 0 \\ 0 \\ 0 \end{bmatrix} \qquad (2.52)
\end{aligned}$$

In steady straight flight, $\beta = 0$. This gives the contribution from thrust:

$$\begin{aligned}
\frac{X_p}{m} &= \frac{T}{m}\cos\alpha = X_{\delta_T}\delta_T \\
\frac{Y_p}{m} &= 0 \\
\frac{Z_p}{m} &= -\frac{T}{m}\sin\alpha = Z_{\delta_T}\delta_T \qquad (2.53) \\
\frac{L_p}{m} &= 0 \\
\frac{M_p}{m} &= 0 \\
\frac{N_p}{m} &= 0
\end{aligned}$$

2.4.6 Total models

Longitudinal

The resulting equations for the longitudinal model from (2.27)-(2.30) (2.37)-(2.39), (2.43)-(2.45) and (2.53) are

$$\begin{aligned}
\dot{u} &= X_u u + X_w w - g\theta + X_{\delta_E}\delta_E + X_{\delta_T}\delta_T \\
\dot{w} &= Z_u u + Z_w w + U_0 q + Z_{\delta_E}\delta_E + Z_{\delta_T}\delta_T \\
\dot{q} &= \tilde{M}_u u + \tilde{M}_w w + \tilde{M}_q q + \tilde{M}_{\delta_E}\delta_E \\
\dot{\theta} &= q
\end{aligned}$$

where we have substituted the equation for $\dot{w}$ into $\dot{q}$ and

$$\begin{aligned}
\tilde{M}_u &= M_u + M_{\dot{w}} Z_u & \tilde{M}_q &= M_q + U_0 Z_u \\
\tilde{M}_w &= M_w + M_{\dot{w}} Z_u & \tilde{M}_\Theta &= -g M_w \sin(\Theta_0)\cos(\Phi_0) \\
\tilde{M}_{\delta_E} &= M_{\delta_E} + M_{\dot{w}} Z_{\delta_E}
\end{aligned}$$

$\tilde{M}_\Theta$ is not present in the equations above, since Θ_0 = 0 in WIND. On vector form we have

$$\begin{bmatrix} \dot{u} \\ \dot{w} \\ \dot{q} \\ \dot{\theta} \end{bmatrix} = \begin{bmatrix} X_u & X_w & 0 & -g \\ Z_u & Z_w & U_0 & 0 \\ \tilde{M}_u & \tilde{M}_w & \tilde{M}_q & 0 \\ 0 & 0 & 1 & 0 \end{bmatrix} \begin{bmatrix} u \\ w \\ q \\ \theta \end{bmatrix} + \begin{bmatrix} X_{\delta_E} & X_{\delta_T} \\ Z_{\delta_E} & Z_{\delta_T} \\ \tilde{M}_{\delta_E} & 0 \\ 0 & 0 \end{bmatrix} \begin{bmatrix} \delta_E \\ \delta_T \end{bmatrix} \tag{2.54}$$

in short

$$\dot{\boldsymbol{\nu}}_{long} = \mathbf{A}_{long}\boldsymbol{\nu}_{long} + \mathbf{B}_{long}\mathbf{u}_{long} \tag{2.55}$$

Lateral

From (2.31)-(2.34), (2.40)-(2.42) and (2.47)-(2.49) we get the lateral model

$$\begin{aligned}
\dot{v} &= Y_v v - U_0 r + g\phi + Y_{\delta_R}\delta_R \\
\dot{p} &= L_v^{'} v + L_p^{'} p + L_r^{'} r + L_{\delta_A}^{'}\delta_A + L_{\delta_R}^{'}\delta_R \\
\dot{r} &= N_v^{'} v + N_p^{'} p + N_r^{'} r + N_{\delta_A}^{'}\delta_A + N_{\delta_R}^{'}\delta_R \\
\dot{\phi} &= p
\end{aligned}$$

where the primed stability derivatives are defined as

$$\begin{aligned}
L_v^{'} &= L_v + I_B N_v & N_v^{'} &= N_v + I_A L_v \\
L_p^{'} &= L_p + I_B N_p & N_p^{'} &= N_p + I_A L_p \\
L_r^{'} &= L_r + I_B N_r & N_r^{'} &= N_r + I_A L_r \\
L_{\delta_A}^{'} &= L_{\delta_A} + I_B L_{\delta_A} & N_{\delta_A}^{'} &= N_{\delta_A} + I_A N_{\delta_A} \\
L_{\delta_R}^{'} &= L_{\delta_R} + I_B L_{\delta_R} & N_{\delta_R}^{'} &= N_{\delta_R} + I_A N_{\delta_R}
\end{aligned}$$

and $I_A = \frac{I_{xz}}{I_{xx}}$ and $I_B = \frac{I_{xz}}{I_{zz}}$. On matrix form we have

$$\begin{bmatrix} \dot{v} \\ \dot{p} \\ \dot{r} \\ \dot{\phi} \end{bmatrix} = \begin{bmatrix} Y_v & 0 & -U_0 & g \\ L_v^{'} & L_p^{'} & L_r^{'} & 0 \\ N_v^{'} & N_p^{'} & N_r^{'} & 0 \\ 0 & 1 & 0 & 0 \end{bmatrix} \begin{bmatrix} v \\ p \\ r \\ \phi \end{bmatrix} + \begin{bmatrix} 0 & Y_{\delta_R} \\ L_{\delta_A}^{'} & L_{\delta_R}^{'} \\ N_{\delta_A}^{'} & N_{\delta_R}^{'} \\ 0 & 0 \end{bmatrix} \begin{bmatrix} \delta_A \\ \delta_R \end{bmatrix} \tag{2.56}$$

in compact form

$$\dot{\boldsymbol{\nu}}_{lat} = \mathbf{A}_{lat}\boldsymbol{\nu}_{lat} + \mathbf{B}_{lat}\mathbf{u}_{lat} \tag{2.57}$$

2.4.7 Dimensionless aerodynamic coefficients

For each aerodynamic derivative, we need to find one or more dimensionless coefficients to calculate them. As mentioned in section 2.3, the aerodynamic coefficients are usually found by wind tunnel tests. I did not have this opportunity and this identification is not the focus of this text, thus the numerical values are obtained from the nonlinear model described in section 2.5. As mentioned in section 2.3, the dimensionless coefficients are nonlinear functions, but in linear aerodynamic theory they are assumed constant.

2.4.8 Simplifications and change of states

As mentioned in the beginning of this chapter, the nonlinear F-16 model assumes different states than the ones the previous derivations have been performed for. This gives some changes in the system matrices.

First, for simplicity, we assume that an external simple speed regulator keeps $U = V_T$ constant, and thus u constant and equal to zero. In this way u can be decoupled from the equations, and the resulting longitudinal system becomes:

$$\begin{bmatrix} \dot{w} \\ \dot{q} \\ \dot{\theta} \end{bmatrix} = \begin{bmatrix} Z_w & U_0 & 0 \\ \tilde{M}_w & \tilde{M}_q & 0 \\ 0 & 1 & 0 \end{bmatrix} \begin{bmatrix} w \\ q \\ \theta \end{bmatrix} + \begin{bmatrix} Z_{\delta_E} \\ \tilde{M}_{\delta_E} \\ 0 \end{bmatrix} \delta_E$$

This is a normal assumption to make, and the possible error imposed by this will hopefully be corrected by the adaptive controller.

For the lateral model, the goal is to control both roll and yaw. Thus the new state ψ needs to be included. In the flight condition considered, ψ will just be the integral of r, and no other states are affected by this.

The nonlinear model expects the states α and β instead of w and v respectively. In this context, α and β means the perturbed angle of attack and side-slip angle. From 2.1 and 2.2

together with the mentioned assumptions, we get

$$\tan(\alpha) = \frac{w}{U_0} \approx \alpha, \;\; \sin(\beta) = \frac{v}{U_0} \approx \beta \tag{2.58}$$

$$\Downarrow$$

$$\dot{\alpha} = \frac{\dot{w}}{U_0}, \;\; \dot{\beta} = \frac{\dot{v}}{U_0} \tag{2.59}$$

This gives the final linear longitudinal model

$$\begin{bmatrix} \dot{\alpha} \\ \dot{q} \\ \dot{\theta} \end{bmatrix} = \begin{bmatrix} Z_\alpha/U_0 & 1 & 0 \\ \tilde{M}_\alpha & \tilde{M}_q & 0 \\ 0 & 1 & 0 \end{bmatrix} \begin{bmatrix} \alpha \\ q \\ \theta \end{bmatrix} + \begin{bmatrix} Z_{\delta_E}/U_0 \\ \tilde{M}_{\delta_E} \\ 0 \end{bmatrix} \delta_E, \tag{2.60}$$

where $Z_\alpha = Z_w U_0$ and $\tilde{M}_\alpha = \tilde{M}_w U_0$, and the final lateral model

$$\begin{bmatrix} \dot{\beta} \\ \dot{p} \\ \dot{r} \\ \dot{\phi} \\ \dot{\psi} \end{bmatrix} = \begin{bmatrix} Y_\beta/U_0 & 0 & -1 & g/U_0 & 0 \\ L'_\beta & L'_p & L'_r & 0 & 0 \\ N'_\beta & N'_p & N'_r & 0 & 0 \\ 0 & 1 & 0 & 0 & 0 \\ 0 & 0 & 1 & 0 & 0 \end{bmatrix} \begin{bmatrix} \beta \\ p \\ r \\ \phi \\ \psi \end{bmatrix} + \begin{bmatrix} 0 & Y_{\delta_R}/U_0 \\ L'_{\delta_A} & L'_{\delta_R} \\ N'_{\delta_A} & N'_{\delta_R} \\ 0 & 0 \\ 0 & 0 \end{bmatrix} \begin{bmatrix} \delta_A \\ \delta_R \end{bmatrix}, \tag{2.61}$$

where $Y_\beta = Y_v U_0$, $L'_\beta = L'_v U_0$ and $N'_\beta = N'_v U_0$. Now, the goal is that an $\mathcal{L}_1$ adaptive controller based on this single linearised model will be able to adapt to the different model changes, and be able to control the aircraft satisfactory for all the different operating points and flight conditions.

2.5 F-16 model

This section introduces the F-16 model used in this text. This model is described in detail in [21]. It is based on the F-16 model from [2] and implemented in Matlab/Simulink. The Matlab and Simulink files have been downloaded from the home pages of the University of Minnesota.

The nonlinear F-16 model can be used directly to test the nonlinear response. Further it includes easy tools to linearise and identify the model parameters and trim values for the different manoeuvres, speed and altitude. It is important to point out that the units used in the F-16 model are a bit different than the ones used in my project report. The difference is that distance and speed is given in ft and ft/s respectively, instead of m and m/s. This will however not effect any dynamics of the system. Also, the states are defined in BODY, and not in WIND as in the derivations in this chapter. This does not change anything in the design of the $\mathcal{L}_1$ adaptive controller, but is important to state.

The linearisation was performed by the F-16 model by specifying the desired altitude and speed. I chose

$$\begin{aligned} U_0 &= 500\ [ft/s] \\ \text{Altitude} &= 15000\ [ft] \end{aligned} \tag{2.62}$$

The linearisation resulted in the following trimmed states and control:

$$\begin{aligned} \Phi_0 &= 0\ [deg] \\ \Theta_0 &= 4.46\ [deg] \\ \Psi_0 &= 0\ [deg] \\ \alpha_0 &= 4.46\ [deg] \\ \beta_0 &= 0\ [deg] \\ P_0 = Q_0 &= R_0 = 0\ [deg/s] \\ \delta_{E0} &= -2.46\ [deg] \\ \delta_{A0} = \delta_{R0} &= 0\ [deg], \\ \text{Thrust}_0 &= 2120.6\ [lbs], \end{aligned}$$

the following longitudinal model:

$$\begin{bmatrix} \dot{\alpha} \\ \dot{q} \\ \dot{\theta} \end{bmatrix} = \begin{bmatrix} -0.6398 & 0.9378 & -0.0000 \\ -1.5679 & -0.8791 & 0 \\ 0 & 1.0000 & 0 \end{bmatrix} \begin{bmatrix} \alpha \\ q \\ \theta \end{bmatrix} + \begin{bmatrix} -0.0777 \\ -6.5121 \\ 0 \end{bmatrix} \delta_E, \tag{2.63}$$

and the lateral model:

$$\begin{bmatrix} \dot{\beta} \\ \dot{p} \\ \dot{r} \\ \dot{\phi} \\ \dot{\psi} \end{bmatrix} = \begin{bmatrix} -0.2022 & 0.0783 & -0.9919 & 0.0641 & 0 \\ -22.9219 & -2.2542 & 0.5408 & 0 & 0 \\ 6.0052 & -0.0404 & -0.3146 & 0 & 0 \\ 0 & 1.0000 & 0.0781 & 0 & 0 \\ 0 & 0 & 1.0030 & 0 & 0 \end{bmatrix} \begin{bmatrix} \beta \\ p \\ r \\ \phi \\ \psi \end{bmatrix} + \begin{bmatrix} 0.0099 & 0.0290 \\ -26.4872 & 3.2579 \\ -1.3965 & -2.6855 \\ 0 & 0 \\ 0 & 0 \end{bmatrix} \begin{bmatrix} \delta_A \\ \delta_R \end{bmatrix}. \tag{2.64}$$

We see that this linearisation gives a bit different result than we would have expected from (2.60) and (2.61). This error may be due to assumptions made during the derivation in this chapter and due to the change of reference system.

Chapter 3

Theory of $\mathcal{L}_1$ adaptive control

This chapter concerns the theoretical background of $\mathcal{L}_1$ adaptive control. The full state-feedback control architectures for different problem formulations are presented as well as the corresponding main theoretical results. The proofs are mostly excluded, but can be found in [7]. This chapter also discusses advantages of the $\mathcal{L}_1$ formulation as well as design challenges.

An ideal adaptive controller would be one that needed no a priori knowledge about the controlled system, introduced no restrictions on the system, would identify the system perfectly on-line, and based on this, control the system perfectly. However, this ideal controller does not exist. We do need some information about the system structure and some assumptions have to be made. Despite this, adaptive controllers may be very helpful. The goal of this text is to design a single $\mathcal{L}_1$ adaptive controller based on the single linearised system developed in chapter 2, that will be able to adapt to the different model changes, and be able to control the aircraft satisfactory for all the different operating points and flight conditions. That is, an $\mathcal{L}_1$ adaptive controller based on the linear identified system on the form

$$\dot{\mathbf{x}}(t) = \mathbf{A}_{id}\mathbf{x}(t) + \mathbf{B}_{id}\mathbf{u}(t), \tag{3.1}$$

is designed to control a general unknown system on the form

$$\dot{\mathbf{x}} = f_x(t, \mathbf{x}(t)) + f_u(t, \mathbf{x}(t), \mathbf{u}(t)). \tag{3.2}$$

Thus, the error between the systems in (3.1) and (3.2) has to be identified on-line and corrected for by the controller. This chapter will show that by imposing some minor assumptions, this goal is possible.

The theory presented in this text is a continuation of the theory presented in my project report [1]. This text, takes the principles of $\mathcal{L}_1$ adaptive control further by removing the assumptions made on the system structure in [1], and thus be able to control systems on the form in (3.2). The final goal of this chapter is an $\mathcal{L}_1$ adaptive controller which can cope with unmatched uncertainties for multi-variable nonlinear systems, and unmodeled actuator dynamics. To better understand the final architecture and the final theoretical results, the problem formulation is extended step by step to include more and more uncertainties. Thus

the problem formulation imposes fewer and fewer limitations to the considered system. For each problem formulation, the corresponding $\mathcal{L}_1$ adaptive control architecture and the theoretical results are presented. This is also the way I have worked my way through the theory. The architectures and the resulting theoretical results are mainly obtained from [7].

3.1 Main theoretical results for systems with unknown constant parameters.

Some of the theoretical results from my project report [1] is of important for this text. To make this text easier to read, to and be able to refer to these results, they are included in this section. The control architecture is not included. For more information about $\mathcal{L}_1$ adaptive controller for systems with unknown constant parameters, see [1], [7] and [8]. The different parameters and symbols used in this section will be defined in the subsequent sections.

Consider the reference system

$$\begin{aligned}
\dot{\mathbf{x}}_{ref}(t) &= \mathbf{A}_{id}\mathbf{x}_{ref}(t) + \mathbf{B}\left(\boldsymbol{\theta}^T\mathbf{x}_{ref}(t) + u_{ref}(t)\right), \mathbf{x}_{ref}(0) = \mathbf{x}_0, \\
u_{ref}(s) &= -C(s)\left(\boldsymbol{\theta}^T\mathbf{x}_{ref}(s) - k_g r(s)\right) - \mathbf{K}_m^T\mathbf{x}_{ref}(s), \\
y_{ref}(s) &= \mathbf{C}^T\mathbf{x}_{ref}(s).
\end{aligned} \tag{3.3}$$

This system defines the best theoretically possible control for the $\mathcal{L}_1$ adaptive controller described in [1], namely when the unknown parameter θ is known.

In [1], subject to the $\mathcal{L}_1$-norm condition, the following relationship between the implementable $\mathcal{L}_1$ adaptive coontroller and the non-implementable reference system was found

$$\|\mathbf{x}_{ref} - \mathbf{x}\|_{\mathcal{L}_\infty} \leq \frac{\gamma_1}{\sqrt{\Gamma}}, \qquad \|u_{ref} - u\|_{\mathcal{L}_\infty} \leq \frac{\gamma_2}{\sqrt{\Gamma}}, \tag{3.4}$$

$$\lim_{t\to\infty}\|\mathbf{x}_{ref}(t) - \mathbf{x}\| = 0, \qquad \lim_{t\to\infty}\|x_{ref}(t) - u\| = 0, \tag{3.5}$$

where

$$\begin{aligned}
\gamma_1 &:= \frac{\|C(s)\|_{\mathcal{L}_1}}{1 - \|G(s)\|_{\mathcal{L}_1}L}\sqrt{\frac{\theta_{\max}}{\lambda_{\min}(P)}}, \\
\gamma_2 &:= \|H_1(s)\|_{\mathcal{L}_1}\sqrt{\frac{\theta_{\max}}{\lambda_{\min}(P)}} + \|C(s)\boldsymbol{\theta}^T + \mathbf{K}_m^T\|_{\mathcal{L}_1}\gamma_1.
\end{aligned}$$

$H_1(s)$ is defined by

$$H_1(s) := C(s)\frac{1}{c_0^T H(s)}c_0^T, \tag{3.6}$$

where $c_0 \in \mathbb{R}^n$ makes H_1 proper and BIBO stable.

Consider the LTI design system

$$\mathbf{x}_{des}(s) = C(s)k_g H(s)r(s) + \mathbf{x}_{in}(s), \tag{3.7}$$
$$u_{des}(s) = k_g C(s)r(s) - C(s)\boldsymbol{\theta}^T\mathbf{x}_{des}(s) - \mathbf{K}_m^T\mathbf{x}_{des}(s), \tag{3.8}$$
$$y_{des}(s) = \mathbf{C}^T\mathbf{x}_{des}(s), \tag{3.9}$$

where $\mathbf{x}_{in}(s) := (s\mathbf{I} - \mathbf{A}_m)^{-1}\mathbf{x}_0$, implying that $\mathbf{x}_{in}(t)$ is exponentially decreasing. This system was introduced to investigate the performance of the $\mathcal{L}_1$ adaptive controller. As opposed to the reference system (3.3), the output of the design system does not depend upon the unknown parameter $\boldsymbol{\theta}$, and is therefore used for introducing the transient specifications. In [1], subject to the $\mathcal{L}_1$-norm condition, the following relationship between the reference system and the design system was found:

$$\|y_{des} - y_{ref}\|_{\mathcal{L}_\infty} \leq \frac{\lambda}{1-\lambda}\|\mathbf{C}^T\|_1 \left(\|k_g H(s)C(s)\|_{\mathcal{L}_1}\|r\|_{\mathcal{L}_\infty} + |\mathbf{x}_{in}\|_{\mathcal{L}_\infty}\right), \tag{3.10}$$
$$\|\mathbf{x}_{des} - \mathbf{x}_{ref}\|_{\mathcal{L}_\infty} \leq \frac{\lambda}{1-\lambda}\left(\|k_g H(s)C(s)\|_{\mathcal{L}_1}\|r\|_{\mathcal{L}_\infty}\right) + |\mathbf{x}_{in}\|_{\mathcal{L}_\infty}\right), \tag{3.11}$$
$$\begin{aligned}\|u_{des} - u_{ref}\|_{\mathcal{L}_\infty} \leq &\frac{\lambda}{1-\lambda}\|C(s)\boldsymbol{\theta}^T + \mathbf{K}_m^T\|_{\mathcal{L}_1} \\ &\cdot \left(\|k_g H(s)C(s)\|_{\mathcal{L}_1}\|r\|_{\mathcal{L}_\infty} + |\mathbf{x}_{in}\|_{\mathcal{L}_\infty}\right)\end{aligned} \tag{3.12}$$

3.2 SISO systems with matched unknown parameters and disturbance, and uncertain system input gain

In this section the $\mathcal{L}_1$ adaptive control strategy and the theoretical results for systems with matched unknown time-varying parameters and disturbances together with uncertain system input gain is presented. Compared to the system considered in my project report [1], this is a step towards the final goal of controlling systems on the general form of (3.2). To get a better insight to the $\mathcal{L}_1$ adaptive control strategy, an introduction through model reference adaptive control (MRAC) is given.

3.2.1 Problem formulation

In this section we consider systems on the form

$$\begin{aligned}\dot{\mathbf{x}}(t) &= \mathbf{A}_m\mathbf{x}(t) + \mathbf{B}\left(\omega u_{ad}(t) + \boldsymbol{\theta}^T(t)\mathbf{x}(t) + \sigma(t)\right),\ \mathbf{x}(0) = \mathbf{x}_0 \\ y(t) &= \mathbf{C}^T\mathbf{x}(t),\end{aligned} \tag{3.13}$$

where $\mathbf{x}(t) \in \mathbb{R}^n$ is the measured system state vector, $u_{ad}(t) \in \mathbb{R}$ is the control signal, $y(t) \in \mathbb{R}$ is the regulated output, $\mathbf{B}$, $\mathbf{C} \in \mathbb{R}^n$ are known constant vectors, $\mathbf{A}_m$ is a known $n \times n$ Hurwitz matrix specifying the desired closed-loop dynamics, $(\mathbf{A}_m, \mathbf{B})$ is controllable, $\omega \in \mathbb{R}$ is an unknown constant with known sign, $\boldsymbol{\theta}(t) \in \mathbb{R}^n$ is a vector of time-varying unknown parameters, and $\sigma(t) \in \mathbb{R}$ models disturbances.

Assumptions

To prove the theoretical results of this section, some assumptions to the systems in (3.13) have to be made.

Assumption 3.2.1 (Uniform boundedness of unknown parameter). *Let*

$$\boldsymbol{\theta}(t) \in \Theta,\ |\boldsymbol{\sigma}(t)| \leq \Delta_0,\ \forall\, t \leq 0,$$

where Θ is a known convex compact set and $\Delta_0 \in \mathbb{R}^+$ is a known conservative bound.

Assumption 3.2.2 (Uniformly boundedness of the rate of variation of parameters). *Let $\boldsymbol{\theta}(t)$ and $\sigma(t)$ be continuously differentiable with uniformly bounded derivatives:*

$$\|\dot{\boldsymbol{\theta}}(t)\| \leq d_\theta < \infty,\ |\dot{\sigma}(t)| \leq d_\sigma < \infty,\ \forall t \geq 0.$$

Assumption 3.2.3 (Partial knowledge of uncertain system input gain). *Let*

$$\omega \in \Omega_0 := [\omega_{l0},\ \omega_{u0}],$$

where $0 < \omega_{l0} < \omega_{u0}$ are given known lower and upper bounds on ω.

3.2.2 Limitations in the problem formulation

Compared to (3.2) we see that the formulation (3.13) still puts some limitations on the systems considered. This section concerns this limitations and names the assumptions needed to get from (3.2) to (3.13).

By looking at (3.13) we see that a linear time-varying system is assumed. This brings us to the first assumption:

Assumption 3.2.4 (Linear time-varying system). *The functions $f_x(t, \mathbf{x}(t)), f_u(t, \mathbf{x}(t)) : \mathbb{R} \times \mathbb{R}^n \to \mathbb{R}^n$ are linear and time-varying, according to*

$$f_x(t, \mathbf{x}(t)) = \mathbf{A}_{real}(t)\mathbf{x}(t)$$
$$f_u(t, \mathbf{x}(t), \mathbf{u}(t)) = \mathbf{B}_{real}(t)(u(t) + \sigma_1(t))$$

where $\mathbf{A}_{real}(t) \in \mathbb{R}^{n\times n}$ is the real unknown time-varying system matrix, $\mathbf{B}_{real}(t) \in \mathbb{R}^n$ is the real unknown time-varying input vector, and $\sigma_1(t) \in \mathbb{R}$ is the input disturbance.

This gives the real system:

$$\begin{aligned} \dot{\mathbf{x}}(t) &= \mathbf{A}_{real}(t)\mathbf{x}(t) + \mathbf{B}_{real}(t)(u(t) + \sigma_1(t)),\ \mathbf{x}(0) = \mathbf{x}_0 \\ y(t) &= \mathbf{C}^T\mathbf{x}(t), \end{aligned} \tag{3.14}$$

where $\mathbf{x}(t) \in \mathbb{R}^n$ is the measured system state vector, $u(t) \in \mathbb{R}$ is the control signal, $y(t) \in \mathbb{R}$ is the regulated output, and $\mathbf{C} \in \mathbb{R}^n$ is the known constant output vector.

Through modelling and system identification, as described in chapter 2, the identified system (3.1) is found. We define the identified system matrix $\mathbf{A}_{id}$, and we define the identified input vector $\mathbf{B}_{id}$. However, as described, the identified system matrix and input vector can not be assumed to be the correct unknown system matrix and input vector for all the flight conditions. To get from (3.14) to (3.13), we need to introduce some additional assumptions on the system.

Assumption 3.2.5 (Linear relationship between $\mathbf{B}_{real}$ and $\mathbf{B}_{id}$). *The input vector $\mathbf{B}_{real}(t)$ is constant, that is $\mathbf{B}_{real}(t) \equiv \mathbf{B}_{real}$, and there exist a constant vector $B_{id} \in \mathbb{R}^n$ and a constant scalar $\omega \in \mathbb{R}$ such that*

$$\mathbf{B}_{real} = \mathbf{B}_{id}\omega.$$

ω is also assumed to belong to the set $\Omega_0 := [\omega_{l_0},\ \omega_{u_0}]$, where $0 < \omega_{l_0} < \omega_{u_0}$.

The next assumption is similar to that in [8].

Assumption 3.2.6 (Matched modelling error). *There exist a matrix $\mathbf{A}_{id} \in \mathbb{R}^{n\times n}$ and a vector $\boldsymbol{\theta}_1(t) \in \mathbb{R}^n$ of ideal parameters such that $(\mathbf{A}_{id}, \mathbf{B}_{real})$ is controllable and*

$$\mathbf{A}_{real}(t) - \mathbf{A}_{id} = \mathbf{B}_{real}\boldsymbol{\theta}_1^T(t).$$

$\boldsymbol{\theta}_1(t)$ is also assumed to belong to the compact convex set Θ_1, that is $\boldsymbol{\theta}_1(t) \in \Theta_1$.

By substituting for A_{real} in (3.14) using assumption 3.2.6, we get

$$\begin{aligned} \dot{\mathbf{x}}(t) &= \mathbf{A}_{id}\mathbf{x}(t) + \mathbf{B}_{real}\left(u(t) + \boldsymbol{\theta}_1^T(t)\mathbf{x}(t) + \sigma_1(t)\right),\ \mathbf{x}(0) = \mathbf{x}_0 \\ y(t) &= \mathbf{C}^T\mathbf{x}(t). \end{aligned} \tag{3.15}$$

To get the desired system matrix $\mathbf{A}_m$, we need to design a state feedback vector that achieves this. However, since the real input vector is unknown, we want to design the feedback vector based on the identified input vector. Since $(\mathbf{A}_{id}, \mathbf{B}_{real})$ is controllable and $\mathbf{B}_{id} = \mathbf{B}_{real}/\omega$, $(\mathbf{A}_{id}, \mathbf{B}_{id})$ is also controllable, and there exist a vector $\mathbf{K}_m \in \mathbb{R}^n$ such that $\mathbf{A}_m = \mathbf{A}_{id} - \mathbf{B}_{id}\mathbf{K}_m^T$ is Hurwitz. Thus, we introduce the control structure

$$u(t) = u_m(t) + u_{ad}(t),\ u_m(t) = -\mathbf{K}_m^T\mathbf{x}(t), \tag{3.16}$$

where $\mathbf{K}_m \in \mathbb{R}^n$ makes $\mathbf{A}_m := \mathbf{A}_{id} - \mathbf{B}_{id}\mathbf{K}_m^T$ Hurwitz and specifies the desired closed loop dynamics, and u_{ad} is the adaptive component. Substituting for $\mathbf{B}_{real}$ and $u(t)$ in (3.15) using assumption 3.2.5 and (3.16), we get

$$\begin{aligned} \dot{\mathbf{x}}(t) &= \mathbf{A}_{id}\mathbf{x}(t) + \mathbf{B}_{id}\omega\left(-\mathbf{K}_m^T\mathbf{x}(t) + u_{ad} + \boldsymbol{\theta}_1^T(t)\mathbf{x}(t) + \sigma_1(t)\right) \\ &= \left(\mathbf{A}_{id} - \mathbf{B}_{id}\mathbf{K}_m^T\omega\right)\mathbf{x}(t) + \mathbf{B}_{id}\left(\omega u_{ad} + \omega\boldsymbol{\theta}_1^T(t)\mathbf{x}(t) + \omega\sigma_1(t)\right) \\ &= \left(\mathbf{A}_{id} - \mathbf{B}_{id}\mathbf{K}_m^T + \mathbf{B}_{id}\mathbf{K}_m^T - \mathbf{B}_{id}\mathbf{K}_m^T\omega\right)\mathbf{x}(t) + \mathbf{B}_{id}\left(\omega u_{ad} + \omega\boldsymbol{\theta}_1^T(t)\mathbf{x}(t) + \omega\sigma_1(t)\right) \\ &= \mathbf{A}_m\mathbf{x}(t) + \mathbf{B}_{id}\mathbf{K}_m^T\left(1-\omega\right)\mathbf{x}(t) + \mathbf{B}_{id}\left(\omega u_{ad} + \omega\boldsymbol{\theta}_1^T(t)\mathbf{x}(t) + \omega\sigma_1(t)\right) \\ y(t) &= \mathbf{C}^T\mathbf{x}(t),\ \mathbf{x}(0) = \mathbf{x}_0. \end{aligned}$$

By defining

$$\boldsymbol{\theta}^T(t) := \mathbf{K}_m^T(1-\omega) + \omega\boldsymbol{\theta}_1^T(t), \tag{3.17}$$
$$\sigma(t) := \omega\sigma_1(t), \tag{3.18}$$

we get

$$\begin{aligned}\dot{\mathbf{x}} &= \mathbf{A}_m\mathbf{x}(t) + \mathbf{B}_{id}\left(\omega u_{ad}(t) + \boldsymbol{\theta}^T(t)\mathbf{x}(t) + \sigma(t)\right),\ \mathbf{x}(0) = \mathbf{x}_0 \\ y &= \mathbf{C}^T\mathbf{x}(t),\end{aligned} \tag{3.19}$$

which has the same structure as (3.13).

This derivation shows that when the identified input vector is equal to the real input vector, that is $\omega = 1$, the feedback u_m imposes no error on $\boldsymbol{\theta}$. Further we can see that u_m is not actually needed. Omitting u_m would result in a larger modelling error, which would have to be taken care of by the adaptive part of the controller, u_{ad}. However, a larger modelling error will be disadvantageous for the design of the controller.

This derivation may also justify the use of the estimate of the unknown constant gain, $\hat{\omega}$, in the design of the feedback signal. By designing

$$u_m = -\frac{1}{\hat{\omega}}\mathbf{K}_m^T\mathbf{x} \tag{3.20}$$

This design would make the error caused by the feedback signal equal to $\mathbf{K}_m^T(1-\frac{\omega}{\hat{\omega}}) \approx 0$ for $\hat{\omega} \approx \omega$.

3.2.3 Model Reference Adaptive Control with state predictor

The theory of $\mathcal{L}_1$ adaptive control is based on the theory of indirect model reference adaptive control (MRAC). To better understand the $\mathcal{L}_1$-theory, this section will include a short summary of the indirect MRAC theory, based on that in [7] and [22].

Consider the system in (3.13):

$$\begin{aligned}\dot{\mathbf{x}}(t) &= \mathbf{A}_m\mathbf{x}(t) + \mathbf{B}\left(\omega u(t) + \boldsymbol{\theta}^T\mathbf{x}(t) + \sigma(t)\right),\ \mathbf{x}(0) = \mathbf{x}_0 \\ y(t) &= \mathbf{C}^T\mathbf{x}(t),\end{aligned} \tag{3.21}$$

The control objective is to make the output $y(t)$ track a given uniformly bounded piecewise continuous input signal $r(t)$. This will be achieved by using the ideal controller

$$u_{id}(t) = \frac{1}{\omega}\left(-\boldsymbol{\theta}^T(t)\mathbf{x}(t) - \sigma(t) + k_g r(t)\right), \tag{3.22}$$

where

$$k_g := \frac{1}{\mathbf{C}^T\mathbf{A}_m^{-1}\mathbf{B}}. \tag{3.23}$$

This choice of controller, u_{id}, makes $y(t)$ track steps in $r(t)$ with zero steady-state error, and provides perfect cancellation of the uncertainty in (3.13). This gives the ideal system

$$\begin{aligned}\dot{\mathbf{x}}_m(t) &= \mathbf{A}_m\mathbf{x}_m(t) + \mathbf{B}k_g r(t),\ \mathbf{x}_m(0) = \mathbf{x}_0 \\ y_m(t) &= \mathbf{C}^T\mathbf{x}_m(t),\end{aligned} \tag{3.24}$$

However, since the controller (3.22) uses the unknown parameters ω, $\boldsymbol{\theta}(t)$ and $\sigma(t)$, this controller is not implementable. Thus, adaptation is needed to find the desired control input $u(t)$.

A state predictor of (3.13) is given by:

$$\begin{aligned}\dot{\hat{\mathbf{x}}}(t) &= \mathbf{A}_m\hat{\mathbf{x}}(t) + \mathbf{B}\left(\hat{\omega}u(t) + \hat{\boldsymbol{\theta}}^T(t)\mathbf{x}(t) + \hat{\sigma}(t)\right),\ \hat{\mathbf{x}}(0) = \mathbf{x}_0, \\ \hat{y}(t) &= \mathbf{C}^T\hat{\mathbf{x}}(t),\end{aligned} \tag{3.25}$$

where $\hat{x} \in \mathbb{R}^n$ is the state of the predictor. The predictor has the same structure as (3.13) with the unknown parameters ω, $\boldsymbol{\theta}(t)$ and $\sigma(t)$ replaced by their estimates $\hat{\omega}$, $\hat{\boldsymbol{\theta}}(t)$ and $\hat{\sigma}(t)$. The prediction error dynamics is obtained by subtracting (3.13) from (3.25):

$$\tilde{\mathbf{x}}(t) = \mathbf{A}_m\tilde{\mathbf{x}}(t) + \mathbf{B}\left(\tilde{\omega}(t)u + \tilde{\boldsymbol{\theta}}^T(t)\mathbf{x}(t) + \tilde{\sigma}(t)\right),\ \tilde{\mathbf{x}}(0) = 0, \tag{3.26}$$

where $\tilde{\mathbf{x}}(t) := \hat{\mathbf{x}}(t) - \mathbf{x}(t)$, $\tilde{\omega}(t) := \hat{\omega}(t) - \omega$, $\tilde{\boldsymbol{\theta}}(t) := \hat{\boldsymbol{\theta}}(t) - \boldsymbol{\theta}(t)$ and $\tilde{\sigma}(t) := \hat{\sigma}(t) - \sigma(t)$. As we can see, (3.26) is independent of u. The adaptive law for the unknown parameters are given by

$$\begin{aligned}\dot{\hat{\omega}}(t) &= \Gamma\text{Proj}(\hat{\omega}(t), -\tilde{\mathbf{x}}^T(t)\mathbf{P}\mathbf{B}u(t)),\ \hat{\omega}(0) = \hat{\omega}_0 \in \Omega, \\ \dot{\hat{\boldsymbol{\theta}}}(t) &= \Gamma\text{Proj}(\hat{\boldsymbol{\theta}}(t), -\tilde{\mathbf{x}}^T(t)\mathbf{P}\mathbf{B}\mathbf{x}(t)),\ \hat{\boldsymbol{\theta}}(0) = \hat{\boldsymbol{\theta}}_0 \in \Theta, \\ \dot{\hat{\sigma}}(t) &= \Gamma\text{Proj}(\hat{\sigma}(t), -\tilde{\mathbf{x}}^T(t)\mathbf{P}\mathbf{B}),\ \hat{\sigma}(0) = \hat{\sigma} \in \Delta,\end{aligned} \tag{3.27}$$

where $\Gamma \in (0, \infty)$ is the adaptation gain, Proj$(\cdot, \cdot)$ is the projection operator and defined in [7], appendix B. The projection operator ensures that the estimated parameters are kept within the known conservative bounds. $\hat{\omega}_0$, $\hat{\boldsymbol{\theta}}_0$ and $\hat{\sigma}_0$ is the best possible guess on the estimates. $\mathbf{P} = \mathbf{P}^T > 0$ solves the algebraic Lyapunov equation

$$\mathbf{A}_m^T\mathbf{P} + \mathbf{P}\mathbf{A}_m = -\mathbf{Q} \tag{3.28}$$

for arbitrary $\mathbf{Q} = \mathbf{Q}^T > 0$. Consider the Lyapunov function candidate:

$$V\left(\tilde{\mathbf{x}}(t), \tilde{\omega}(t), \tilde{\boldsymbol{\theta}}(t), \tilde{\sigma}(t)\right) = \tilde{\mathbf{x}}^T(t)\mathbf{P}\tilde{\mathbf{x}}(t) + \frac{1}{\Gamma}\left(\tilde{\omega}^2(t) + \tilde{\boldsymbol{\theta}}^T(t)\tilde{\boldsymbol{\theta}}(t) + \tilde{\sigma}^2(t)\right). \tag{3.29}$$

The time-derivative $\dot{V}(t)$ of $V\left(\tilde{\mathbf{x}}(t), \tilde{\boldsymbol{\theta}(t)}\right)$ along the system trajectories (3.26)-(3.27) is, [22]

$$\dot{V}(t) = -\tilde{\mathbf{x}}^T(t)\mathbf{Q}\tilde{\mathbf{x}}(t) - \frac{2}{\Gamma}\left(\tilde{\boldsymbol{\theta}}^T(t)\dot{\boldsymbol{\theta}}^T(t) + \tilde{\sigma}(t)\dot{\sigma}(t)\right). \tag{3.30}$$

From this inequality, we obtain the uniform bound, [22]

$$\|\tilde{\mathbf{x}}(t)\| \leq \frac{\gamma_0}{\sqrt{\Gamma}}, \ \forall \, t \geq 0, \tag{3.31}$$

where

$$\gamma_0 := \sqrt{\frac{\theta_{mi}}{\lambda_{min}(P)}}, \ \theta_{mi} := 4\boldsymbol{\theta}_{max}^2 + 4\sigma_b^2 + (\omega_{max} - \omega_{min})^2 + 4\frac{\lambda_{max}(P)}{\lambda_{min}(Q)}(\theta_{max} d_\theta + \sigma_b d_\sigma), \tag{3.32}$$

and

$$\theta_{max} := \max_{\theta \in \Theta} \|\boldsymbol{\theta}\|, \tag{3.33}$$

However, since we have not specified $u(t)$ we can not conclude convergence of $\tilde{\mathbf{x}}(t)$ to zero. $\mathbf{x}$ and $\hat{\mathbf{x}}$ may both diverge at the same rate.

Based on the ideal controller (3.22), by replacing the real unknown parameters with the estimated ones, we get the controll law

$$u(t) = \frac{1}{\hat{\omega}} \left(-\hat{\boldsymbol{\theta}}^T(t)\mathbf{x}(t) - \hat{\sigma}(t) + k_g r(t) \right), \tag{3.34}$$

with the estimates updated according to (3.27). If we substitute this in (3.25), we get

$$\begin{aligned} \dot{\hat{\mathbf{x}}}(t) &= \mathbf{A}_m \hat{\mathbf{x}}(t) + \mathbf{B} k_g r(t), \ \hat{\mathbf{x}}(0) = \mathbf{x}_0, \\ \hat{y}(t) &= \mathbf{C}^T \hat{\mathbf{x}}(t), \end{aligned} \tag{3.35}$$

which replicates the bounded ideal system (3.24). Since $\mathbf{x}(t) = \hat{\mathbf{x}}(t) - \tilde{\mathbf{x}}(t)$ and $\hat{\mathbf{x}}(t)$ replicates the bounded ideal system (3.24), $\mathbf{x}(t)$ is uniformly bounded. The architecture of the MRAC with state predictor is given in figure 3.1 from [22].

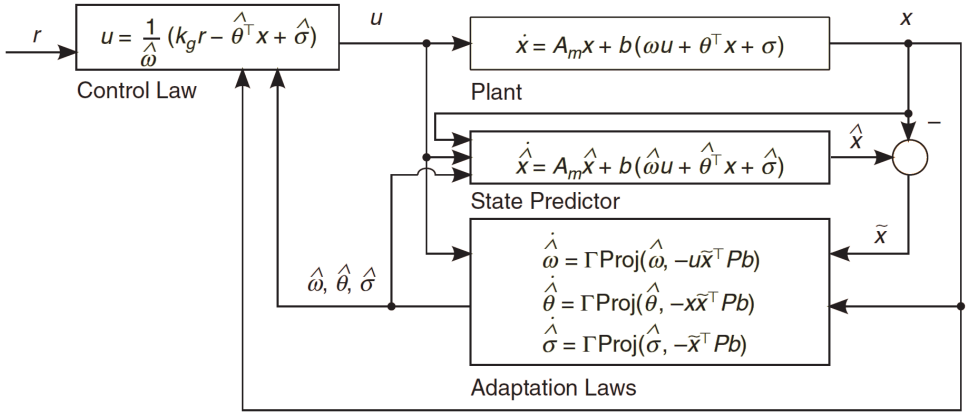

Figure 3.1: Closed loop MRAC architecture with state predictor, from [22].

3.2.4 Why $\mathcal{L}_1$ adaptive control?

From (3.31) we get the upper bound on the prediction error

$$\|\tilde{\mathbf{x}}\| \leq \sqrt{\frac{\theta_{mi}}{\lambda_{min}(P)\Gamma}},\ \forall\, t \geq 0. \tag{3.36}$$

This shows that the tracking error can be arbitrary reduced by increasing the adaptation gain. This holds for all $t \geq 0$, also in the transient phase. However, from the choice of control law (3.27) and (3.34) we see that large adaptive gains introduce high-gain feedback control, which may lead poor robustness and rapid oscillations on the control signal. Another problem with the MRAC structure is when the adaptation is within the same frequency range as the closed loop dynamics. Then these two processes may interfere and it is difficult to know if errors in the parameters are handled by the adaptation or by the controller. Thus, the tuning of MRAC represents a major challenge.

The idea of the $\mathcal{L}_1$ controller is to decouple adaptation from control. Then it is possible to introduce high adaptation gain to give fast adaptation of the unknown parameters. The robustness is resolved via conventional methods from classical and robust control. In this way, the $\mathcal{L}_1$ adaptive controller approximates a non-adaptive linear controller. The next sections show these theoretical results.

3.2.5 $\mathcal{L}_1$ adaptive control architecture

Consider the system in (3.13). The control objective is to design a full-state feedback $\mathcal{L}_1$ adaptive controller to ensure that $y(t)$ tracks a given piecewise-continuous reference signal $r(t)$ with quantifiable performance bounds.

State predictor

Just as in the MRAC design, we consider the following state predictor:

$$\begin{aligned}\dot{\hat{\mathbf{x}}}(t) &= \mathbf{A}_m\hat{\mathbf{x}}(t) + \mathbf{B}\left(\hat{\omega}(t)u_{ad} + \hat{\boldsymbol{\theta}}^T(t)\mathbf{x}(t) + \hat{\sigma}(t)\right),\ \hat{\mathbf{x}}(0) = \mathbf{x}_0 \\ \hat{y}(t) &= \mathbf{C}^T\hat{\mathbf{x}}(t).\end{aligned} \tag{3.37}$$

This has the same structure as (3.13) with the unknown parameters replaced by the adaptive estimates.

Adaptation laws

The estimates are again updated according to

$$\begin{aligned}\dot{\hat{\omega}}(t) &= \Gamma \text{Proj}(\hat{\omega}(t), -\tilde{\mathbf{x}}^T(t)\mathbf{P}\mathbf{B}u_{ad}(t)),\ \hat{\omega}(0) = \hat{\omega}_0 \in \Omega,\\ \dot{\hat{\boldsymbol{\theta}}}(t) &= \Gamma \text{Proj}(\hat{\boldsymbol{\theta}}(t), -\tilde{\mathbf{x}}^T(t)\mathbf{P}\mathbf{B}\mathbf{x}(t)),\ \hat{\boldsymbol{\theta}}(0) = \hat{\boldsymbol{\theta}}_0 \in \Theta,\\ \dot{\hat{\sigma}}(t) &= \Gamma \text{Proj}(\hat{\sigma}(t), -\tilde{\mathbf{x}}^T(t)\mathbf{P}\mathbf{B}),\ \hat{\sigma}(0) = \hat{\sigma} \in \Delta,\end{aligned} \tag{3.38}$$

where $\tilde{\mathbf{x}}(t) := \hat{\mathbf{x}}(t) - \mathbf{x}(t)$, $\Gamma \in \mathbb{R}^+$ is the adaptation rate, and $P = P^T > 0$ is the solution of the algebraic Lyapunov equation (3.28) for arbitrary $\mathbf{Q} = \mathbf{Q}^T > 0$. When the projection operator is to be implemented, we replace the sets Ω_0 and Δ_0 by $\Omega := [\omega_l,\ \omega_u]$ and Δ, defined by

$$\Delta_0 < \Delta, \quad 0 < \omega_l < \omega_{l_0} < \omega_{u_0} < \omega_u. \tag{3.39}$$

This definition is made due to the extra error a time delay would impose on the system, and is used in [7] in the time-delay analysis. [7] derives an analytical expression, amongst others dependent on the time delay, to find a conservative bound, Δ. This is however beyond the scope of this text, and the projection bounds are assumed chosen large enough to include all possible error. See [7] for more on this topic.

Control law

Just as in the MRAC control design, we want the control signal to compensate for the uncertainties, ω, $\boldsymbol{\theta}$ and σ, and track the reference, $r(t)$, with zero steady-state error. As in the design presented in [1], we want to filter the input signal to decouple adaptation from control. Intuitively, it would be reasonable to suggest a control law where the lowpass filter is directly applied to the control signal, that is:

$$u_f(s) = C_f(s)u(s),$$

where $u(s)$ is the Laplace transform of

$$u(t) = \frac{1}{\hat{\omega}(t)}(k_g r(t) - \hat{\boldsymbol{\theta}}^T\mathbf{x}(t) - \hat{\sigma}(t)), \tag{3.40}$$

and $C_f(s)$ is a lowpass filter. However, in the presence of the unknown input gain, this can not be done directly. The following explanation to why this is problematic follows that in [22]. Let $c_f(t)$ be the impulse response of $C_f(s)$. Then

$$u_f(t) = c_f(t) * u(t) = c_f(t) * \left(\frac{(k_g r(t) - \hat{\theta}\mathbf{x}(t) - \hat{\sigma}(t)}{\hat{\omega}(t)}\right), \tag{3.41}$$

where $*$ is the convolution operator. Substituting for u_{ad} in the predictor (3.37), using (3.41), we get

$$\dot{\hat{\mathbf{x}}}(t) = \mathbf{A}_m\hat{\mathbf{x}}(t) + \mathbf{B}\left(\hat{\omega}(t)c_f(t) * \left(\frac{(k_g r(t) - \hat{\boldsymbol{\theta}}^T\mathbf{x}(t) - \hat{\sigma}(t)}{\hat{\omega}(t)}\right) + \hat{\boldsymbol{\theta}}^T(t)\mathbf{x}(t) + \hat{\sigma}(t)\right) \tag{3.42}$$

As we can see from this expression, $\hat{\omega}$ can not be cancelled due to the convolution operator. Since we introduce fast adaptation, $\hat{\omega}$ may change rapidly which may result in unpredictable consequences on the systems performance [22].

Instead, the the $\mathcal{L}_1$ adaptive control law is given as

$$u_{ad}(s) = -kD(s)\left(\hat{\eta}(s) - k_g r(s)\right), \tag{3.43}$$

where $r(s)$ and $\hat{\eta}$ are the Laplace transforms of $r(t)$ and $\hat{\eta}(t) := \hat{\omega}(t)u_{ad}(t) + \hat{\boldsymbol{\theta}}^T(t)\mathbf{x}(t) + \hat{\sigma}(t)$ respectively, $k_g := -1/(\mathbf{C}^T\mathbf{A}_m^{-1}\mathbf{B}$, $k > 0$ is a feedback gain and $D(s)$ a strictly proper transfer function leading to a strictly proper stable

$$C(s) := \frac{\omega k D(s)}{1 + \omega k D(s)} \; \forall \, \omega \in \Omega_0, \tag{3.44}$$

with DC gain $C(0) = 1$. In the approach presented in (3.43) $\hat{\omega}$ can be viewed as a time-varying gain of the filter (3.44), which compensates for $\hat{\omega}$ in (3.42).

The choice $D(s) = 1/s$ and k>0 results in the exponentially stable strictly proper transfer-function

$$C(s) = \frac{\omega k}{s + k\omega}, \tag{3.45}$$

similar to the filter considered in the project report. As in [1], we define

$$L := \max_{\boldsymbol{\theta}\in\Theta} \|\boldsymbol{\theta}\|_1, \; H(s) := (s\mathbb{I} - \mathbf{A}_m)^{-1}\mathbf{B}, \; G(s) := H(s)(1 - C(s)). \tag{3.46}$$

The $\mathcal{L}_1$ adaptive controller is defined by combining the feedback controller defined in (3.16), the predictor (3.37), the adaptation rule (3.38) and the adaptive control law (3.43) subject to the $\mathcal{L}_1$-norm condition

$$\lambda := \|G(s)\|_{\mathcal{L}_1}\|L\| < 1. \tag{3.47}$$

The architecture of the $\mathcal{L}_1$ adaptive controller for systems with uncertain input gain is found in figure 3.2 from [22].

3.2.6 Theoretical results

The following part presents the main theoretical results for the $\mathcal{L}_1$ adaptive controller considered in this section. The proofs are mostly omitted in this text, but can be found in [7].

Prediction error

Subtracting the system dynamics (3.13) from the predictor (3.37), we get the prediction error

$$\dot{\tilde{\mathbf{x}}}(t) = \mathbf{A}_m\tilde{\mathbf{x}}(t) + \mathbf{B}(\tilde{\omega}(t)u(t) + \tilde{\boldsymbol{\theta}}^T(t)\mathbf{x}(t) + \tilde{\sigma}(t)), \tilde{\mathbf{x}}(0) = 0, \tag{3.48}$$

where $\tilde{\boldsymbol{\theta}}(t) := \hat{\boldsymbol{\theta}}(t) - \boldsymbol{\theta}(t)$, $\tilde{\sigma} := \hat{\sigma}(t) - \sigma(t)$, and $\tilde{\omega}(t) := \hat{\omega}(t) - \omega$. The following result holds for the prediction error, [7]

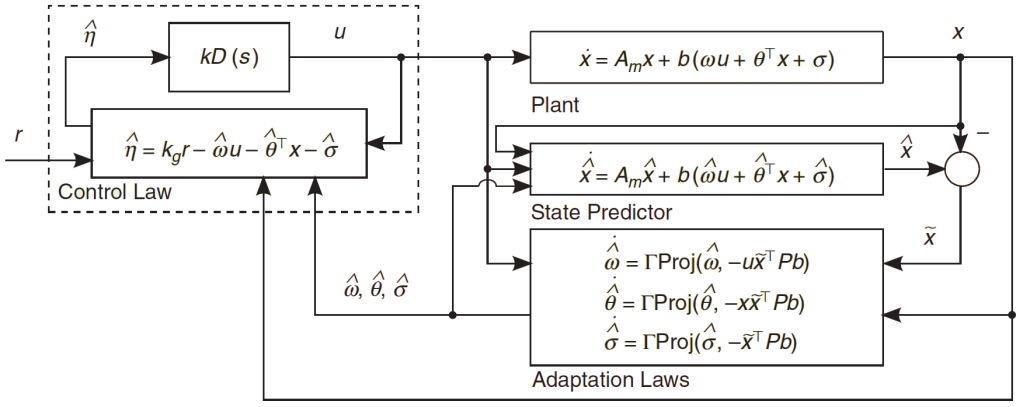

Figure 3.2: L1 adaptive control architecture, from [22].

Lemma 3.2.1. *The prediction error* $\tilde{\mathbf{x}}(t)$ *is uniformly bounded,*

$$\|\tilde{\mathbf{x}}\|_{\mathcal{L}_\infty} \leq \sqrt{\frac{\theta_m}{\lambda_{min}(\mathbf{P})\Gamma}}, \tag{3.49}$$

where

$$\theta_m := 4 \max_{\boldsymbol{\theta} \in \Theta} \|\boldsymbol{\theta}\|^2 + 4\Delta^2 + (\omega_u - \omega_l)^2 + 4\frac{\lambda_{max}(\mathbf{P})}{\lambda_{min}(\mathbf{Q})} \left(d_\theta \max_{\theta \in \Theta} \|\boldsymbol{\theta}\| + d_\sigma \Delta \right). \tag{3.50}$$

We can see that by increasing the adaptation gain, the bound on the prediction error can be made arbitrarily small.

Performance

To investigate the best theoretically possible control for the $\mathcal{L}_1$ adaptive controller, we again introduce the reference system. This is the non-adaptive version of the $\mathcal{L}_1$ adaptive controller, where all uncertainties are assumed known. In this case, the controller (3.43) takes the form:

$$u_{ref}(s) = -kD(s)(\eta_{ref}(s) + \omega u_{ref}(s) - k_g r(s)), \tag{3.51}$$

where $r(s)$ and $\eta_{ref}(s)$ are the Laplace transforms of $r(t)$ and $\eta_{ref}(t) := \boldsymbol{\theta}^T(t)\mathbf{x}_{ref}(t) + \sigma(t)$ respectively. Solving for $u_{ref}(s)$ gives

$$u_{ref}(s) = \frac{kD(s)}{1 + kD(s)\omega}(k_g r(s) - \eta_{ref}(s)) \tag{3.52}$$

$$= \frac{1}{\omega} C(s)(k_g r(s) - \eta_{ref}(s)), \tag{3.53}$$

where $C(s)$ is defined in (3.44). By this, we see that the control formulation (3.43) and the definition (3.44) of the filter can resolves the problem imposed by the convolution in (3.42).

Further, we see that the reference controller equals the filtered version of the ideal MRAC-controller. However, as opposed to the idel MRAC-controlelr, the reference controller only compensates for the uncertainties within the bandwidth of $C(s)$.

We now consider the reference system

$$\begin{aligned}\dot{\mathbf{x}}_{ref}(t) &= \mathbf{A}_m\mathbf{x}_{ref}(t) + \mathbf{B}\left(\omega u_{ref}(t) + \boldsymbol{\theta}^T(t)\mathbf{x}_{ref}(t) + \sigma(t)\right), \mathbf{x}_{ref}(0) = \mathbf{x}_0,\\ u_{ref}(s) &= \frac{C(s)}{\omega}\left(k_g r(s) - \eta_{ref}(s)\right),\\ y_{ref}(t) &= \mathbf{C}^T\mathbf{x}_{ref}(t).\end{aligned} \tag{3.54}$$

In the frequency domain, the closed loop reference system can be written as

$$\mathbf{x}_{ref}(s) = H(s)C(s)k_g r(s) + G(s)\eta_{ref}(s) + x_{in}, \tag{3.55}$$

where $x_{in}(s) := (s\mathbb{I} - \mathbf{A}_m)^{-1}\mathbf{x}_0$ is the Laplace transform of the ideal response tue to the initial condition $\mathbf{x}_0$. We also recognise $H(s)$ as the transfer function from u_{ref} to $\mathbf{x}_{ref}$ and $G(s)$ as the transfer function from the uncertainties η_{ref} to $\mathbf{x}_{ref}$. From (3.55) we get the upper bound

$$\|\mathbf{x}_{ref\ \tau}\|_{\mathcal{L}_\infty} = \|H(s)C(s)k_g\|_{\mathcal{L}_1}\|r\|_{\mathcal{L}_\infty} + \|G(s)\|_{\mathcal{L}_1}\|\eta_{ref\ \tau}\|_{\mathcal{L}_\infty} + \|x_{in}\|_{\mathcal{L}_\infty}. \tag{3.56}$$

An upper bound on η_{ref} is given by

$$\|\eta_{ref\ \tau}\|_{\mathcal{L}_\infty} \leq L\|\mathbf{x}_{ref\ \tau}\|_{\mathcal{L}_\infty} + \|\sigma_\tau\|_{\mathcal{L}_\infty} = L\|\mathbf{x}_{ref\ \tau}\|_{\mathcal{L}_\infty} + \Delta, \tag{3.57}$$

where L is defined in (3.46). Now, assuming that the $\mathcal{L}_1$-norm condition (3.47) holds, we get by substituting an solving for $\|\mathbf{x}_{ref\ \tau}\|_{\mathcal{L}_\infty}$:

$$\|\mathbf{x}_{ref\ \tau}\|_{\mathcal{L}_\infty} = \frac{\|H(s)C(s)k_g\|_{\mathcal{L}_1}\|r\|_{\mathcal{L}_\infty} + \|G(s)\|_{\mathcal{L}_1}\Delta + \|x_{in}\_\mathcal{L}_\infty}{1 - \|G(s)\|_{\mathcal{L}_1}L}. \tag{3.58}$$

This result motivates the need for the $\mathcal{L}_1$-norm condition, since it is the key to prove stability of the reference system. This result also proves the following following result, [7]

Lemma 3.2.2. *If k and $D(s)$ verify the $\mathcal{L}_1$-norm condition in* (3.47)*, the closed-loop reference system in* (3.54) *is BIBS stable with respect to $r(t)$ and $\mathbf{x}_0$*

Further, the following theorem from [7] gives the relationship between the nonimplementable reference system and the implementable $\mathcal{L}_1$ adaptive controller.

Theorem 3.2.1. *Given the system in* (3.13) *and the $\mathcal{L}_1$ adaptive controller defined via* (3.37), (3.38), *and* (3.43), *subject to the $\mathcal{L}_1$-norm condition in* (3.47), *we have*

$$\|\mathbf{x}_{ref} - \mathbf{x}\|_{\mathcal{L}_\infty} \leq \frac{\gamma_1}{\sqrt{\Gamma}}, \;\; \|u_{ref} - u\|_{\mathcal{L}_1} \leq \frac{\gamma_2}{\sqrt{\Gamma}}, \tag{3.59}$$

where

$$\begin{aligned}\gamma_1 &:= \frac{\|C(s)\|_{\mathcal{L}_1}}{1 - \|G(s)\|_{\mathcal{L}_1}L}\sqrt{\frac{\theta_m}{\lambda_{min}(P)}},\\ \gamma_2 &:= \left\|\frac{C(s)}{\omega}\right\|_{\mathcal{L}_1} L\gamma_1 + \left\|\frac{H_1(s)}{\omega}\right\|_{\mathcal{L}_1}\sqrt{\frac{\theta_m}{\lambda_{min}(P)}},\end{aligned} \tag{3.60}$$

and $H_1(s) = C(s)\frac{1}{c_0^T H(s)}c_0^T$ was defined in (3.6)

We see that by increasing the adaptation gain Γ, the system controlled by the $\mathcal{L}_1$ adaptive controller can get its states and the control input arbitrarily close to the reference system's states and control input. Since the reference system represents the best possible performance possible, we thus conclude that a high adaptation gain is desired.

Robustness

In linear system theory, the two most common measures of robustness is the phase margin and the gain margin. These stability margins can be found from the bode plot of the system. Equivalently to the phase and gain margin, we can measure the robustness of a system by the time delay margin. The time delay margin is defined as the amount of delay the system can tolerate before it becomes unstable.

When the adaptation gain Γ is large, the $\mathcal{L}_1$ adaptive controller defined in section 3.2.5 approximates the non-adaptive reference system (3.54). Thus, in the case of fast adaptation, we can study the robustness of the $\mathcal{L}_1$ controller by studying (3.54), but since this is a nonlinear closed-loop system, linear theory can not be used. However, [7] states that the following loop transfer function can be used to study the robustness of (3.54):

$$L_o(s) = \frac{C(s)}{1 - C(s)}(1 + \boldsymbol{\theta}^T \bar{H}(s)), \tag{3.61}$$

where

$$\bar{H}(s) := (s\mathbf{I} - \mathbf{A}_m - \mathbf{B}\boldsymbol{\theta}^T)^{-1}\mathbf{B}$$

The time delay margin of (3.61) is given by

$$\mathcal{T} = \frac{\phi_m}{\omega_{gc}}, \tag{3.62}$$

where ϕ_m is the phase margin, found from the bode plot, and ω_{gc} is the gain crossover frequency. This time delay gives a guaranteed lower bound on the time delay margin of the reference system (3.54). Equivalent to Corollary 2.2.1 in [7] we can state the following:

Corollary 3.2.1. *Subject to* (3.47)*, and* $\tau < \mathcal{T}$*, if* Γ *and* Δ *are selected appropriately large, the closed loop system in* (3.13)*, with the input from the controller defined by* (3.37)*,* (3.38) *and* (3.43) *delayed by* τ *seconds, is stable.*

Thus, as long as the time delay is smaller than the time delay margin found from (3.61), the $\mathcal{L}_1$ adaptive controller provides a stable system.

3.3 Design challenges: Trade-off between robustness and performance

The previous section presented the $\mathcal{L}_1$ adaptive control strategy and the corresponding theoretical results. This chapter sums up the main design challenges. Further, we will see

that the design of an $\mathcal{L}_1$ adaptive controller imposes a trade-off between robustness and performance. The reason for including this section before the final control architecture is introduced, it that it is easier to understand the theory behind the principles when considering the more simpler systems, while the same principals are valid for the more advanced architectures.

From theorem 3.2.1 we know that by increasing the adaptation gain, the controlled system can follow the reference system arbitrarily close. Thus, the adaptation gain should be chosen as large as the cpu and sample rate permits. The case of a limited sampling rate is investigated in chapter 4. By choosing a large adaptation gain, the control objective is reduced to the selection of k_m and $C(s)$ such that the reference system has the desired response.

To further investigate the separation effect of the filter and its relationship to the adaptation gain Γ we consider the following. From (3.21) and (3.43) it follows that

$$\mathbf{x}(s) = k_g H(s)C(s)r(s) + H(s)\boldsymbol{\theta}^T\mathbf{x}(s) - H(s)C(s)\hat{\eta}(s) + \mathbf{x}_{in}(s), \tag{3.63}$$

and the state predictor can be rewritten as

$$\hat{\mathbf{x}}(s) = k_g H(s)C(s)r(s) + H(s)(1 - C(s))\hat{\eta}(s) + \mathbf{x}_{in}(s) \tag{3.64}$$

This shows that the low-frequency part of the parameter estimate $C(s)\hat{\eta}(s)$ goes to the system state, while the high-frequency part $(1 - C(s))\hat{\eta}(s)$ goes to the state predictor. Since we only want the system to affected by the low frequency part of the parameter estimate, we need to chose Γ large enough to produce frequencies beyond the bandwidth of $C(s)$. The same goes for the control input, defined by (3.43), in which we want to compensate for the low-frequency component of the parameter update. Choosing Γ too low, will make the update frequencies lie inside the bandwidth of $C(s)$, and may introduce oscillations in the control input.

Further, the results from [1], given in (3.10)-(3.12), show that by minimising $\lambda := \|G(s)\|_{\mathcal{L}_1} L$, the difference between the reference system and the design system can be made arbitrarily small. Since $C(s)$ is a low-pass filter and $H(s)$ is a low-pass system, $G(s) = H(s)(1 - C(s))$ can be viewed as a cascade of a low-pass system $H(s)$ and a high-pass system $(1 - C(s))$. Thus, either decreasing the bandwidth of $H(s)$ or increasing the bandwidth of $C(s)$ may make $\|H(s)(1 - C(s))\|_{\mathcal{L}_1}$ arbitrary small, and make the controlled system follow the design system. The control objective is now reduced to the selection of k_m and $C(s)$ such that $C(S)\mathbf{C}^T H(s)$, which is independent of the uncertainties, has the desired transient and steady state performance, while simultaneously keeping the value of λ small. In general, k_m is selected such that $\mathbf{A}_m$ specifies the desired closed loop response, while $C(s)$ is designed such that the uncertainties within the desired frequencies are compensated for, and such that the controller reacts fast enough to track the desired reference signals.

As we can see, choosing a large bandwidth for the filter $C(s)$ is beneficial for performance. Another proof of this is by considering the reference control signal in (3.54). Letting $k \to \infty$ we get $C(s) \to 1$ and thus the reference controller perfectly cancels the uncertainties, and becomes the ideal system in (3.24). However, for $C(s) = 1$, $H_1(s)$ is improper, and thus its $\mathcal{L}_1$-norm does not exist. This implies that the bound on the controller in theorem 3.2.1 is lost,

and we get the same problems as discussed in section 3.2.4. Further, from (3.61) we see that increasing the bandwidth of $C(s)$makes the time delay margin go to zero.

As we can see, the choice of the filter $C(s)$ controls the trade-off between robustness and performance. The optimal design of $C(s)$ with respect to robustness and performance is the main design challenge of the $\mathcal{L}_1$ adaptive control theory. There is different methods for optimizing $C(s)$ based on robustness and performance specifications. [7] chapter 2.6 and [23] concerns and provide design guidelines for this topic. However, this problem is still largely open and hard to address [7].

3.4 SISO systems with matched nonlinear uncertainties

In this section the $\mathcal{L}_1$ adaptive control strategy and the theoretical results for systems with nonlinear matched uncertainties are presented. This a new step towards the final goal of controlling systems on the general form of (3.2). In the design and theoretical analysis of the $\mathcal{L}_1$ adaptive controller considered in this section, a lot of definitions are made, and it is challenging to get a good grip on the results. Thus, a section summing up the main results is included. As before, the $\mathcal{L}_1$ adaptive controller consists of a state predictor, an adaptive law and a control law, subject to an $\mathcal{L}_1$-norm condition.

3.4.1 Problem formulation

In this section we consider systems on the form:

$$\begin{aligned} \dot{\mathbf{x}}(t) &= \mathbf{A}_m\mathbf{x}(t) + \mathbf{B}(\omega u_{ad}(t) + f(t,\mathbf{x}(t))),\ \mathbf{x}(0) = \mathbf{x}_0 \\ y(t) &= \mathbf{C}^T\mathbf{x}(t), \end{aligned} \tag{3.65}$$

where $\mathbf{x}(t) \in \mathbb{R}^n$ is the measured system state; $\mathbf{A}_m \in \mathbb{R}^{n\times n}$ is a known Hurwitz matrix specifying the desired-closed loop dynamics; $\mathbf{B}, \mathbf{C} \in \mathbb{R}^n$ are known constant vectors; $u_{ad}(t) \in \mathbb{R}$ is the control input; $\omega \in \mathbb{R}$ is an unknown constant parameter with known sign, representing uncertainty in the system input gain; $f(t,\mathbf{x}) : \mathbb{R} \times \mathbb{R}^n \to \mathbb{R}$ is an unknown nonlinear map continuous in its arguments; and $y(t) \in \mathbb{R}$ is the regulated output. The initial states are assumed to be inside an arbitrarily large known set, that is $\|\mathbf{x}_0\|_\infty \leq \rho_0 < \infty$ with known $\rho_0 > 0$.

Assumptions

To prove the theoretical results of this section, some assumptions to the systems in (3.65) have to be made.

Assumption 3.4.1 (Partial knowledge of uncertain system input gain). *Let*

$$\omega \in \Omega := [\omega_l,\ \omega_u],$$

where $0 < \omega_l < \omega_u$ are given known conservative lower and upper bounds on ω.
Assumption 3.4.2 (Uniform boundedness of $\mathbf{f}(\mathbf{t}, \mathbf{0})$). *There exist $B > 0$ such that*

$$|f(t,0)| \leq B, \ \forall\, t \geq 0.$$

Assumption 3.4.3 (Semiglobal uniform boundedness of partial derivatives). *For arbitrary $\delta > 0$ there exist $d_{f_x}(\delta) > 0$ and $d_{f_t}(\delta) > 0$ independent of time, such that for arbitrary $\|\mathbf{x}\|_\infty \leq \delta$, the partial derivatives of $f(t,x)$ are piecewise-continuous and bounded,*

$$\left\| \frac{\delta f(t,x)}{\delta x} \right\|_1 \leq d_{f_x}(\delta), \ \left| \frac{\delta f(t,x)}{\delta t} \right| \leq d_{f_t}(\delta),$$

3.4.2 Limitations in the problem formulation

Compared to (3.2) we see that the formulation (3.104) still puts some limitations on the systems considered. This section concerns this limitations and names the assumptions needed to get from (3.2) to (3.104).

Now, as we consider systems with nonlinear dynamics with respect to time and state, we do not have to assume a linear function $f_x(\,\cdot\,)$, we do however need to assume a linear function $f_u(\,\cdot\,)$:
Assumption 3.4.4 (Linear time-varying input function). *The function $f_u(t, \mathbf{x}(t), \mathbf{u}(t)) : \mathbb{R} \times \mathbb{R}^n \to \mathbb{R}^n$ is linear and time-varying, according to*

$$f_u(t, \mathbf{x}(t), \mathbf{u}(t)) = \mathbf{B}_{real}(t)(u(t) + \sigma_1(t))$$

where $\mathbf{B}_{real}(t) \in \mathbb{R}^n$ is the real unknown time-varying input vector, and $\sigma_1(t) \in \mathbb{R}$ is the input disturbance.

This gives the new real system

$$\begin{aligned} \dot{\mathbf{x}}(t) &= f_x(t, \mathbf{x}(t)) + \mathbf{B}_{real}(t)(u(t) + \sigma_1(t)) \\ y(t) &= \mathbf{C}^T \mathbf{x}(t), \end{aligned} \tag{3.66}$$

where $\mathbf{x}(t) \in \mathbb{R}^n$ is the measured system state vector, $u(t) \in \mathbb{R}$ is the control signal, $y(t) \in \mathbb{R}$ is the regulated output, $B_{real}(t) \in \mathbb{R}^n$ is the real unknown time-varying input vector, $C \in \mathbb{R}^n$ is the known constant output vector, $f_x(t, \mathbf{x}(t)) : \mathbb{R} \times \mathbb{R}^n \to \mathbb{R}^n$ is the unknown nonlinear map, and $\sigma(t) \in \mathbb{R}$ is the unknown input disturbance.

Through modelling and system identification, as described in chapter 2, the identified linearised system (3.1) is found. Again, we define the identified system matrix $\mathbf{A}_{id}$, and we define the identified input vector $\mathbf{B}_{id}$. As discussed, we know that the identified system matrix and input vector will not be able to model the nonlinear system correctly. To get from (3.66) to (3.65), we again need to make some additional assumptions.

Assumption 3.4.5 (Linear relationship between $\mathbf{B}_{real}$ and $\mathbf{B}_{id}$). *The input vector $\mathbf{B}_{real}(t)$ is constant, that is $\mathbf{B}_{real}(t) \equiv \mathbf{B}_{real}$, and there exist a constant vector $B_{id} \in \mathbb{R}^n$ and a constant scalar $\omega \in \mathbb{R}$ such that*

$$\mathbf{B}_{real} = \mathbf{B}_{id}\omega.$$

ω is also assumed to belong to the set $\Omega := [\omega_l,\ \omega_u]$, where $0 < \omega_l < \omega_u$.

Assumption 3.4.6 (Matched modelling error). *There exist a matrix $\mathbf{A}_{id} \in \mathbb{R}^{n\times n}$ and a nonlinear function $f_1(t, \mathbf{x}(t)) : \mathbb{R} \times \mathbb{R}^n \to \mathbb{R}$, continuous in its arguments, such that $(\mathbf{A}_{id}, \mathbf{B}_{real})$ is controllable, and*

$$f_x(t, \mathbf{x}(t)) - \mathbf{A}_{id}\mathbf{x} = \mathbf{B}_{real} f_1(t, \mathbf{x}(t)).$$

By substituting for f_x in (3.66) using assumption 3.4.6, we get

$$\begin{aligned} \dot{\mathbf{x}}(t) &= \mathbf{A}_{id}\mathbf{x} + \mathbf{B}_{real}\left(u(t) + f_1(t, \mathbf{x}(t)) + \sigma_1(t)\right),\ \mathbf{x}(0) = \mathbf{x}_0 \\ y(t) &= \mathbf{C}^T\mathbf{x}(t), \end{aligned} \tag{3.67}$$

As before, and based on the same argumentation, we introduce the control structure

$$u(t) = u_m(t) + u_{ad}(t),\ u_m(t) = -\mathbf{K}_m^T\mathbf{x}(t), \tag{3.68}$$

where $\mathbf{K}_m \in \mathbb{R}^n$ makes $\mathbf{A}_m := \mathbf{A}_{id} - \mathbf{B}_{id}\mathbf{K}_m^T$ Hurwitz and specifies the desired closed loop dynamics, and u_{ad} is the adaptive component. Substituting for $\mathbf{B}_{real}$ and $u(t)$ in (3.67) using assumption 3.4.5 and (3.68), we get

$$\begin{aligned} \dot{\mathbf{x}}(t) &= \mathbf{A}_{id}\mathbf{x}(t) + \mathbf{B}_{id}\omega\left(-\mathbf{K}_m^T\mathbf{x}(t) + u_{ad} + f_1(t, \mathbf{x}(t)) + \sigma_1(t)\right) \\ &= \left(\mathbf{A}_{id} - \mathbf{B}_{id}\mathbf{K}_m^T\omega\right)\mathbf{x}(t) + \mathbf{B}_{id}\left(\omega u_{ad} + \omega f_1(t, \mathbf{x}(t)) + \omega\sigma_1(t)\right) \\ &= \mathbf{A}_m\mathbf{x}(t) + \mathbf{B}_{id}\mathbf{K}_m^T\left(1 - \omega\right)\mathbf{x}(t) + \mathbf{B}_{id}\left(\omega u_{ad} + \omega f_1(t, \mathbf{x}(t)) + \omega\sigma_1(t)\right) \\ y(t) &= \mathbf{C}^T\mathbf{x}(t),\ \mathbf{x}(0) = \mathbf{x}_0. \end{aligned}$$

By defining

$$f(t, \mathbf{x}(t)) := \omega f_1(t, \mathbf{x}(t)) + \mathbf{K}_m^T(1 - \omega)\mathbf{x}(t) + \omega\sigma_1(t), \tag{3.69}$$

we get

$$\begin{aligned} \dot{\mathbf{x}}(t) &= \mathbf{A}_m\mathbf{x}(t) + \mathbf{B}_{id}\left(\omega u_{ad} + f(t, \mathbf{x}(t))\right), \mathbf{x}(0) = \mathbf{x}_0 \\ y(t) &= \mathbf{C}^T\mathbf{x}(t), \end{aligned} \tag{3.70}$$

which has the same structure as (3.65).

3.4.3 $\mathcal{L}_1$ adaptive control architecture

Consider the system in (3.66):

$$\begin{aligned} \dot{\mathbf{x}}(t) &= \mathbf{A}_m\mathbf{x}(t) + \mathbf{B}(\omega u_{ad}(t) + f(t, \mathbf{x}(t))),\ \mathbf{x}(0) = \mathbf{x}_0 \\ y(t) &= \mathbf{C}^T\mathbf{x}(t), \end{aligned} \tag{3.71}$$

As before, the control objective is to design a full-state feedback $\mathcal{L}_1$ adaptive controller which ensure that $y(t)$ tracks a given bounded piecewise-continuous reference signal $r(t)$ with quantifiable performance bounds.

State predictor

Again we need to specify a state predictor as a reference to the system responce. To be able to find adaptive laws for systems specified by (3.65) we need to parametrize the nonlinear function $f(t, \mathbf{x}(\mathbf{t}))$. We consider the following state predictor:

$$\begin{aligned} \dot{\hat{\mathbf{x}}} &= \mathbf{A}_m\hat{\mathbf{x}}(t) + \mathbf{B}(\hat{\omega}(t)u_{ad}(t) + \hat{\theta}(t)\|\mathbf{x}(t)\|_\infty + \hat{\sigma}), \quad \hat{\mathbf{x}}_0 = x_0, \\ \hat{y} &= \mathbf{C}^T\hat{\mathbf{x}}(t), \end{aligned} \tag{3.72}$$

where $\hat{\omega} \in \mathbb{R}$, and $\hat{\sigma} \in \mathbb{R}$ are adaptive estimates. This semi-linear formulation is similar to the linear formulation considered in the previous section. The reason for this choice of predictor will be clear shortly.

Adaptive Laws:

Similar to the previous section, the estimates are updated according to

$$\begin{aligned} \dot{\hat{\omega}}(t) &= \Gamma\text{Proj}(\hat{\omega}(t), -\tilde{\mathbf{x}}^T(t)\mathbf{P}\mathbf{B}u_{ad}(t)), \ \hat{\omega}(0) = \hat{\omega}_0 \in \Omega, \\ \dot{\hat{\theta}}(t) &= \Gamma\text{Proj}(\hat{\theta}(t), -\tilde{\mathbf{x}}^T(t)\mathbf{P}\mathbf{B}\|\mathbf{x}(t)\|_\infty), \ \hat{\theta}(0) = \hat{\theta}_0 \in \Theta, \\ \dot{\hat{\sigma}}(t) &= \Gamma\text{Proj}(\hat{\sigma}(t), -\tilde{\mathbf{x}}^T(t)\mathbf{P}\mathbf{B}), \ \hat{\sigma}(0) = \hat{\sigma} \in \Delta, \end{aligned} \tag{3.73}$$

where $\tilde{\mathbf{x}} := \hat{\mathbf{x}}(t) - \mathbf{x}(t)$, $\Gamma \in \mathbb{R}^+$ is the adaption gain, while $\mathbf{P} = \mathbf{P}^T > 0$ is the solution to the agebraic Lyapunov equation $\mathbf{A}_m^T\mathbf{P} + \mathbf{P}\mathbf{A}_m = -\mathbf{Q}$, for arbitrary $\mathbf{Q} = \mathbf{Q}^T > 0$. The projection operator ensures that $\hat{\omega}(t) \in \Omega$, $\hat{\theta}(t) \in \Theta := [-\theta_b, \theta_b]$, $|\hat{\sigma}(t)| \leq \Delta$, where θ_b and Δ are defined as

$$\theta_b := d_{f_x}(\rho), \quad \Delta := B + \epsilon, \tag{3.74}$$

where ρ is defined in (3.79) and $\epsilon > 0$.

Control law

As before, we want the control signal to compensate for the uncertainties and track the reference $r(t)$ with zero steady-state error. Similar to (3.43) the control law is given by

$$u_{ad}(s) = -kD(s)(\hat{\eta}(s) - k_g r(s)), \tag{3.75}$$

where $\hat{\eta}(s)$ and $r(s)$ are the Laplace transforms of $\hat{\eta}(t) := \hat{\omega}(t)u_{ad} + \hat{\theta}(t)\|\mathbf{x}(t)\|_\infty + \hat{\sigma}(t)$ and $r(t)$ respectively, and $k_g := -1/\mathbf{C}^T\mathbf{A}_m^{-1}\mathbf{B}$. As in the previous section, $k > 0$ is a feedback gain and $D(s)$ is a strictly proper transfer function leading to a strictly proper stable

$$C(s) := \frac{\omega k D(s)}{1 + \omega k D(s)} \ \forall\, \omega \in \Omega_0, \tag{3.76}$$

with DC gain $C(0) = 1$.

$\mathcal{L}_1$-norm condition

Now the sufficient $\mathcal{L}_1$-norm condition for stability is presented. This require some definitions.

Since $\mathbf{A}_m$ is Hurwitz, $\|x_{in}\|_{\mathcal{L}_\infty} \leq \rho_{in}$ [7], where $\rho_{in} := \|s(s\mathbb{I} - \mathbf{A}_m)^{-1}\|_{\mathcal{L}_\infty}\rho_0$, $x_{in}(s) := (s\mathbb{I} - \mathbf{A}_m)^{-1}\mathbf{x}_0$ as before, and ρ_0 is previously defined as the bound on $\mathbf{x}_0$. Further, we define

$$L_\delta := \frac{\bar{\delta}(\delta)}{\delta} d_{f_x}(\bar{\delta}(\delta)),\ \bar{\delta}(\delta) := \delta + \bar{\gamma}_1, \tag{3.77}$$

where $d_{f_x}(\,\cdot\,)$ was introduced in assumption 3.4.2 and $\bar{\gamma} > 0$ is an arbitrary positive constant.

To be able to prove stability and the performance bounds, k and $D(s)$ also need to ensure that for a given ρ_0, there exist $\rho_r > \rho_{in}$, such that the following $\mathcal{L}_1$-norm condition can be met:

$$\|G(s)\|_{\mathcal{L}_1} < \frac{\rho_r - \|H(s)C(s)k_g\|_{\mathcal{L}_1}\|r\|_{\mathcal{L}_\infty} - \rho_{in}}{L_{\rho_r}\rho_r + B}, \tag{3.78}$$

where $G(s) := H(s)(1 - C(s))$, $H(s) := (S\mathbb{I} - A_m)^{-1}b$.

The $\mathcal{L}_1$ adaptive controller is defined by combining the feedback controller defined in (3.68), the predictor (3.72), the adaptation rule (3.73) and the adaptive control law (3.75) subject to the $\mathcal{L}_1$-norm condition in (3.78).

3.4.4 Theoretical results

The following part presents the main theoretical results for the $\mathcal{L}_1$ adaptive controller considered in this section. The proofs are ommitted in this text, but can be found in [7].

Definitions

Before we continue, we make some definitions to make the following text easier to read. Let

$$\rho := \rho_r + \bar{\gamma}_1, \tag{3.79}$$

where ρ_r and $\bar{\gamma}_1$ were introduced in (3.78) and (3.77) respectively, and we let γ_1 be given by

$$\gamma_1 := \frac{\|C(s)\|_{\mathcal{L}_1}}{1 - \|G(s)\|_{\mathcal{L}_1}L_{\rho_r}}\gamma_0 + \beta, \tag{3.80}$$

where β and γ_0 are arbitrary small positive constants such that $\gamma_1 \leq \bar{\gamma}_1$. Further, let

$$\rho_u := \rho_{ur} + \gamma_2, \tag{3.81}$$

where ρ_{ur} and γ_2 are defined as

$$\rho_{ur} := \left\| \frac{C(s)}{\omega} \right\|_{\mathcal{L}_1} (|k_g| \|r\|_{\mathcal{L}_\infty} + L_{\rho_r} \rho_r + B). \tag{3.82}$$

$$\gamma_2 := \left\| \frac{C(s)}{\omega} \right\|_{\mathcal{L}_1} L_{\rho_r} \gamma_1 + \left\| \frac{H_1(s)}{\omega} \right\|_{\mathcal{L}_1} \gamma_0, \tag{3.83}$$

where $H_1(s) = C(s) \frac{1}{c_0^T H(s)} c_0^T$ was defined in (3.6).

Equivalent semi-linear time-varying system

Next we show how the nonlinear system can be transformed to an equivalent semi-linear time varying system. This result supports the choice of state predictor and adaptation laws. Subject to assumption 3.4.2 and 3.4.3, the following holds, [7]

Lemma 3.4.1. *Let $\mathbf{x}(t)$ be a continuous and (piecewise)-differentiable function of t for $t \geq 0$. If $\|\mathbf{x}_\tau\|_{\mathcal{L}_\infty} \leq \rho$ and $\|\dot{\mathbf{x}}_\tau\|_{\mathcal{L}_\infty} \leq d_x$ for $\tau \geq 0$, where ρ and d_x are some positive constants, then there exist continuous $\theta(t)$ and $\sigma(t)$ with (piecewise)-continuous derivative, such that for all $t \in [0, \tau]$*

$$f(t, \mathbf{x}(t)) = \theta(t) \|\mathbf{x}(t)\|_\infty + \sigma(t), \tag{3.84}$$

where

$$\begin{aligned} |\theta(t)| &< \theta_\rho, \quad |\dot{\theta}| < d_\theta, \\ |\sigma(t)| &< \sigma_b, \quad |\dot{\sigma}| < d_\sigma, \end{aligned} \tag{3.85}$$

with $\theta_\rho := d_{f_x}(\rho)$, $\sigma_b := B + \epsilon$, where $\epsilon > 0$ is an arbitrary constant, and d_θ, d_σ are computable bounds.

Since

$$\|\mathbf{x}_0\|_\infty \leq \rho_0 < \rho, \;\; u(0) = 0,$$

and $\mathbf{x}(t)$, $u(t)$ are continuous, there will always exist τ such that

$$\|\mathbf{x}_\tau\|_{\mathcal{L}_\infty} \leq \rho, \;\; \|u_\tau\|_{\mathcal{L}_\infty} \leq \rho_u \tag{3.86}$$

Thus, it follows from Lemma 3.4.1 that the system in (3.71) can be rewritten over $t \in [0, \tau]$ for arbitrary $\tau \geq 0$ as a semi-linear time-varying system:

$$\begin{aligned} \dot{\mathbf{x}} &= \mathbf{A}_m \mathbf{x}(t) + \mathbf{B}(\omega u(t) + \theta(t) \|\mathbf{x}(t)\|_\infty + \sigma(t)), \quad \mathbf{x}(0) = \mathbf{x}_0, \\ y &= \mathbf{C}^T \mathbf{x}(t), \end{aligned} \tag{3.87}$$

with the unknown parameters bounded according to

$$|\theta(t)| < \theta_b, \;\; |\sigma| < \Delta, \;\; \forall t \in [0, \tau]. \tag{3.88}$$

$$|\dot{\theta}(t)| < d_\theta(\rho, \rho_u), \;\; |\dot{\sigma}| < d_\sigma(\rho, \rho_u), \;\; \forall t \in [0, \tau], \tag{3.89}$$

where $d_\theta(\rho, \rho_u) > 0$ and $d_\sigma(\rho, \rho_u) > 0$ being the bounds specified by Lemma 3.4.1.

Prediction error

From (3.72) and (3.87) we get that over $[0, \tau]$ the prediction error dynamics can be written as

$$\dot{\tilde{\mathbf{x}}}(t) = \mathbf{A}_m \tilde{\mathbf{x}}(t) + \mathbf{B}\left(\tilde{\omega}(t)u(t) + \tilde{\theta}(t)\|\mathbf{x}(t)\|_\infty + \tilde{\sigma}(t)\right),\ \tilde{\mathbf{x}}(0) = 0, \tag{3.90}$$

where

$$\tilde{\omega}(t) := \hat{\omega}(t) - \omega, \quad \tilde{\theta}(t) := \hat{\theta}(t) - \theta(t), \quad \tilde{\sigma}(t) := \hat{\sigma} - \sigma(t) \tag{3.91}$$

The following result hold for the prediction error, [7]

Lemma 3.4.2. *For the system in* (3.90)*, if* $u(t)$ *is continuous, and moreover the following bounds hold:*

$$\|\mathbf{x}_\tau\|_{\mathcal{L}_\infty} \leq \rho, \ \ \|u_\tau\|_{\mathcal{L}_\infty} \leq \rho_u, \tag{3.92}$$

then

$$\|\tilde{\mathbf{x}}_\tau\|_{\mathcal{L}_\infty} \leq \sqrt{\frac{\theta_m(\rho, \rho_u)}{\lambda_{\min}(P)\Gamma}} \tag{3.93}$$

where

$$\theta_m(\rho, \rho_u) := 4\theta_b^2 + 4\Delta^2 + (\omega_u - \omega_l)^2 + 4\frac{\lambda_{\max}(P)}{\lambda_{\min}(q)}(\theta_b d_\theta(\rho, \rho_u) + \Delta d_\sigma(\rho, \rho_u)). \tag{3.94}$$

Performance

Again, we consider the reference system which specifies the best theoretically possible $\mathcal{L}_1$ adaptive control result.

$$\begin{aligned}
\dot{\mathbf{x}}_{ref}(t) &= \mathbf{A}_m \mathbf{x}_{ref}(t) + \mathbf{B}\left(\omega u_{ref}(t) + f(t, \mathbf{x}_{ref}(t))\right),\ \mathbf{x}_{ref}(0) = \mathbf{x}_0, \\
u_{ref}(s) &= \frac{C(s)}{\omega}\left(k_g r(s) - \eta_{ref}(s)\right), \\
y_{ref}(t) &= \mathbf{C}^T \mathbf{x}_{ref}(t)
\end{aligned} \tag{3.95}$$

where $\eta_{ref}(s)$ is the Laplace transform of the signal $\eta_{ref}(s) := f(t, x_{ref}(t))$. The following result holds for the stability of the reference system [7]

Lemma 3.4.3. *For the closed-loop reference system in* (3.95)*, subject to the* $\mathcal{L}_1$*-norm condition in* (3.78)*, if*

$$\|\mathbf{x}_0\|_\infty \leq \rho_0$$

then

$$\|\mathbf{x}_{ref}\|_{\mathcal{L}_\infty} < \rho_r, \tag{3.96}$$

$$\|u_{ref}\|_{\mathcal{L}_\infty} < \rho_{ur}, \tag{3.97}$$

where ρ_r *and* ρ_{ur} *were introduced in* (3.78) *and* (3.82) *respectively.*

The following theorem is the main theoretical result of this section, and gives the relationship between the adaptation gain, the prediction error, and the performance of the controller relative to the reference system. The proof is found in [7].

Theorem 3.4.1. *Consider the closed-loop reference system in* (3.95) *and the closed-loop system consisting of the system in* (3.71) *and* $\mathcal{L}_1$ *adaptive controller in* (3.72), (3.73) *and* (3.75) *subject to the* $\mathcal{L}_1$*-norm condition* (3.78)*. If the adaptive gain is chosen to verify the design constraint*

$$\Gamma \geq \frac{\theta_m(\rho, \rho_u)}{\lambda_{\min}(P)\gamma_0^2}, \tag{3.98}$$

then we have

$$\|\tilde{\mathbf{x}}\|_{\mathcal{L}_\infty} \leq \gamma_0, \tag{3.99}$$
$$\|\mathbf{x}_{ref} - \mathbf{x}\|_{\mathcal{L}_\infty} \leq \gamma_1, \tag{3.100}$$
$$\|u_{ref} - u\|_{\mathcal{L}_\infty} \leq \gamma_2, \tag{3.101}$$

where γ_1 *and* γ_2 *are as defined in* (3.80) *and* (3.83)*, respectively.*

Remarks

First, consider the $\mathcal{L}_1$-norm condition in (3.78). This slightly more complex formulation, as compared to the $\mathcal{L}_1$- norm condition in (3.47), is due to the assumption of semiglobal boundedness of the partial derivatives of $f(t, \mathbf{x}(t))$ in assumption 3.4.2. If $f(t, \mathbf{x}(t))$ has a uniform bound for the partial derivative with respect to $\mathbf{x}$, that is, $\|\frac{\delta f}{\delta \mathbf{x}}\| \leq d_{f_x} = L$ for all $\mathbf{x} \in \mathbb{R}$, then

$$\lim_{\rho_r \to \infty} \frac{\rho_r - \|H(s)C(s)k_g\|_{\mathcal{L}_\infty} - \rho_{in}}{L\rho_r + B} = \frac{1}{L}. \tag{3.102}$$

Thus, the $\mathcal{L}_1$-norm condition in (3.78) changes to

$$\|G(s)\|_{\mathcal{L}_1} L < 1, \tag{3.103}$$

which is the same as the $\mathcal{L}_1$-norm condition (3.47), considered in the previous section.

From theorem 3.4.1 we see that we can achieve an arbitrarily small prediction error γ_0 by increasing the adaptation gain Γ. From (3.80) and (3.83) we see that by minimising γ_0, we can achieve arbitrarily small performance bounds γ_1 and γ_2 simultaneously. Thus, we can achieve arbitrary close tracking performance for both the output and the input signal simultaneously, both in transient and steady-state, by increasing the adaptation gain.

The theory on $\mathcal{L}_1$ adaptive control include no analytical bound on the time delay-margin for nonlinear systems, such as the result presented in the previous section. By letting $k \to \infty$ and thus $C(s) \to 1$, we again see that the reference controller cancels the uncertainties perfectly, and equals the ideal system. However as before, setting $C(s) = 1$ takes away the uniform bound on the control signal.

3.5 MIMO systems with unmatched nonlinear uncertainties

In this section, the $\mathcal{L}_1$ adaptive control strategy and the theoretical results for general nonlinear systems are presented. This is the final goal for the $\mathcal{L}_1$ adaptive control design considered in this text. The design and the theory presented in this section is quite similar to the design and theory presented in the previous section. Until now, all the uncertainties considered has been assumed matched. This assumption imposes major limitations to the systems considered. This section shows how the $\mathcal{L}_1$ adaptive controller can be redesigned to cope with unmatched uncertainties. Further, the design is made for multivariable systems, which is important for the lateral model. With this design we will see that we only need to make some minor assumptions on the system in (3.2), and we thus achieve the final goal of this text. The problem formulation considered in this section is not explicitly described in [7], but is based on the theory presented there. All the results presented in this section can be reformulated without any loss of generality, such that the proofs in [7] can be used.

3.5.1 Problem formulation

In this section, we consider systems on the form:

$$\begin{aligned}\dot{\mathbf{x}}(t) &= \mathbf{A}_m\mathbf{x}(t) + \mathbf{B}_m\boldsymbol{\omega}\mathbf{u}_{ad}(t) + \mathbf{f}(t,\mathbf{x}(t)),\ \mathbf{x}(0) = \mathbf{x}_0 \\ \mathbf{y}(t) &= \mathbf{C}^T\mathbf{x}(t),\end{aligned} \tag{3.104}$$

where $\mathbf{x}(t) \in \mathbb{R}^n$ is the measured system state; $\mathbf{A}_m \in \mathbb{R}^{n\times n}$ is a known Hurwitz matrix specifying the desired-closed loop dynamics; $\mathbf{B}_m \in \mathbb{R}^{n\times m}$ is a known full-rank constant matrix, $(\mathbf{A}_m, \mathbf{B}_m)$ is observable; $\mathbf{C} \in \mathbb{R}^{n\times m}$ is a known full-rank constant matrix, $(\mathbf{A}_m, \mathbf{C})$ is observable; $u_{ad}(t) \in \mathbb{R}^m$ is the control input ($m \leq n$); $\omega \in \mathbb{R}^{m\times m}$ is the uncertain system input gain matrix; $f(t,\mathbf{x}) : \mathbb{R}\times\mathbb{R}^n \to \mathbb{R}^n$ is an unknown nonlinear map continuous in its arguments; and $y(t) \in \mathbb{R}^m$ is the regulated output. The initial states are assumed to be inside an arbitrarily large known set, that is $\|\mathbf{x}_0\|_\infty \leq \rho_0 < \infty$ with known $\rho_0 > 0$.

Again we consider the system (3.2), now for multiple inputs and outputs. First, we need to make a minor assumptions on $\mathbf{f}_u(\,\cdot\,)$.

Assumption 3.5.1 (Linear relationship with respect to u). *The function $\mathbf{f}_u(t,\mathbf{x}(t),\mathbf{u}(t)) : \mathbb{R}\times\mathbb{R}^n\times\mathbb{R}^m \to \mathbb{R}^n$ is linear and time-varying with respect to u, according to*

$$f_u(t,\mathbf{x}(t),\mathbf{u}(t)) = \mathbf{B}_{real}(t,\mathbf{x}(t))\mathbf{u}(t),$$

where $\mathbf{B}_{real}(t,\mathbf{x}(t)) \in \mathbb{R}^{n\times m}$ is the real unknown time-varying input vector.

If the controller can deal with time-varying B_{real}-matrix, most cases are probably covered by this formulation. The new real system formulation becomes:

$$\begin{aligned}\dot{\mathbf{x}}(t) &= \mathbf{f}_x(t,\mathbf{x}(t)) + \mathbf{B}_{real}(t,\mathbf{x}(t))\mathbf{u}(t) \\ \mathbf{y}(t) &= \mathbf{C}^T\mathbf{x}(t),\end{aligned} \tag{3.105}$$

where $\mathbf{x}(t) \in \mathbb{R}^n$ is the measured system state vector, $u(t) \in \mathbb{R}^m$ is the control signal, $y(t) \in \mathbb{R}^m$ is the regulated output, $\mathbf{B}_{real}(t, \mathbf{x}(t)) \in \mathbb{R}^{n \times m}$ is the real unknown input vector, $C \in \mathbb{R}^{n \times m}$ is the known constant output vector, and $f_x(t, \mathbf{x}(t)) : \mathbb{R} \times \mathbb{R}^n \to \mathbb{R}^n$ is the unknown nonlinear map.

Through modelling and system identification, as described in chapter 2, The linearised system (3.1) is found. Again, we define the identified system matrix $\mathbf{A}_{id}$, and we define the identified input vector $\mathbf{B}_{id}$. We need that $(\mathbf{A}_{id}, \mathbf{B}_{id})$ is controllable. As before, the identified system matrix and input vector will not be able to model the nonlinear system correctly. However, unlike the previous sections we do not need to make any assumptions to get from the real system (3.105) to the starting point for the $\mathcal{L}_1$ theory (3.104). It is sufficient with some definitions. First we define:

$$\tilde{\mathbf{f}}_x(t, \mathbf{x}(t)) := \mathbf{f}_x(t, \mathbf{x}(t)) - \mathbf{A}_{id}\mathbf{x}, \tag{3.106}$$

$$\tilde{\mathbf{B}}(t, \mathbf{x}(t)) := \mathbf{B}_{real}(t, \mathbf{x}(t)) - \mathbf{B}_{id}\boldsymbol{\omega}, \tag{3.107}$$

where $\tilde{\mathbf{f}} : \mathbb{R} \times \mathbb{R}^n \to \mathbb{R}^n$ is an unknown nonlinear function, $\tilde{\mathbf{B}} \in \mathbb{R}^{n \times m}$ is an unknown matrix, and $\boldsymbol{\omega} \in \mathbb{R}m \times m$ is an unknown matrix. We see that the use of $\boldsymbol{\omega}$ is not really necessary. It could be set to 1, and it would only change the value of $\tilde{\mathbf{B}}$.

Substituting for $\mathbf{f}_x$ and $\mathbf{B}_{real}$ in (3.105) using these definitions, we get

$$\begin{aligned} \dot{\mathbf{x}}(t) &= \mathbf{A}_{id}\mathbf{x}(t) + \mathbf{B}_{id}\boldsymbol{\omega}\mathbf{u}(t) + \tilde{\mathbf{f}}_x(t, \mathbf{x}(t)) + \tilde{\mathbf{B}}(t, \mathbf{x}(t))\mathbf{u}(t) \\ \mathbf{y}(t) &= \mathbf{C}^T\mathbf{x}(t) \end{aligned} \tag{3.108}$$

As before, we introduce the control structure

$$\mathbf{u}(t) = \mathbf{u}_m + \mathbf{u}_{ad}, \;\; \mathbf{u}_m(t) = -\mathbf{K}_m^T\mathbf{x}(t), \tag{3.109}$$

where $\mathbf{K}_m \in \mathbb{R}^{n \times m}$ makes $\mathbf{A}_m := \mathbf{A}_{id} - \mathbf{B}_{id}\mathbf{K}_m^T$ Hurwitz and specifies the desired closed loop dynamics, and $\mathbf{u}_{ad}$ is the adaptive component. Substituting for $\mathbf{u}(t)$ in (3.108) using (3.109), we get

$$\begin{aligned} \dot{\mathbf{x}}(t) &= \mathbf{A}_{id}\mathbf{x}(t) + \mathbf{B}_{id}\boldsymbol{\omega}(\mathbf{u}_{ad} - \mathbf{K}_m^T\mathbf{x}(t)) + \tilde{\mathbf{f}}_x(t, \mathbf{x}(t)) + \tilde{\mathbf{B}}(t, \mathbf{x}(t))(\mathbf{u}_{ad} - \mathbf{K}_m^T\mathbf{x}(t)) \\ &= \mathbf{A}_m\mathbf{x}(t) + \mathbf{B}_{id}\boldsymbol{\omega}\mathbf{u}_{ad} + \mathbf{B}_{id}\mathbf{K}_m^T(\mathbb{I} - \boldsymbol{\omega})\mathbf{x}(t) + \tilde{\mathbf{f}}_x(t, \mathbf{x}(t)) \\ &\quad + \tilde{\mathbf{B}}(t, \mathbf{x}(t))(\mathbf{u}_{ad} - \mathbf{K}_m^T\mathbf{x}(t)) \\ \mathbf{y}(t) &= \mathbf{C}^T\mathbf{x}(t), \;\; \mathbf{x}(0) = \mathbf{x}_0 \end{aligned}$$

By defining

$$\mathbf{f}(t, \mathbf{x}(t)) := \mathbf{B}_{id}\mathbf{K}_m^T(\mathbb{I} - \boldsymbol{\omega})\mathbf{x}(t) + \tilde{\mathbf{f}}_x(t, \mathbf{x}(t)) + \tilde{\mathbf{B}}(t, \mathbf{x}(t))(\mathbf{u}_{ad} - \mathbf{K}_m^T\mathbf{x}(t)), \tag{3.110}$$

we get

$$\dot{\mathbf{x}}(t) = \mathbf{A}_m\mathbf{x}(t) + \mathbf{B}_{id}\boldsymbol{\omega}\mathbf{u}_{ad} + \mathbf{f}(t, \mathbf{x}(t)), \;\; \mathbf{x}(0) = \mathbf{x}_0 \tag{3.111}$$

$$\mathbf{y}(t) = \mathbf{C}^T\mathbf{x}(t), \tag{3.112}$$

which has the same structure as (3.104). Considering the definition of $\mathbf{f}$ in 3.110, we see a possible problem due to the dependency of u_{ad}. u_{ad} is dependent on the input $r(t)$ and nonlinearly on the states $x(t)$. This should thus not be a problem, but it may be difficult to find the limits for this function.

Reformulation

(3.104) can be written as

$$\begin{aligned}\dot{\mathbf{x}}(t) &= \mathbf{A}_m\mathbf{x}(t) + \mathbf{B}_m(\boldsymbol{\omega}\mathbf{u}_{ad}(t) + \mathbf{f}_1(t,\mathbf{x}(t))) + \mathbf{B}_{um}\mathbf{f}_2(t,\mathbf{x}(t))\ \mathbf{x}(0) = \mathbf{x}_0 \\ \mathbf{y}(t) &= \mathbf{C}^T\mathbf{x}(t),\end{aligned} \tag{3.113}$$

where $\mathbf{B}_{um} \in \mathbb{R}^{n\times n-m}$ is a constant matrix such that $\mathbf{B}_m^T\mathbf{B}_{um} = 0$ and $\text{rank}([\mathbf{B}_m, \mathbf{B}_{um}]) = n$; and $\mathbf{f}_1 : \mathbb{R}\times\mathbb{R}^n \to \mathbb{R}^m$ and $\mathbf{f}_2 : \mathbb{R}\times\mathbb{R}^n \to \mathbb{R}^{(n-m)}$ such that

$$\begin{bmatrix}\mathbf{f}_1(t,\mathbf{x}(t))\\ \mathbf{f}_2(t,\mathbf{x}(t))\end{bmatrix} = \left[\mathbf{B}_m\mathbf{B}_{um}\right]^{-1}\mathbf{f}(t,\mathbf{x}(t)). \tag{3.114}$$

In this way, $\mathbf{f}_1(\,\cdot\,)$ represents the matched component of the unknown nonlinearities, while $\mathbf{B}_{um}\mathbf{f}_2(\,\cdot\,)$ represents the unmatched uncertainties.

Assumptions

The assumptions needed to prove the theoretical results are almost the same as those for the case of matched uncertainties. However, some adjustments must be done since we consider a MIMO-system, and one new assumption is made due to the unmatched uncertainties.

Assumption 3.5.2 (Partial knowledge of uncertain system input gain). *The system input gain matrix $\boldsymbol{\omega}$ is assumed to be an unknown (nonsingular strictly row-diagonally dominant matrix with sgn(ω_{ii}) known. Also, we assume that there exists a known compact convex set Ω such that $\boldsymbol{\omega} \in \Omega \subset \mathbb{R}^{m\times m}$.*

Assumption 3.5.3 (Boundedness of $\mathbf{f_i}(\mathbf{t},\mathbf{0})$). *There exist $B_{i0} > 0$ such that $\|f_i(t,0)\|_\infty \leq B_{i0}$, holds for all $t \geq 0$, and for $i = 1, 2$.*

Assumption 3.5.4 (Semiglobal uniform boundedness of partial derivatives). *For $i = 1, 2$ and arbitrary $\delta > 0$ there exist $d_{f_{xi}}(\delta) > 0$ and $d_{f_{ti}}(\delta) > 0$ independent of time, such that for all $\|\mathbf{x}\|_\infty < \delta$, the partial derivatives of $f_i(t,x)$ are piecewise-continuous and bounded:*

$$\left\|\frac{\delta f_i(t,\mathbf{x})}{\delta\mathbf{x}}\right\|_\infty \leq d_{f_{xi}}(\delta),\ \left\|\frac{\delta f_i(t,\mathbf{x})}{\delta t}\right\|_\infty \leq d_{f_{ti}}(\delta), \tag{3.115}$$

where the first is a matrix induced ∞-norm, while the second is a vector ∞-norm.

Assumption 3.5.5 (Stability of matched transmission zeros). *The transmission zeros of the transfer matrix $H_m(s) = C(s\mathbb{I} - \mathbf{A}_m)^{-1}\mathbf{B}_m K_g(s)$ lie in the open left half plane.*

3.5.2 $\mathcal{L}_1$ adaptive control architecture

Consider the system in (3.113). The control objective is to design a full-state feedback $\mathcal{L}_1$ adaptive controller which ensures that $y(t)$ tracks the output response of a desired system $M(s)$ defined as

$$M(s) := C(s\mathbb{I} - \mathbf{A}_m)^{-1}\mathbf{B}_m K_g(s), \tag{3.116}$$

where $K_g(s)$ is a feedforward prefilter, to a given bounded piecewise-continuous reference signal $r(t)$ in both transient and steady-state, while all other signals remain bounded.

The slight change in control objective is due to the consideration of MIMO-systems. Thus it may be impossible to achieve tracking of all the references simultaneously. Now, the prefilter K_g has to be defined to give the desired properties, and different design methods from multivariable control theory may be used. In this text, the constant matrix

$$K_g = -(\mathbf{C}\mathbf{A}_\mathbf{m}^{-\mathbf{1}}\mathbf{B}_\mathbf{m})^{-1} \tag{3.117}$$

is used. This gives the diagonal elements of the desired transfer matrix DC gain equal to one, and the off-diagonal elements have zero DC gain. Before continuing, it is useful to include the following definitions:

$$H_{xm}(s) := (s\mathbb{I}_n - \mathbf{A}_m)^{-1}\mathbf{B}_m, \tag{3.118}$$
$$H_{xum}(s) := (s\mathbb{I}_n - \mathbf{A}_m)^{-1}\mathbf{B}_{um}, \tag{3.119}$$
$$H_m(s) := \mathbf{C}^T H_{xm}(s) = \mathbf{C}^T(s\mathbb{I}_n - \mathbf{A}_m)^{-1}\mathbf{B}_m, \tag{3.120}$$
$$H_{um}(s) := \mathbf{C}^T H_{xum}(s) = \mathbf{C}^T(s\mathbb{I}_n - \mathbf{A}_m)^{-1}\mathbf{B}_{um}. \tag{3.121}$$

In this section, the subscripts m and um refers to matched and unmatched respectively. We see that H_{xm} and H_m are the transfer functions from the matched input signals to the states and output respectively, while H_{xum} and H_{um} are the transfer functions from the unmatched input signals to the states and output respectively.

State predictor

As before, we need to specify a state predictor. Similar to the state predictor in the previous section, we parametrize the nonlinear functions $\mathbf{f}_1$ and $\mathbf{f}_2$, and consider the following state predictor:

$$\begin{aligned}\dot{\hat{\mathbf{x}}}(t) &= \mathbf{A}_m\hat{\mathbf{x}}(t) + \mathbf{B}_m(\hat{\boldsymbol{\omega}}\mathbf{u}(t) + \hat{\boldsymbol{\theta}}_1(t)\|\mathbf{x}_t\|_\infty + \hat{\boldsymbol{\sigma}}_1(t)) + \mathbf{B}_{um}(\hat{\boldsymbol{\theta}}_2(t)\|\mathbf{x}_t\|_\infty + \hat{\boldsymbol{\sigma}}_2(t)), \\ \hat{\mathbf{y}}(t) &= \mathbf{C}^T\hat{\mathbf{x}}(t),\end{aligned} \tag{3.122}$$

where $\hat{\boldsymbol{\omega}} \in \mathbb{R}^{m\times m}$, $\hat{\boldsymbol{\theta}}_1(t) \in \mathbb{R}^m$, $\hat{\boldsymbol{\sigma}}_1(t) \in \mathbb{R}^m$, $\hat{\boldsymbol{\theta}}_2(t) \in \mathbb{R}^{n-m}$, and $\hat{\boldsymbol{\sigma}}_2(t) \in \mathbb{R}^{n-m}$ are the adaptive estimates.

Adaptive laws

The following adaptive laws are similar to the ones considered in the previous section. However, now we need to update the estimates for both the matched and the unmatched part of

the uncertainties. The estimates are updated according to

$$\begin{aligned}
\dot{\hat{\boldsymbol{\omega}}}(t) &= \Gamma \text{Proj}(\hat{\boldsymbol{\omega}}(t), -(\tilde{\mathbf{x}}^T(t)\mathbf{P}\mathbf{B}_m)^T\mathbf{u}^T(t)), \;\; \hat{\boldsymbol{\omega}}(0) = \hat{\boldsymbol{\omega}}_0 \\
\dot{\hat{\boldsymbol{\theta}}}_1(t) &= \Gamma \text{Proj}(\hat{\boldsymbol{\theta}}_1(t), -(\tilde{\mathbf{x}}^T(t)\mathbf{P}\mathbf{B}_m)^T\|\mathbf{x}_t\|_\infty), \;\; \hat{\boldsymbol{\theta}}_1(0) = \hat{\boldsymbol{\theta}}_{1_0} \\
\dot{\hat{\boldsymbol{\sigma}}}_1(t) &= \Gamma \text{Proj}(\hat{\boldsymbol{\sigma}}_1(t), -(\tilde{\mathbf{x}}^T(t)\mathbf{P}\mathbf{B}_m)^T), \;\; \hat{\boldsymbol{\sigma}}_1(0) = \hat{\boldsymbol{\sigma}}_{1_0} \\
\dot{\hat{\boldsymbol{\theta}}}_2(t) &= \Gamma \text{Proj}(\hat{\boldsymbol{\theta}}_2(t), -(\tilde{\mathbf{x}}^T(t)\mathbf{P}\mathbf{B}_{um})^T\|\mathbf{x}_t\|_\infty), \;\; \hat{\boldsymbol{\theta}}_2(0) = \hat{\boldsymbol{\theta}}_{2_0} \\
\dot{\hat{\boldsymbol{\sigma}}}_2(t) &= \Gamma \text{Proj}(\hat{\boldsymbol{\sigma}}_2(t), -(\tilde{\mathbf{x}}^T(t)\mathbf{P}\mathbf{B}_{um})^T), \;\; \hat{\boldsymbol{\sigma}}_2(0) = \hat{\boldsymbol{\sigma}}_{2_0}
\end{aligned} \tag{3.123}$$

where $\tilde{\mathbf{x}} := \hat{\mathbf{x}}(t) - \mathbf{x}(t)$, $\Gamma \in \mathbb{R}^+$ is the adaption gain, while $\mathbf{P} = \mathbf{P}^T > 0$ is the solution to the agebraic Lyapunov equation $\mathbf{A}_m^T\mathbf{P} + \mathbf{P}\mathbf{A}_m = -\mathbf{Q}$, for arbitrary $\mathbf{Q} = \mathbf{Q}^T > 0$. The projection operator ensures that $\hat{\omega}(t) \in \Omega$, $\|\hat{\theta}(t)\|_\infty \leq \theta_{bi}$, $|\hat{\sigma}_i(t)| \leq \Delta_i$, where θ_{bi} and Δ_i are defined as

$$\theta_{bi} := L_{i\rho}, \quad \Delta_i := B_{i0} + \epsilon_i, \quad i = 1, 2, \tag{3.124}$$

where $L_{i\delta}$ is defined in (3.132), ρ is defined in (3.137), and $\epsilon_i > 0$.

Control law

As always, we want the control signal to compensate for the uncertainties and track the reference $r(t)$ with zero steady-state error. Similar to (3.75) the control law is given by

$$\mathbf{u}_{ad}(s) = -\mathbf{K}D(s)\hat{\eta}(s), \tag{3.125}$$

where $\hat{\eta}$ is the Laplace transform of the signal

$$\hat{\eta}(t) := \hat{\boldsymbol{\omega}}(t)\mathbf{u}(t) + \hat{\eta}_1(t) + \hat{\eta}_{2m}(t) - r_g(t) \tag{3.126}$$

with $r_g(s) := K_g(s)\mathbf{r}(s)$, $\hat{\eta}_{2m}(s) := H_m^{-1}(s)H_{um}(s)\hat{\eta}_2(s)$, and with $\hat{\eta}_1$ and $\hat{\eta}_2$ being defined as $\hat{\eta}_i(t) := \hat{\theta}_i(t)\|\mathbf{x}(t)\|_\infty + \hat{\sigma}_i(t), i = 1, 2$. The prefilter $K_g(s)$ is given in (3.117).

Compared to the control law in the previous section, $\eta(s)$ is defined a bit different. This is due to the unmatched uncertainties. The purpose of the controller is to compensate for the uncertainties. However, the control signal can not compensate for the unmatched uncertainties directly. This can be solved by inverting the matrices, or by consider the transfer matrices. Here, the latter solution is used. By saying that we only want the control signal to compensate for the part of the unmatched uncertainties which affects the output, the goal becomes:

$$\frac{y}{u}(s)u(s) = \frac{y}{\eta_2}(s)\hat{\eta}_2(s) \tag{3.127}$$

Using the definitions in (3.120) and (3.121) we get

$$H_m(s)u(s) = H_{um}(s)\hat{\eta}_2(s) \tag{3.128}$$

$$u(s) = H_m^{-1}(s)H_{um}(s)\hat{\eta}_2 \tag{3.129}$$

This derivation explains the choice of η_{2m}. This is also the reason for the need of assumption 3.5.5. Similar to before, $K \in \mathbb{R}^{m\times m}$ is the feedback gain matrix, and $D(s)$ is a $m \times m$ strictly proper transfer matrix, which lead, for all $\omega \in \Omega$, to a strictly proper stable

$$C(s) := \boldsymbol{\omega}\mathbf{K}D(s)(\mathbb{I}_m + \boldsymbol{\omega}\mathbf{K}D(s))^{-1}, \tag{3.130}$$

with DC-gain $C(0) = \mathbb{I}_m$. Due to the unmatched uncertainties, the choice of $D(s)$ also needs to ensure that $C(s)H_m^{-1}(s)$ is a proper stable transfer matrix. Similar to before, a simple of $D(s)$ might be $D(s) = \frac{1}{s}\mathbb{I}_m$. This choice results in a strictly proper $C(s)$ on the form

$$C(s) = \boldsymbol{\omega}\mathbf{K}(s\mathbb{I}_m + \boldsymbol{\omega}\mathbf{K})^{-1} \tag{3.131}$$

$\mathcal{L}_1$-norm condition

Now, the sufficient $\mathcal{L}_1$-norm condition is presented. Again, this require some definitions, similar to the ones in the previous section.

Let $\mathbf{x}_{in}(t)$ be the signal with Laplace transform $\mathbf{x}_{in}(s) := (s\mathbb{I}_n - \mathbf{A}_m)^{-1}\mathbf{x}_0$ and $\rho_{in} := \|s(s\mathbb{I} - \mathbf{A}_m)^{-1}\|_{\mathcal{L}_1}\rho_0$. Since $\mathbf{A}_m$ is Hurwitz and $\mathbf{x}_0$ is bounded, then we have from [7] that $\|\mathbf{x}_{in}\|_{\mathcal{L}_\infty} \leq \rho_{in}$.

Further, for every $\delta > 0$, we define

$$L_{i\delta} := \frac{\bar{\delta}(\delta)}{\delta} d_{f_{xi}}(\bar{\delta}(\delta), \;\; \bar{\delta}(\delta) := \delta + \bar{\gamma}_1, \tag{3.132}$$

where $d_{f_{xi}(\cdot)}$ was introduced in assumption 3.5.4 with $\bar{\gamma}$ being an arbitrary small positive constant.

To be able to prove stability and the performance bounds, K and $D(s)$ also need to ensure that for a given ρ_0, there exist $\rho_r > \rho_{in}$, such that the following $\mathcal{L}_1$-norm condition can be met:

$$\|G_m(s)\|_{\mathcal{L}_1} + \|G_{um}(s)\|_{\mathcal{L}_1} l_0 < \frac{\rho_r - \|H_{xm}(s)C(s)K_g(s)\|_{\mathcal{L}_1}\|r\|_{\mathcal{L}_\infty} - \rho_{in}}{L_{1\rho_r}\rho_r + B_0}, \tag{3.133}$$

where

$$G_m(s) := H_{xm}(s)(\mathbb{I}_m - C(s)), \tag{3.134}$$

$$G_{um}(s) := \left(\mathbb{I}_n - Hxm(s)C(s)H_m^{-1}(s)\mathbf{C}\right) H_{xum}(s), \tag{3.135}$$

while

$$l_0 := \frac{L_{2\rho_r}}{L_{1\rho_r}}, \quad B_0 := \max\left\{B_{10}, \frac{B_{20}}{l_0}\right\}. \tag{3.136}$$

The $\mathcal{L}_1$ adaptive controller is defined by combining the feedback controller defined in (3.109), the predictor (3.122), the adaptation rule (3.123) and the adaptive control law (3.125) subject to the $\mathcal{L}_1$-norm condition in (3.133).

3.5.3 Theoretical results

The following part presents the main theoretical results for the $\mathcal{L}_1$ adaptive controller considered in this section. The proofs are ommitted in this text, but can be found in [7].

Definitions

Before we continue, we make some definitions to make the following text easier to read. Let

$$\rho := \rho_r + \bar{\gamma}_1, \tag{3.137}$$

where ρ_r and $\bar{\gamma}_1$ were defined in (3.133) and (3.132) respectively, and let γ_1 be given by

$$\gamma_1 := \frac{\|H_{xm}(s)C(s)H_m^{-1}(s)\mathbf{C}\|_{\mathcal{L}_1}}{1 - \|G_m(s)\|_{\mathcal{L}_1}L_{1\rho_r} - \|G_{um}(s)\|_{\mathcal{L}_1}L_{2\rho_r}}\gamma_0 + \beta, \tag{3.138}$$

where γ_0 and β are arbitrarily small positive constants such that $\gamma_1 \leq \bar{\gamma}_1$. Next, let

$$\rho_u := \rho_{ur} + \gamma_2, \tag{3.139}$$

where ρ_{ur} and γ_2 are defined as

$$\begin{aligned}
\rho_{ur} :=& \left\|\omega^{-1}C(s)\right\|_{\mathcal{L}_1}(L_{1\rho_r}\rho_r + B_{10}) + \left\|\omega^{-1}C(s)H_m^{-1}(s)H_{um}(s)\right\|_{\mathcal{L}_1}(L_{2\rho_r}\rho_r + B_{20}) \\
&+ \left\|\omega^{-1}C(s)K_g(s)\right\|_{\mathcal{L}_1}\|r\|_{\mathcal{L}_\infty}, \\
\gamma_2 :=& \left(\left\|\omega^{-1}C(s)\right\|_{\mathcal{L}_1}L_{1\rho_r}\rho_r + \left\|\omega^{-1}C(s)H_m^{-1}(s)H_{um}(s)\right\|_{\mathcal{L}_1}L_{2\rho_r}\right)\gamma_1 \\
&+ \left\|\omega^{-1}C(s)H_m^{-1}(s)C\right\|_{\mathcal{L}_1}\gamma_0
\end{aligned} \tag{3.140}$$

Equivalent semi-linear timevarying system

Based on the same argumentation as in the previous section, the system in (3.104) can be rewritten over $t \in [0, \tau]$ for arbitrary $\tau \geq 0$ as a semi-linear time-varying system:

$$\begin{aligned}
\dot{\mathbf{x}} &= \mathbf{A}_m\mathbf{x}(t) + \mathbf{B}_m(\omega u(t) + \theta_1(t)\|\mathbf{x}(t)\|_\infty + \sigma_1(t)) \\
&\quad + \mathbf{B}_{um}(\theta_2(t)\|\mathbf{x}(t)\|_\infty + \sigma_2(t)),\ \mathbf{x}(0) = \mathbf{x}_0, \\
y &= \mathbf{C}^T\mathbf{x}(t),
\end{aligned} \tag{3.141}$$

with the unknown parameters bounded according to

$$|\theta_i(t)| < \theta_{bi} = \theta_{bi}(\rho_r),\ |\sigma_i| < \Delta_i = \Delta_i(\rho_r),\ \ \forall t \in [0, \tau]. \tag{3.142}$$

$$|\dot{\theta}_i(t)| < d_{\theta_i}(\rho_r),\ |\dot{\sigma}_i| < d_{\sigma_i}(\rho_r),\ \ \forall t \in [0, \tau], \tag{3.143}$$

where $d_{\theta_i}(\rho, \rho_u) > 0$ and $d_{\sigma_i}(\rho, \rho_u) > 0$ being the bounds specified by Lemma 3.4.1.

Prediction error

From (3.122) and (3.142) we get that over $[0, \tau]$ the prediction error dynamics can be written as

$$\dot{\tilde{\mathbf{x}}}(t) = \mathbf{A}_m \tilde{\mathbf{x}}(t) + \mathbf{B}_m \left(\tilde{\omega}(t)u(t) + \tilde{\eta}_1(t)\right) + \mathbf{B}_{um}\tilde{\eta}_2(t),\ \tilde{\mathbf{x}}(0) = 0, \tag{3.144}$$

where $\tilde{\eta}_i(t) := \hat{\eta}(t) - \eta_i(t)$ with $\eta_i := \theta_i(t)\|\mathbf{x}(t)\|_\infty + \sigma_i(t), i = 1, 2$.

The following result hold for the prediction error, [7]

Lemma 3.5.1. *Let the adaptive gain be lower bounded by*

$$\Gamma > \frac{\theta_m(\rho_r)}{\lambda_{\min}(P)\gamma_0^2}, \tag{3.145}$$

where

$$\theta_m(\rho_r) := 4\left(\max_{\omega\in\Omega} tr(\boldsymbol{\omega}^T\boldsymbol{\omega}) + \left(\theta_{b_1}^2 + \sigma_{b_1}^2\right)m + \left(\theta_{b_2}^2 + \sigma_{b_2}^2\right)(n-m)\right) \tag{3.146}$$

$$+ 4\frac{\lambda_{\max}(P)}{\lambda_{\min}(Q)}\left(\left(\theta_{b_1}d_{\theta_1} + \sigma_{b_1}d_{\sigma_1}\right)m + \left(\theta_{b_1}d_{\theta_1} + \sigma_{b_1}d_{\sigma_1}\right)(n-m)\right), \tag{3.147}$$

and the projection be confined to the bounds

$$\hat{\boldsymbol{\omega}}(t) \in \Omega,\ \ \|\hat{\theta}_i(t)\|_\infty \le \theta_{b_i},\ \ \|\hat{\sigma}_i(t)\|_\infty \le \sigma_{b_i},\ \ i = 1, 2. \tag{3.148}$$

Given the system in (3.113) *and the $\mathcal{L}_1$ adaptive controller defined by combining* (3.122), (3.123) *and* (3.125) *subject to the $\mathcal{L}_1$-norm condition in* (3.133), *if*

$$\|\mathbf{x}_\tau\|_{\mathcal{L}_\infty} \le \rho,\ \ \|u_\tau\|_{\mathcal{L}_\infty} \le \rho_u, \tag{3.149}$$

then

$$\|\tilde{\mathbf{x}}_\tau\|_{\mathcal{L}_\infty} < \gamma_0, \tag{3.150}$$

where γ_0 was introduced in (3.138).

Performance

Again, we consider the reference system which specifies the best theoretically possible $\mathcal{L}_1$ adaptive control result. Consider the reference system given by

$$\begin{aligned}
\dot{\mathbf{x}}_{ref}(t) &= \mathbf{A}_m\mathbf{x}_{ref}(t) + \mathbf{B}_m\left(\omega u_{ref}(t) + \mathbf{f}_1(t, \mathbf{x}_{ref}(t))\right) \\
&\quad + \mathbf{B}_{um}\mathbf{f}_2(t, \mathbf{x}_{ref}(t)),\ \mathbf{x}_{ref}(0) = \mathbf{x}_0, \\
u_{ref}(s) &= \boldsymbol{\omega}^{-1}C(s)\left(K_g r(s) - \eta_{1ref}(s) - H_m^{-1}(s)H_{um}(s)\eta_{2ref}(s)\right), \\
y_{ref}(t) &= \mathbf{C}^T\mathbf{x}_{ref}(t)
\end{aligned} \tag{3.151}$$

where $\eta_{1ref}(s)$ and $\eta_{2ref}(s)$ are the Laplace transforms of the signals $\eta_{iref}(s) := f_1(t, x_{ref}(t)), i = 1, 2$. The following result holds for the stability of the reference system [7]

Lemma 3.5.2. *For the closed-loop reference system in* (3.151)*, subject to the $\mathcal{L}_1$-norm condition in* (3.133)*, if*

$$\|\mathbf{x}_0\|_\infty \leq \rho_0$$

then

$$\|\mathbf{x}_{ref}\|_{\mathcal{L}_\infty} < \rho_r, \tag{3.152}$$
$$\|u_{ref}\|_{\mathcal{L}_\infty} < \rho_{ur}, \tag{3.153}$$

where ρ_r and ρ_{ur} were introduced in (3.78) *and* (3.82) *respectively.*

The following theorem is the main theoretical result of this section, and gives the relationship between the adaptation gain, the prediction error, and the performance of the controller relative to the reference system. The proof is found in [7].

Theorem 3.5.1. *Let the adaptive gain be lower bounded as in* (3.145) *and the projection be confined to the bounds in* (3.148)*. Given the closed-loop system in* (3.113) *with the $\mathcal{L}_1$ adaptive controller defined by combining* (3.122)*,* (3.123) *and* (3.125) *subject to the $\mathcal{L}_1$-norm condition in* (3.133)*, and the closed loop reference system in* (3.151)*, if*

$$\|\mathbf{x}_0\|_\infty \leq \rho_0,$$

then we have

$$\|\mathbf{x}\|_{\mathcal{L}_\infty} < \rho, \tag{3.154}$$
$$\|\mathbf{u}\|_{\mathcal{L}_\infty} < \rho_u, \tag{3.155}$$
$$\|\tilde{\mathbf{x}}\|_{\mathcal{L}_\infty} \leq \gamma_0, \tag{3.156}$$
$$\|\mathbf{x}_{ref} - \mathbf{x}\|_{\mathcal{L}_\infty} \leq \gamma_1, \tag{3.157}$$
$$\|\mathbf{u}_{ref} - \mathbf{u}\|_{\mathcal{L}_\infty} \leq \gamma_2, \tag{3.158}$$
$$\|y_{ref} - y\|_{\mathcal{L}_\infty} \leq \|\mathbf{C}\|_\infty \gamma_1, \tag{3.159}$$

where γ_1 and γ_2 were defined in (3.138) *and* (3.140)*, respectively.*

Remarks

From theorem 3.5.1 we again see that we can achieve an arbitrarily small prediction error γ_0 by increasing the adaptation gain Γ. From (3.138) and (3.140) we see that by minimising γ_0, we can again achieve arbitrarily small performance bounds γ_1 and γ_2 simultaneously. Thus, since the bounds are specified for the $\mathcal{L}_\infty$-norm of the signals, we can achieve arbitrary close tracking performance for both the output and the input signal simultaneously, both in transient and steady-state, by increasing the adaptation gain.

In this section we have only considered the response of the $\mathcal{L}_1$ adaptive controller relative to the reference system. In section 3.3 we considered the design system, which opposed to the reference system was not dependent on the uncertainties. We saw that it was beneficial to

minimise λ to get the desired performance. We now consider the ideal control signal for the system in (3.113),

$$u_{id} = -\boldsymbol{\omega}^{-1}\left(\eta_1(s) + H_m^{-1}(s)H_{um}(s)\eta_2(s) - K_g(s)r(s)\right), \tag{3.160}$$

which results in the desired ideal output responce

$$\mathbf{y}_{id} = H_m(s)K_g(s)r(s) \tag{3.161}$$

by canceling the uncertainties perfectly. Similar to the result in section 3.1 where we saw that it was beneficial with respect to performance, to minimise λ, the output response y_{ref} can be made as close as possible to (3.161) by minimising $(\|G_m(s)\|_{\mathcal{L}_1} + \|G(_{um}(s)\|_{\mathcal{L}_1} l_0)$ [7]. We saw in section 3.3 that by increasing the bandwidth of the filter $C(s)$, λ could be made arbitrarily small. However, in the general case with unmatched uncertainties, the design of K and $D(s)$ which satisfy (3.133) is an open problem [7]. [7] allso note that the presence of unmatched uncertainties may limit the choise of the desired state matrix $\mathbf{A}_m$.

3.6 Systems with unmodeled actuator dynamics

This section extends the problem formulations considered, by introducing unmodeled actuator dynamics. This section will not cover all the theoretical results, but will discuss the assumptions and the design changes needed to cope with this extension. This section covers the design for SISO-systems, but may be extended to MIMO-systems. For more details on the subject, see [7].

3.6.1 Problem formulation

The extension covered in this section can be made for all the problem formulations described earlier. The change is that $\omega u_a d(t)$ is exchanged by $\mu(t)$ and

$$\mu(s) = F(s)u(s), \tag{3.162}$$

where $\mu \in \mathbb{R}^m$ is the output of the unmodeled actuator system, $u(t) \in \mathbb{R}^m$ is the control input, and $F(s)$ is an unknown BIBO-stable transfer function with known sign of its DC gain. We further need to make some assumptions on $F(s)$

Assumption 3.6.1 (Partial knowledge of actuator dynamics). *There exists $L_F > 0$ verifying $\|F(s)\|_{\mathcal{L}_1} \leq L_F$. Also, we assume that there exist known constants $\omega_l, \omega_u \in \mathbb{R}$ satisfying*

$$0 < \omega_l \leq F(0) \leq \omega_u, \tag{3.163}$$

where we have assumed, without loss of generality, that $F(0) > 0$. Finally, we assume that we know a set $\mathbb{F}_\Delta$ of all admissible actuator dynamics.

The control objective is the same as for the different problem formulations considered.

3.6.2 Control architecture

The extension of considering actuator dynamics does not change the architectures directly, but it imposes some new limitations. The most important is the filter $C(s)$, which now is defined as

$$C(s) := \frac{kF(s)D(s)}{1 + kF(s)D(s)} \tag{3.164}$$

Now, k and $D(s)$ need to imply that this new $C(s)$ is a strictly proper and stable transfer function with DC gain $C(0) = 1$ for all $F(s) \in \mathbb{F}_\Delta$. For the proofs of stability, this new filter need to ensure that the $\mathcal{L}_1$-norm condition, dependent on the given problem formulation considered, holds.

Equivalent linear time-varying system

To be able to find adaptation laws for the systems with unmodeled actuator dynamics, we want, similar to the case with nonlinear systems, an equivalent linear time-varying system for the actuator dynamics. From [7] we get the following result.

Lemma 3.6.1. *Consider the system in* (3.162)*. If for some* $\tau > 0$

$$\|u_\tau\|_{\mathcal{L}_\infty} \leq \rho_u, \quad \|\dot{u}_\tau\|_{\mathcal{L}_\infty} \leq d_u, \tag{3.165}$$

then there exist ω *and differentiable* $\sigma(t)$ *over* $t \in [0, \tau]$*, such that*

$$\mu(t) = \omega u(t) + \sigma_\mu(t), \tag{3.166}$$

where

$$\omega \in (\omega_l, \omega_u), \quad |\sigma_\mu(t)| \leq \Delta_\mu, \quad |\dot{\sigma}_\mu(t)| \leq d_{\sigma_\mu}, \tag{3.167}$$

with $\Delta_\mu := \|F(s) - (\omega_l + \omega_u)/2\|_{\mathcal{L}_1}\rho_u$*, and* $d_{\sigma_\mu} := \|F(s) - 8\omega_l + \omega_u)/2\|_{\mathcal{L}_1} d_u$*.*

New modelling error

One point not considered in [7] is the extra error caused by the filtering of $u_m := -k_m x$. To get the desired system $\mathbf{A}_m$ we need to use this feedback signal, and if a system has unmodeled actuator dynamics, this has to affect the feedback signal u_m as well as u_{ad}. We will now show how this affects the modelling error.

Similar to before, we separate the control signal between the feedback control part and the adaptive control part. We define

$$\mu(s) := \mu_{ad}(s) + \mu_m(s) := F(s)u_{ad}(s) + F(s)u_m(s), \tag{3.168}$$

where u_{id} and u_m are introduced in (3.109). From lemma 3.6.1, considering the same assumptions, we get that the system can be written as

$$\mu(t) = \omega u_m(t) + \sigma_{\mu_m} + \omega u_{ad}(t) + \sigma_{\mu_{ad}} = \omega u + \sigma_\mu(t) \tag{3.169}$$

where $\sigma_\mu := \sigma_{\mu_m} + \sigma_{\mu_{ad}}$, and the bounds on ω, σ_{μ_m} and $\sigma_{\mu_{ad}}$ are given by lemma 3.6.1. This extra modelling error must be considered in the design. To see how this effects the modelling error, we first redefine

$$\tilde{\mathbf{B}}(t, \mathbf{x}(t)) := \mathbf{B}_{real}(t, \mathbf{x}(t)) - \mathbf{B}_{id}, \tag{3.170}$$

and consider this combined with (3.106) and (3.105), with $u(t)$ exchanged with $\mu(t)$, to get:

$$\begin{aligned}
\dot{\mathbf{x}}(t) &= \mathbf{A}_{id}\mathbf{x}(t) + \mathbf{B}_{id}\mu(t) + \tilde{f}_x(t, \mathbf{x}(t)) + \tilde{\mathbf{B}}(t, \mathbf{x}(t))\mu(t) \\
\dot{\mathbf{x}}(t) &= \mathbf{A}_{id}\mathbf{x}(t) + \mathbf{B}_{id}(\omega u_m(t) + \omega u_{id}(t) + \sigma_\mu(t)) + \tilde{f}_x(t, \mathbf{x}(t)) \\
&\quad + \tilde{\mathbf{B}}(t, \mathbf{x}(t))(\omega u_m(t) + \omega u_{id}(t) + \sigma_\mu(t)) \\
\dot{\mathbf{x}}(t) &= \mathbf{A}_{id}\mathbf{x}(t) + \mathbf{B}_{id}(-\omega \mathbf{K}_m\mathbf{x}(t) + \omega u_{id}(t) + \sigma_\mu(t)) + \tilde{f}_x(t, \mathbf{x}(t)) \\
&\quad + \tilde{\mathbf{B}}(t, \mathbf{x}(t))(-\omega \mathbf{K}_m\mathbf{x} + \omega u_{id}(t) + \sigma_\mu(t)) \\
\dot{\mathbf{x}}(t) &= \mathbf{A}_m\mathbf{x}(t) + \mathbf{B}_{id}(\omega u_{id}(t) + \sigma_\mu(t)) + \mathbf{B}_{id}\mathbf{K}_m^T(1-\omega)\mathbf{x}(t) + \tilde{f}_x(t, \mathbf{x}(t)) \\
&\quad + \tilde{\mathbf{B}}(t, \mathbf{x}(t))(-\omega \mathbf{K}_m\mathbf{x} + \omega u_{id}(t) + \sigma_\mu(t)) \\
\mathbf{y}(t) &= \mathbf{C}^T\mathbf{x}(t).
\end{aligned}$$

By defining

$$\begin{aligned}
f(t, \mathbf{x}(t)) := \mathbf{B}_{id}(\mathbf{K}_m^T(1-\omega)\mathbf{x}(t) + \sigma_\mu(t)) + \tilde{f}_x(t, \mathbf{x}(t)) \\
+ \tilde{\mathbf{B}}(t, \mathbf{x}(t))(\omega u_{ad} - \omega \mathbf{K}_m^T\mathbf{x}(t) + \sigma_\mu(t)),
\end{aligned} \tag{3.171}$$

we get

$$\dot{\mathbf{x}}(t) = \mathbf{A}_m\mathbf{x}(t) + \mathbf{B}_{id}\omega u_{ad} + f(t, \mathbf{x}(t)), \;\; \mathbf{x}(0) = \mathbf{x}_0 \tag{3.172}$$

$$y(t) = \mathbf{C}^T\mathbf{x}(t), \tag{3.173}$$

which has the same structure as (3.104), only for SISO systems. Comparing (3.171) with (3.110), we see that we get an extra error $\mathbf{B}_{real}(t, \mathbf{x}(t))\sigma_\mu$. As mentioned in section 3.5.1, ω was not really needed and could be put to 1, so we also get an extra error due to ω.

Thus, with unmodeled dynamics, we can estimate and predict the system just as before. However, the projection bounds on $\hat{\sigma}$ must consider the new modelling error given in (3.171), with the bounds on σ specified by lemma 3.6.1.

Chapter 4

Simulation results and discussion

This chapter presents the simulation results performed in this text. The control design of the $\mathcal{L}_1$ adaptive controller for the SISO longitudinal and the MIMO lateral modes are presented, and simulations are performed. To investigate the performance and robustness of the $\mathcal{L}_1$ adaptive controller, two different cases for each of the longitudinal and the lateral modes, including different nonlinear unmatched uncertainties and unmodelled actuator dynamics, are simulated. All the simulations are performed using the same control design. Considering the scope of this report, these cases are not based on any nonlinear aircraft modelling. Instead, the basis for the systems considered are the linearised models and trim conditions presented in section 2.5 and elaborated in section 4.1, with additional nonlinear dynamics and disturbances, and unmodelled actuator dynamics added to these linear systems. These nonlinear effects are chosen more or less randomly to test the robustness and performance of the controller. In this way we have full knowledge of the unmodelled dynamics and are able to see how the different modelling errors affect the performance and robustness of the controllers. However, after these cases are presented and discussed, simulations of the longitudinal mode on the realistic nonlinear F-16 model are performed and discussed, without any retuning of the controller.

As a reference to the performance of the $\mathcal{L}_1$ adaptive controller, this chapter presents simulations for the longitudinal system where the control signal is produced from MRAC and PID control and compare the results to the results from the $\mathcal{L}_1$ controller.

Lastly, this chapter discusses how implementation issues not considered in the theory chapter of this text, affects the performance of the $\mathcal{L}_1$ adaptive controller. Specifically the case of limited sampling rate is simulated and discussed, and a redesign of the control architecture designed to handle this case is presented.

4.1 Simulation values

This section presents the parameters used in all of the simulations.

Linearised modelled dynamics

The considered model in this text is the one presented in section 2.5. One design change is however made. In the linearising of the nonlinear F-16 model, the angles $[\theta, \phi, \psi]$ was considered as the euler angles. As mentioned, the control goal is that the $\mathcal{L}_1$ adaptive controller controls the inner control loops, while an outer controller sets the desired references to the $\mathcal{L}_1$ controller. Thus, we want the outer controller to find the desired references based on the position and the attitude (euler angles), while the references sent to the inner $\mathcal{L}_1$ controllers are relative to the BODY-frame. Thus, we redefine the angles considered by the $\mathcal{L}_1$ adaptive controllers as the integral of its associated rate. The models then become:

$$\begin{bmatrix} \dot{\alpha} \\ \dot{q} \\ \dot{\theta} \end{bmatrix} = \begin{bmatrix} -0.6398 & 0.9378 & -0.0000 \\ -1.5679 & -0.8791 & 0 \\ 0 & 1 & 0 \end{bmatrix} \begin{bmatrix} \alpha \\ q \\ \theta \end{bmatrix} + \begin{bmatrix} -0.0777 \\ -6.5121 \\ 0 \end{bmatrix} \delta_E, \tag{4.1}$$

$$\begin{bmatrix} \dot{\beta} \\ \dot{p} \\ \dot{r} \\ \dot{\phi} \\ \dot{\psi} \end{bmatrix} = \begin{bmatrix} -0.2022 & 0.0783 & -0.9919 & 0.0641 & 0 \\ -22.9219 & -2.2542 & 0.5408 & 0 & 0 \\ 6.0052 & -0.0404 & -0.3146 & 0 & 0 \\ 0 & 1 & 0 & 0 & 0 \\ 0 & 0 & 1 & 0 & 0 \end{bmatrix} \begin{bmatrix} \beta \\ p \\ r \\ \phi \\ \psi \end{bmatrix} + \begin{bmatrix} 0.0099 & 0.0290 \\ -26.4872 & 3.2579 \\ -1.3965 & -2.6855 \\ 0 & 0 \\ 0 & 0 \end{bmatrix} \begin{bmatrix} \delta_A \\ \delta_R \end{bmatrix}. \tag{4.2}$$

By definition, we will thus have no modelling error in the states $[\theta, \phi, \psi]$. The modelling error induced by the difference between the redefined $[\theta, \phi, \psi]$ and the real euler angles, will be handled by the adaptation in the $\mathcal{L}_1$ adaptive controller.

To make the text easier to read, we repeat the trim values from section 2.5:

$$\begin{aligned} U_0 &= 500\ [ft/s] \\ \text{Altitude} &= 15000\ [ft] \\ \Phi_0 &= 0\ [deg] \\ \Theta_0 &= 4.46\ [deg] \\ \Psi_0 &= 0\ [deg] \\ \alpha_0 &= 4.46\ [deg] \\ \beta_0 &= 0\ [deg] \\ P_0 = Q_0 &= R_0 = 0\ [deg/s] \\ \delta_{E0} &= -2.46\ [deg] \\ \delta_{A0} = \delta_{R0} &= 0\ [deg], \\ \text{Thrust}_0 &= 2120.6\ [lbs]. \end{aligned}$$

The eigenvalues are

$$\lambda_{long} = \begin{bmatrix} -0.7594 + j1.2067 \\ -0.7594 - j1.2067 \\ 0 \end{bmatrix}, \tag{4.3}$$

$$\lambda_{lat} = \begin{bmatrix} 0 \\ -0.3177 + j2.7404 \\ -0.3177 - j2.7404 \\ -2.1198 \\ -0.0158 \end{bmatrix}, \tag{4.4}$$

where λ_{long} and λ_{lat} denote the eigenvalues for the longitudinal and the lateral model respectively.

Unmodeled actuator dynamics

To further test the performance of the $\mathcal{L}_1$ adaptive controller, unmodeled actuator dynamics is considered. This models the response of the control surfaces to the control signal from the controller. The actuator dynamic may also model the effect that a sudden deflection in one control surface will not give an instant responding force. This effect is however something that could be modelled and considered in the design of the desired system response $\mathbf{A}_m$. In ether way, the introduction of the unmodeled actuator dynamic is a good way to test the performance and robustness of the $\mathcal{L}_1$ adaptive controller and will also prevent unrealistically fast control.

The actual actuator dynamic considered in this text is given by the first order low-pass filter

$$F(s) = \frac{20.2}{s + 20.2} \tag{4.5}$$

This is used for all the control surfaces and is the actuator dynamic considered in the F-16 model [21]. Further, a limitation in the control surfaces are given according to

$$|\delta_E| \leq 25^\circ \tag{4.6}$$
$$|\delta_A| \leq 21.5^\circ \tag{4.7}$$
$$|\delta_R| \leq 30^\circ \tag{4.8}$$
$$\tag{4.9}$$

4.2 $\mathcal{L}_1$ adaptive control design for the longitudinal system

This section presents the control design used for the simulations considering the longitudinal system in this chapter. The controller is designed based on the linearised model in section 4.1, and the control laws are kept unchanged for all the considered cases. The $\mathcal{L}_1$

adaptive controller is defined by combining the feedback controller defined in (3.109), the predictor (3.122), the adaptation rule (3.123) and the adaptive control law (3.125). The parameters used and the design of the different control elements are presented in following of this section. The implementation of the $\mathcal{L}_1$ adaptive controller for the longitudinal system can be found in Appendix A.

4.2.1 Design of the feedback gain K_m

The design of the feedback vector K_m to get the desired closed loop dynamics specified by $\mathbf{A}_m$ can be performed in different ways. This design challenge is not a big part of the theory presented in [7], or any other papers considering $\mathcal{L}_1$ adaptive control theory. Some of the strengths of $\mathcal{L}_1$ adaptive control is the way that we can choose the desire response and robustness specifications based on classical control theory, while ignoring the part about modelling errors. After the desired response is specified, the adaptive part of the controller is designed to handle the errors. However, the choice of $\mathbf{A}_m$ affects $G(s)$ and thus the norm in the $\mathcal{L}_1$-norm condition, which puts the limits on the adaptive part of the controller.

In this text the design of the feedback gain K_m is done through LQR-design. This design method calculates the optimal gain vector (or matrix) K_m such that the feedback law $u = -K_m u$ minimizes the cost function

$$J = \int \mathbf{x}^T Q\mathbf{x} + \mathbf{u}^T R\mathbf{u} \, \mathrm{d}t$$

subject to the system dynamics $\dot{\mathbf{x}} = \mathbf{A}_{id}\mathbf{x} + \mathbf{B}_{id}\mathbf{u}$. In this way we can calculate the optimal control by weighting each state and control input through the matrices Q and R respectively. For more theory on the topic of LQR-design, see [2] [13] [14].

By using LQR-design, the design parameters are the matrices Q and R. The choice of these matrices can be done by trial and error, but by considering the control goal, we can get a good first guess. The goal is to control θ. Thus it is important to weight this state pretty high. Further, it may be a goal that the rate do not get to high. In this case one would give some weight on q. Considering the angle of attack, α, this is unimportant in this context. Further, the available actuator does not affect this state much. Simulations performed, where there were any weight on α, show that this ruins the control of θ.

One other fact to take into consideration, is the presence of the actuator dynamics. This puts a limit to how fast the response can be made, and thus to high weight on θ may cause instability in the presence of the actuator dynamics. This effect was examined through the Bode plot of the transfer function from the reference r to the output y. For this analysis, we assume that we have a good insight in the actuator dynamics even though we have not used it directly in the model. The transfer function is

$$\frac{y}{r}(s) = \mathbf{C}\left(s\mathbb{I}_n - (\mathbf{A}_{id} - \mathbf{B}_{id}F(s)K_m)\right)^{-1} k_g \mathbf{B}_{id}F(s) \tag{4.10}$$

Following the discussion above, and by some trial and error, I chose

$$Q = \begin{bmatrix} 0 & 0 & 0 \\ 0 & 0 & 0 \\ 0 & 0 & 30 \end{bmatrix}$$
$$R = 10$$

Using the lqr-function in matlab, this resulted in the feedback vector

$$K_m = \begin{bmatrix} 0.2130 \\ -0.5643 \\ -1.7321 \end{bmatrix}, \tag{4.11}$$

which again resulted in the system matrix

$$\mathbf{A}_m = \begin{bmatrix} -0.6232 & 0.8939 & -0.1346 \\ -0.1808 & -4.5535 & -11.2793 \\ 0 & 1.0000 & 0 \end{bmatrix}, \tag{4.12}$$

with the eigenvalues

$$\lambda_m = \begin{bmatrix} -0.6094 \\ -2.2837 + j2.5060 \\ -2.2837 - j2.5060 \end{bmatrix}$$

This resulted in the bode plot in figure 4.1 of $\frac{y}{r}(s)$ in 4.10, where the filter $F(s)$ in (4.5) was considered.
We see that we get a gain margin of 17.7 dB and a phase margin of 180 degrees, which are acceptable margins [11].

4.2.2 Specifying the projection bounds

This part requires some knowledge of the system considered. Since we specify the error in the considered cases, we can chose conservative bounds based on that. The kind of uncertainties considered in the simulations are

$$\tilde{f}_x(t, \mathbf{x}(t)) = \mathbf{A}_\Delta(t)\mathbf{x}(t) + \sigma(t), \tag{4.13}$$
$$\tilde{\mathbf{B}}(t, \mathbf{x}(t)) = \tilde{\mathbf{B}}(t) \tag{4.14}$$

Further, the unmodeled actuator dynamics causes an extra unknown error since

$$\mu(t) = \omega u + \sigma_\mu(t) \tag{4.15}$$

From (3.171) and the results above, we get that the modelling error becomes

$$\begin{aligned} f(t, \mathbf{x}(t)) = \mathbf{B}_{id}\mathbf{K}_m^T(1-\omega)\mathbf{x}(t) + \mathbf{A}_\Delta(t)\mathbf{x}(t) + \sigma(t) + (\mathbf{B}_{id} + \tilde{\mathbf{B}}(t))\sigma_\mu(t) \\ + \tilde{\mathbf{B}}(t)(\omega u_{ad} - \omega\mathbf{K}_m^T\mathbf{x}(t)) \end{aligned} \tag{4.16}$$

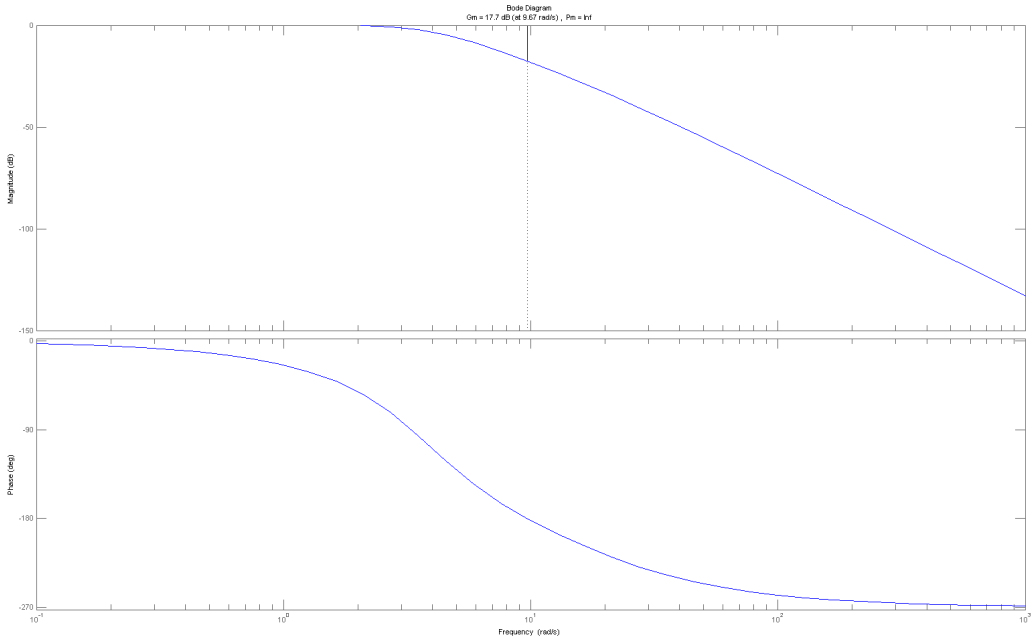

Figure 4.1: Bode plot of $\frac{y}{r}(s) = \mathbf{C}\left(s\mathbb{I}_n - (\mathbf{A}_{id} - \mathbf{B}_{id}F(s)K_m)\right)^{-1} k_g \mathbf{B}_{id}F(s)$

Specifying Δ_i

From (4.16) we have

$$f(t,0) = \sigma(t) + (\mathbf{B}_{id} + \tilde{\mathbf{B}})\sigma_{\mu_{ad}}(t) + \tilde{\mathbf{B}}\omega u_{ad}(t) \tag{4.17}$$

where σ is the only signal we have knowledge about. From (3.114) we have that

$$\begin{bmatrix}\mathbf{f}_1(t,\mathbf{x}(t))\\ \mathbf{f}_2(t,\mathbf{x}(t))\end{bmatrix} = \begin{bmatrix}\mathbf{B}_m & \mathbf{B}_{um}\end{bmatrix}^{-1} f(t,\mathbf{x}(t)). \tag{4.18}$$

In the cases considered in this text, $\sigma_{max} := \|\sigma(t)\|_\infty = 10\pi/180 \approx 0.175$. We find a lower bound on the error:

$$\|\mathbf{f}_1(t,0)\|_\infty \geq \left\| \begin{bmatrix}1&0&0\\0&0&0\\0&0&0\end{bmatrix} \begin{bmatrix}\mathbf{B}_m & \mathbf{B}_{um}\end{bmatrix}^{-1} \right\|_\infty \sigma_{max} \tag{4.19}$$

$$\|\mathbf{f}_2(t,0)\|_\infty \geq \left\| \begin{bmatrix}0&0&0\\0&1&0\\0&0&1\end{bmatrix} \begin{bmatrix}\mathbf{B}_m & \mathbf{B}_{um}\end{bmatrix}^{-1} \right\|_\infty \sigma(t)_{max} \tag{4.20}$$

This gives

$$\|\mathbf{f}_1(t,0)\|_\infty \geq 0.0268 \tag{4.21}$$

$$\|\mathbf{f}_2(t,0)\|_\infty \geq 0.1766 \tag{4.22}$$

Based on this, and proven to give good results through simulations, the projection bounds defined in (3.124) is chosen as

$$\Delta_1 = 0.1 \tag{4.23}$$
$$\Delta_2 = 0.3 \tag{4.24}$$

Specifying θ_{bi}

From (4.16) we have

$$\frac{\delta f(t,\mathbf{x})}{\delta \mathbf{x}} = \mathbf{B}_{id}\mathbf{K}_m^T(1-\omega) + \mathbf{A}_\Delta(t) - \tilde{\mathbf{B}}\omega\mathbf{K}_m^T + \tilde{\mathbf{B}}\omega\frac{\delta u_{ad}}{\delta \mathbf{x}} + (\mathbf{B}_{id} + \tilde{\mathbf{B}}(t))\frac{\delta \sigma_\mu}{\delta \mathbf{x}}, \tag{4.25}$$

for all $\|\mathbf{x}\|_\infty < \infty$. We known that $F(0) = 1$, thus $\omega = 1$. Further, from the cases considered we have that

$$\max_{\mathbf{A}_\Delta(t)} \left\| \begin{bmatrix} 1 & 0 & 0 \\ 0 & 0 & 0 \\ 0 & 0 & 0 \end{bmatrix} \begin{bmatrix} \mathbf{B}_m & \mathbf{B}_{um} \end{bmatrix}^{-1} \mathbf{A}_\Delta \right\|_\infty = 1.54 \tag{4.26}$$

$$\max_{\mathbf{A}_\Delta(t)} \left\| \begin{bmatrix} 0 & 0 & 0 \\ 0 & 1 & 0 \\ 0 & 0 & 1 \end{bmatrix} \begin{bmatrix} \mathbf{B}_m & \mathbf{B}_{um} \end{bmatrix}^{-1} \mathbf{A}_\Delta \right\|_\infty = 0.43 \tag{4.27}$$

and

$$\max_{\tilde{\mathbf{B}}(t)} \left\| \begin{bmatrix} 1 & 0 & 0 \\ 0 & 0 & 0 \\ 0 & 0 & 0 \end{bmatrix} \begin{bmatrix} \mathbf{B}_m & \mathbf{B}_{um} \end{bmatrix}^{-1} \tilde{\mathbf{B}} K_m^T \right\|_\infty = 0.87 \tag{4.28}$$

$$\max_{\tilde{\mathbf{B}}(t)} \left\| \begin{bmatrix} 0 & 0 & 0 \\ 0 & 1 & 0 \\ 0 & 0 & 1 \end{bmatrix} \begin{bmatrix} \mathbf{B}_m & \mathbf{B}_{um} \end{bmatrix}^{-1} \tilde{\mathbf{B}} K_m^T \right\|_\infty = 0 \tag{4.29}$$

The last addends $\tilde{\mathbf{B}}\frac{\delta u_{ad}}{\delta \mathbf{x}}$ and $\tilde{\mathbf{B}}(t))\frac{\delta \sigma_\mu}{\delta \mathbf{x}}$ we have no control over. Thus we get

$$L_1 = \left\| \frac{\delta f_1(t,\mathbf{x})}{\delta \mathbf{x}} \right\|_\infty \geq 2.41 \tag{4.30}$$

$$L_2 = \left\| \frac{\delta f_1(t,\mathbf{x})}{\delta \mathbf{x}} \right\|_\infty \geq 0.43 \tag{4.31}$$

Bases on these calculations, we choose a conservative bound on the projection bound, defined in (3.124), as

$$\theta_{b1} = 3, \tag{4.32}$$
$$\theta_{b2} = 1 \tag{4.33}$$

Specifying Ω

In the cases considered in the simulations, we know that $F(0) = 1$. However, it may be beneficial to let some of the error $\mathbf{B}$ be taken care of by $\hat{\omega}$. Further it is interesting to see how this adaptation affect the control. In the simulations considered, the bounds on ω are given as

$$\Omega = [0.5, 2]. \tag{4.34}$$

Initial conditions

The initial conditions for the estimates have to be specified. The only requirement from the $\mathcal{L}_1$ theory is that the initial values are chosen within the specified projection bounds. For all the simulations performed for the longitudinal system the initial guess is that there is no modelling error, that is:

$$\hat{\theta}_{10} = 0 \tag{4.35}$$

$$\hat{\theta}_{20} = \begin{bmatrix} 0 \\ 0 \end{bmatrix} \tag{4.36}$$

$$\hat{\sigma}_{10} = 0 \tag{4.37}$$

$$\hat{\sigma}_{20} = \begin{bmatrix} 0 \\ 0 \end{bmatrix} \tag{4.38}$$

$$\hat{\omega}_0 = 1 \tag{4.39}$$

4.2.3 Designing the filter $C(s)$

The design of k and $D(s)$ to specify the desired filter $C(s) := kD(s)F(s)/(1 + kD(s)F(s))$ is the most challenging part of the $\mathcal{L}_1$ adaptive control design. We know that $C(s)$ has to be a BIBO-stable strictly proper filter with DC-gain $C(0) = 0$. Further, for the theoretical results to be valid, $C(s)$ has to verify the $\mathcal{L}_1$-norm condition (3.133). Other than this, the filter may be chosen freely. There exist no concrete guidelines to how this filter should be designed, and as mentioned in section 3.5, the design of k and $D(s)$ which satisfy the $\mathcal{L}_1$-norm condition in (3.133) is still an open problem. We know from the theory that minimising $(\|G_m(s)\|_{\mathcal{L}_1} + \|G(_{um}(s)\|_{\mathcal{L}_1} l_0)$ is good for performance, while increasing the bandwidth of $C(s)$ affects the robustness.

One simple choice of $D(s)$ that is mentioned in [7], is

$$D(s) = \frac{1}{s}. \tag{4.40}$$

This is the one considered in this text, and has proven to give good results for this system. Other choices of $D(s)$ inspired by the ones mentioned in [7] has been tested. This were

$D(s) = \dfrac{s+0.1}{s(s+9)}$ and $D(s) = \dfrac{1}{s(\frac{s}{90}+1)(\frac{s}{300}+1)(\frac{s^2}{140^2}+\frac{1.8s}{140}+1)}$. Neither of them seemed to give any better simulation results nor improve the $\mathcal{L}_1$-norm in the $\mathcal{L}_1$-norm condition.

Now the feedback gain k, which specifies the bandwidth, has to be chosen. As we have discussed, the purpose of the filter is to separate robustness from adaptation. That is, make the controller compensate for the uncertainties within the bandwidth of $C(s)$ while the higher frequencies are used in the adaptation. Thus, high adaptation gain will not ruin the robustness of the system. For the given choice of $D(s)$, we consider the plot of $\|G_m(s)\|_{\mathcal{L}_1}L_1 + \|G(_{um}(s)\|_{\mathcal{L}_1}L_2$ versus k. This can be seen in figure 4.2. The values for L_1 and L_2 used in the plot are found in (4.30) and (4.31) respectively. As we can see, up until

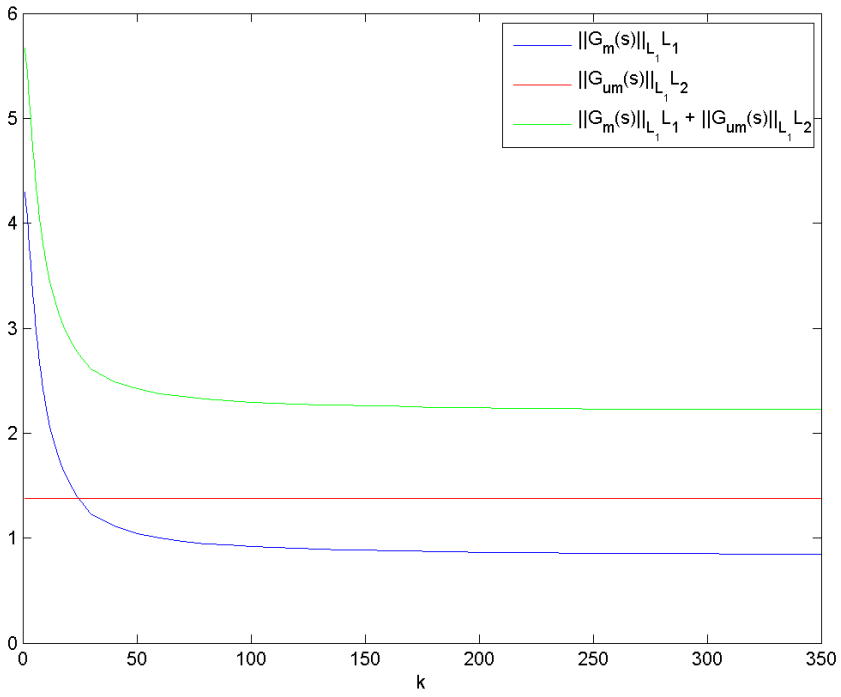

Figure 4.2: $\mathcal{L}_1$-norm condition as a function of k.

about $k = 150$, increasing k decreases the value of $\|G_m(s)\|_{\mathcal{L}_1}L_1 + \|G(_{um}(s)\|_{\mathcal{L}_1}L_2$. However, the plot level off and it does not look like it is possible to satisfy the $\mathcal{L}_1$-norm condition by increasing k.

Figure 4.3 shows the control input for case 2, described in section 4.3.3, with $k = 150$. We see that a too high value on k makes the controller compensate for undesired frequencies and thus start to oscillate rapidly, and makes the system unstable. Thus, there is no point checking the $\mathcal{L}_1$-norm conditions for higher values of k. A good starting point for the design of the bandwidth of $C(s)$ is by considering the bandwidth and the bode-plot of $\dfrac{y}{r}(s)$ in figure 4.1. We want the bandwidth of $C(s)$ to be larger than the bandwidth of the system to get the

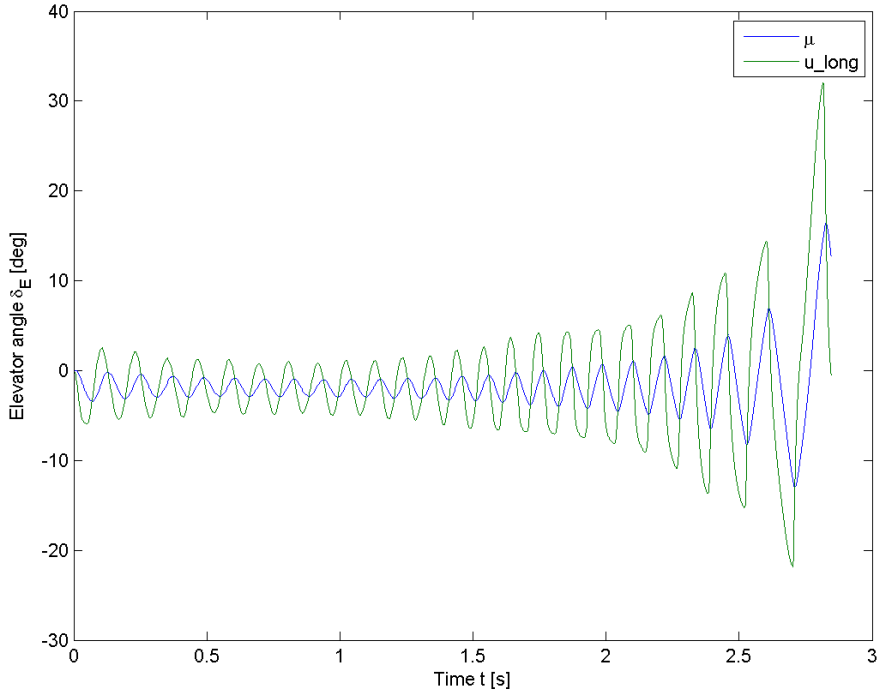

Figure 4.3: Control input, case 2, with k = 150, and reference r_1.

desired response. Through lots of simulations the choice according to

$$k = 30 \tag{4.41}$$

seems to give good results, even though the $\mathcal{L}_1$-norm condition is not met. This choice results in the filter

$$C(s) = \frac{606s + 12240}{s^3 + 40.4s^2 + 1014s + 12240} \tag{4.42}$$

with the bode plot given in figure 4.4. Compared to the bode plot of $\frac{y}{r}(s)$, we see that the bandwidth of $C(s)$ is large enough to make the controller compensate for the desired frequencies.

4.2.4 Choosing the adaptation gain Γ

From the theoretical results, we know that a large adaptation gain as possible is beneficial for good performance. We also want the update frequencies of the uncertainties to lie outside of the bandwidth of $C(s)$ to prevent oscillations in the control signal. For the simulations performed in this text, when not considering limited sampling frequencies, the value

$$\Gamma = 10000 \tag{4.43}$$

is used. The update gain when considering limited sampling frequencies is considered later in this chapter.

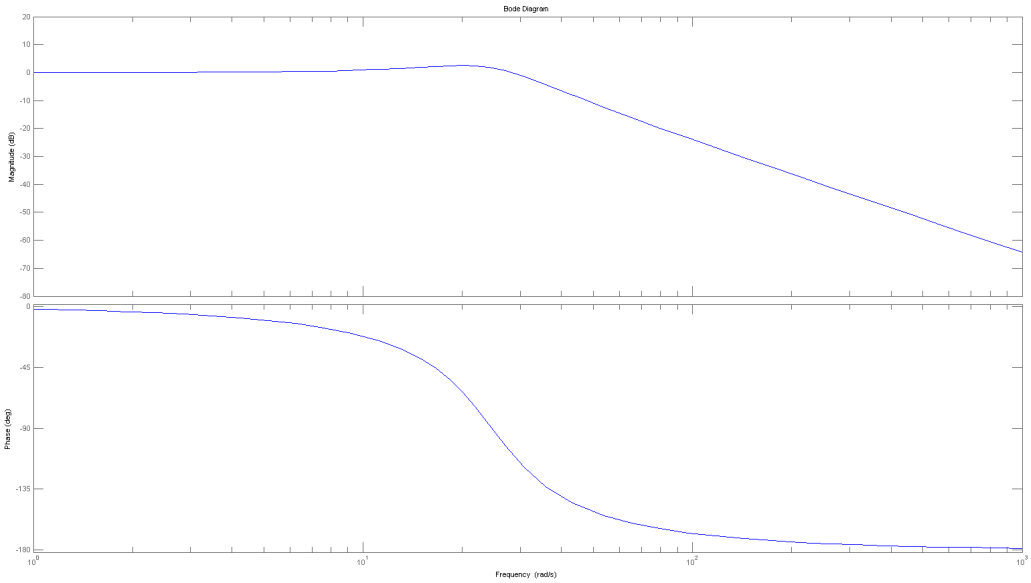

Figure 4.4: Bode plot of $C(s)$

4.3 Simulation results and discussion for the longitudinal system

In this section, the simulation results of the $\mathcal{L}_1$ adaptive controller for the longitudinal system are presented. It would be impossible to consider and simulate all the different nonlinear effects the aircraft could encounter. However, in this section we present two different cases which together gives a good insight in the robustness and the performance of the $\mathcal{L}_1$ adaptive controller. All the simulations presented in this section are performed with the solver ODE45 and a relative tolerance of 10^{-3}. Implementation issues like limited sampling time and measurement errors are considered in section 4.8.

The simulations in this section are performed for two types of reference inputs:

$$r_{10}(t) = \begin{cases} 5^\circ & , \ 5\ s < t < 25\ s \\ 0^\circ & , \ \text{otherwise} \end{cases} \tag{4.44}$$

$$r_{20}(t) = 5^\circ \sin \frac{\pi}{4} t \tag{4.45}$$

Further, to prevent to aggressive change, the reference signals are filtered:

$$r_i(s) = F_r(s) r_{i0}, \tag{4.46}$$

where $F_r(s) = \dfrac{5}{s+5}$

4.3.1 Design system

First, as a reference to the best possible control result one could hope for, the ideal case with no modelling error is presented. This represents the design system. The simulation is performed by setting the adaptation gain to zero, and removing all error. The resulting plots for the system output, the control signal together with the real control input, and the states are shown in figures 4.5, 4.6 and 4.7 respectively.

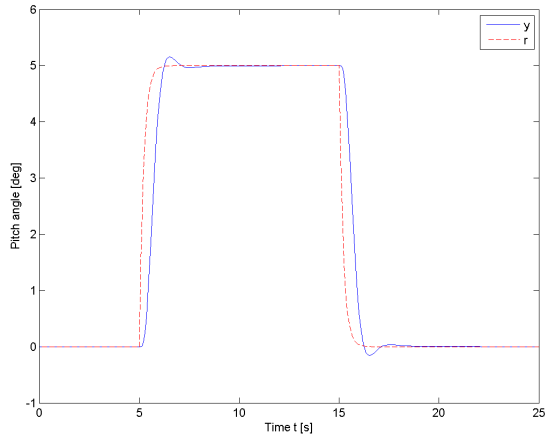

(a) System output with reference r_1

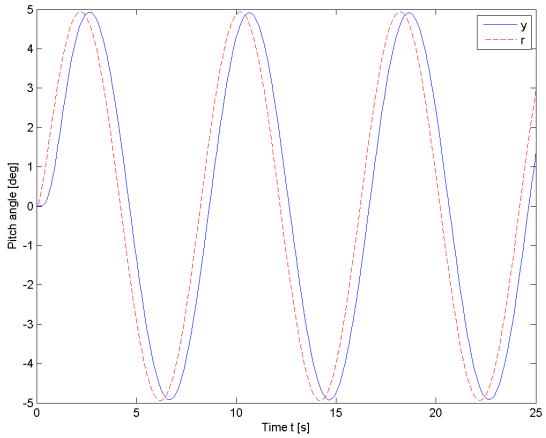

(b) System output with reference r_2

Figure 4.5: System output in the case of no modelling error.

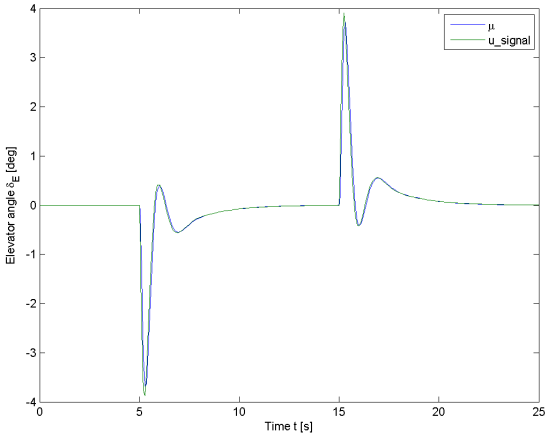

(a) Control signal with reference r_1

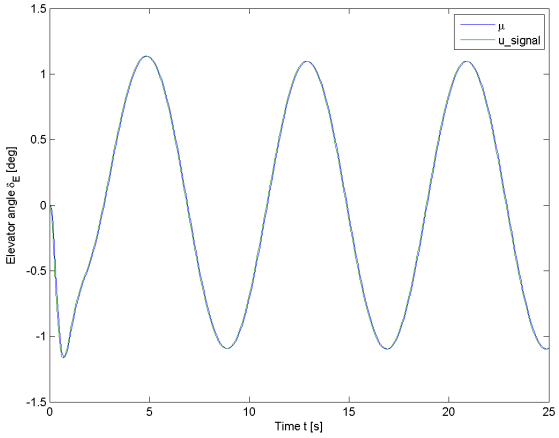

(b) Control signal with reference r_2

Figure 4.6: Control input in the case of no modelling error.

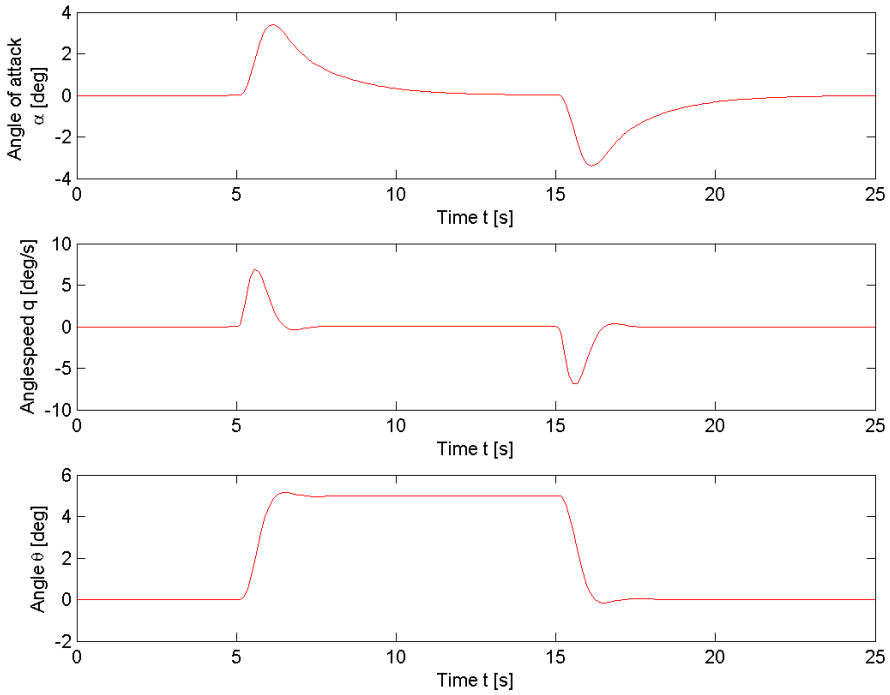

(a) System states with reference r_1

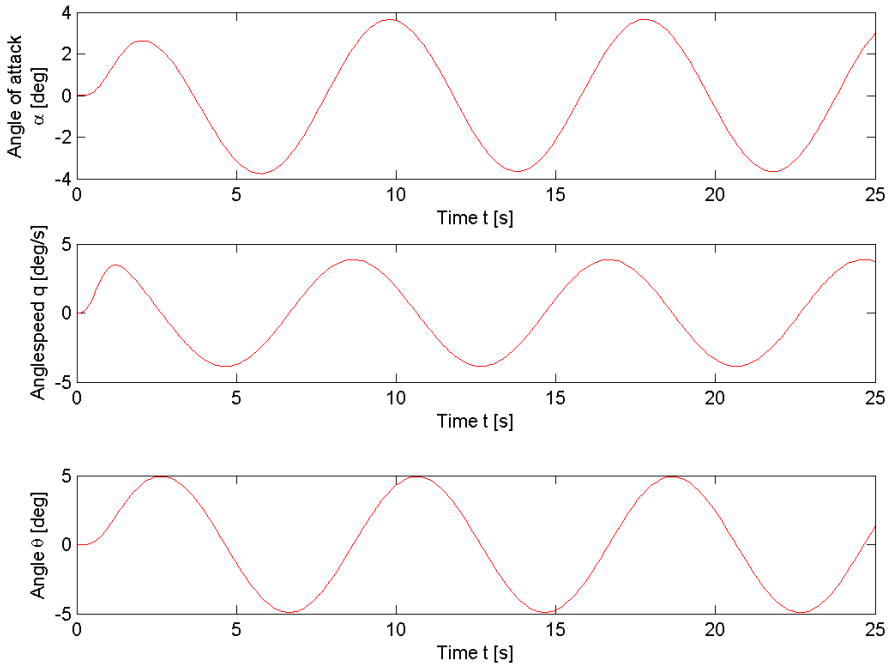

(b) System states with reference r_2

Figure 4.7: System states in the case of no modelling error.

4.3.2 Simulation case 1

As the aircraft flies and the angle of attack α change, a normal effect is that the coefficient C_{m_α} change. This is due to the change of center of pressure on the aircraft. To imitate this affect and test how this affects the control and the robustness of the aircraft, a simulation is performed where an extra error is put on $\bar{M}_\alpha$. A sinusoidal error is added to this parameter according to:

$$f(t, \mathbf{x}(t)) = \mathbf{A}_\Delta(t)x, \tag{4.47}$$

where

$$\mathbf{A}_\Delta(t) = \begin{bmatrix} 0 & 0 & 0 \\ 10 \sin \frac{\pi}{2} t & 0 & 0 \\ 0 & 0 & 0 \end{bmatrix} \tag{4.48}$$

This error is highly nonlinear, and makes the system change between being stable and being unstable. Further, the amplitude of the sinusoidal is much larger than the initial value on $\bar{M}_\alpha$. The resulting plots for the system output, the control signal together with the real control input, the prediction estimates, and the states together with the state estimates are shown in figures 4.8, 4.9, 4.10 and 4.11 respectively.

As a reference, the output of a simulation where the adaptation gain is zero is shown in figure 4.12.

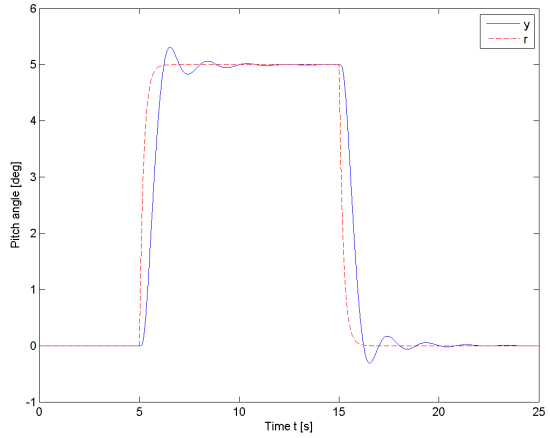

(a) System output with reference r_1

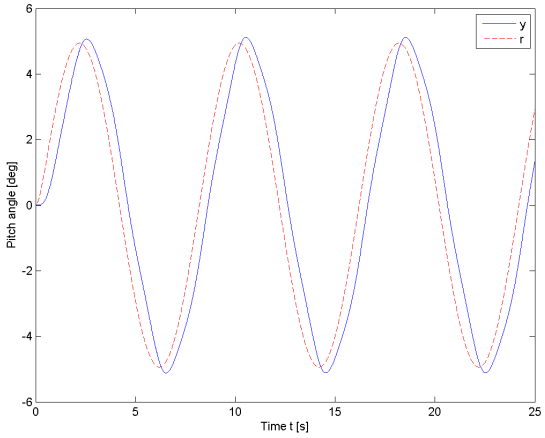

(b) System output with reference r_2

Figure 4.8: System output of the $\mathcal{L}_1$ adaptive controlled longitudinal system, for simulation case 1.

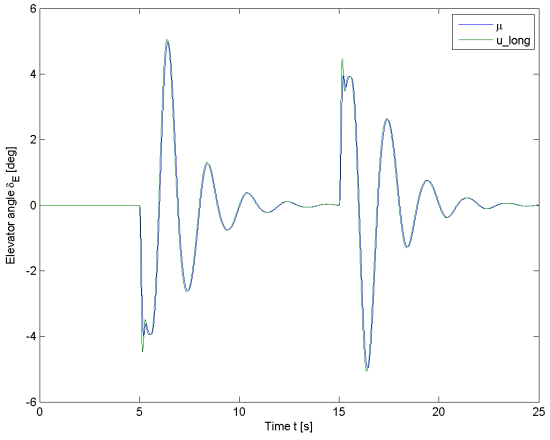

(a) Control signal with reference r_1

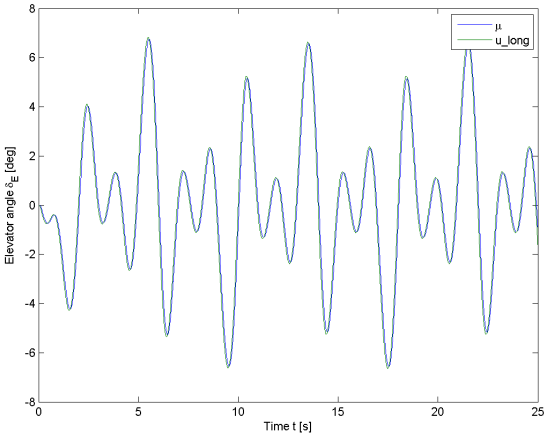

(b) Control signal with reference r_2

Figure 4.9: L1 adaptive control input to the longitudinal system, for simulation case 1.

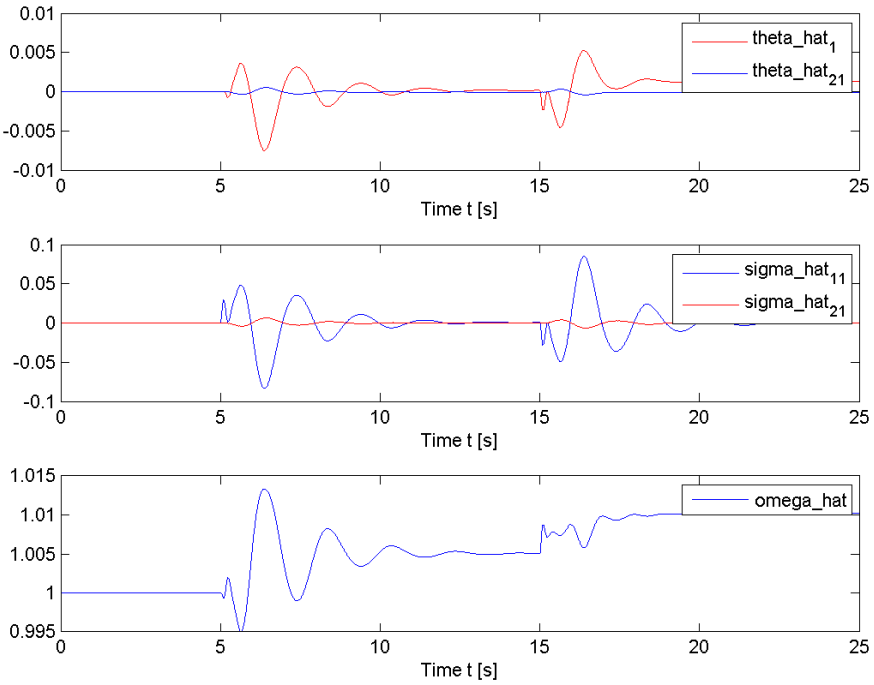

(a) Adaptive estimates with reference r_1

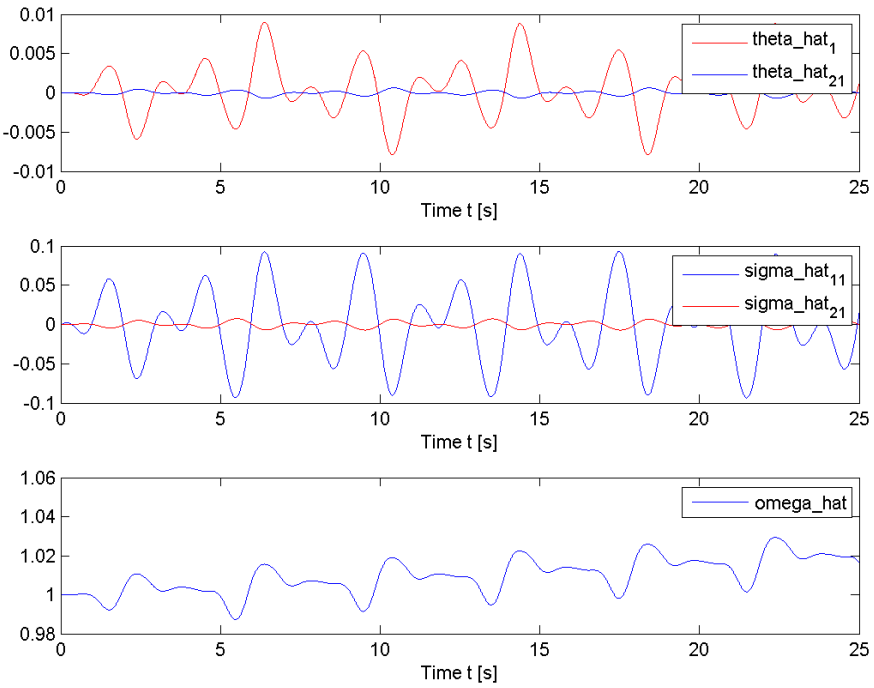

(b) Adaptive estimates with reference r_2

Figure 4.10: Adaptive estimates for the $\mathcal{L}_1$ adaptive controlled longitudinal system, for simulation case 1.

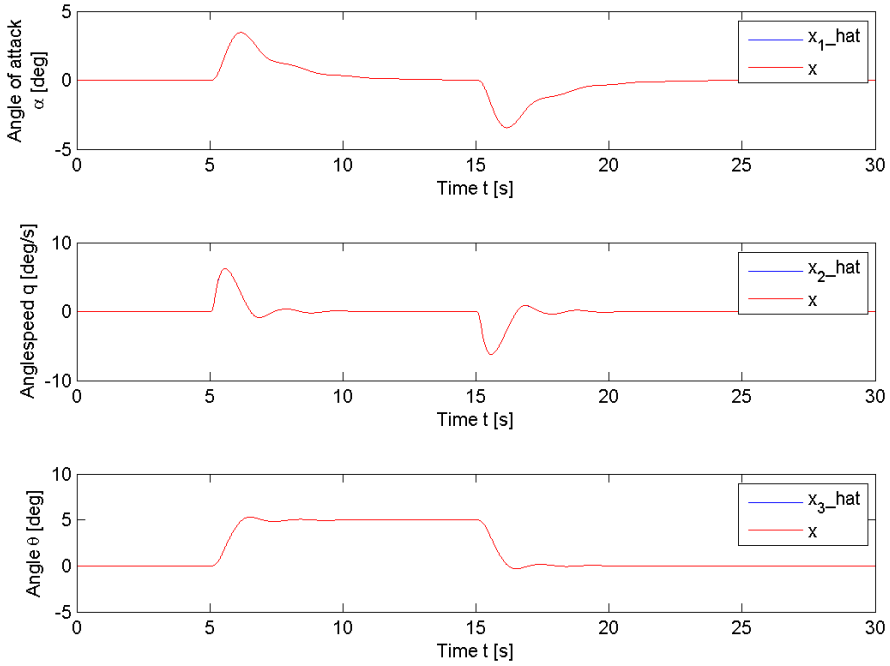

(a) System states with reference r_1

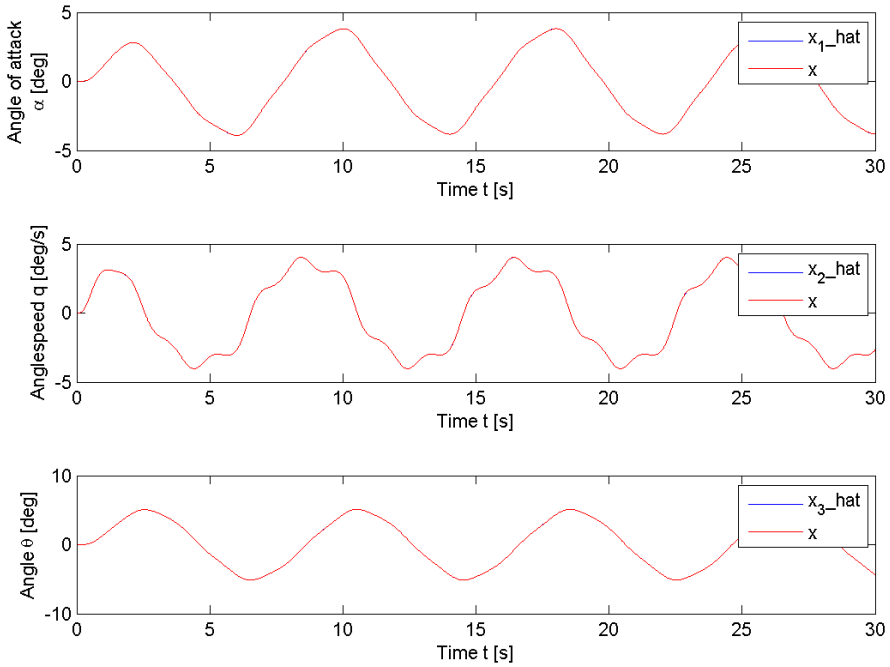

(b) System states with reference r_2

Figure 4.11: Real and predicted states of the $\mathcal{L}_1$ adaptive controlled longitudinal system, for simulation case 1.

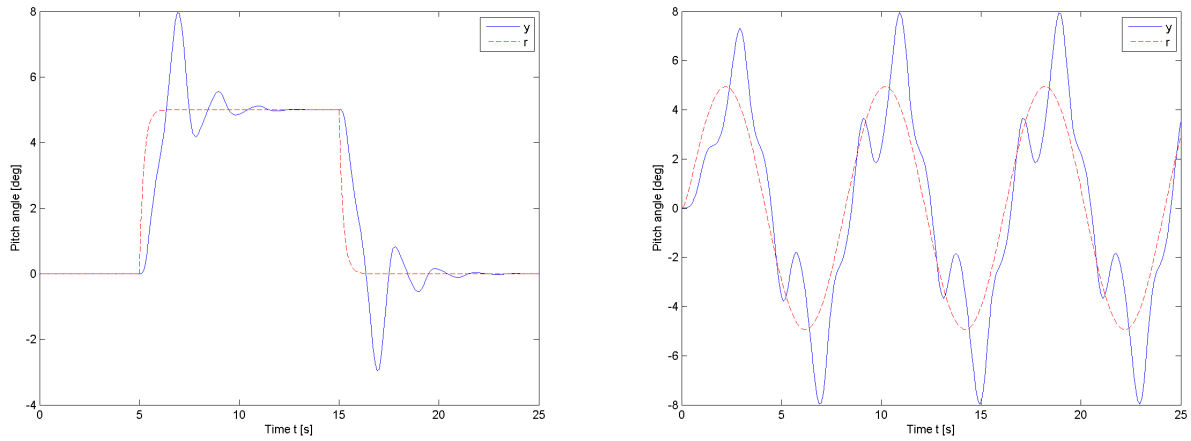

(a) System output with reference r_1

(b) System output with reference r_2

Figure 4.12: System output of the $\mathcal{L}_1$ adaptive controlled longitudinal system, for simulation case 1, without adaptation.

4.3.3 Simulation case 2

The simulation case now presented is designed to put the $\mathcal{L}_1$ adaptive controller to the test. The system considered in the following simulation is given as

$$\dot{\mathbf{x}}(t) = (\mathbf{A}_{id} + \mathbf{A}_{\Delta}(t))\mathbf{x}(t) + \mathbf{B}(t)\mu(t) + \sigma(t), \tag{4.49}$$

where

$$\mathbf{A}_{\Delta}(t) = \begin{bmatrix} 0 & 0.5\sin\left(\frac{\pi}{3}t + \frac{\pi}{5}\right) & 0 \\ 0 & 6 & 0 \\ 0 & 0 & 0 \end{bmatrix}, \tag{4.50}$$

$$\mathbf{B}(t) = \left(1 + 0.5\sin\left(\frac{\pi}{5}t - \frac{\pi}{9}\right)\right)\mathbf{B}_{id}, \tag{4.51}$$

$$\sigma(t) = \begin{bmatrix} \frac{5\pi}{180}\sin\left(\frac{\pi}{3.5}t + \frac{\pi}{7}\right) \\ \frac{10\pi}{180}\sin\left(\frac{\pi}{6}t + \frac{\pi}{3}\right) \\ 0 \end{bmatrix} \tag{4.52}$$

The resulting plots for the system output, the control signal together with the real control input, the prediction estimates, and the states together with the state estimates are shown in figures 4.13, 4.14, 4.15 and 4.16 respectively.

As a reference, it is interesting to see how the controller performs without the adaptation. However, since element $(2, 2)$ in $\mathbf{A}_{\Delta}$ makes the total feedback system unstable, the output of a simulation where the adaptation gain is zero is done with element $(2, 2)$ in $\mathbf{A}_{\Delta}$ equal to zero. This simulation is shown in figure 4.17.

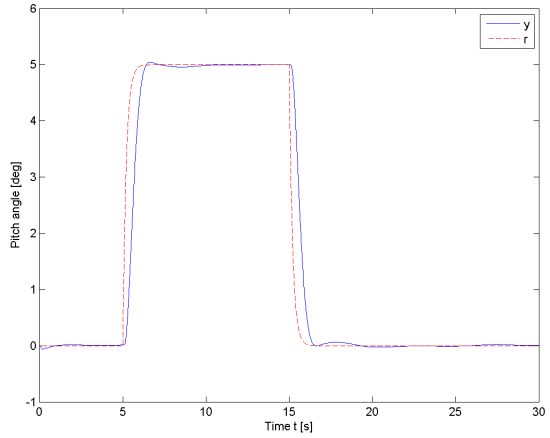

(a) System output with reference r_1

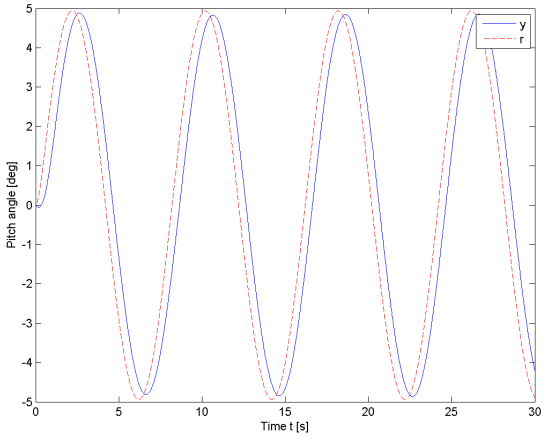

(b) System output with reference r_2

Figure 4.13: System output of the $\mathcal{L}_1$ adaptive controlled longitudinal system, for simulation case 2.

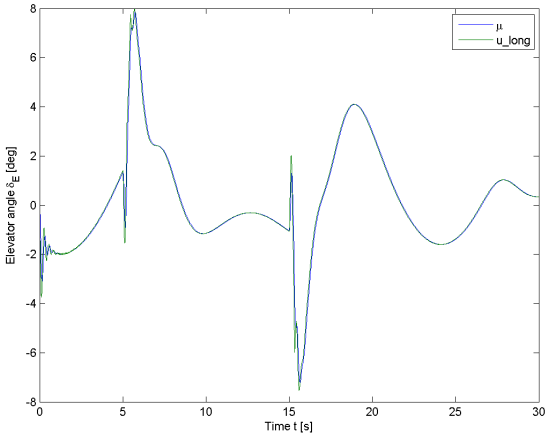

(a) Control signal with reference r_1

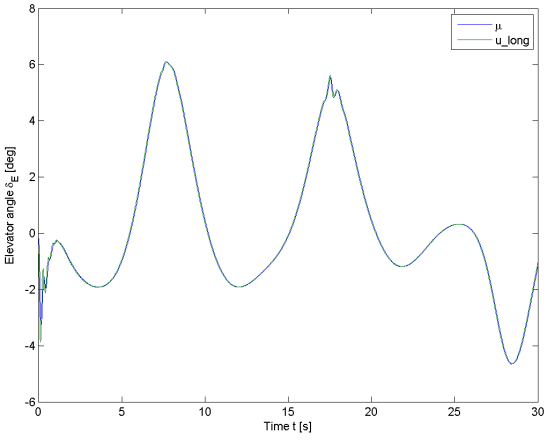

(b) Control signal with reference r_2

Figure 4.14: $\mathcal{L}_1$ adaptive control input to the longitudinal system, for simulation case 2.

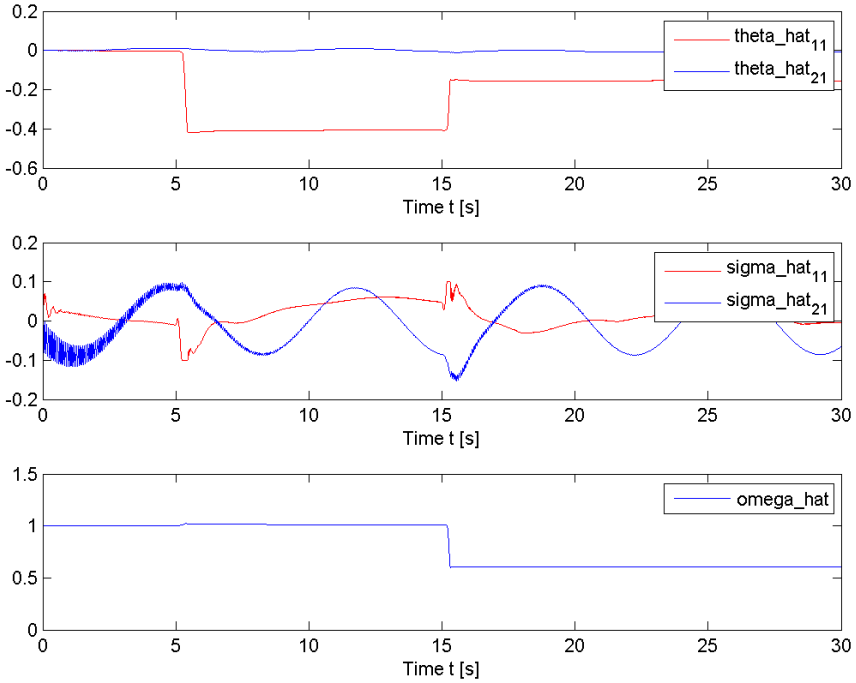

(a) Adaptive estimates with reference r_1

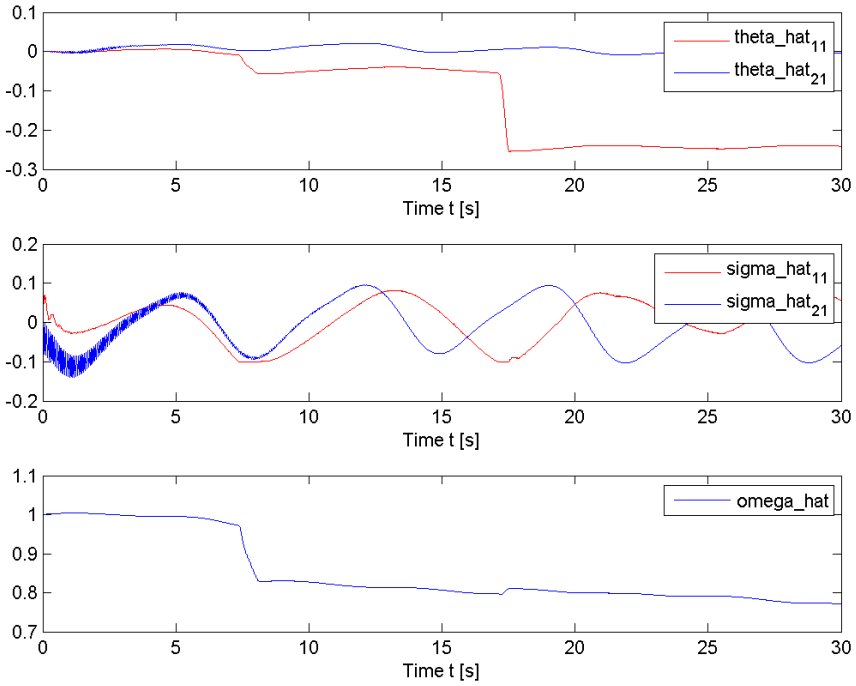

(b) Adaptive estimates with reference r_2

Figure 4.15: Adaptive estimates for the $\mathcal{L}_1$ adaptive controlled longitudinal system, for simulation case 2.

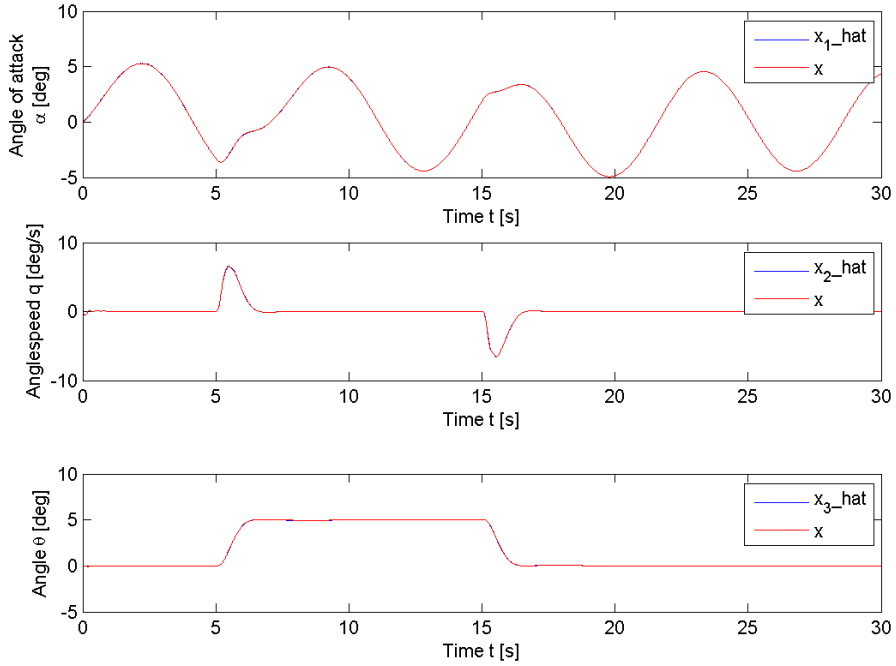

(a) System states with reference r_1

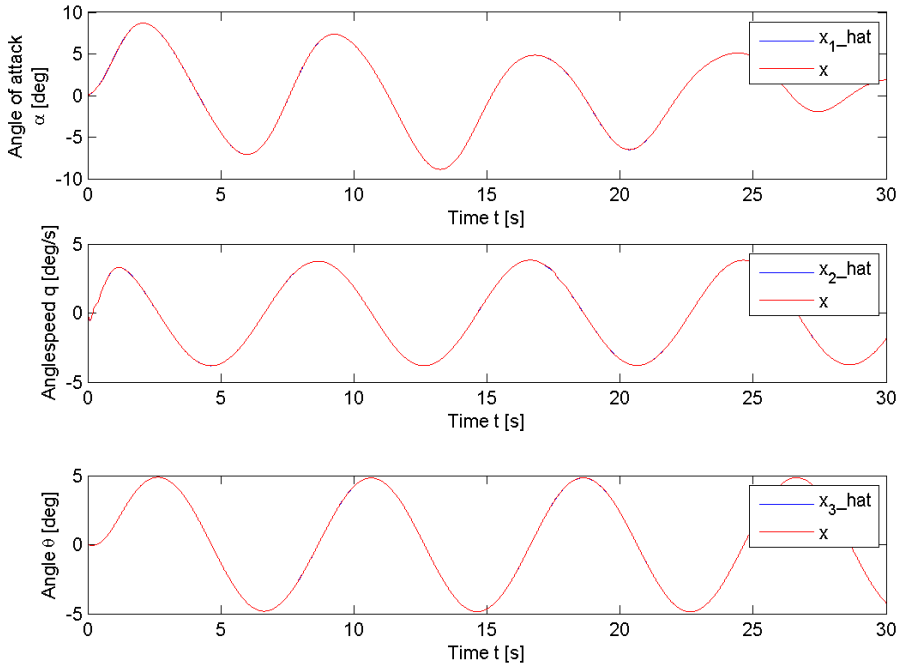

(b) System states with reference r_2

Figure 4.16: Predicted and real system states of the $\mathcal{L}_1$ adaptive controlled longitudinal system, for simulation case 2.

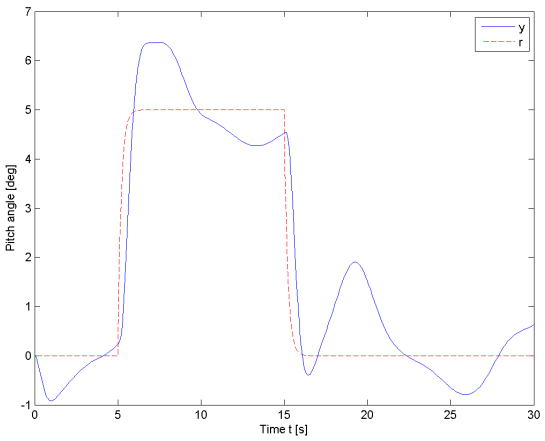

(a) System output with reference r_1

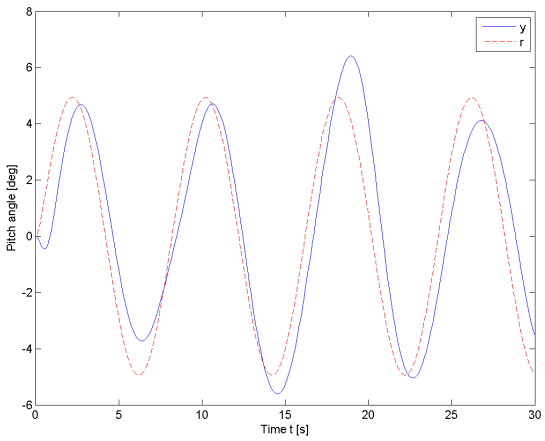

(b) System output with reference r_2

Figure 4.17: System output of the $\mathcal{L}_1$ adaptive controlled longitudinal system, for simulation case 2, without adaptation.

4.3.4 MRAC control of simulation case 2

As explained in chapter 3, the developments of $\mathcal{L}_1$ adaptive control is based on the theory of model reference adaptive control. Since we have argued how $\mathcal{L}_1$ adaptive control is supposed to be a better control strategy than MRAC, it is interesting to perform simulations where an MRAC strategy is used. This section presents this results. The simulations are performed for case 2, described in section 4.3.3. As we will see, one simulation case is enough to show the effect of the filtering in the $\mathcal{L}_1$ adaptive control formulation.

The design of the model reference adaptive controller is identical to the $\mathcal{L}_1$ adaptive control design presented in section 3.5.2 and 4.2 except for some important points:

No filter

Most importantly is the point that the control signal is no longer filtered. Thus, $D(s)$ and the feedback gain k is removed such that the adaptive control signal is defined as

$$u_a d = \frac{1}{\hat{\omega}} \left(k_g r - \hat{\eta}_1 - \hat{\eta}_{2m} \right). \tag{4.53}$$

Handling of the unmatched uncertainties

One other point is that η_{2m}, as defined in (3.126), can no longer be implemented. This is because H_m^{-1} is not proper. Thus, the compensation for the unmatched uncertainties must be done by using vector inversion. Our goal is that the control cancels the effect of the unmatched uncertainties. Thus we want:

$$\mathbf{B}_m u_m = \mathbf{B}_{um} \hat{\eta}_2 \tag{4.54}$$

$$\Downarrow \tag{4.55}$$

$$u_m = \mathbf{B}_m^{\dagger} \mathbf{B}_{um} \hat{\eta}_2, \tag{4.56}$$

where † denotes the left matrix inverse. Thus, for the MRAC, we redefine

$$\hat{\eta}_{2m} := \mathbf{B}_m^{\dagger} \mathbf{B}_{um} \hat{\eta}_2. \tag{4.57}$$

Tuning of Γ

The adaptation gain Γ must be tuned since we no longer has a output filter $C(s)$. Through simulations for Case 2, it was found that the system was stable for

$$\Gamma \geq 118. \tag{4.58}$$

For the simulations performed, $\Gamma = 1000$ has been used.

New projection bounds

Finally, the projection bounds have been changed. This is because the bounds specified for the $\mathcal{L}_1$ adaptive controller seems to be very conservative, and actually makes the MRAC-controller unstable. The bounds used was found more or less by coincidence, but seem to work well. The bounds are chosen as

$$\theta_{bi} = 0.1, i = 1, 2, \tag{4.59}$$

$$\Delta_i = 0.3, i = 1, 2. \tag{4.60}$$

Except for these changes, the design is unchanged.

The resulting plots for the system output, the control signal together with the real control input, the prediction estimates, and the states together with the state estimates are shown in figures 4.18, 4.19, 4.20 and 4.21 respectively.

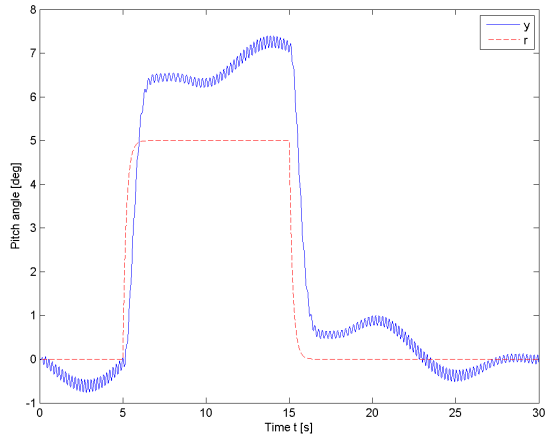

(a) System output with reference r_1

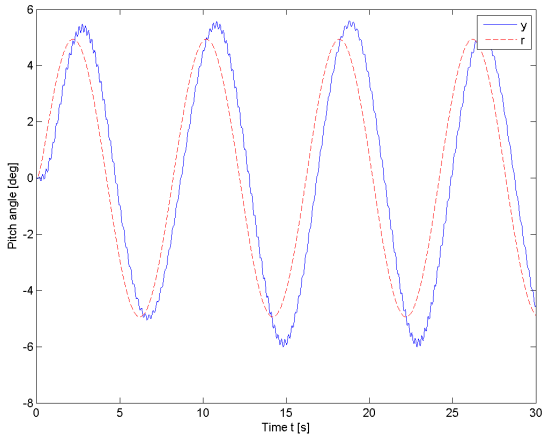

(b) System output with reference r_2

Figure 4.18: MRAC controlled system output of simulation case 2.

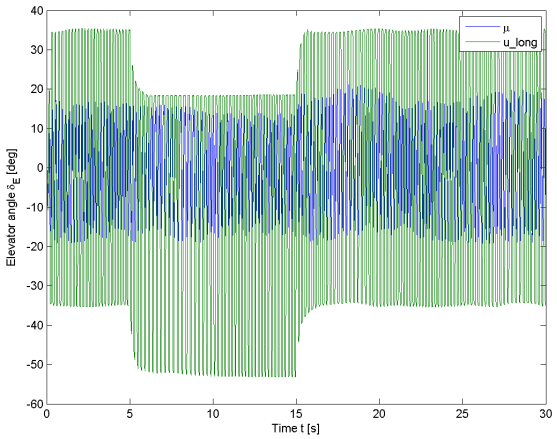

(a) Control signal with reference r_1

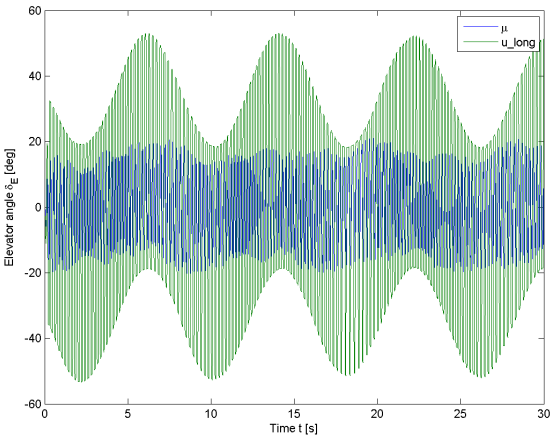

(b) Control signal with reference r_2

Figure 4.19: MRAC control input of simulation case 2.

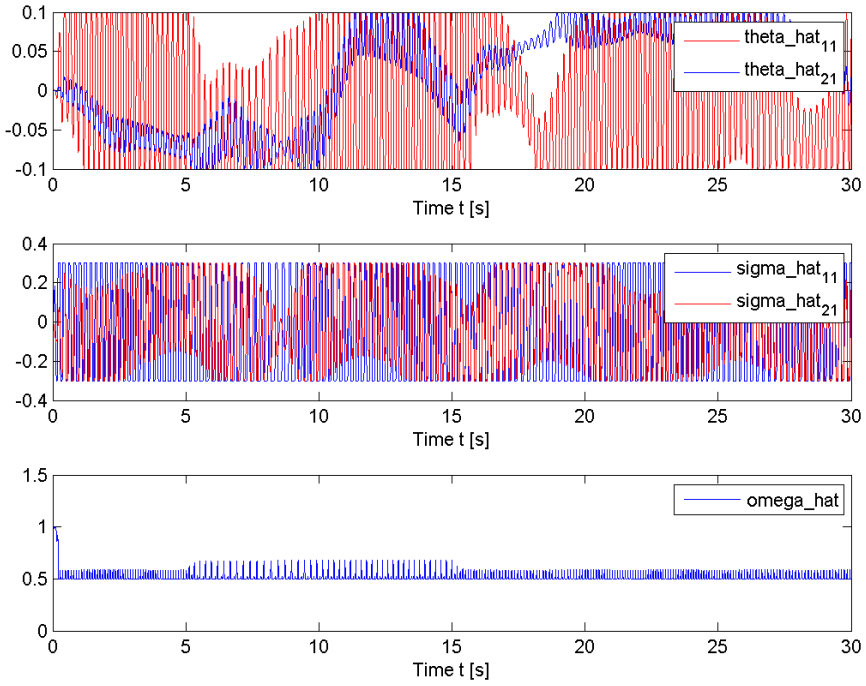

(a) Adaptive estimates with reference r_1

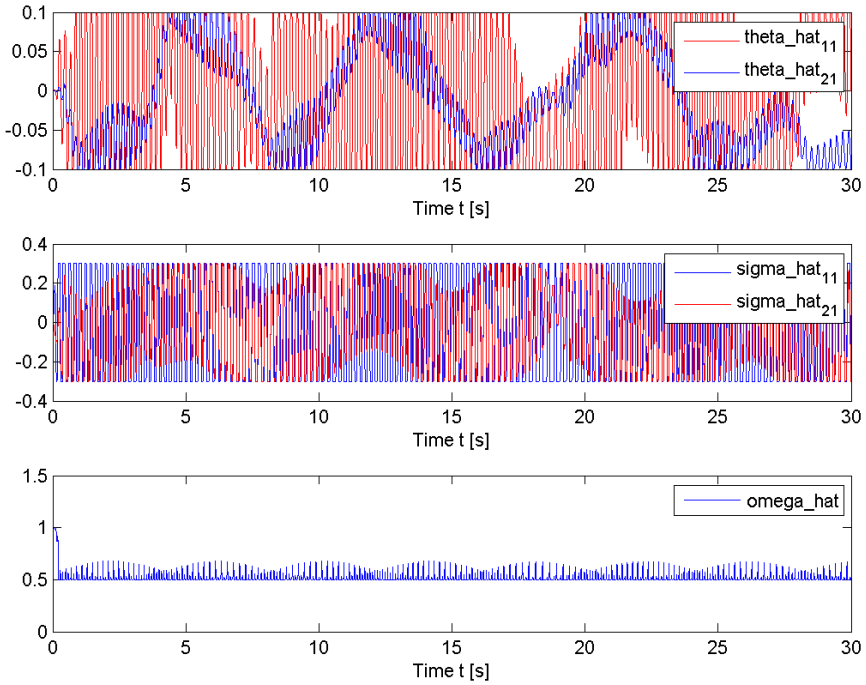

(b) Adaptive estimates with reference r_2

Figure 4.20: Adaptive estimates for MRAC controlled system, simulation case 2.

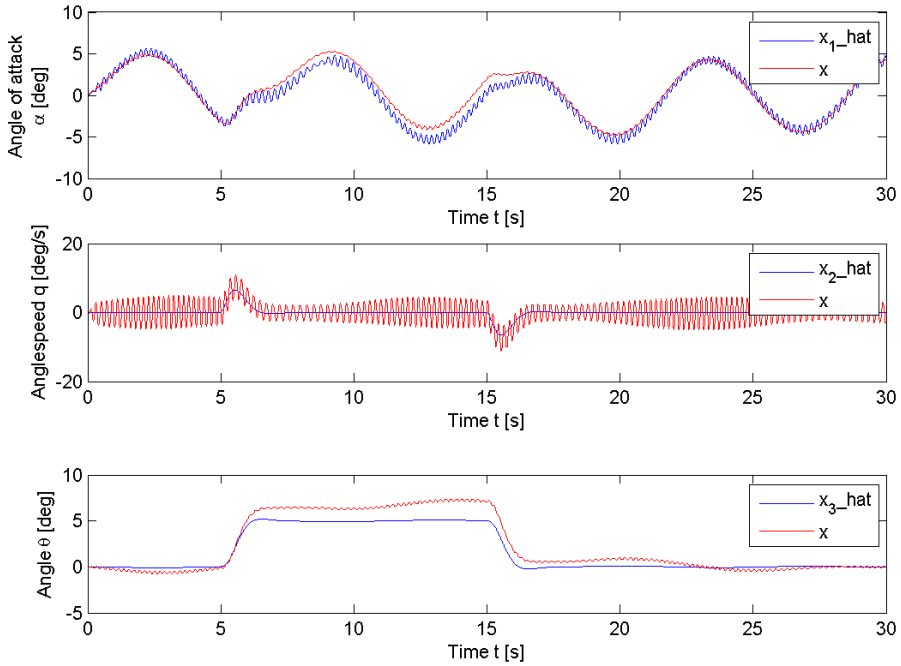

(a) System states with reference r_1

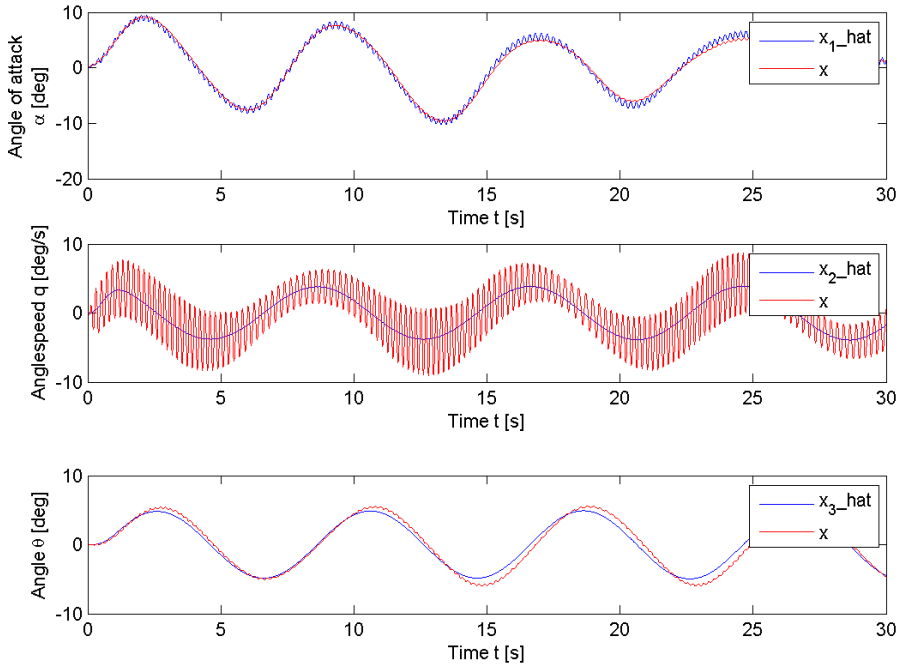

(b) System states with reference r_2

Figure 4.21: MRAC controlled system states of simulation case 2.

4.3.5 Discussion

In this section the simulation results for the longitudinal system, presented in section 4.3 and section 4.3.4 are discussed. Two different cases are presented which shows the response and robustness of the $\mathcal{L}_1$ adaptive controller.

Design system

Section 4.3.1 presents the simulation results for the design system. That is the system results when the modelling errors are equal to zero. The actuator dynamics are however included. This controller is not implementable, but represents the goal of the $\mathcal{L}_1$ adaptive controller and is the basis for the design of K_m. From figure 4.5 (a) we see that the output gets a small overshoot before it settles after approximately 2 seconds. Due to the actuator dynamics, we can not make the system more aggressive without loose robustness. Further, figure 4.5 and 4.7 shows the control signals and the system states for the non-implementable system.

Simulation case 1

Section 4.3.2 presents the simulation results for the first case. This case is designed to test the response of the $\mathcal{L}_1$ adaptive controller for the nonlinear effect that a changing α has on the system matrix. The modelling error is implemented as a sinusoidal change on element $(2,1)$ on the system matrix. Compared to the identified system matrix in (4.1), we see that the amplitude of the error is more than six times the initial value. Thus, this presents a major change in the system response. We also note that when the sinusoidal is at its peak, such that the error in element $(2,1)$ equals 10, the eigenvalues of A becomes

$$\lambda = \begin{bmatrix} -3.5740 \\ 2.0552 \\ 0.0000 \end{bmatrix}.$$

This means that the real system changes between being stable and being unstable as the time goes. Lastly, we note that this represents an unmatched uncertainty.

As we can see from figure 4.8, the $\mathcal{L}_1$ adaptive controller handles this nonlinear modelling error really well, both for the filtered step in reference, and for the sinusoidal reference signal. Compared to the design system in figure 4.5, where the modelling error is set to zero, we see that we achieve almost the same result for the $\mathcal{L}_1$ controlled system in Case 1. The most notable difference is with reference r_1, where the output of the $\mathcal{L}_1$ controlled system oscillates a few more timed before it settles on the desired angle. This oscillation has however a max peak of less than half a degree, and is thus a really good result. Comparing figure 4.7 and figure 4.11, we see that the response of system states becomes quite similar for the ideal case and the $\mathcal{L}_1$ controlled system in Case 1.

Further, in figure 4.12 we see the response of the system output without adaptation, that is when $\Gamma = 0$. We see that the output gets an overshoot of about 3 degrees for both of the reference signals. This shows how well the adaptation works to compensate for the error. The $\mathcal{L}_1$ adaptive controller senses the model error and adapts fast to this change to correct the control input and give close to the desired response.

Comparing the control signals of the ideal system in figure 4.6 with the control signals of the $\mathcal{L}_1$ controlled system 4.9, we notice some clear differences. We see how the control signal from the $\mathcal{L}_1$ adaptive controller constantly has to work to compensate for the modelling error. This is especially clear for the simulation with reference $r2$, where the input signal looks like a simple sinusoidal curve for the ideal case, while the control signal for the $\mathcal{L}_1$ adaptive control gets a more complex shape. Comparing the control signal u with the real control input μ we see that μ lags a little behind u. This is equivalent to a time delay, which we know is bad for the robustness. We see that the choice of $\mathbf{K}_m$ together with the adaptation makes the $\mathcal{L}_1$ adaptive controller robust enough to cope with this.

Figure 4.10 shows the adaptive estimates during the simulation of case 2. For both the reference signals, we see that $\hat{\omega}$ is kept almost constant to 1 through the simulation. We know that $F(0) = 1$, so we see that the prediction of ω is good. Comparing the estimates of σ and θ with each other, we see that they have almost the exact same shape. Considering the adaptation laws in (3.123), this is not a very surprising result. The only difference between them is that the adaptation law for $\hat{\theta}$ is multiplied by the ∞-norm of $\mathbf{x}$. Thus, only a scalar number differ the adaptation rates of $\hat{\theta}$ and $\hat{\sigma}$. This suggests that it may be sufficient to only adapt $\hat{\sigma}$, and let this take care of all the modelling error. In section 4.8 considering the case of limited sampling time, we will see that this actually is the case, and discuss this topic further.

From the plot of the system states and the predicted states in figure 4.11 we can see no error between the real and the predicted states. It therefore seems like the adaptation gain is chosen large enough to compensate for the modelling errors.

Simulation case 2

Section 4.3.3 presents the simulation results for the second case. This case is designed to put the $\mathcal{L}_1$ adaptive controller to the test. In this case we have included a sinusoidal error with an amplitude of 0.5 in element $(1, 2)$ of the system matrix, and a constant error of 6 on element $(2, 2)$. Further, a sinusoidal gain is multiplied with the input vector, and sinusoidal disturbance is applied to α and q. All the sinusoidal signals have different frequencies and phase shift. Thus, the system will experience nonlinear modelling errors and nonlinear disturbances. Further, due to the error in element $(2, 2)$ of the system matrix, the system with the feedback loop through K_m is unstable. We note that the modelling errors and disturbances considered in Case 2 are unmatched uncertainties.

From figure 4.13 we see that the $\mathcal{L}_1$ adaptive controller again gives a really good result. Even when the system with feedback is unstable, the $\mathcal{L}_1$ adaptive controller compensates for this and keeps the system stable. Further, the nonlinear modelling error and disturbances are

quickly compensated for, and we see almost no effect from them on the system output. Figure 4.17 shows the system output when there is no adaptation and the error on element $(1, 2)$ is sat to zero. The reason for setting the specific error to zero is because it makes the feedback system unstable. This figure shows how the changing nonlinear modelling errors affects the output, when the adaptation is turned off. For the simulation with reference r_1, we see that the output oscillates around the reference, and is unable to achieve tracking. For the simulation with reference r_2 we see that the result is a bit better, but compared to the $\mathcal{L}_1$ adaptive controller performs poorly. This again proves the good result of the $\mathcal{L}_1$ adaptive controller.

Similar to Case 1 we see from figure 4.14 how the controller have to work to compensate for the disturbances. Even when the output is kept constant, the controller changes dependent on the disturbances.

Considering the adaptive estimates in figure 4.15 we see that this time $\hat{\omega}$ wanders more off the right value than before. Again we notice some similarities in the estimates of $\hat{\theta}$ and $\hat{\sigma}$. However, with the exception of the sudden steps in $\hat{\theta}$, this estimate is kept quite constant. It looks like $\hat{\sigma}$ takes care of most of the adaptation.

MRAC-control

To investigate the effect of the filter $C(s)$, a simulation with an MRAC-controller has been performed for Case 2. The design and the resulting plots are presented in section 4.3.4. First of all, we see from figure 4.18 that the MRAC-controller manages to keep the system stable, but the performance of the MRAC-controller is far from the performance of the $\mathcal{L}_1$ controller. The most distinct difference between MRAC and $\mathcal{L}_1$ adaptive control can be seen from figure 4.19 and 4.20, which shows the control input and the estimates respectively. We see that the estimates is almost constantly oscillating between one end of the projection bound to the other end of the projection bound. This again goes directly back to the control signal which also oscillates rapidly. This is consistent with the problems of MRAC pointed out in section 3.2.4. We also see from figure 4.21 that the predicted states differ from the real states.

General remarks

As discussed in section 4.2.3, the $\mathcal{L}_1$-norm condition is not verified. Thus, none of the theoretical results can be proven to hold. Since we for real implementations can have no exact knowledge about the uncertainties, the $\mathcal{L}_1$-norm condition is impossible to prove to be verified in practice. However, as we have seen in the simulations presented, the $\mathcal{L}_1$ adaptive controller manages to give a robust response and a good performance for different types of uncertainties and disturbances, without any retuning, and without persistence of excitation. This imply that the $\mathcal{L}_1$-norm condition is quite conservative. From figure 4.10 and figure 4.15 we also see that the estimated values of θ are never near the bounds found in (4.33) and (4.33). This further imply that the bounds specified in the theory are chosen very conservative and thus contribute to making the $\mathcal{L}_1$-norm condition conservative. We have thus

shown that even though the $\mathcal{L}_1$-norm condition is not met, following the design strategies presented in chapter 3, we can achieve the same results as the ones proved in theory.

As mentioned in section 4.1, the model used in the simulations include a limitation in the control surfaces. As we can see from the presented simulations of the $\mathcal{L}_1$ adaptive controller, the control signal have never been near this limitation. What has been experienced through simulations is that $\mathcal{L}_1$ adaptive control does not work well when the control input is saturated. What happens when the control signal is saturated is that the we get an error between the predicted state and the real state due to the error between the assumed output and the real output. This error causes the estimated values of ω and σ to change. As the estimations are updated, the adaptive controller wants to compensate for this modelling error, and thus increases the control signal. This increase again makes the prediction error larger. Thus, we see that we get a wind-up situation. To prevent this from happening the feedback vector K_m must be designed such that the control is not to aggressive. It is also important that the changes in the reference r is not to quick. Keeping this in mind, as have been done for the designs considered in this text, the $\mathcal{L}_1$ adaptive controller works well with control limits.

4.4 $\mathcal{L}_1$ adaptive control design for the lateral system

This section presents the control design used in the simulations of the lateral system in this chapter. Again, the controller is designed based on the linearised model in section 4.1, and the control laws are kept unchanged for the considered cases. The $\mathcal{L}_1$ adaptive controller is defined by combining the feedback controller defined in (3.109), the predictor (3.122), the adaptation rule (3.123) and the adaptive control law (3.125). The parameters used and the design of the different control elements are presented in the following of this section. The implementation of the $\mathcal{L}_1$ adaptive controller for the lateral system can be found in Appendix 2.

4.4.1 Design of the feedback gain K_m

As for the longitudinal system, we again choose to use LQR-design when specifying the feedback matrix. Compared to for instance pole placement, we get much better control on which states are important to control. In this case these states are of course the output states ϕ and ψ. Thus we want to weight these states relatively high. Again, we need to take into consideration the actuator dynamics. By some trial and error, considering both the

robustness and the desired response, the I chose

$$Q = \begin{bmatrix} 0 & 0 & 0 & 0 & 0 \\ 0 & 10 & 0 & 0 & 0 \\ 0 & 0 & 10 & 0 & 0 \\ 0 & 0 & 0 & 125 & 0 \\ 0 & 0 & 0 & 0 & 125 \end{bmatrix} \tag{4.61}$$

$$R = \begin{bmatrix} 5 & 0 \\ 0 & 5 \end{bmatrix} \tag{4.62}$$

Using the lqr-function in Matlab, this resulted in the feedback matrix

$$K_m = \begin{bmatrix} 0.3241 & -1.8649 \\ -1.4370 & 0.2411 \\ -0.3482 & -1.9091 \\ -4.9169 & 0.8030 \\ -1.0851 & -4.8808 \end{bmatrix} \tag{4.63}$$

which again resulted in the system matrix

$$\mathbf{A}_m = \begin{bmatrix} -0.1514 & 0.0855 & -0.9332 & 0.0894 & 0.1522 \\ -8.2619 & -41.1021 & -2.4633 & -132.8518 & -12.8408 \\ 1.4497 & -1.3998 & -5.9279 & -4.7099 & -14.6227 \\ 0 & 1.0000 & 0 & 0 & 0 \\ 0 & 0 & 1.0000 & 0 & 0 \end{bmatrix} \tag{4.64}$$

with the eigenvalues

$$\lambda = \begin{bmatrix} -37.6475 \\ -0.1229 \\ -2.9324 + j2.7157 \\ -2.9324 - j2.7157 \\ -3.5461 \end{bmatrix} \tag{4.65}$$

The bode plots of $\frac{y}{r}(s)$ in (4.10) can be seen in figure 4.22. We see that the choice of K_m gives a gain margin for the response from r_1 to y_1 of 15.2 dB and a phase margin of 165 degrees, for the response from r_2 to y_2 we get a gain margin of 18.2 dB and a phase margin of 180 degrees, for the response from r_1 to y_2 we get a gain margin of 27.4 dB and an infinite phase margin, and for the response from r_2 to y_1 we get a gain margin of 35.4 dB and an infinite phase margin. These are acceptable margins [11].

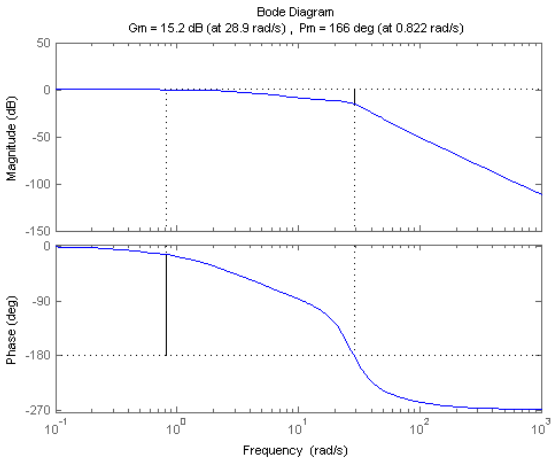

(a) Bode plot from reference r_1 to output y_1.

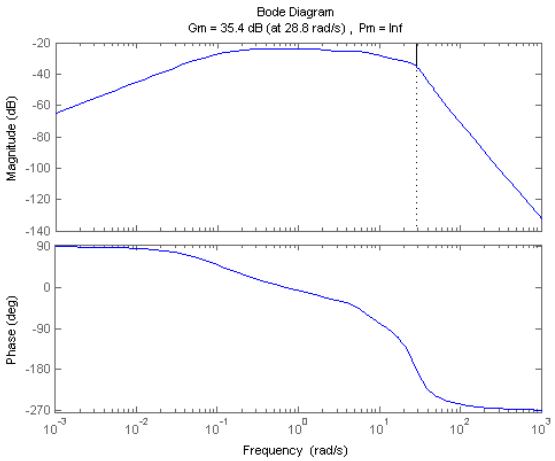

(b) Bode plot from reference r_1 to output y_2.

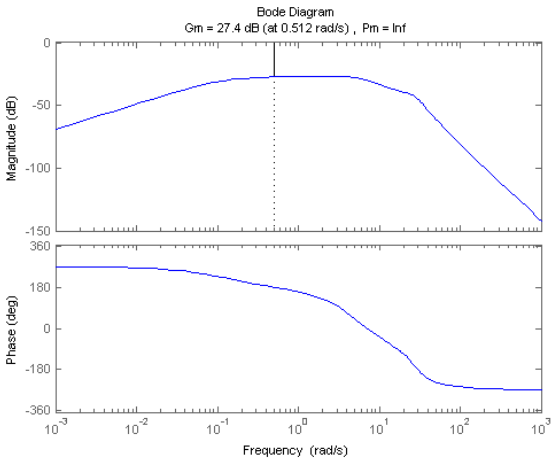

(c) Bode plot from reference r_2 to output y_1.

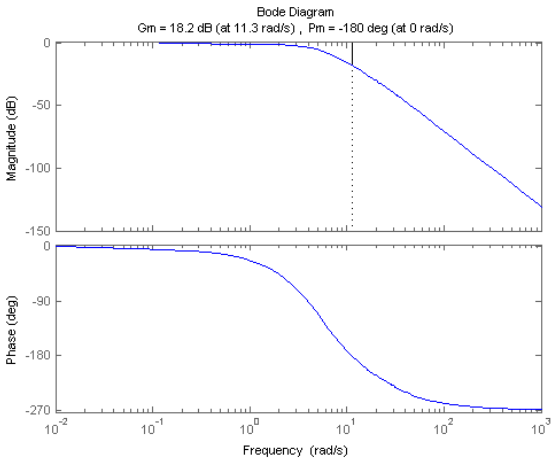

(d) Bode plot from reference r_2 to output y_2.

Figure 4.22: Bode plot of $\frac{y}{r}(s) = \mathbf{C}\left(s\mathbb{I}_n - \left(\mathbf{A}_{id} - \mathbf{B}_{id}F(s)K_m\right)\right)^{-1} k_g\mathbf{B}_{id}F(s)$

4.4.2 Specifying the projection bounds

Again, we need some knowledge about the uncertainties to find the projection bounds. The kind of uncertainties considered in the following simulations are

$$\tilde{\mathbf{f}}_x(t, \mathbf{x}(t)) = \mathbf{A}_\Delta \mathbf{x}(t) + \boldsymbol{\sigma}(t), \tag{4.66}$$

$$\tilde{\mathbf{B}}(t, \mathbf{x}(t)) = \tilde{\mathbf{B}} \tag{4.67}$$

Further, the unmodeled actuator dynamics causes an extra unknown error since

$$\boldsymbol{\mu}(t) = \boldsymbol{\omega} u + \boldsymbol{\sigma}_\mu(t) \tag{4.68}$$

From (3.171) and the results above, we get that the modelling error becomes

$$\begin{aligned}\mathbf{f}(t, \mathbf{x}(t)) = \mathbf{B}_{id}\mathbf{K}_m^T(\mathbb{I} - \boldsymbol{\omega})\mathbf{x}(t) + \mathbf{A}_\Delta \mathbf{x}(t) + \boldsymbol{\sigma}(t) + (\mathbf{B}_{id} + \tilde{\mathbf{B}})\boldsymbol{\sigma}_\mu(t) \\ + \tilde{\mathbf{B}}\boldsymbol{\omega}(\mathbf{u}_{ad} - \mathbf{K}_m^T \mathbf{x}(t))\end{aligned} \tag{4.69}$$

Specifying Δ_1

From (4.69) we have

$$\mathbf{f}(t, 0) = \boldsymbol{\sigma}(t) + (\mathbf{B}_{id} + \tilde{\mathbf{B}})\boldsymbol{\sigma}_\mu(t) + \tilde{\mathbf{B}}\boldsymbol{\omega}\mathbf{u}_{ad}(t) \tag{4.70}$$

where σ is the only signal we have knowledge about. From (3.114) we again have that

$$\begin{bmatrix}\mathbf{f}_1(t, \mathbf{x}(t)) \\ \mathbf{f}_2(t, \mathbf{x}(t))\end{bmatrix} = \begin{bmatrix}\mathbf{B}_m & \mathbf{B}_{um}\end{bmatrix}^{-1} f(t, \mathbf{x}(t)). \tag{4.71}$$

In the cases considered in this text, $\sigma_{max} := \|\boldsymbol{\sigma}(t)\|_\infty = 50\pi/180 \approx 0.873$. We find a lower bound on the error:

$$\|\mathbf{f}_1(t, 0)\|_\infty \geq \left\| \begin{bmatrix}1 & 0 & 0 \\ 0 & 0 & 0 \\ 0 & 0 & 0\end{bmatrix} \begin{bmatrix}\mathbf{B}_m & \mathbf{B}_{um}\end{bmatrix}^{-1} \right\|_\infty \sigma_{max} \tag{4.72}$$

$$\|\mathbf{f}_2(t, 0)\|_\infty \geq \left\| \begin{bmatrix}0 & 0 & 0 \\ 0 & 1 & 0 \\ 0 & 0 & 1\end{bmatrix} \begin{bmatrix}\mathbf{B}_m & \mathbf{B}_{um}\end{bmatrix}^{-1} \right\|_\infty \sigma_{max} \tag{4.73}$$

This gives

$$\|\mathbf{f}_1(t, 0)\|_\infty \geq 0.3247 \tag{4.74}$$

$$\|\mathbf{f}_2(t, 0)\|_\infty \geq 0.8820 \tag{4.75}$$

Based on this, and proven to give good results through simulations, the projection bound defined in (3.124) is chosen as

$$\Delta_1 = 0.6 \tag{4.76}$$

$$\Delta_2 = 1.2. \tag{4.77}$$

Specifying θ_{bi}

From (4.69) we have

$$\frac{\delta \mathbf{f}(t,\mathbf{x})}{\delta \mathbf{x}} = \mathbf{B}_{id}\mathbf{K}_m^T(\mathbb{I}-\boldsymbol{\omega}) + \mathbf{A}_\Delta - \tilde{\mathbf{B}}\mathbf{K}_m^T + (\mathbf{B}_{id}+\tilde{\mathbf{B}})\frac{\delta \boldsymbol{\sigma}_\mu}{\delta \mathbf{x}} + \tilde{\mathbf{B}}\frac{\delta \mathbf{u}_{ad}}{\delta \mathbf{x}}, \tag{4.78}$$

for all $\|\mathbf{x}\|_\infty < \infty$. We known that $F(0) = \mathbb{I}$, thus $\omega = \mathbb{I}$. Further, from the cases considered we have that

$$\max_{\mathbf{A}_\Delta} \left\| \begin{bmatrix} 1 & 0 & 0 & 0 & 0 \\ 0 & 1 & 0 & 0 & 0 \\ 0 & 0 & 0 & 0 & 0 \\ 0 & 0 & 0 & 0 & 0 \\ 0 & 0 & 0 & 0 & 0 \end{bmatrix} \begin{bmatrix} \mathbf{B}_m & \mathbf{B}_{um} \end{bmatrix}^{-1} \mathbf{A}_\Delta \right\|_\infty = 4.8070 \tag{4.79}$$

$$\max_{\mathbf{A}_\Delta} \left\| \begin{bmatrix} 0 & 0 & 0 & 0 & 0 \\ 0 & 0 & 0 & 0 & 0 \\ 0 & 0 & 1 & 0 & 0 \\ 0 & 0 & 0 & 1 & 0 \\ 0 & 0 & 0 & 0 & 1 \end{bmatrix} \begin{bmatrix} \mathbf{B}_m & \mathbf{B}_{um} \end{bmatrix}^{-1} \mathbf{A}_\Delta \right\|_\infty = 0.1470 \tag{4.80}$$

and

$$\max_{\tilde{\mathbf{B}}} \left\| \begin{bmatrix} 1 & 0 & 0 & 0 & 0 \\ 0 & 1 & 0 & 0 & 0 \\ 0 & 0 & 0 & 0 & 0 \\ 0 & 0 & 0 & 0 & 0 \\ 0 & 0 & 0 & 0 & 0 \end{bmatrix} \begin{bmatrix} \mathbf{B}_m & \mathbf{B}_{um} \end{bmatrix}^{-1} \tilde{\mathbf{B}} K_m^T \right\|_\infty = 1.4391 \tag{4.81}$$

$$\max_{\tilde{\mathbf{B}}} \left\| \begin{bmatrix} 0 & 0 & 0 & 0 & 0 \\ 0 & 0 & 0 & 0 & 0 \\ 0 & 0 & 1 & 0 & 0 \\ 0 & 0 & 0 & 1 & 0 \\ 0 & 0 & 0 & 0 & 1 \end{bmatrix} \begin{bmatrix} \mathbf{B}_m & \mathbf{B}_{um} \end{bmatrix}^{-1} \tilde{\mathbf{B}} K_m^T \right\|_\infty = 0.0075 \tag{4.82}$$

The last addends $(\mathbf{B}_{id}+\tilde{\mathbf{B}})\frac{\delta \boldsymbol{\sigma}_\mu}{\delta \mathbf{x}} + \tilde{\mathbf{B}}\frac{\delta u_{ad}}{\delta \mathbf{x}}$ we have no control over. Thus we get

$$L_1 = \left\| \frac{\delta f_1(t,\mathbf{x})}{\delta \mathbf{x}} \right\|_\infty \geq 6.2461 \tag{4.83}$$

$$L_2 = \left\| \frac{\delta f_1(t,\mathbf{x})}{\delta \mathbf{x}} \right\|_\infty \geq 0.1545 \tag{4.84}$$

Bases on these calculations, we choose a conservative bound on the projection bound, defined in (3.124), as

$$\theta_{bi} = 8 \tag{4.85}$$

$$\theta_{bi} = 1. \tag{4.86}$$

Specifying Ω

In the cases considered in the simulations, we know that $F(0) = \mathbb{I}$. However, it may be beneficial to let some of the error in **B** be taken care of by $\hat{\boldsymbol{\omega}}$. Further it is interesting to see how this adaptation affect the control. In the simulations considered, the bounds on $\boldsymbol{\omega}$ are given as

$$\hat{\boldsymbol{\omega}} \in \begin{bmatrix} [0.5, 2] & [-0.3, 0.3] \\ [-0.3, 0.3] & [0.5, 2] \end{bmatrix} = \Omega. \tag{4.87}$$

Initial conditions

The initial conditions for the estimates have to be specified. The only requirement from the $\mathcal{L}_1$ theory is that the initial values are chosen within the specified projection bounds. For all the simulations performed for the lateral system the initial guess is that there is no modelling error, that is:

$$\hat{\theta}_{10} = \begin{bmatrix} 0 \\ 0 \end{bmatrix} \tag{4.88}$$

$$\hat{\theta}_{20} = \begin{bmatrix} 0 \\ 0 \\ 0 \end{bmatrix} \tag{4.89}$$

$$\hat{\sigma}_{10} = \begin{bmatrix} 0 \\ 0 \end{bmatrix} \tag{4.90}$$

$$\hat{\sigma}_{20} = \begin{bmatrix} 0 \\ 0 \\ 0 \end{bmatrix} \tag{4.91}$$

$$\hat{\boldsymbol{\omega}}_0 = \begin{bmatrix} 1 & 0 \\ 0 & 1 \end{bmatrix} \tag{4.92}$$

4.4.3 Designing the filter $C(s)$

The same guidelines for the design of $C(s)$ holds for the MIMO lateral system as for the SISO longitudinal system. Similar to the longitudinal controller, we chose $D(s)$ according to

$$D(s) = \mathbb{I}_m \frac{1}{s} \tag{4.93}$$

We consider the feedback gain $K = \mathbb{I}_m k$. For the given choice of $D(s)$, we consider the plot of $\|G_m(s)\|_{\mathcal{L}_1} L_1 + \|G(_{um}(s)\|_{\mathcal{L}_1} L_2$ versus k. This can be seen in figure 4.23. The values for L_1 and L_2 used in the plot are the ones found in (4.83) and (4.84) respectively. As we can see the value of $\|G_m(s)\|_{\mathcal{L}_1} L_1$ is actually increasing as k increases. This is a bit strange result compared to the $\mathcal{L}_1$ theory. This may be due to numerical errors in the computations. Some

problems occurred in the computations when the systems became large. Thus, the Matlab function balred() was used to reduce the order of the systems. This may have given bad results in the computation of the $\mathcal{L}_1$-norms. It does however not seems like it is possible to meet the $\mathcal{L}_1$-norm condition, and thus the design must be based on a different analysis.

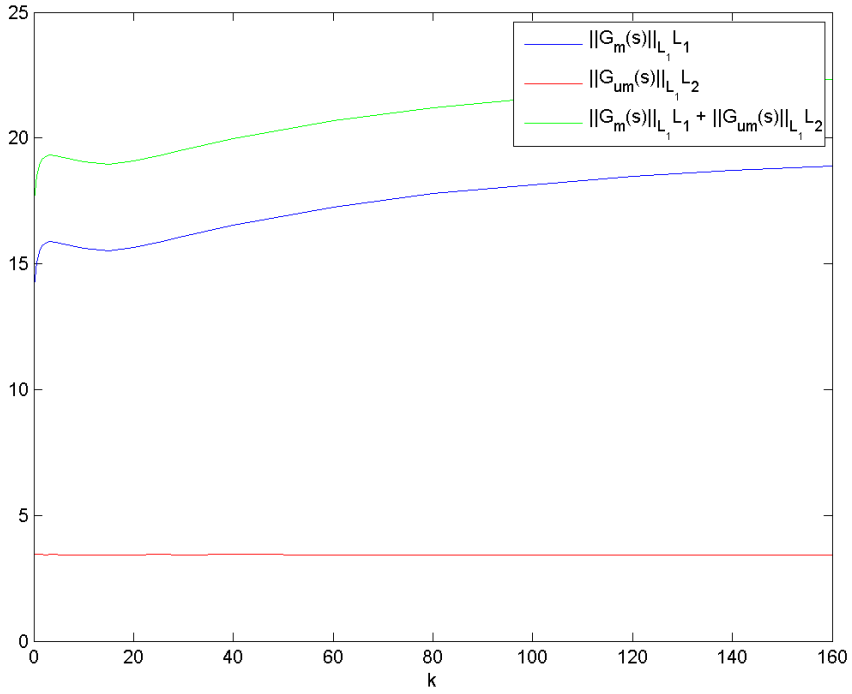

Figure 4.23: $\mathcal{L}_1$-norm condition as a function of k.

Figure 4.24 shows the system output and the control input for a simulation of case 1, described in section 4.5.2, with $K = \mathbb{I}_m 12.5$. We see that the system becomes unstable, and that the response of the control signals u_1 and u_2 are to fast for the real inputs μ_1 and μ_2 to keep up. Thus we know that we need to choose a smaller value for k to keep the system stable. However, considering the system output of the simulation of case 2, described in section 4.5.3, with the same $K = \mathbb{I}_m 12.5$, we see that the response is very good, and actually better than the one achieved with the actual choice of K, seen in figure 4.35. Based on lots of simulations, the choice

$$K = \begin{bmatrix} 2.5 & 0 \\ 0 & 2.5 \end{bmatrix} \tag{4.94}$$

seems to give good results, even though the $\mathcal{L}_1$-norm condition is not met. This choice results in the filter

$$C(s) = \mathbb{I}_m \frac{50.5s^2 + 1020s}{s^4 + 40.4s^3 + 458.5s^2 + 1020s} \tag{4.95}$$

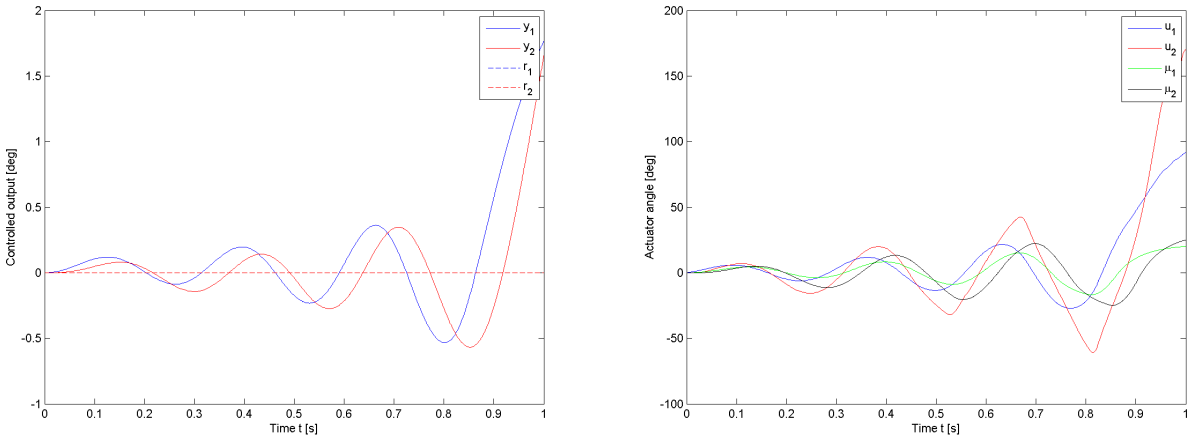

(a) System output

(b) Control input

Figure 4.24: Simulation of case 1 with $K = \mathbb{I}_m 12.5$, and reference r_1.

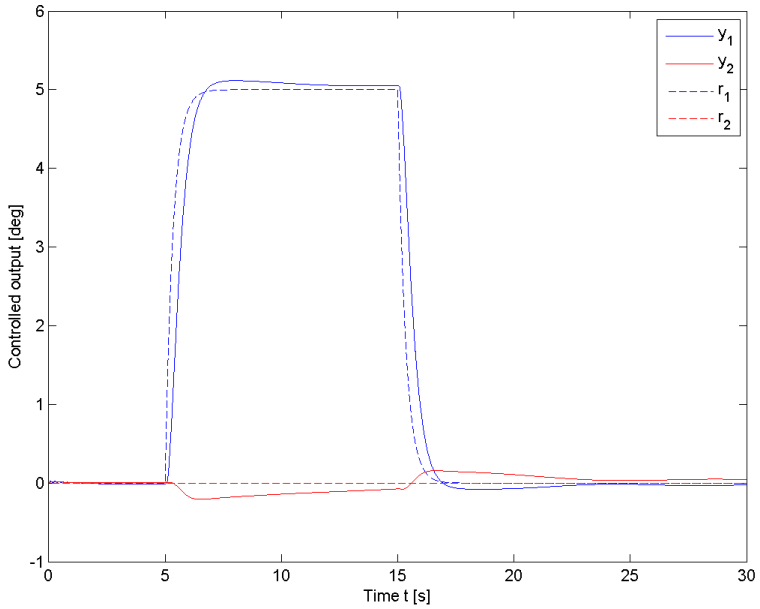

Figure 4.25: System output of simulation case 2, with $K = \mathbb{I}_m 12.5$, and reference r_1.

with the bode plot given in figure 4.26. Compared to the bode-plot of the bode plot of $\frac{y}{r}(s)$ in figure 4.22 we see that the bandwidth of $C(s)$ is a bit low to be able to compensate for the desired frequencies. This is the result we see by comparing the plots of case 2 with $k = 12.5$, in figure 4.25, with simulations of the same case and $k = 2.5$, in figure 4.35. However as shown, increasing k makes the controller lose the robustness needed to control case 1.

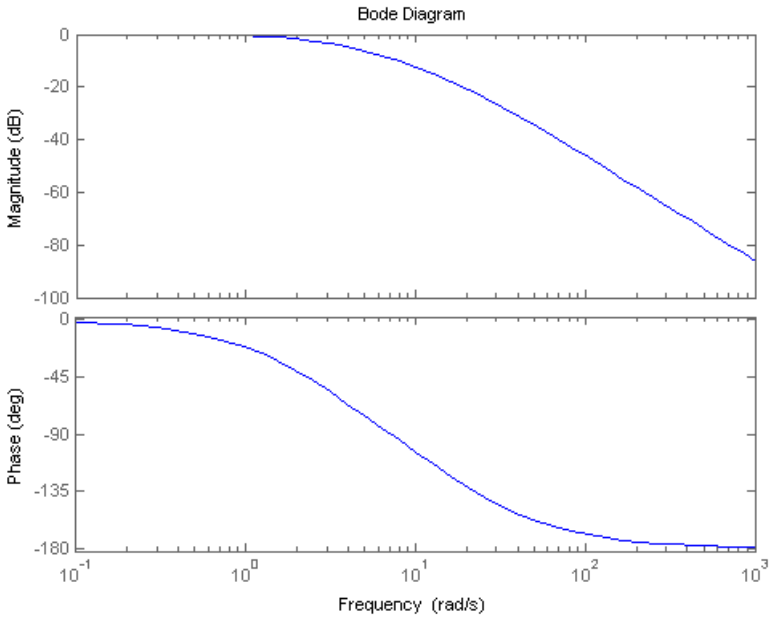

Figure 4.26: Bode plot of $C(s)$.

4.4.4 Choosing the adaptation gain Γ

Again, we know that a large as possible adaptation gain is beneficial for performance. The adaptation gain considered in the simulation is

$$\Gamma = 20000 \tag{4.96}$$

4.5 Simulation results and discussion for the lateral system

In this section, the simulation results of the $\mathcal{L}_1$ adaptive controller for the lateral system are presented. Is before, it would be impossible to consider and simulate all the different non-linear effects the aircraft could encounter. Two different cases are chosen and presented, which try to give a good insight in the robustness and the performance of the $\mathcal{L}_1$ adaptive controller. All the simulations presented in this section are performed with the solver ODE45 and a relative tolerance of 10^{-9}. Implementation issues like limited sampling time and measurement errors are considered in section 4.8.

The simulations in this section are performed for two types of reference inputs:

$$r_{10}(t) = \begin{cases} \begin{bmatrix} 5^\circ \\ 0^\circ \end{bmatrix} & , \ 5\ s < t < 25\ s \\ \begin{bmatrix} 0^\circ \\ 0^\circ \end{bmatrix} & , \ \text{otherwise} \end{cases} \tag{4.97}$$

$$r_{20}(t) = \begin{bmatrix} 5^\circ \sin \frac{\pi}{4} t \\ 0^\circ \end{bmatrix} \tag{4.98}$$

Further, to prevent to aggressive change, the reference signals are filtered:

$$r_i(s) = F_r(s) r_{i0}, \tag{4.99}$$

where $F_r(s) = \dfrac{3}{s+3}$.

4.5.1 Design system

First, as a reference to the best possible control result one could hope for, the ideal case with no modelling error is presented. This represents the design system. The simulation is performed by setting the adaptation gain to zero, and removing all error. The resulting plots for the system output, the control signal together with the real control input, and the states are shown in figures 4.27, 4.28 and 4.29 respectively.

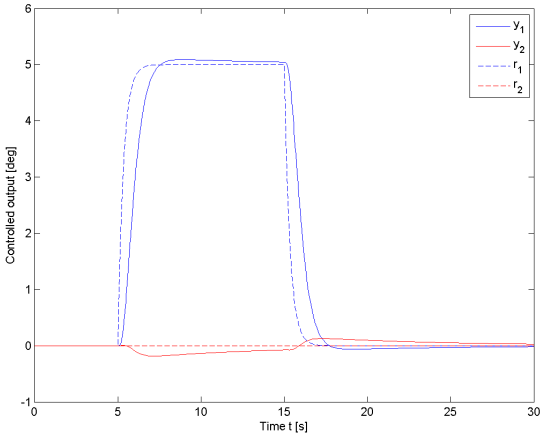

(a) System output with reference r_1

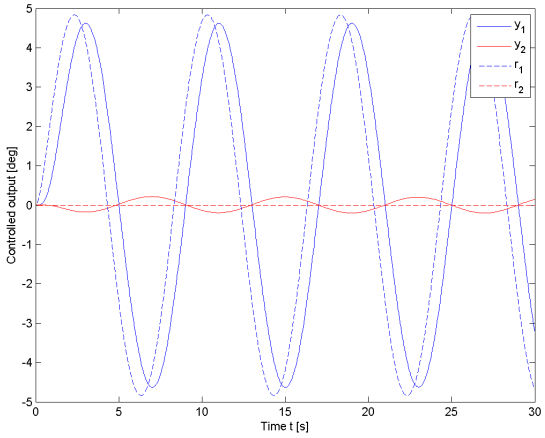

(b) System output with reference r_2

Figure 4.27: System output in the case of no modelling error.

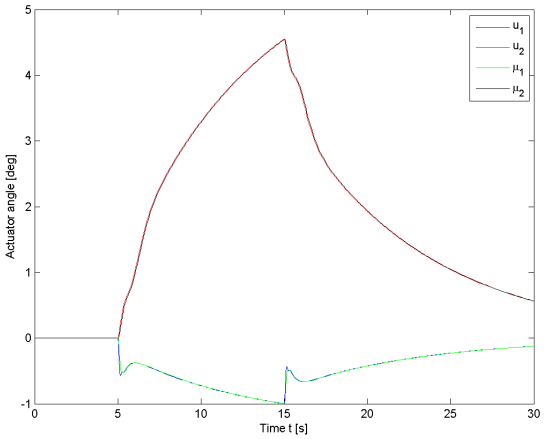

(a) Control signal and real control input with reference r_1

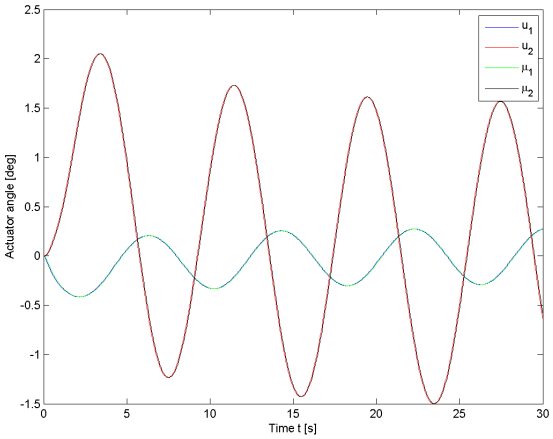

(b) Control signal and real control input with reference r_2

Figure 4.28: Control input in the case of no modelling error.

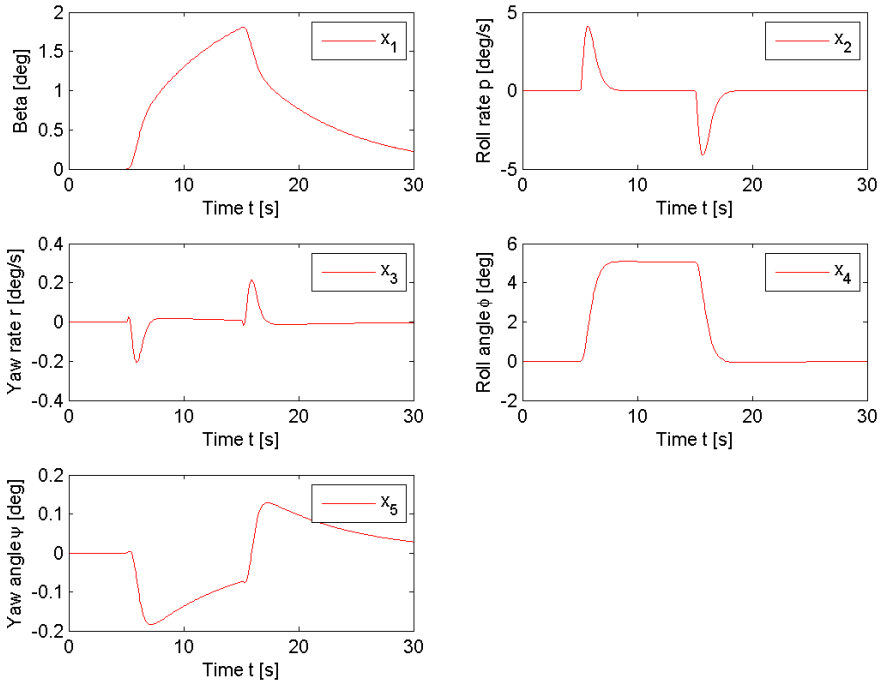

(a) System states with reference r_1

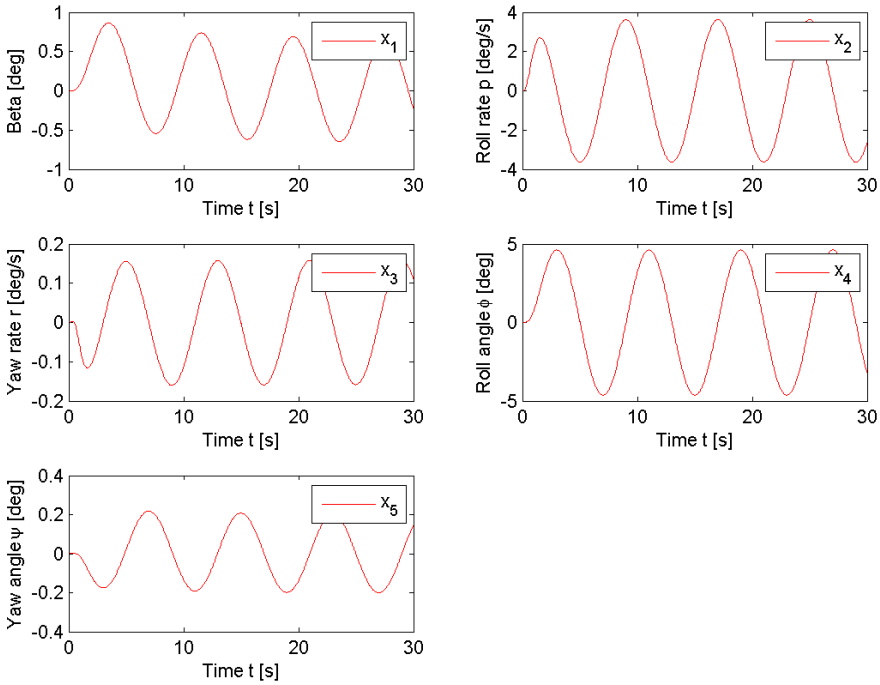

(b) System states with reference r_2

Figure 4.29: System states in the case of no modelling error.

4.5.2 Simulation case 1

As mentioned, the goal is to show the robustness and the performance of the $\mathcal{L}_1$ adaptive controller. Two cases are chosen for this purpose. The system considered in this case is given as

$$\dot{\mathbf{x}}(t) = (\mathbf{A}_{id} + \mathbf{A}_{\Delta})\mathbf{x}(t) + (\mathbf{B}_{id} + \mathbf{B}_{\Delta})\mu(t) + \sigma, \tag{4.100}$$

where

$$\mathbf{A}_{\Delta} = \begin{bmatrix} 0 & 0 & 0 & 0 & 0 \\ 0 & 10 & 5 & 0 & 0 \\ 0 & 14 & 0 & 0 & 0 \\ 0 & 0 & 0 & 0 & 0 \end{bmatrix}, \tag{4.101}$$

$$\mathbf{B}_{\Delta} = \begin{bmatrix} 0 & 0 \\ 5 & 0 \\ 0 & 0 \\ 0 & 0 \\ 0 & 0 \end{bmatrix} \tag{4.102}$$

$$\sigma = \begin{bmatrix} 0 \\ \frac{30\pi}{180} \\ 0 \\ 0 \\ 0 \end{bmatrix} \tag{4.103}$$

The resulting plots for the system output, the control signal together with the real control input, the prediction estimates, and the states together with the state estimates are shown in figures 4.30, 4.31, 4.32 and 4.33 respectively.

As a reference, it is interesting to see how the controller performs without the adaptation. This simulation is shown in figure 4.34.

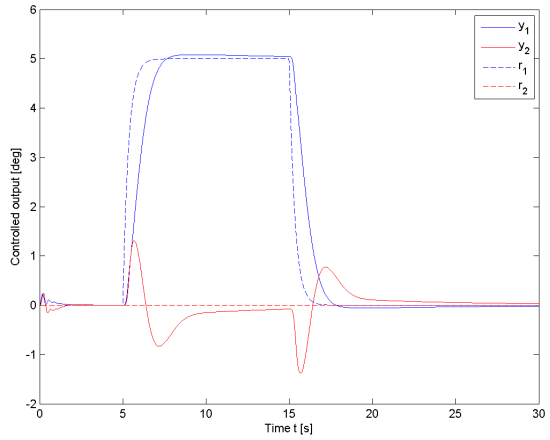

(a) System output with reference r_1

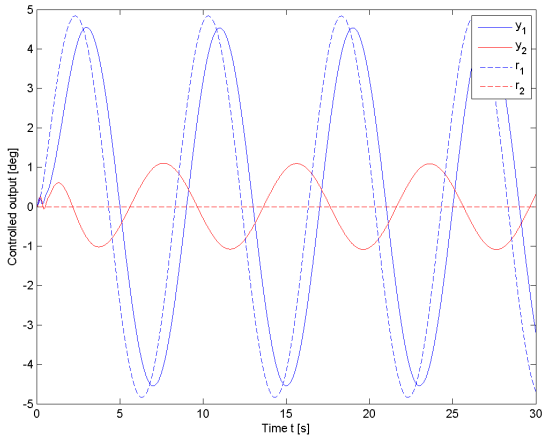

(b) System output with reference r_2

Figure 4.30: System output of the $\mathcal{L}_1$ adaptive controlled lateral system, for simulation case 1.

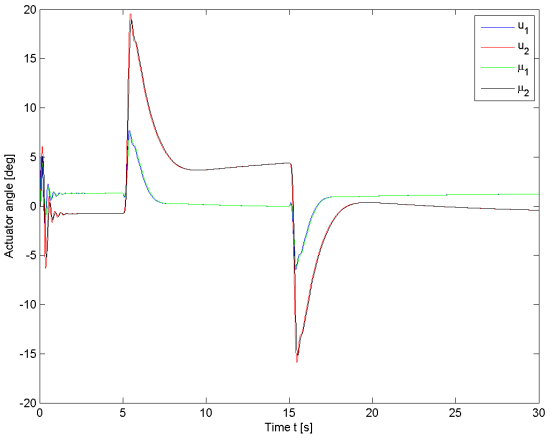

(a) Control signal with reference r_1

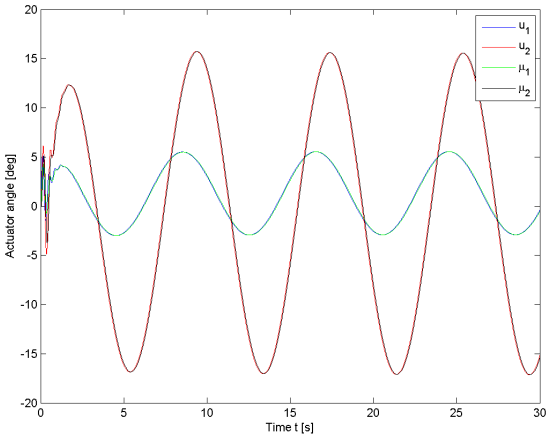

(b) Control signal with reference r_2

Figure 4.31: Control input to the $\mathcal{L}_1$ adaptive controlled lateral system, for simulation case 1.

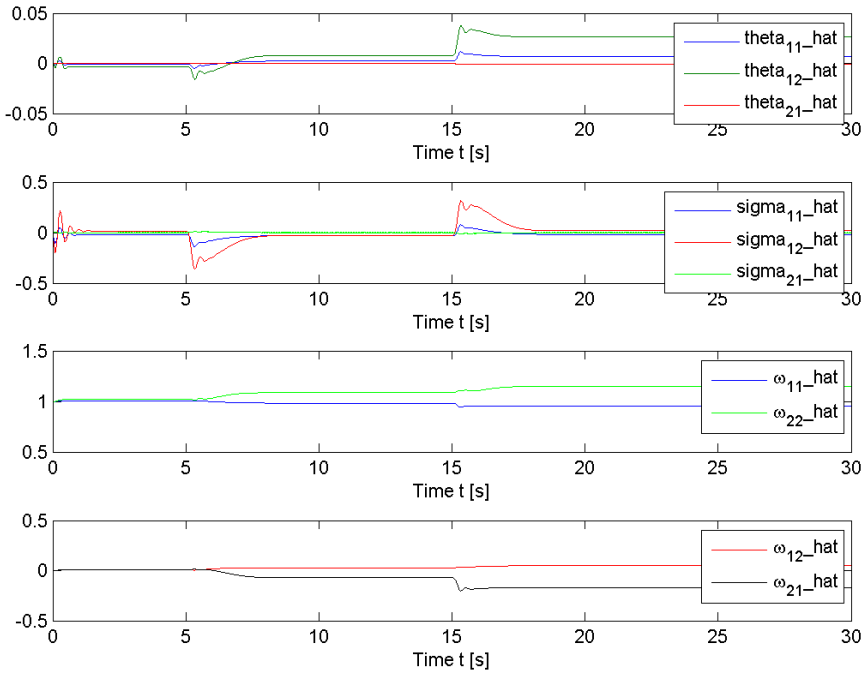

(a) Adaptive estimates with reference r_1

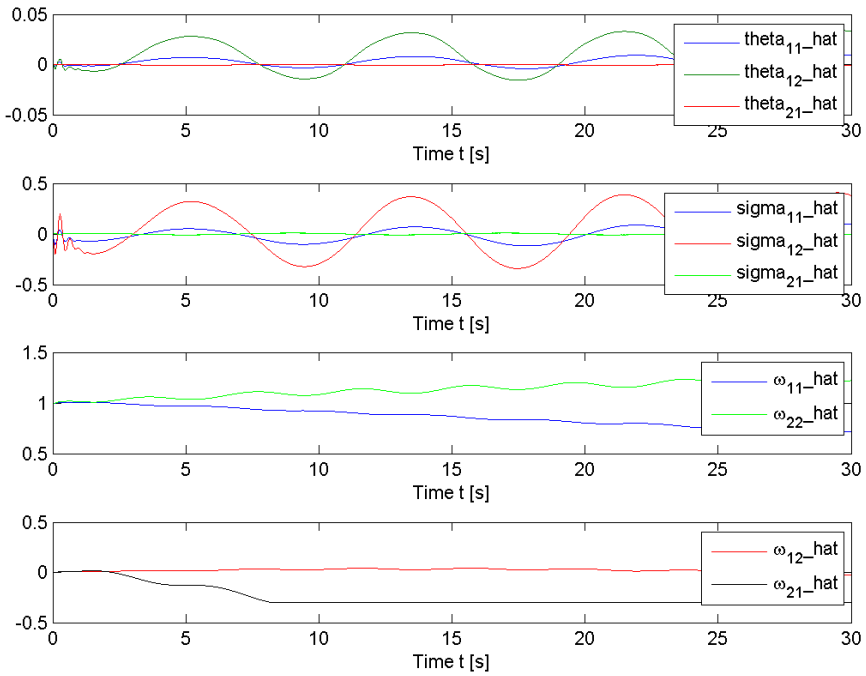

(b) Adaptive estimates with reference r_2

Figure 4.32: Adaptive estimates for the $\mathcal{L}_1$ adaptive controlled lateral system, for simulation case 1.

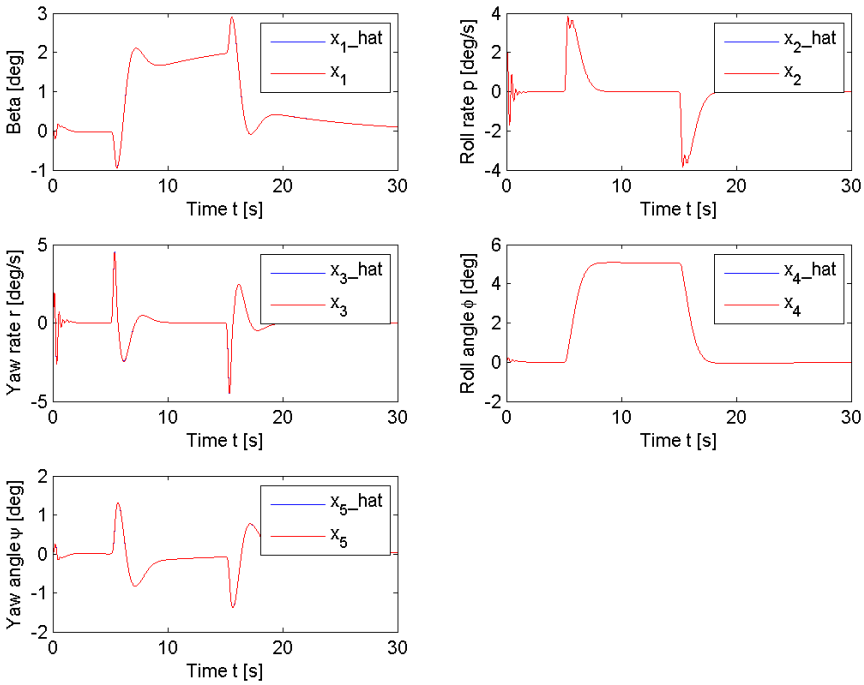

(a) System states with reference r_1

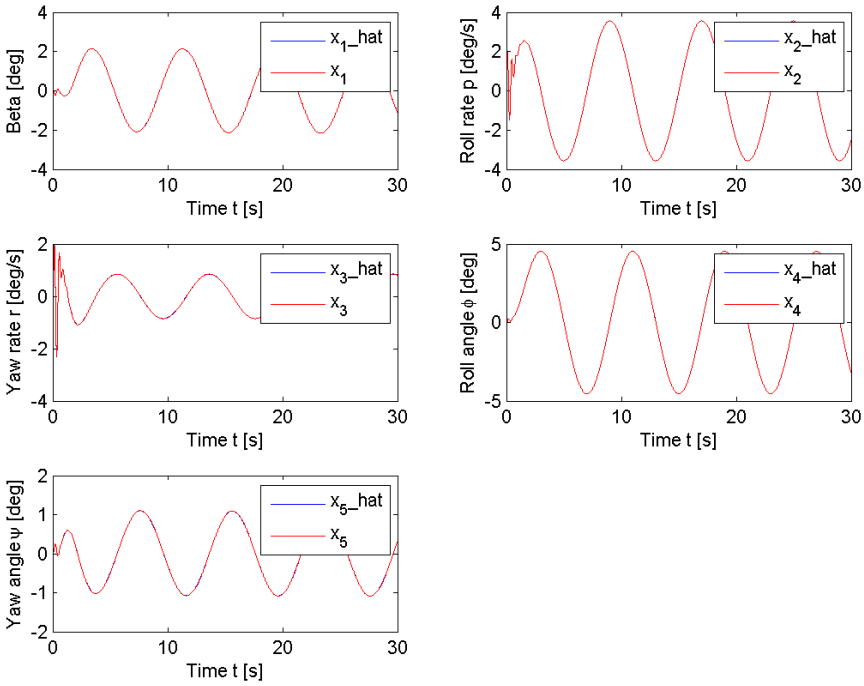

(b) System states with reference r_2

Figure 4.33: Predicted and real system states of the $\mathcal{L}_1$ adaptive controlled lateral system, for simulation case 1.

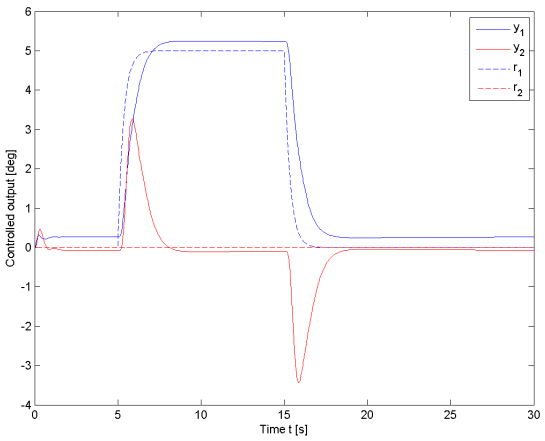

(a) System output with reference r_1

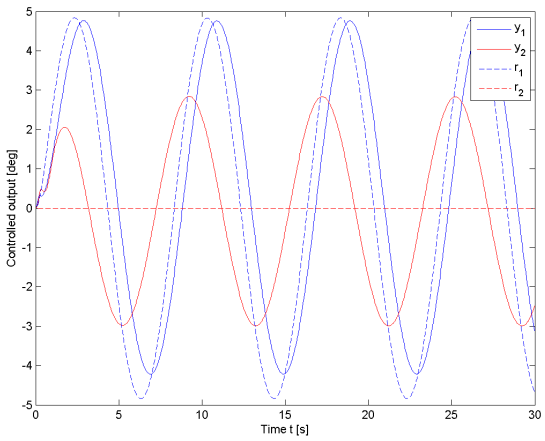

(b) System output with reference r_2

Figure 4.34: System output of the $\mathcal{L}_1$ adaptive controlled lateral system, for simulation case 1, without adaptation.

4.5.3 Simulation case 2

In the simulation case 2, we consider timevarying disturbances. The system considered in this case is given as

$$\dot{\mathbf{x}}(t) = \mathbf{A}_{id}\mathbf{x}(t) + \mathbf{B}_{id}\mu(t) + \sigma(t), \tag{4.104}$$

where

$$\sigma(t) = \begin{bmatrix} \frac{3\pi}{180}\sin\left(\frac{\pi}{7}t - \frac{\pi}{7}\right) \\ \frac{50\pi}{180}\sin\left(\frac{\pi}{4}t - \frac{\pi}{9}\right) \\ \frac{5\pi}{180}\sin\left(\frac{\pi}{5}t - \frac{\pi}{3}\right) \\ 0 \\ 0 \end{bmatrix} \tag{4.105}$$

The resulting plots for the system output, the control signal together with the real control input, the prediction estimates, and the states together with the state estimates are shown in figures 4.35, 4.36, 4.37 and 4.38 respectively.

As a reference, it is interesting to see how the controller performs without the adaptation. This simulation is shown in figure 4.39.

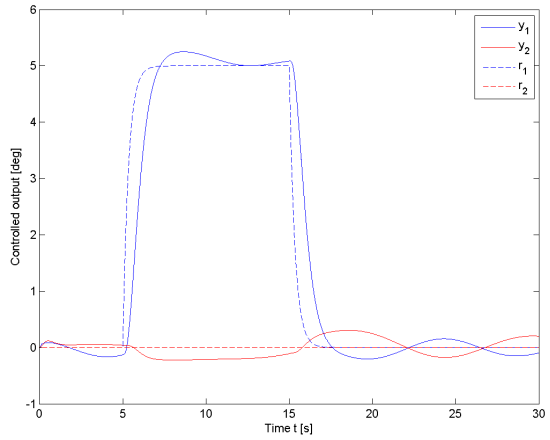

(a) System output with reference r_1

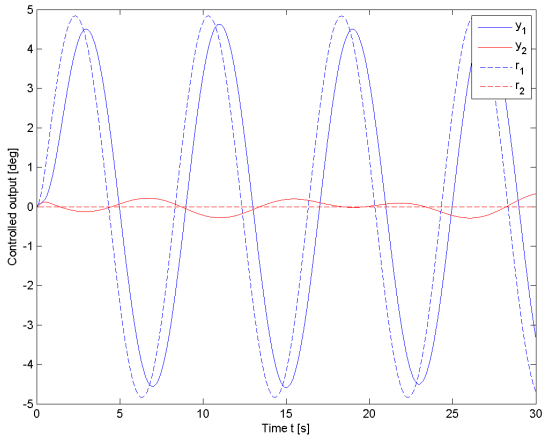

(b) System output with reference r_2

Figure 4.35: System output of the $\mathcal{L}_1$ adaptive controlled lateral system, for simulation case 2.

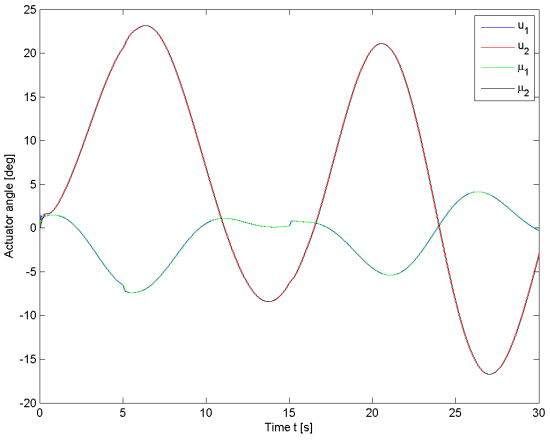

(a) Control signal with reference r_1

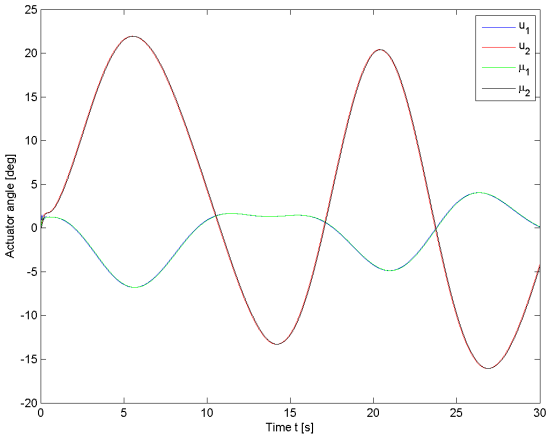

(b) Control signal with reference r_2

Figure 4.36: Control input to the $\mathcal{L}_1$ adaptive controlled lateral system, for simulation case 2.

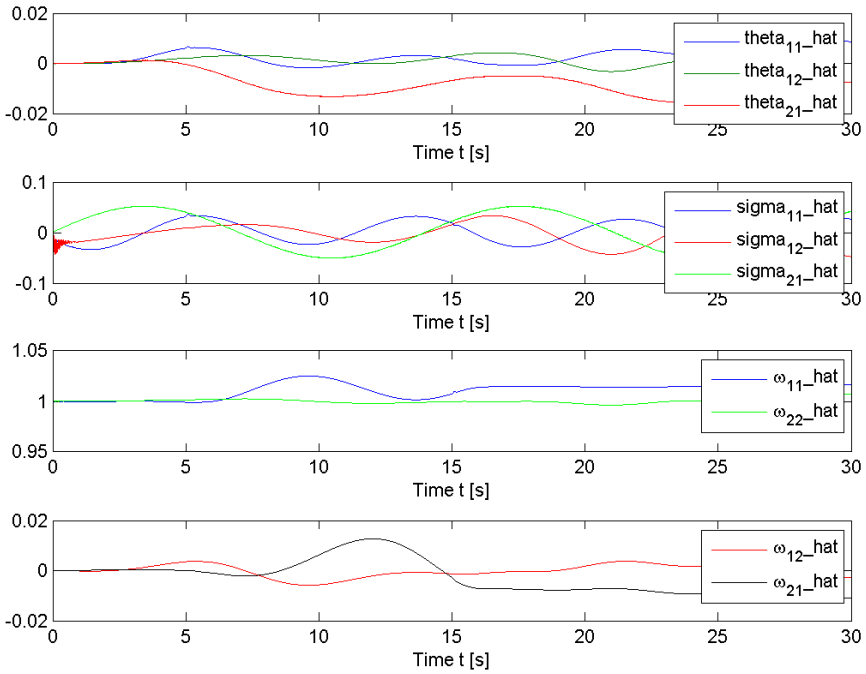

(a) Adaptive estimates with reference r_1

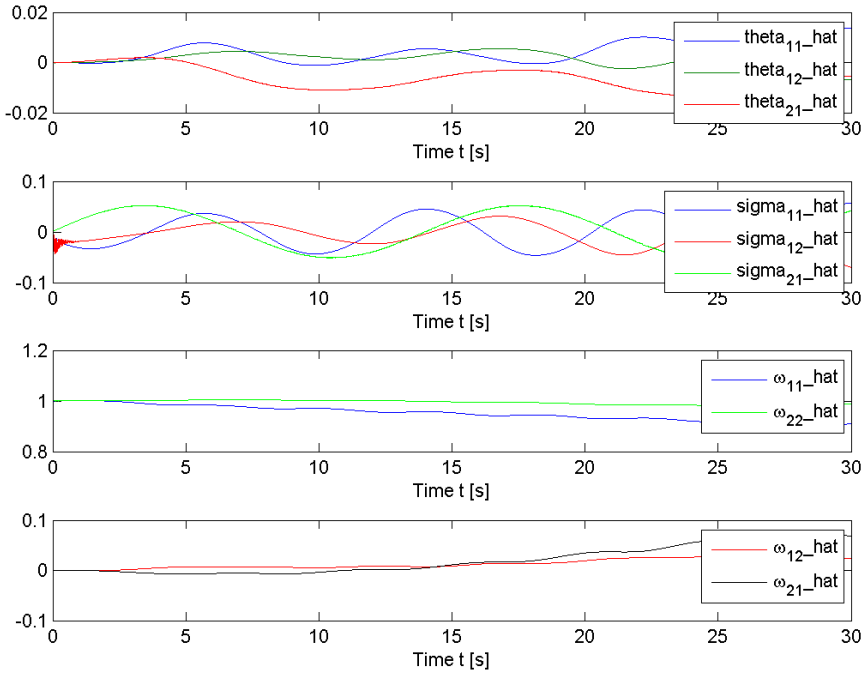

(b) Adaptive estimates with reference r_2

Figure 4.37: Adaptive estimates for the $\mathcal{L}_1$ adaptive controlled lateral system, for simulation case 2.

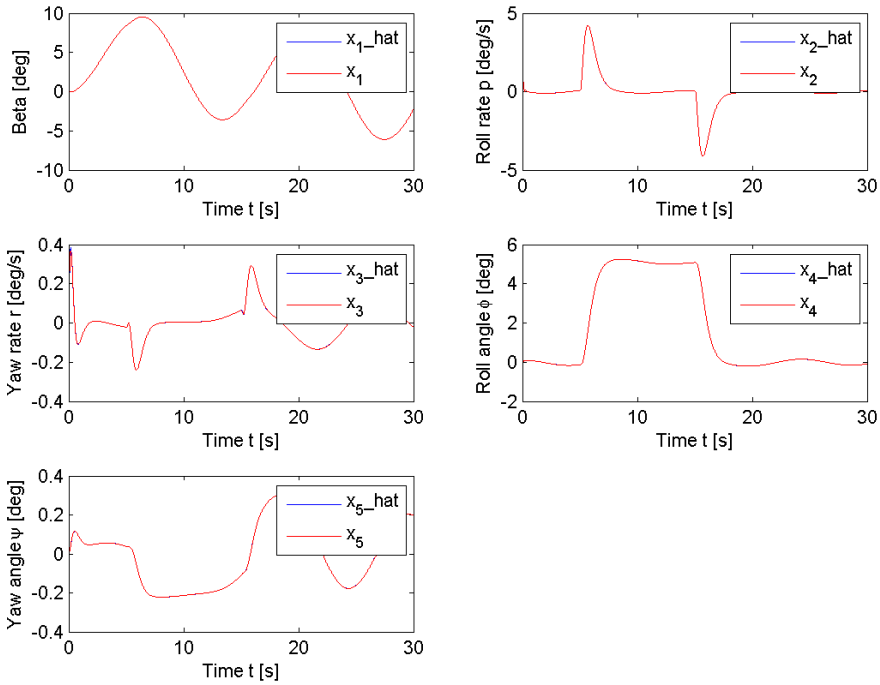

(a) System states with reference r_1

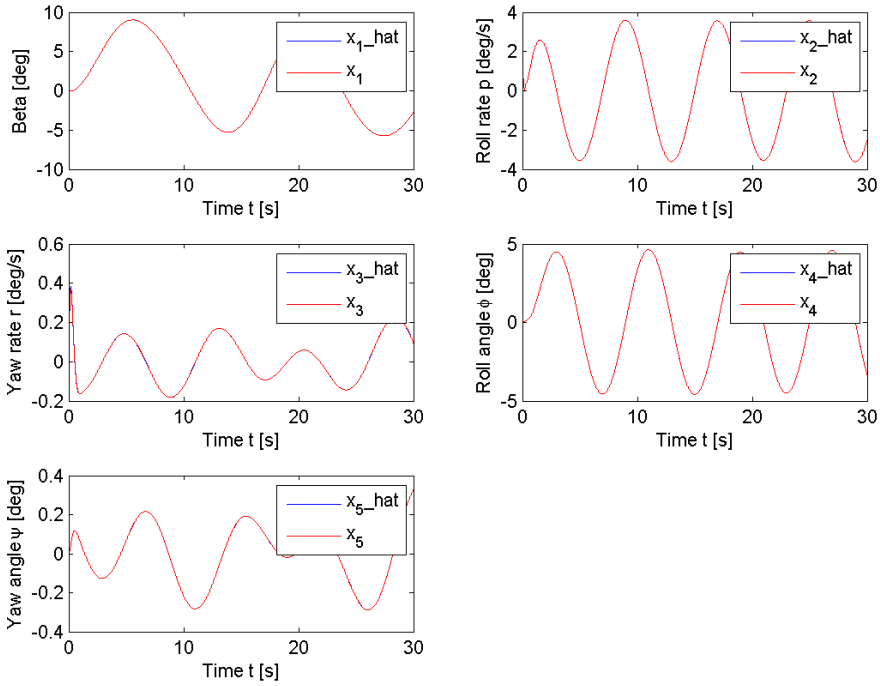

(b) System states with reference r_2

Figure 4.38: Predicted and real system states of the $\mathcal{L}_1$ adaptive controlled lateral system, for simulation case 2.

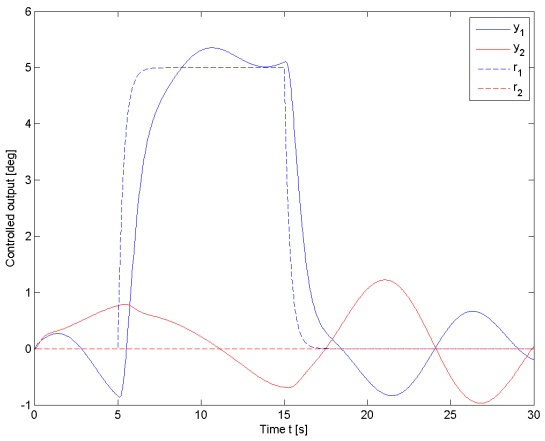

(a) System output with reference r_1

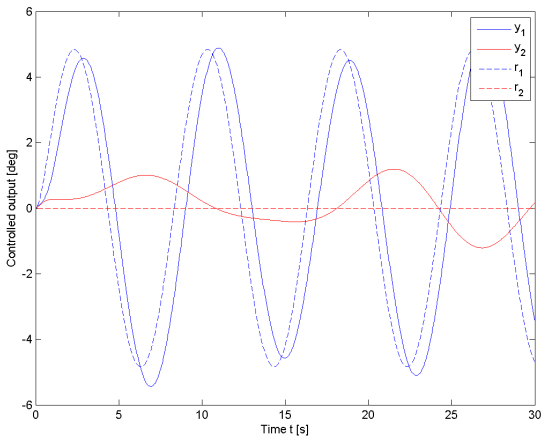

(b) System output with reference r_2

Figure 4.39: System output of the $\mathcal{L}_1$ adaptive controlled lateral system, for simulation case 2, without adaptation.

4.5.4 Discussion

In this section the simulation results for the lateral system, presented in section 4.5 are discussed. Again, two different cases are presented which shows the responce and robustness of the $\mathcal{L}_1$ adaptive controller.

Design system

Section 4.5.1 presents the simulation results for the design system. That is the system results when the modelling errors are equal to zero. The actuator dynamics are however included. This controller is not implementable, but represents the goal of the $\mathcal{L}_1$ adaptive controller and is the basis for the design of K_m. Figure 4.27 shows the best possible output with the chosen K_m and $C(s)$. We see that we do not achieve perfect tracking of both roll and yaw, but not far from it. To be able to achieve a better tracking, we would need a more aggressive controller, but due to the actuator dynamics this would make the controller loose its robustness.

Simulation case 1

Section 4.5.2 presents the simulation results for the $\mathcal{L}_1$ adaptive controller for Case 1. This case introduce constant modelling error in the state matrix. This error reduces the stability in roll, and increases the coupling between roll and yaw. Further a constant error in the input matrix is introduced, which decreases the effect of δ_A to roll. Lastly, a constant disturbance on to the roll rate is introduced. All the modelling errors and the disturbance are unmatched.

Figure 4.30 shows the output response of the $\mathcal{L}_1$ adaptive controller for Case 1. Compared to the output of the design system in figure 4.27, we see that the $\mathcal{L}_1$ adaptive controller manages to control the roll angle really well. Due to the extra coupling between roll and yaw, we see that when we change the roll angle, we get an unwanted yaw angle with a maximum of little over one degree. In figure 4.34 we see the output of Case 1 without adaptation in the controller. Here we see that we get an unwanted yaw angle of about three times the size as compared to the $\mathcal{L}_1$ adaptive controller. Further, we see that due to the constant disturbance in roll, the roll angle gets a stationary deviation in roll, which the $\mathcal{L}_1$ adaptive controller manages to correct for.

Considering the plots of the control inputs in figure 4.31 we notice a bit different signal as compared to the case with no model error in figure 4.28. We also see that the real control input lags a little behind the control signal, just as for the longitudinal system.

Considering the plots of the states and the state predictions in figure 4.33, we see that the predictions follow the real states. We can thus conclude that the adaptation gain is large enough and the estimates capture the uncertainties. However, even though the estimates capture the uncertainties and the predicted states follow the real states, we see that we are

not able to get the same response as the design system. This has to do with the relationship between the reference system and the design system, as discussed in section 3.3 and in the remarks of section 3.5.3. The bandwidth of $C(s)$ is not large enough to let $\mathbf{u}_{ad}$ respond fast enough to the modelling errors. However, as we can see from figure 4.24, increasing the bandwidth makes the system unstable.

Figure 4.32 shows the estimates used in the $\mathcal{L}_1$ adaptive controller. Considering $\hat{\boldsymbol{\omega}}$ it looks like this estimate takes care of some of the modelling error in $\mathbf{B}$. Considering $\hat{\boldsymbol{\theta}}$ we see that the estimates are far from the projection bounds specified in (4.85) and (4.86). Again is seems like these bounds are very conservative. Similar to the simulations of the longitudinal system, we notice the same similarity in the shapes of $\hat{\boldsymbol{\theta}}$ and $\hat{\boldsymbol{\sigma}}$.

Simulation case 2

Section 4.5.3 presents the simulation results for the second case. This case include no modelling error in neither $\mathbf{A}$ nor $\mathbf{B}$, but presents sinusoidal unmatched disturbances on β, roll and yaw. All the sinusoidal signals have different frequencies and phase. Thus, this case tests the $\mathcal{L}_1$ adaptive controller's response to external disturbance.

Figure 4.35 shows the output response of the $\mathcal{L}_1$ adaptive controller for Case 2. We see that the controller manages to follow the reference quite well. Compared to the design system, we see how the disturbances affects the output. However, this deviation from the response of the design system is less than a half degree for both yaw and roll. Compared to the output response when there is no adaptation in figure 4.39, we see that the adaptation manages to reduce the effect to about one half.

The plot of the control inputs in figure 4.36 shows how the controller have to work to counter the effect of the disturbances. We see that the rudder angle gets larger than 20 degrees to counter the disturbances.

Considering the plot of the states and the predicted state in figure 4.38, we again see that the predictions follow closely to the real states. This again shows that the adaptation gain is chosen large enough. In figure 4.25 we can see the response of the $\mathcal{L}_1$ adaptive controller for Case 2 with a larger bandwidth of the filter $C(s)$. We see that the response in this case is almost identical to the design system response. This again indicates that the chosen bandwidth is too small to let $\mathbf{u}_{ad}$ respond fast enough to the disturbances, and a larger bandwidth of $C(s)$ would better the performance of the $\mathcal{L}_1$ adaptive controller when the system is affected by disturbances.

Considering the plots of the estimates in figure 4.37 we notice that even though we have no error in the input matrix, $\boldsymbol{\omega}$ deviates from its initial condition as the time passes. However, this is a very small deviation. Again we notice that the shapes of $\hat{\boldsymbol{\theta}}$ and $\hat{\boldsymbol{\sigma}}$ are very similar, and that the projection bounds specified by the theory seems to be very conservative.

General remarks

Just as the case for the longitudinal system, the $\mathcal{L}_1$ adaptive controller for the lateral system can not verify the $\mathcal{L}_1$-norm condition. However, as we have seen, the $\mathcal{L}_1$ adaptive controller improve the performance in cases of uncertainties and disturbances as compared to a constant feedback.

What has been experienced through lots of simulations is that the designed $\mathcal{L}_1$ adaptive controller for the lateral system does not cope with instabilities as good as the $\mathcal{L}_1$ controller designed for the longitudinal system. While the $\mathcal{L}_1$ controller for the longitudinal system managed to handle modelling errors that made the feedback control unstable, this was not achieved for the lateral system. The choice $D(s) = \mathbb{I}1/s$, used in this text, is most likely not the optimal choice for this system. With this choice an optimal bandwidth of $C(s)$ for some cases makes the system unstable for other cases. Without the actuator dynamics, it would be much easier to design the controller. This is because the control signal could have a much more aggressive response without causing instability. Thus, one could increase the bandwidth of $C(s)$ without problems. However, the implemented actuator dynamics makes the system more realistic, and shows some of the design challenges experienced with a real implementation.

4.6 Alternative control

As a reference to the result of the $\mathcal{L}_1$ adaptive controller, we want to consider a more traditional control law. This is done for the longitudinal system. For this purpose we consider a PID-controller with anti windup. Unlike the state feedback LQR-controller considered earlier, the PID controller is not model based. Thus, changes in the considered model does not necessarily ruin the PID-controller's performance. Further, the integral term makes the PID-controller able to correct for disturbances, which the the LQR-controller considered is not.

4.6.1 PID control design

The PID-controller was designed using the PID tuning tool in Simulink. This tool automatically linearises the system and produces the optimal control parameters for the linearised system based on the desired response time. The control law of the PID-controller is given as

$$u(s) = \left(P + I\frac{1}{s} + D\frac{N}{1 + N\frac{1}{s}} \right) e(s), \tag{4.106}$$

where, P is the proportional gain, I is the integral gain, D is the derivative gain, N is the filter coefficient, and $e(t) = y(t) - r(t)$ is the tracking error. By considering the system without modelling errors, the tuning was performed by trying different response times and testing

for the different cases. What seemed to give the best result was a response time of 0.0334 seconds, which resulted in the following parameters:

$$\begin{aligned} P &= -45.1631278872384, \\ I &= -15.7728902394785, \\ D &= -28.7327844651241, \\ N &= 6841.43177754918. \end{aligned}$$

4.6.2 Simulations

The PID-controller was tested for the same cases as the longitudinal $\mathcal{L}_1$ adaptive controller and for the case on no modelling error. The resulting plots are shown in figures 4.40 - 4.45.

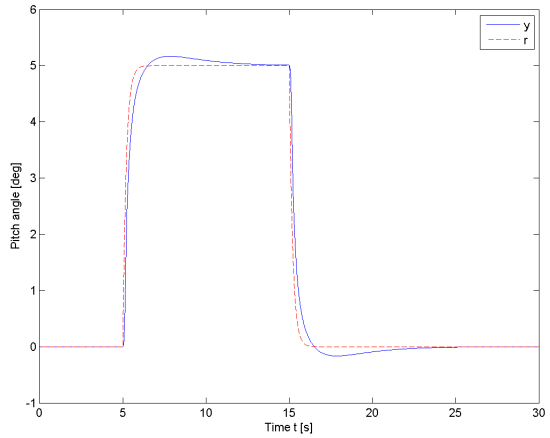

(a) System output with reference r_1

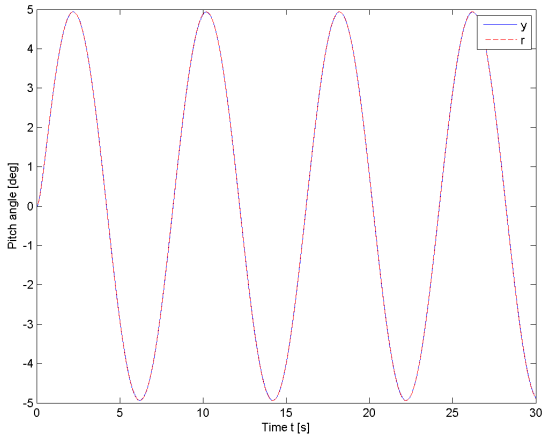

(b) System output with reference r_2

Figure 4.40: PID-controlled longitudinal system output, with no modelling error.

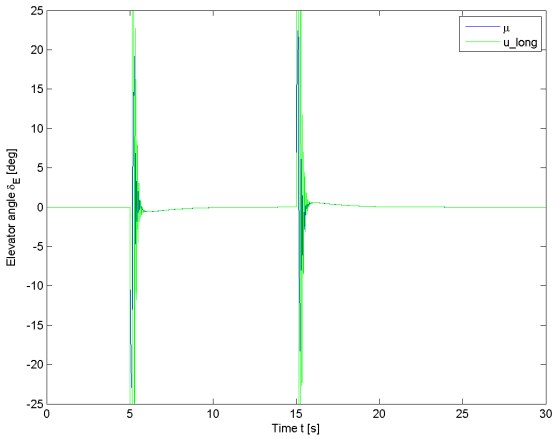

(a) Control input with reference r_1

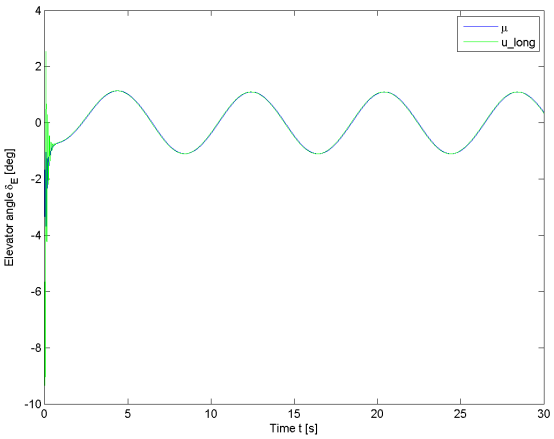

(b) Control input with reference r_2

Figure 4.41: PID control input to the longitudinal system, with no modelling error.

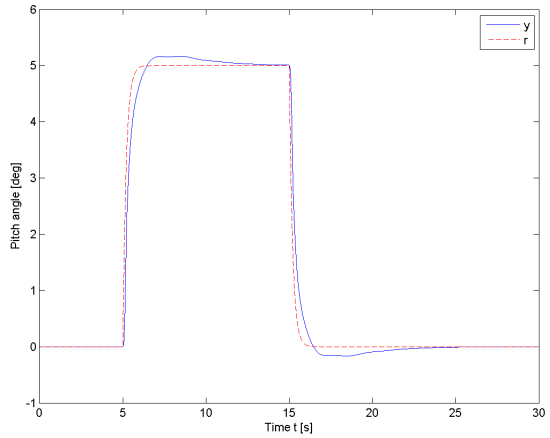

(a) System output with reference r_1

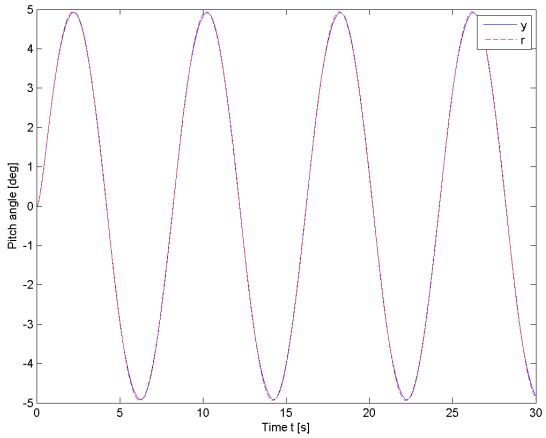

(b) System output with reference r_2

Figure 4.42: System output of the PID-controlled longitudinal system, for simulation case 1.

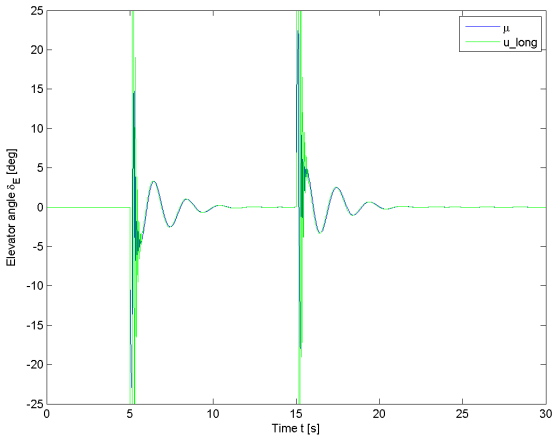

(a) Control input with reference r_1

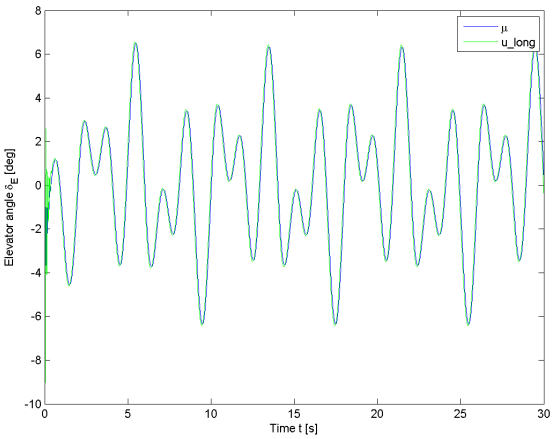

(b) Control input with reference r_2

Figure 4.43: Control input to the PID-controlled longitudinal system, for simulation case 1.

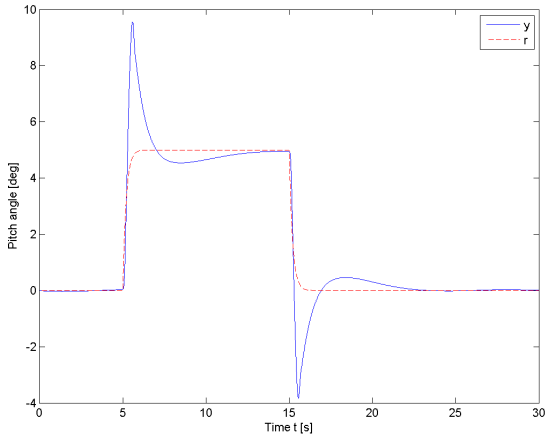

(a) System output with reference r_1

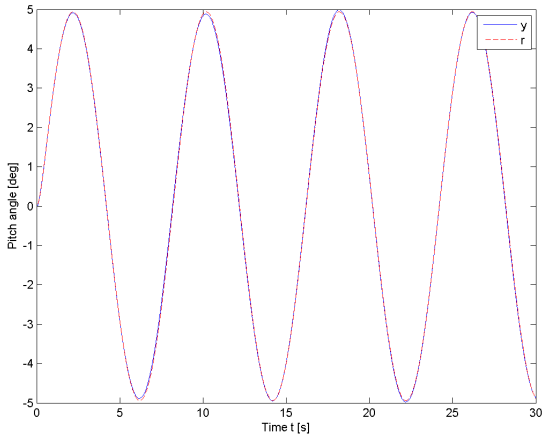

(b) System output with reference r_2

Figure 4.44: System output of the PID-controlled longitudinal system, for simulation case 2.

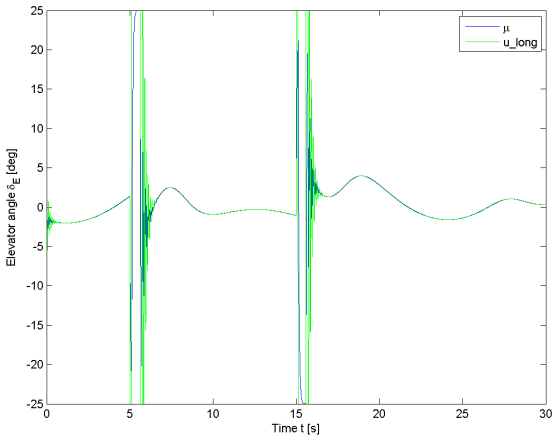

(a) Control input with reference r_1

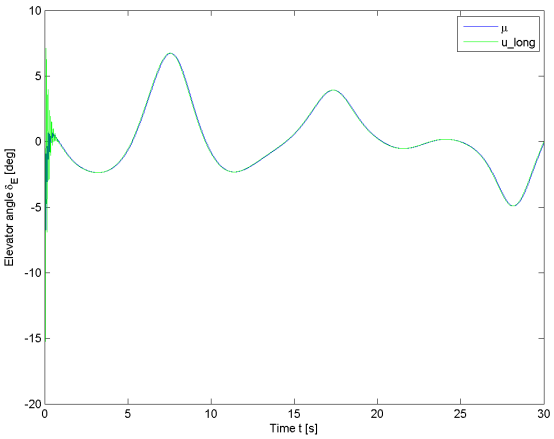

(b) Control input with reference r_2

Figure 4.45: Control input to the PID-controlled longitudinal system, for simulation case 2.

4.6.3 Discussion

As mentioned, unlike the LQR-design, the PID control design is not model based. The control parameters must be design such that the PID-controller has desired robustness specifications. That is, the parameters are chosen such that the system is kept stable within a given set of modelling error. As we can see from the plots above, the PID-controller manages to keep the system stable for all of the given cases, and thus the chosen parameters gives the desired robustness.

From figure 4.40 and 4.41 we see the response of the PID-controller when there is no modelling error. We see that the controller makes the output follow changes in the reference really good. As we can see from figure 4.40 (b) with reference r_2 we achieve almost perfect tracking. Considering the output of Case 1 in figure 4.42, we see that we get almost the same result. However, considering the control signals, we see how the controller for case 1 has to work to compensate for the changing model dynamics. From figure 4.44 and 4.45 we see the response for Case 2. Now we see that the output with reference r_1 gets an overshoot to almost twice the desired reference value. Further, it takes about 18 seconds before the desired constant value is achieved. With reference r_2 however, we again see that we achieve almost perfect tracking.

The interest now lies in the comparison of the PID-controller to the $\mathcal{L}_1$ adaptive controller. From the plots above, we see that the PID-controller is quite aggressive. This is due to the nature of the PID-formulation. To increase the robustness of the PID-controller, it needs to be more aggressive. However, a too aggressive controller makes the system unstable again. The $\mathcal{L}_1$ adaptive controller however, specifies the desired response without considering the possible model changes. This makes the PID- controller able to track the changes in reference good, but considering the control signals we see rapid changes which bounces between the saturations.

For the case with no model error and Case 1, we see that the output response of the PID controller is quite similar to the response of the $\mathcal{L}_1$ adaptive controller. We do however notice that due to the integral part, the PID-controller uses some time to reach the desired step, for reference r_1. For Case 2, we see that the performance of the PID-controller is poor compared to the $\mathcal{L}_1$ adaptive controller. It gets a large overshoot and uses about 18 seconds before the desired constant value is achieved. For the same case, the $\mathcal{L}_1$ adaptive controller manages to suppress the disturbances much better and achieves the desired constant value just as fast as the design system. We also see that this is achieved for the $\mathcal{L}_1$ adaptive controller with a maximum control angle of 8 degrees, while the PID-controller hits the saturation of 25 degrees.

As we have seen, the PID controller manages to compensate for modelling errors and disturbances. However, while the PID-controller only compensates for tracking error on the output, the $\mathcal{L}_1$ adaptive controller detects the model changes for each of the states, and can immediately calculate the correct control to compensate for exactly this disturbance. The

effect of this design differences was evident for simulation Case 2.

4.7 Simulation of the nonlinear F-16 model

This section presents the simulations performed on the full nonlinear F-16 model presented in section 2.5. The same controllers presented in the previous sections are the one used in the simulations, without any retuning. Due to the scope of this report, the simulations performed are done for the pitch control only. However, since the nonlinear F-16 model is a full 6 DOF model, the $\mathcal{L}_1$ adaptive controller for the lateral mode was used to keep the references in roll and yaw equal to zero. The reference on pitch was chosen such that the aircraft would experience quite large change in alpha. Further, the thrust was reduced to 1000 [lbs] such that the aircraft would experience a change in speed. All of these choices was made to try to challenge the pitch controller. The reference used in the simulation is given by:

$$r_0(t) = \begin{cases} 60^\circ & , \ 3\ s < t < 8\ s \\ -30^\circ & , \ 25\ s < t < 35\ s \\ 0^\circ & , \ \text{otherwise} \end{cases} \tag{4.107}$$

Further, to prevent to aggressive change in the reference, it is filtered:

$$r(s) = F_r(s) r_{i0}, \tag{4.108}$$

where $F_r(s) = \dfrac{10}{s+10}$, and the rate of change has got the limit

$$-10^\circ/s \leq \dot{r}(t) \leq 20^\circ/s. \tag{4.109}$$

4.7.1 Simulations

The simulations are performed with the fixed-step solver Bogacki-Shampine and a step size of 0.0001. Besides the nonlinearities included in the F-16 model introduced in section 2.5, the simulations include no disturbances nor measurement errors. The purpose of the simulations presented is to test the different control strategies response to the nonlinearities presented in the F-16 model. Beside the known linearisation of the F-16 model for the given trim conditions, the model is treated as a black box. In this way we test the goal of the $\mathcal{L}_1$ adaptive controller, namely that it can be based in a single linearisation, and perform well for the entire flight envelope.

$\mathcal{L}_1$ adaptive control

The simulation results of the pitch control of the nonlinear F-16 model, with the $\mathcal{L}_1$ adaptive controller are shown in figure 4.46.

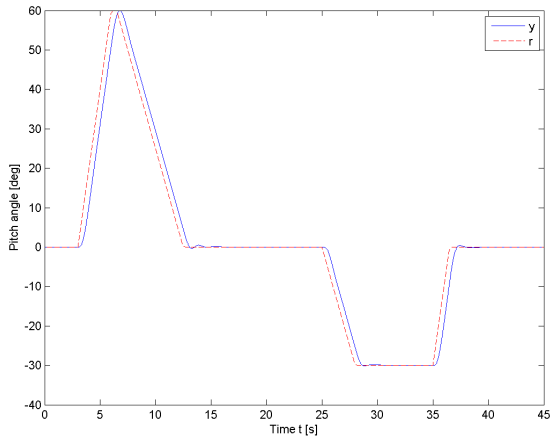

(a) System output and reference r

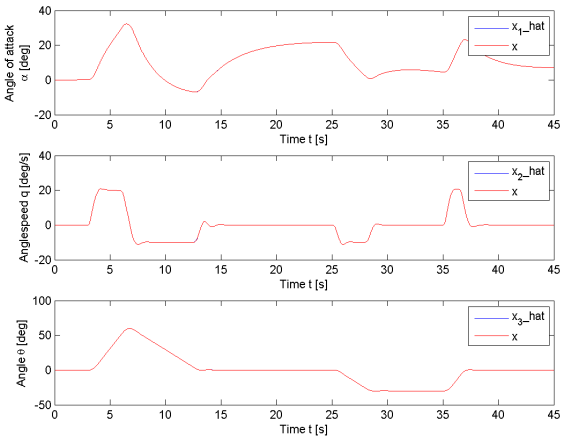

(b) Longitudinal states

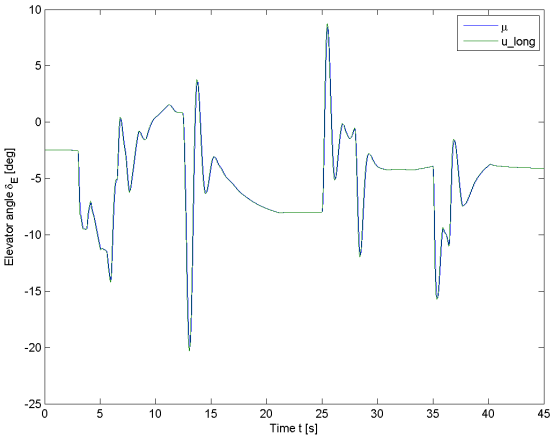

(c) Elevator input

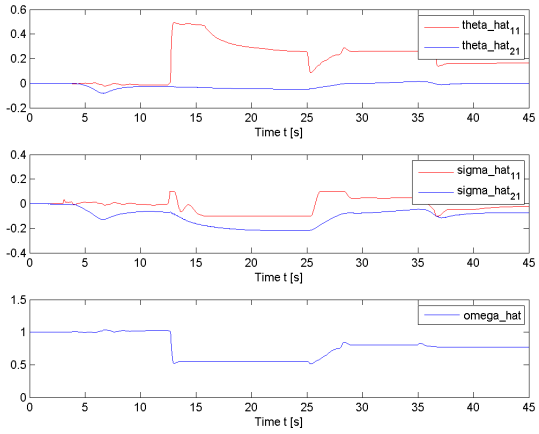

(d) Prediction estimates

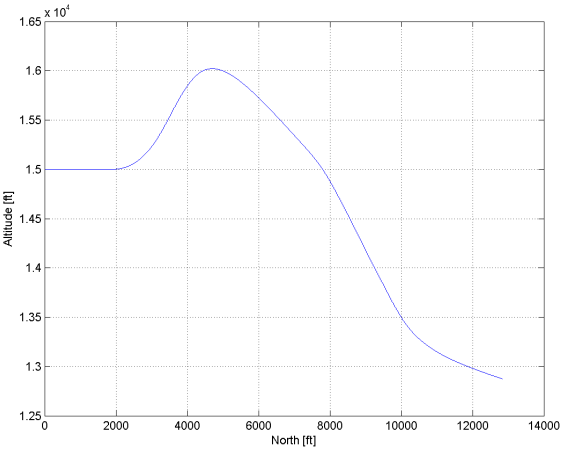

(e) Flight path

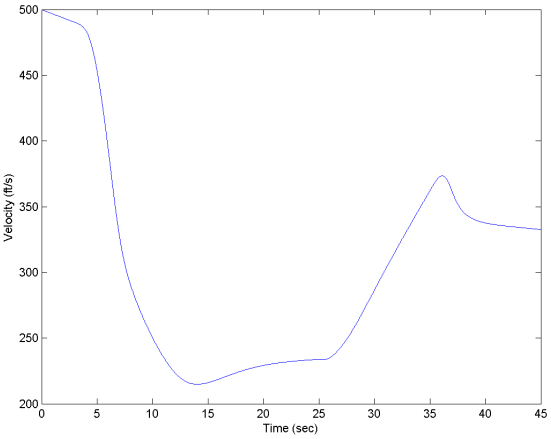

(f) Aircraft velocity

Figure 4.46: Simulation of the nonlinear F-16 model, with $\mathcal{L}_1$ adaptive controlled pitch.

$\mathcal{L}_1$ without adaptation

As before, it is interesting to see the effect of the nonlinearities on the system when the adaptation is turned off. The simulation results of the pitch control of the nonlinear F-16 model, with the $\mathcal{L}_1$ controller without adaptation are shown in figure 4.47.

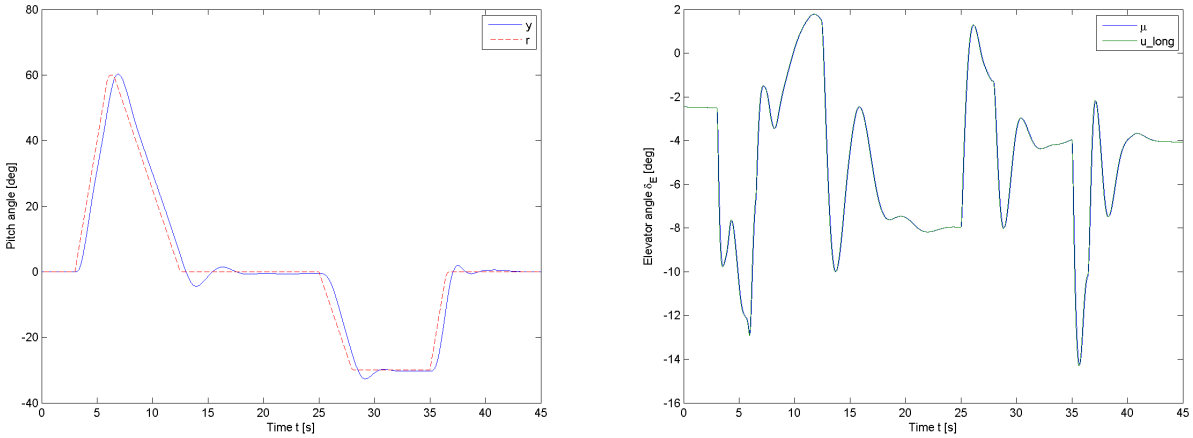

(a) System output and reference r

(b) Elevator input

Figure 4.47: Simulation of the nonlinear F-16 model, with $\mathcal{L}_1$ adaptive controlled pitch, without adaptation.

PI control

As a reference to the $\mathcal{L}_1$ adaptive controller it is interesting to see how the PID-controller designed in the previous section performes for the nonlinear F-16 model. The simulation result is shown in figure 4.48

4.7.2 Discussion

From figure 4.46 (a) we see that the $\mathcal{L}_1$ adaptive controller manages to control the pitch of the aircraft really well. We see that the output has a delay with respect to the reference. This is, as we know due to the formulation of $\mathbf{A}_m$. Other than this, we see that the output hits the reference when it flattens out with almost no overshoot. The output settles on the correct value in about 3 seconds. From figure 4.46 (b) we see that the predicted and the real states are as good as equal, and from figure 4.46 (c) we see how the estimates change to keep them so. Thus, we see that the adaptation gain is chosen satisfactory. From figure 4.46 (f) we see that the aircraft experience a drastic loss in speed, and from figure 4.46 (b) we see that it experience a high alpha of over 32 degrees. As we know, the $\mathcal{L}_1$ adaptive controller is designed based on the single linearising point presented in 4.1. As we can see from the

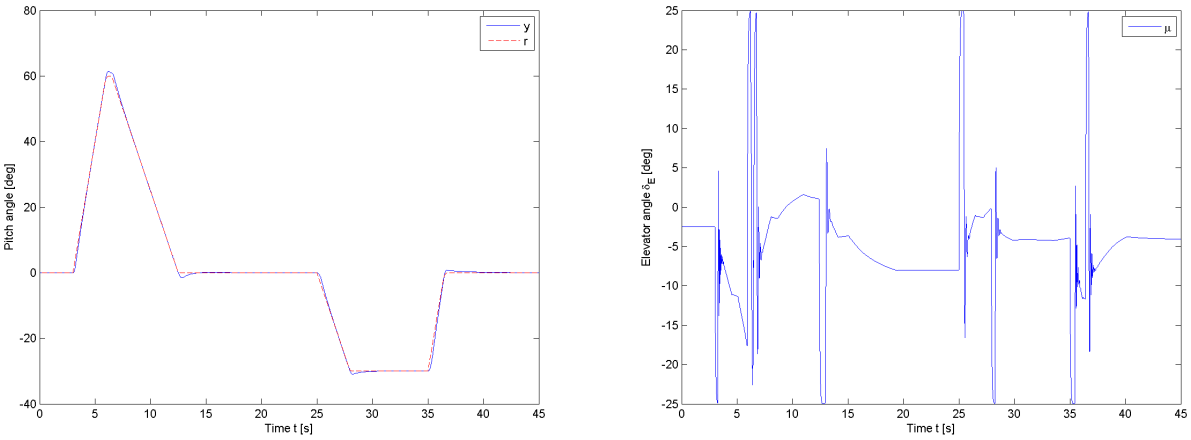

(a) System output and reference r

(b) Elevator input

Figure 4.48: Simulation of the nonlinear F-16 model, with PID controlled pitch.

plots, the $\mathcal{L}_1$ adaptive controller manages to compensate for the model changes due to the low speed and the high α, and give the desired response.

Considering the output of the system when the adaptation is turned off, in figure 4.47, we see that the system is still kept stable. However, we see that the output experiences overshoot with a maximum of over 4 degrees. Further, the settling time is about 5 seconds, and the controller does not manage to hit the correct constant references. This shows the improvements of the adaptation in the $\mathcal{L}_1$ adaptive controller.

Considering figure 4.48 we see the response of the PID controller for the simulation on the nonlinear F-16 model. As we can see, despite the nonlinearities, the PID-controller manages to track the reference really good. We see that the output get some small overshoots of between 1 to 1.5 degrees, but the controller manages to reduce the error to less than 0.2 degrees in about 1.5 seconds, and is thus just as quick as the $\mathcal{L}_1$ adaptive controller. Thus we see that for the performance of the pitch control of the nonlinear F-16 model, there is no advantage of the $\mathcal{L}_1$ adaptive controller over the simple PID-controller. However, considering the control input of the two controllers, we again see some distinct differences. As before, we see that the PID control input is really aggressive. The control signal oscillates rapidly and hits the saturation often.

4.8 Implementation issues and assumptions made

For the design presented in this text, some assumptions have been made implicitly, which may not always be possible to meet when implementing the controller on a real system. This section discusses these implementation issues and emphasize the case of limited sampling rate, which is in particular an important issue concerning $\mathcal{L}_1$ adaptive control.

4.8.1 Control redesign for limited sampling rate

The reason why the case of limited sampling rate is important to discuss when considering $\mathcal{L}_1$ adaptive control, is due to the high adaptation gain considered in the formulation of the controller. When we combine the adaptation law defined in (3.123), where Γ is chosen as a large value, with a limited sampling rate, the result is most likely adaptive estimates which bounces between the projection bounds, which quickly makes the system unstable. This has been experienced through simulations and can be seen in figure 4.49. This is because the real prediction error will not be updated before the adaptive estimate already has gone far beyond the real value, due to the fast adaptation. Thus, the adaptation gain needs to be tuned dependent on the sampling rate. Further, the adaptation law and the state predictor have to be redesigned. This section present how this redesign can be performed. The resulting simulations of the longitudinal system for Case 2, with this redesign implemented for sample rates of 20 Hz and 100 Hz are presented in section 4.8.2.

The design presented in this section is inspired by the design for piecewise constant adaption laws presented in [7]. However, we consider a different adaptation law than in the book. This section presents no theoretical results, but present the design changes done to cope with the case of limited sampling frequency. The goal is to get the same result as for the theory presented in chapter 3. See [7] for theoretical results and for the different adaptation law.

When we have a limited sampling rate $\frac{1}{T_s}$, where T_s is the sampling time, we need to make some adjustments to the $\mathcal{L}_1$ adaptive controller defined in 3.5.2. We still design the controller as if it is continuous, but since the measurements are sampled, we need to discretize the adaptation law. We also make a change to the state predictor. As we have seen from the simulations of both the longitudinal and the lateral systems, it looks like the estimate $\boldsymbol{\theta}$ is redundant. To simplify, we thus remove this estimate. In the derivations of the modelling error we have also seen that $\boldsymbol{\omega}$ is redundant. A change in the real input gain would only change the value of $\boldsymbol{\sigma}$. Thus, to make the system even simpler we just consider $\hat{\boldsymbol{\sigma}}$ and let this estimate take care off all the modelling error and disturbances.

State predictor

Based on the discussion above, we consider the state predictor:

$$\dot{\hat{\mathbf{x}}} = \mathbf{A}_m + \mathbf{B}_m(\boldsymbol{\omega}_0 u_{ad}(t) + \hat{\boldsymbol{\sigma}}_1(t)) + \mathbf{B}_{um}\hat{\boldsymbol{\sigma}}_2(t), \tag{4.110}$$

$$\hat{\mathbf{y}} = \mathbf{C}\hat{\mathbf{x}}, \tag{4.111}$$

where $\boldsymbol{\omega}_0 \in \mathbb{R}^{m\times m}$ is an initial guess of the real $\boldsymbol{\omega}$, and $\hat{\boldsymbol{\sigma}}_1 \in \mathbb{R}^m$ and $\hat{\boldsymbol{\sigma}}_1 \in \mathbb{R}^{n-m}$ are the adaptive estimates.

Adaptation law

For the derivation of the discrete adaptation law, we use the continuous adaptation law as a starting point, without considering the projection operator:

$$\begin{aligned}
\dot{\hat{\boldsymbol{\sigma}}}_1(t) &= -\Gamma\mathbf{B}_m^T\mathbf{P}\tilde{\mathbf{x}}(t)\\
\dot{\hat{\boldsymbol{\sigma}}}_2(t) &= -\Gamma\mathbf{B}_{um}^T\mathbf{P}\tilde{\mathbf{x}}(t)\\
&\Downarrow\\
\dot{\hat{\boldsymbol{\sigma}}}(t) &= -\Gamma\mathbf{B}^T\mathbf{P}\tilde{\mathbf{x}}(t)
\end{aligned} \tag{4.112}$$

where $\hat{\boldsymbol{\sigma}} := \begin{bmatrix}\hat{\boldsymbol{\sigma}}_1\\ \hat{\boldsymbol{\sigma}}_2\end{bmatrix}$, and $\mathbf{B} := [\mathbf{B}_m, \mathbf{B}_{um}]$. By assuming

$$\tilde{\mathbf{x}}(iT_s + t) \equiv \tilde{\mathbf{x}}(iT_s), t \in [iT_s, (i+1)T_s), \tag{4.113}$$

where T_s is the sampling time, we can integrate both sides of (4.112) and get

$$\begin{aligned}
\hat{\boldsymbol{\sigma}}((i+1)T_s) &= -\int_{T_s}^{(i+1)T_s} \Gamma\mathbf{B}^T\mathbf{P}\tilde{\mathbf{x}}(\tau)\, d\tau + \hat{\boldsymbol{\sigma}}(iT_s)\\
&= -\Gamma T_s\mathbf{B}^T\mathbf{P}\tilde{\mathbf{x}}(T_s) + \hat{\boldsymbol{\sigma}}(T_s)
\end{aligned} \tag{4.114}$$

Based on this, we specify the new adaptation law:

$$\hat{\boldsymbol{\sigma}}(t) = \hat{\boldsymbol{\sigma}}((i+1)T_s), t \in [iT_s, (i+1)T_s), \tag{4.115}$$

where $\hat{\boldsymbol{\sigma}}((i+1)T_s)$ is given in (4.114).

Control law

The control law is the same as before except that $\hat{\boldsymbol{\omega}}$ and $\hat{\boldsymbol{\theta}}$ are no longer considered:

$$\mathbf{u}(s) = -\mathbf{K}D(s)\hat{\eta}(s), \tag{4.116}$$

where $\hat{\eta}(s)$ is the Laplace transform of the signal

$$\hat{\eta} := \boldsymbol{\omega}_0 u(t) + \hat{\eta}_1(t) + \hat{\eta}_{2m}(t) - r_g(t), \tag{4.117}$$

where $r_g(s) := \mathbf{K}_g(s)r(s)$, $\hat{\eta}_{2m} := H_m^{-1}(s)H_{um}(s)\hat{\eta}_2(s)$, and $\hat{\eta}_i := \hat{\boldsymbol{\sigma}}_i, i = 1, 2$.

Control parameters

The feedback gain K_m and the filter $C(s)$ is exactly the same as for the case with continuous measurements. The initial guess of ω is chosen as $\omega_0 = 1$. The adaptation gain Γ needs to be tuned for the different sampling rates. The simulations presented are performed for two different sampling times: $T_{s1} = 0.05$ and $T_{s2} = 0.01$. Through simulations we found that with the sampling time T_{s1}, the system was stable for

$$293 \leq \Gamma_1 \leq 397, \tag{4.118}$$

and with the sampling time T_{s2}, the system was stable for

$$413 \leq \Gamma_2 \leq 7580. \tag{4.119}$$

We want the adaptation gain to be as high as possible to get as fast adaptation as possible. However, when the adaptation gain is close to its maximum value, the control signal oscillates rapidly. Further, the margins were only tested for Case 2, so for other cases, these may change. For the simulations presented in this section the following adaptation gains were used

$$\Gamma_1 = 380, \tag{4.120}$$
$$\Gamma_2 = 7400. \tag{4.121}$$

The control redesign of the adaptation law and the predictor for systems with limited sampling rate is shown in Appendix A.

4.8.2 Simulation with limited sample rate

This section presents the simulations for the case of limited sampling rate. All the simulations are performed for Case 2 of the longitudinal system, with reference r_1. The result of the simulation with the $\mathcal{L}_1$ adaptive controller with a sampling rate or 20 Hz, without any redesign, but with a reduced $\Gamma = 380$, is presented in figure 4.49. The resulting plots for the system output, the control signal together with the real control input, the prediction estimates, and the states together with the state estimates for the redesigned $\mathcal{L}_1$ controller, are shown in figures 4.50, 4.51, 4.52 and 4.53 respectively.

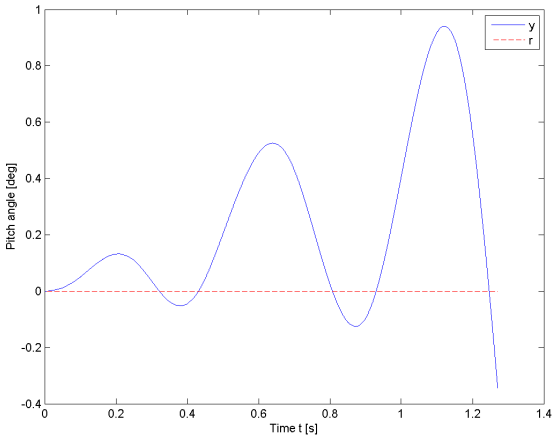

(a) System output with sample rate of 20 Hz

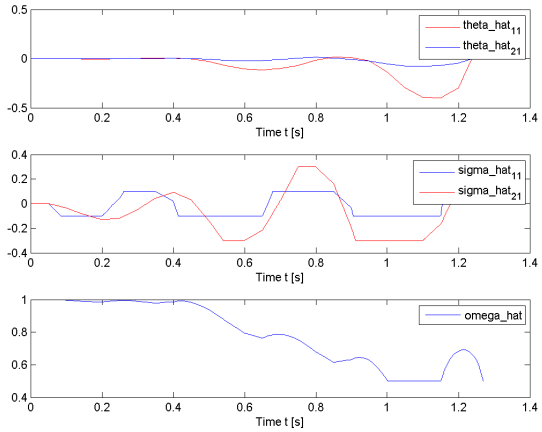

(b) Adaptive estimates with sample rate of 20 Hz

Figure 4.49: Simulation of the original $\mathcal{L}_1$ adaptive control design for simulation case 2 of the longitudinal system, with a limited sample rate of 20 Hz.

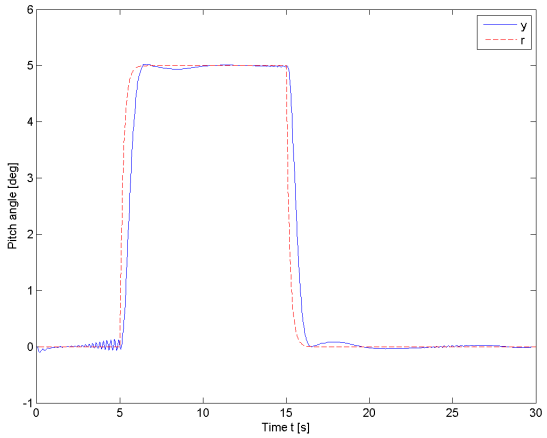

(a) System output with sample rate of 20 Hz

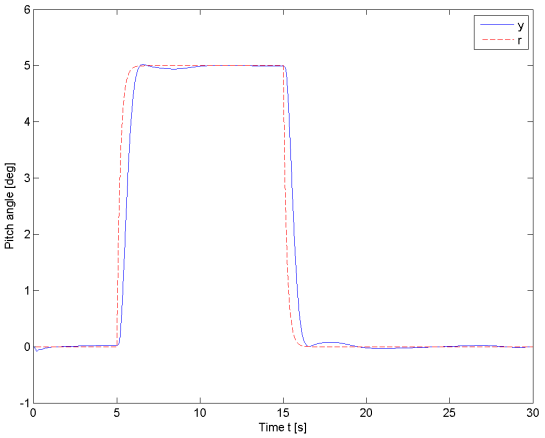

(b) System output with sample rate of 100 Hz

Figure 4.50: System output of the $\mathcal{L}_1$ adaptive controlled longitudinal system, for simulation case 2, with limited sampling rate and reference r_1.

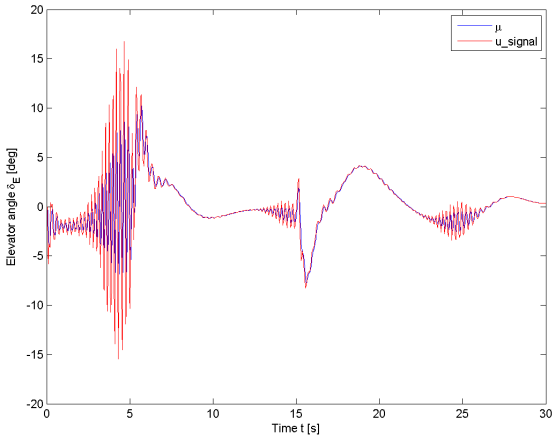

(a) Control signal with sample rate of 20 Hz

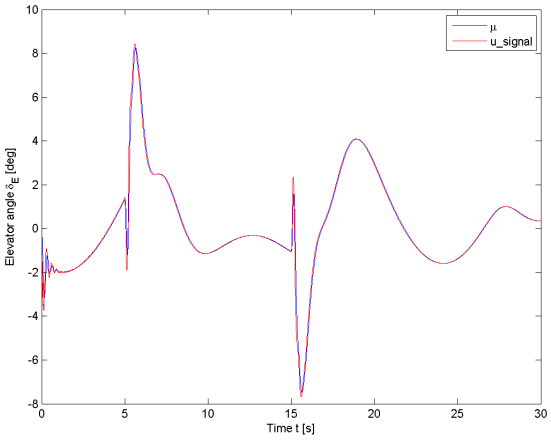

(b) Control signal with sample rate of 100 Hz

Figure 4.51: Control input to the $\mathcal{L}_1$ adaptive controlled longitudinal system, for simulation case 2, with limited sampling rate and reference r_1.

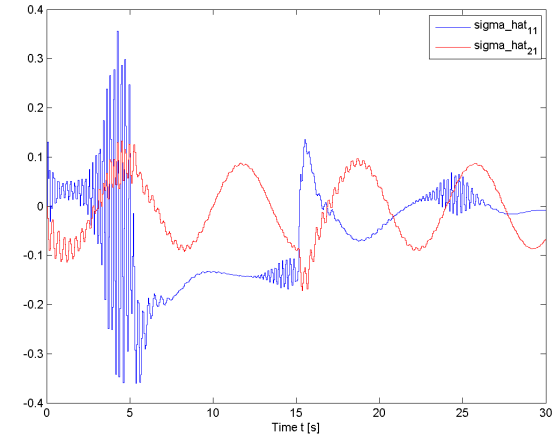

(a) Adaptive estimates with sample rate of 20 Hz

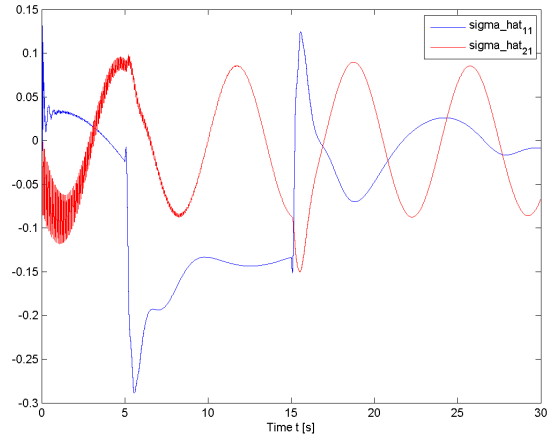

(b) Adaptive estimates with sample rate of 100 Hz

Figure 4.52: Adaptive estimates of the $\mathcal{L}_1$ adaptive controlled longitudinal system, for simulation case 2, with limited sampling rate and reference r_1.

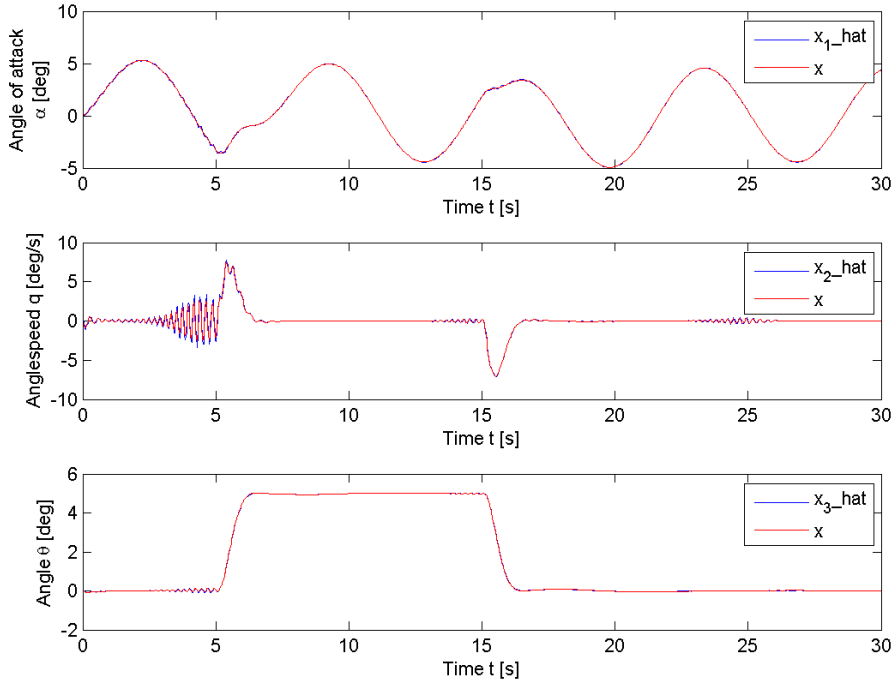

(a) System states with sample rate of 20 Hz

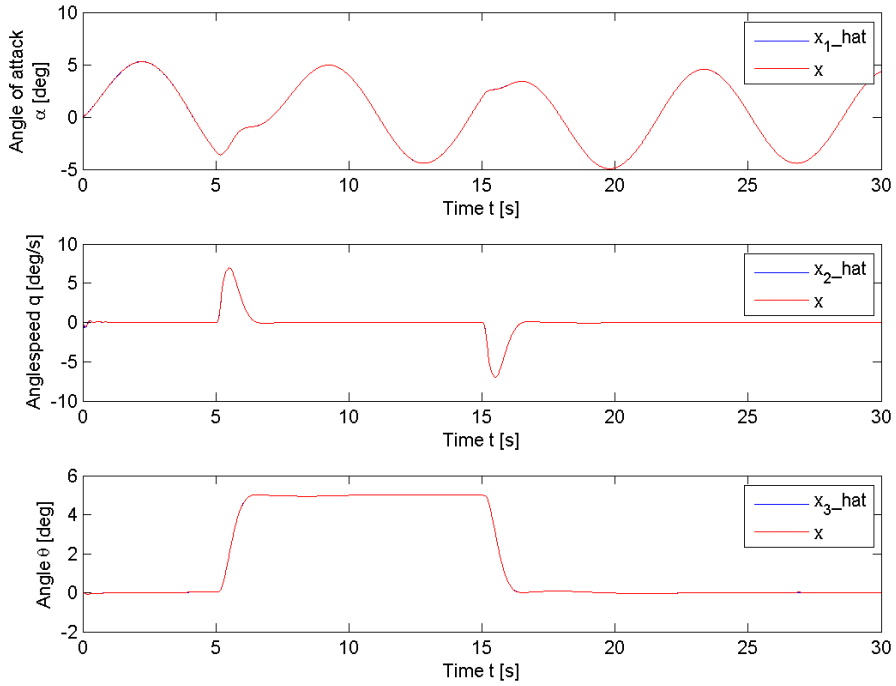

(b) System states with sample rate of 100 Hz

Figure 4.53: Predicted and real system states of the $\mathcal{L}_1$ adaptive controlled longitudinal system, for simulation case 2, with limited sampling rate and reference r_1.

4.8.3 Discussion

As discussed, an important issue with regards to implementing the $\mathcal{L}_1$ adaptive controller on a real system, is the case of limited sampling rate. Why this is a problem can be seen in figure 4.49, where the original design is simulated with a limited sampling rate of 20 Hz. Even though the adaptation gain is limited to the same value as we use in the redesigned controller for a sample rate of 20 Hz, we see that the system becomes unstable. We also see that the adaptive estimates $\hat{\sigma}$ hits the saturation bounds very quickly. This shows that the original design with the projection based adaptation, used to get the theoretical results, is no good in practice. The resulting plots for the redesign presented in section 4.8.1 are shown in figures 4.50 - 4.53. We see that even with a sampling rate as low as 20 Hz the redesigned $\mathcal{L}_1$ adaptive controller manages to keep the system stable. At some points we see that we get some rapid oscillations on the adaptive estimates and on the control signal. These are however bounded, and does not make the system unstable. Considering the real and the predicted states in figure 4.53 (a), we see that the predicted states follow the real states quite good.

As we can see from the simulation results with a sampling frequency of 100 Hz, we get almost the identical result as for the continuous case, presented in figures 4.13 - 4.16. This shows that by increasing the sampling rate, we can get the same results as for the continuous case. Thus, since no other control parameters but the adaptation gain are changed in these simulations, we can design the filter and the desired system response based on the principles as presented in chapter 3, and adjust Γ to the available sample rate. [7] presents an alternative adaptation law directly dependent on the available sampling rate. This has not been considered in this text.

The simulations above also shows that the adaptive estimate $\hat{\boldsymbol{\sigma}}$ alone captures all the uncertainties and disturbances. This confirms the points made earlier, that both $\hat{\omega}$ and $\hat{\theta}$ are redundant. Without considering how the modelling error occurred: if it is a nonlinear dependence on the states, if there are unmodelled dynamics or unmodelled actuator dynamics, or if the errors are due to an external disturbance, due to the fast adaptation, $\hat{\boldsymbol{\sigma}}(t)$ takes care of all the modelling errors and makes u_{ad} do the necessary corrections. The state predictor considered in this section is the one successfully used in the implemented $\mathcal{L}_1$ adaptive controller in the test flights of NASA's GTM (AirSTAR) and the Boeing X-48B.

An other assumption made in the design of the $\mathcal{L}_1$ adaptive controller is that we have perfect state measurements. This is however not an unrealistic assumption since full state feedback has been used in the implementations mentioned. If we should experience measurement errors, the $\mathcal{L}_1$ adaptive controller is not made to correct for this. A bias in the measurement would result in a bias in the output. The biggest challenge with regards to the measurements is a measurement delay. This is again related to the fast adaptation. If we have a measurement delay, the adaptive estimates is based on the wrong state measurement, and the fast adaptation may lead to instability. Thus the $\mathcal{L}_1$ adaptive controller has to be designed with this in mind. Simulations of the $\mathcal{L}_1$ adaptive controller with a sample rate of 100 Hz, without

any retuning, showed that the system was stable for a measure delay of 1,6 ms, but unstable for larger measurement delays.

Chapter 5

Conclusion

This master's thesis has considered control design of the inner loop of an aircraft control system. The goal has been to design a single controller based on a linearised model of the aircraft, to give satisfactory robustness and performance specifications for the complete flight envelope. Thus, the theory of linear aircraft modelling has been presented. Further, the numerical values for this model has been obtained from a nonlinear F-16 model.

Further, the $\mathcal{L}_1$ adaptive control architecture for MIMO systems with nonlinear unmatched uncertainties and unmodeled actuator dynamics has been presented. This has been presented through a step by step expansion of the problem formulations considered. Through the theoretical results, not proven in this text, we have seen how the filter $C(s)$ decouples adaptation from the control and that fast adaptation thus is possible. Further it was proven that a large adaptation gain as possible is beneficial since it decreases the performance bounds. By choosing the feedback matrix $\mathbf{K}_m$ to specify the the desired performance, the control problem was reduced to the proper selection of $D(s)$ and $\mathbf{K}$ to get the desired trade-off between robustness and performance.

The final $\mathcal{L}_1$ adaptive control architecture was used to design one $\mathcal{L}_1$ adaptive controller for the SISO longitudinal system, and one for the MIMO lateral system. We saw that it was hard to verify the $\mathcal{L}_1$-norm condition required to prove the theoretical results. However, even though the $\mathcal{L}_1$-norm condition was not met, we saw that by considering the same design strategies discussed in the theory, the $\mathcal{L}_1$ adaptive controller managed to give good tracking, and suppress the unmatched nonlinear modelling errors and disturbances. This was true for both the longitudinal and the lateral systems, however, for the lateral system it was shown likely that a different filter $D(s)$ would give an even better result. To see the effect of the filter $C(s)$ the MRAC formulation was considered. This resulted in heavy oscillations in both the adaptation estimates, and the control input, which clearly shows the benefits of the $\mathcal{L}_1$ adaptive control formulation.

As a comparison, a simple PID-controller was tested for the longitudinal system. The result showed that the PID controller performed poorer than the $\mathcal{L}_1$ adaptive controller for the steps in reference, but actually better than the $\mathcal{L}_1$ adaptive controller for the sinusoidal reference. The greatest performance improvement of the $\mathcal{L}_1$ adaptive controller over the

PID-controller was in the case with a step response and large disturbances. It seems like the fact that the $\mathcal{L}_1$ adaptive controller can detect prediction errors and correct for them directly, instead of compensating for tracking error, is very beneficial in these cases.

Further, the longitudinal controllers was tested on the nonlinear "black box" F-16 model without any retuning. Again we saw that both the $\mathcal{L}_1$ adaptive controller and the PID-controller performed really well. Based only on the nonlinearities presented in the F-16 model, without disturbances, we can not conclude that the $\mathcal{L}_1$ adaptive controller is a better choice for the longitudinal system, especially considering the extra design challenges it presents. However, considering the control signals of the two controllers, we have seen that the PID-controller is much more aggressive. This is a great advantage of the $\mathcal{L}_1$ adaptive controller, that we can specify the desired performance and aggressiveness without considering the modelling error it has to handle.

Lastly the implementation issues with regards to $\mathcal{L}_1$ adaptive control was considered. We saw that by redesigning the $\mathcal{L}_1$ adaptive control architecture and retuning the adaptation gain, we achieved almost the same result for limited sampling rate as for the continuous formulation. Further we saw that by increasing the sampling rate, we could increase the adaptation which we know is beneficial. However, a direct relationship between the sampling rate and the adaptation gain was not found. What was also seen is that the single prediction estimate $\boldsymbol{\sigma}$ manages to capture all the nonlinearities and disturbances, due to the fast adaptation.

The $\mathcal{L}_1$ adaptive control strategy has proven to give good results. The positive effects of the filter $C(s)$ are clear, and the opportunity to introduce fast adaptation without imposing high gain feedback has been shown very positive. However, for the simple longitudinal system it seems like a simple PID-controller gives almost as good result. Some differences has however been seen in favor of the $\mathcal{L}_1$ adaptive controller. This is mainly the possibility of specifying the desired system response without considering the modelling error, and the ability to sense the modelling error and disturbance at the state it affects the system, and take the correcting action based on this information. For a more complex system this difference in the formulations probably makes the performance error more evident. The difference in performance between the $\mathcal{L}_1$ adaptive controller and a PID-controller for the lateral system is impossible to guess. However, the fact that the $\mathcal{L}_1$ adaptive controller can be designed for the complete multi-variable system is probably beneficial compared to the PID-controller.

5.1 Future work

Since we in this text only got the time to test the nonlinear F-16 controller for the pitch control, future work should include tests for the complete 6DOF nonlinear model.

Through this master's thesis, a good understanding of the principles of $\mathcal{L}_1$ adaptive control and the effects of the filter $C(s)$ has been achieved. However, the design of $D(s)$ and K need to be made specific for the different systems considered. The lack of a general design strategy is what makes the design of the $\mathcal{L}_1$ adaptive controller hard. Due to the scope of

this text, much research on the specific filter design for each of the systems considered was not included. This should be a focus in a future work.

Bibliography

[1] Ø. H. Holhjem, "L1 Adaptive Aontrol of UAV," NTNU, 2011.

[2] B. L. Stevens and F. L. Lewis, *Aircraft Control and Simulation*, 2nd ed. John Wiley & Sons, 2003.

[3] S. Bergbreiter, "Moving from practice to theory: Automatic control after world war ii," UC Berkeley, 2005.

[4] K. J. Åstrøm, "Adaptive control around 1960," in *IEEE Conference on Decision and Control*, New Orleans, LA, December 1995.

[5] P. A. Ioannou and J. Sun, *Robust adaptive control*. PTR Prentice-Hall, 1996.

[6] E. L. Zachary T. Dydek, Anuradha M. Annaswamy, "Adaptive control and the nasa x-15 program: A concise history, lessons learned, and a provably correct design," in *2008 American Control Conference*, Westin Seattle Hotel, Seattle, Washington, USA, June 2008.

[7] N. Hovakimyan and C. Cao, *L1 Adaptive Control Theory*, 1st ed. Sosiety for Industrial & Applied Mathematics, 2010.

[8] C. Cao and N. Hovakimyan, "Design and analysis of a novel l1 adaptive controller, part i," in *Proceedings of the 2006 American Control Conference*.

[9] Aerospaceweb.org.

[10] H. K. Khalil, *Nonlinear Systems*, 3rd ed. Prentice Hall, 2002.

[11] J. G. Balchen, T. Andresen, and B. A. Foss, *Reguleringsteknikk*, 5th ed. Department of Engineering Cybernetics, 2003.

[12] C.-T. Chen, *Linear System Theory and Design*. Oxford University Press, Inc., 1999.

[13] J. M. Maciejowski, *Predictive Control with Constraints*. Prentice Hall, 2000.

[14] T. I. Fossen, *Handbook of Marine Craft Hydrodynamics and Motion Control*, 1st ed. John Wiley & Sons, 2011.

[15] M. V. Cook, *Flight Dynamics Principles*, 2nd ed. Elsevier, 2007.

[16] D. McLean, *Automatic Flight Control Systems*, 1st ed. Prentice Hall, 1990.

[17] T. I. Fossen, *Mathematical Models for Control of Aircraft and Satellites*, 2nd ed. John Wiley & Sons, 2011.

[18] R. Stengel, *Flight Dynamics*, 1st ed. Princeton University Press, 2004.

[19] C.-T. E. Lan and J. Roskam, *Airplane Aerodynamics and Performance*, 3rd ed. Design, Analysis and Research Corporation, 2003.

[20] J. B. Høstmark, "Modelling simulation and control of fixed-wing uav: Cyberswan," Master's thesis, Norwegian University of Science and Technology, 2007.

[21] R. S. Russell, "Non-linear f-16 simulation using simulink and matlab," University of Minnesota, 2003.

[22] N. Hovakimyan, C. Cao, E. Kharisov, E. Xargay, and I. M. Gregory, "L1 adaptive control for safety-critical systems," *IEEE CONTROL SYSTEMS MAGAZINE*, 2011.

[23] D. Li, V. V. Patel, C. Chao, and N. Hovakimyan, "Optimization of the time-delay margin of $\mathcal{L}_1$ adaptive controller via the design of the underlying filter," in *AIAA Guidance, Navigation and Control Conference and Exhibit*.

Appendix A

Simulink diagrams

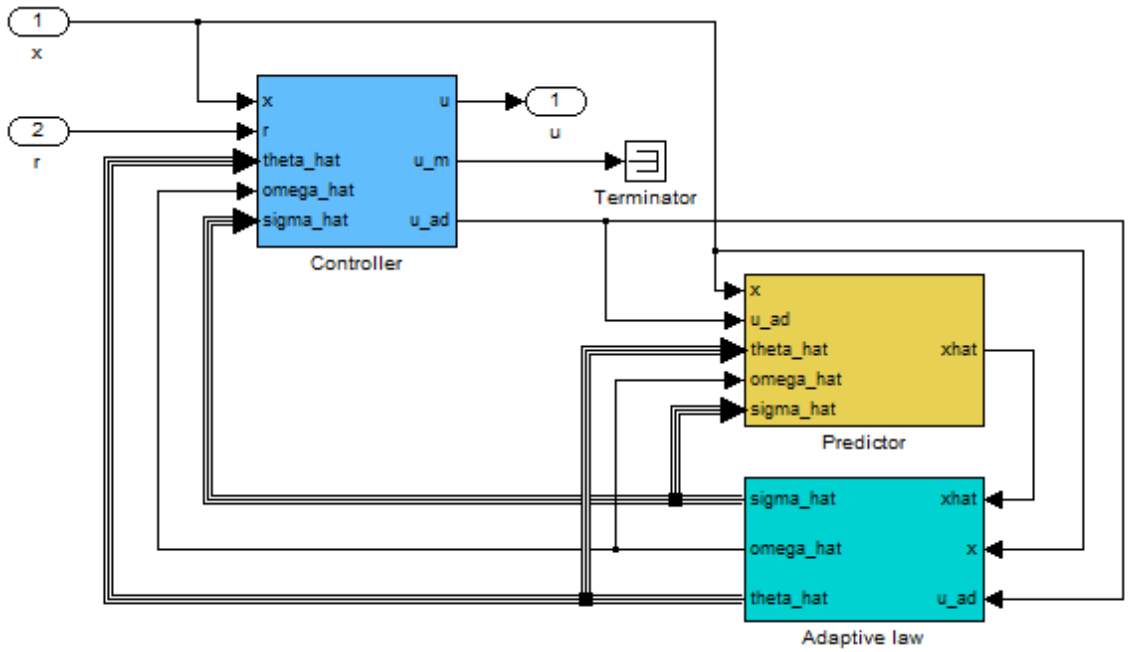

Figure A.1: Simulink implementation of the $\mathcal{L}_1$ adaptive control structure.

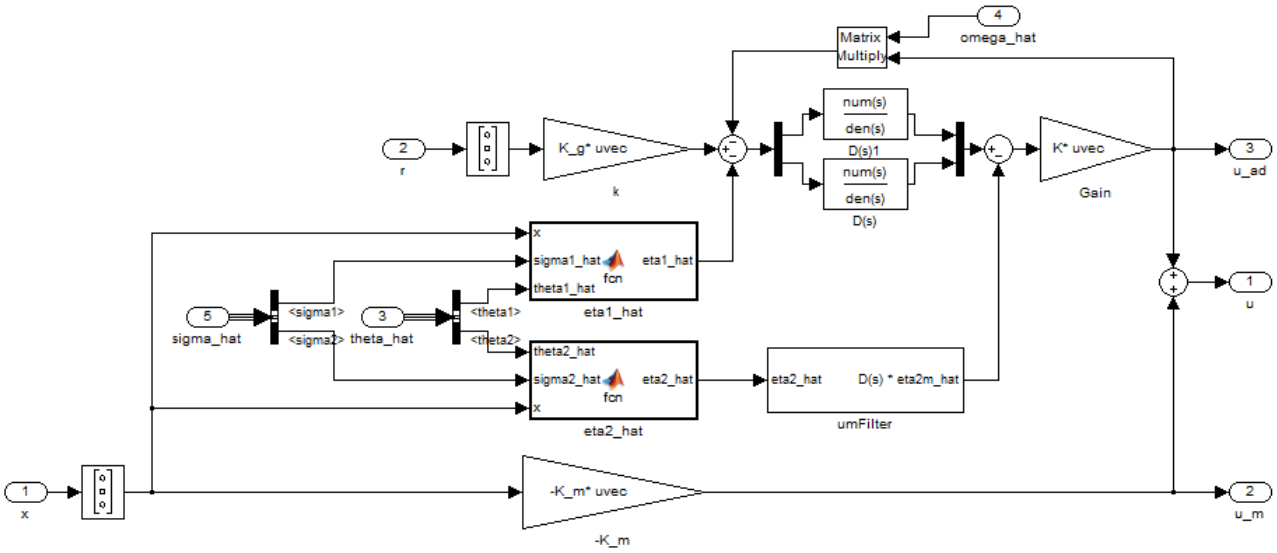

Figure A.2: Simulink implementation of controller.

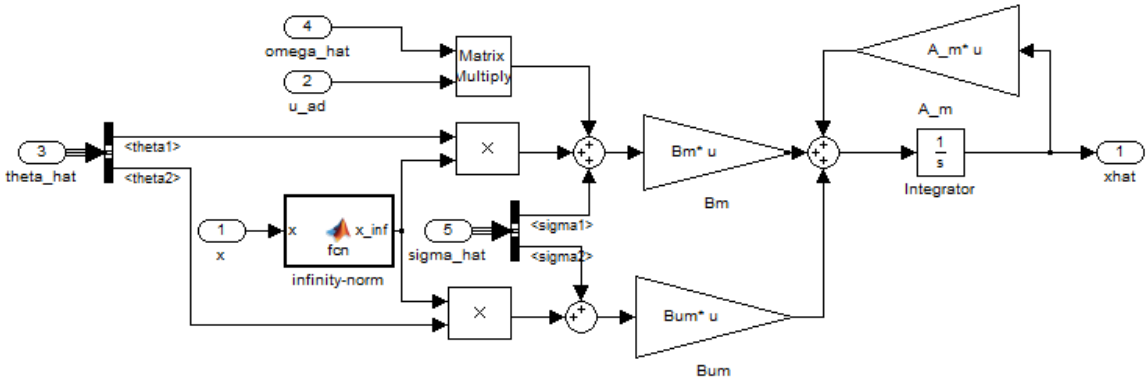

Figure A.3: Simulink implementation of the state predictor.

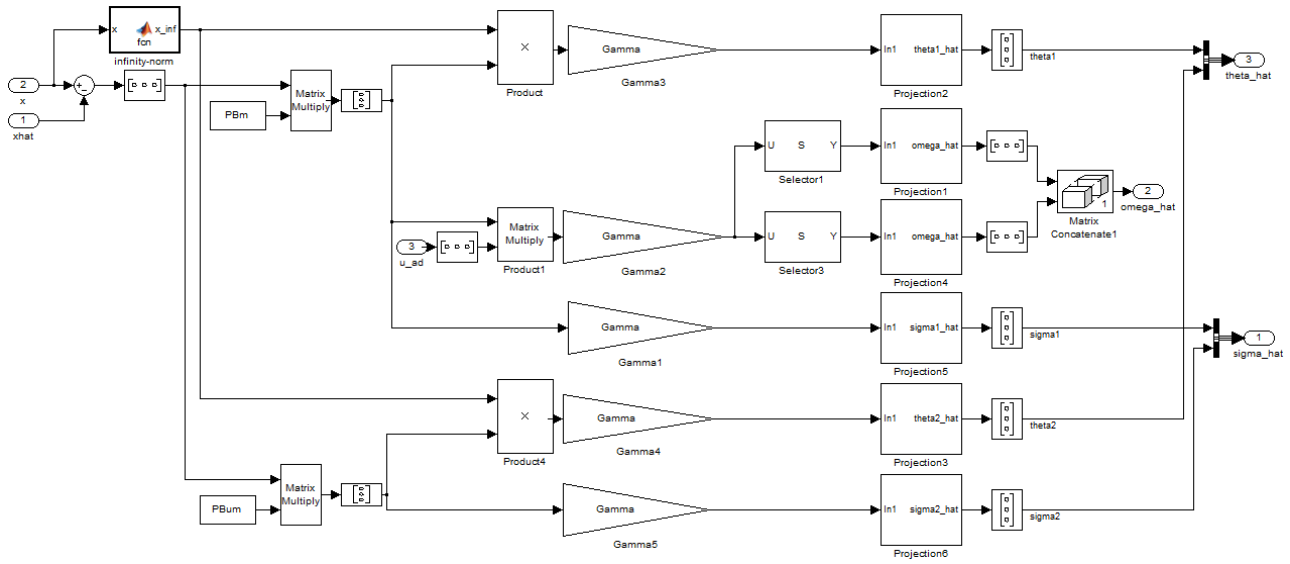

Figure A.4: Simulink implementation of the adaptive law.

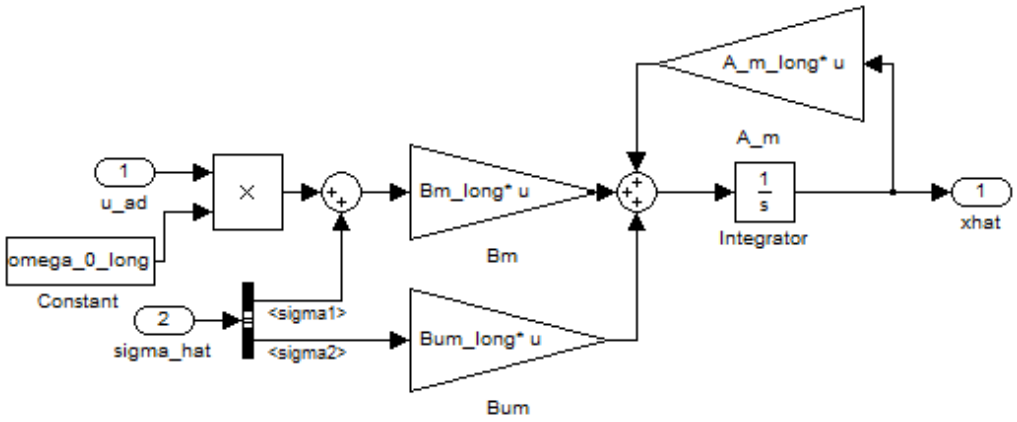

Figure A.5: Simulink implementation of the state predictor with limited sampling rate.

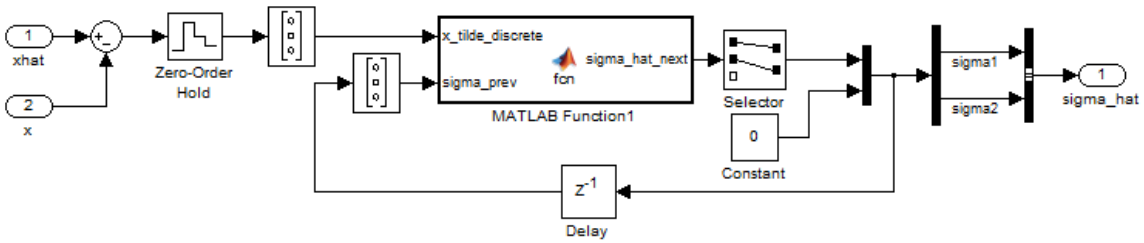

Figure A.6: Simulink implementation of the adaptive law with limited sampling rate.